JUSTUS-LIEBIG-
UNIVERSITÄT
GIESSEN

Aus dem Institut für Ernährungswissenschaften
Professur für Biochemie und Molekularbiologie
der Justus-Liebig-Universität Gießen

Functional characterisation of *Plasmodium* actin-like proteins Alp1 and Alp2b

INAUGURAL-DISSERTATION

zur Erlangung des Grades
Doktor der Naturwissenschaften

– Dr. rer. nat. –

im Fachbereich Agrarwissenschaften, Ökotrophologie und
Umweltmanagement der Justus-Liebig-Universität Gießen

vorgelegt von

Yukino Kobayashi

aus Saitama, Japan

Gießen, 2025

Mit Genehmigung des Fachbereichs Agrarwissenschaften,
Ökotrophologie und Umweltmanagement der
Justus-Liebig-Universität Gießen

Prüfungskommission:

1. Gutachter: **Prof. Dr. Jude M. Przyborski**

2. Gutachter: **Prof. Dr. Christoph Grevelding**

Prüfer: **Prof. Dr. Ross G. Douglas**

Prüfer: **Prof. Dr. Kai Thormann**

Vorsitzender: **Prof. Dr. Marc F. Schetelig**

Verteidigung am 26. Februar 2025

Erklärung gemäß der Promotionsordnung des Fachbereichs 09 vom 07. Juli 2004 § 17 (2)

„Ich erkläre: Ich habe die vorgelegte Dissertation selbständig und ohne unerlaubte fremde Hilfe und nur mit den Hilfen angefertigt, die ich in der Dissertation angegeben habe. Alle Textstellen, die wörtlich oder sinngemäß aus veröffentlichten Schriften entnommen sind, und alle Angaben, die auf mündlichen Auskünften beruhen, sind als solche kenntlich gemacht. Bei den von mir durchgeführten und in der Dissertation erwähnten Untersuchungen habe ich die Grundsätze guter wissenschaftlicher Praxis, wie sie in der „Satzung der Justus-Liebig-Universität Gießen zur Sicherung guter wissenschaftlicher Praxis“ niedergelegt sind, eingehalten.“

Gießen, 2025

_____
Yukino Kobayashi

Acknowledgement

Certainly my PhD journey wouldn't have even started without the kind support of Prof. Dr. Ross Douglas, who has the patience of a diamond. Thank you so much for your guidance. The greatest luck of my PhD life has been to have such a competent, dynamic team, including Caroline Busse, Tarek Holzapfel, Evangelia Nikolaou, Andrea Diers, Amélie Moll, Jana Niermann, Rebecca Schuld and Jennifer Feuser. I would also like to give my sincere appreciation to Annika Binder and Felix Mikus, the talented students of the laboratory of Prof. Dr. Freddy Frischknecht, who begun working with Alps and laid an excellent foundation.

It was a great honour to be a member of Prof. Dr. Jude Przyborski's highly professional team, full of scientific inspiration and ambition, which has always motivated me. I would also like to thank Dr. Stefan Rahlfs for sharing his research and teaching expertise with me.

During my PhD, I had numerous opportunities to present my research at scientific conferences and seminars. I cannot thank Prof. Dr. Christoph Grevelding enough for all these valuable experiences and also for being the second supervisor of this thesis.

I would like to extend my gratitude to Prof. Dr. Kai Thormann for his interest in my work and for kindly accepting the role of my examiner. Prof. Dr. Marc Schetelig, who supervised my Master's thesis, has once again joined my examination committee as chairman. Thank you very much for your continued support.

My special thanks go to Prof. Dr. Franco Falcone and his team, who were always so open and provided me with enormous help, both technically and academically.

This entire PhD project has been funded by the LOEWE Center DRUID, which has granted me not only the research opportunities, but also countless educational chances to grow professionally.

Finally, I would like to thank my family, even though they may not have been fully aware of what I have been facing in Europe. Soon I will no longer be a student.

Sometimes words of gratitude are not adequate to express my deepest feelings. Nevertheless, I hope this will reach everyone who has supported my academic journey until today.

Danke schön.

Summary

Malaria, the disease caused by *Plasmodium* parasites transmitted via *Anopheles* mosquitoes, remains a significant global health threat, responsible for over 600,000 deaths annually. The current treatments are constrained by inefficacy and the spread of drug resistance, which highlights the necessity for alternative strategies to prevent parasite transmission. The actin-like proteins (Alps), Alp1 and Alp2b, are unique actin-related proteins and specific to Apicomplexa. They play critical roles in *Plasmodium* transmission, yet their exact functions are still unknown. The aim of this thesis was therefore to characterise these Alps through elucidation of their specific biological functions, especially during the mammal-to-insect transmission stages.

The production of recombinant *P. berghei* Alp1 and Alp2b was attempted using the *E. coli* system to allow *in vitro* biochemical assays. Despite sufficient expression levels, purification and solubilisation of Alp1 and Alp2b, respectively, required further technical optimisation.

The partial and full knock-out of Alp1 in the rodent model species *P. berghei* demonstrated the essential role of this protein in facilitating ookinete gliding motility, with its C-terminus having no effect on either parasite growth or motility. Notably, *alp1* from human-pathogenic species *P. falciparum* could not rescue *P. berghei* motility when complemented as cDNA, underlining the potential significance of the introns. Cellular localisation of Alp1 was investigated through generation of the Alp1-3xHA line. Despite the critical role of Alp1 in gliding motility, no anticipated spatial association with the cytoskeletal motor machinery was observed. The actin chromobody was successfully utilised to visualise diverse structures of actin filaments in ookinetes. It further revealed that the absence of Alp1 leads to a moderate stabilisation of actin filaments. This suggests that Alp1 may contribute to the dynamic turnover of actin filaments, which ultimately affects the operation of the gliding motor machinery.

Alp2b is crucial for microgametogenesis and exflagellation. Here, a quantitative assay was established to precisely compare the exflagellation activity of different Alp2b mutants. While structurally similar *P. falciparum* Alp2b was partially functional in *P. berghei*, the exchange of the Alp2b D-loop or H-plug with the equivalent structures of actin completely arrested exflagellation. This result indicates that the Alp2b-specific larger D-loop and H-plug are functionally critical. More selective mutations in each region identified critical amino acid residues within the D-loop, while the conserved residues at the tip of the H-plug are interchangeable with the corresponding actin sequence. Collectively, this shows that Alp2b function relies on specific conserved amino acid residues within its unique regions, while some residues may also contribute to structural integrity. The deletion of Alp2b in *P. berghei*

resulted in a delay in axonemal development and the absence of nuclear segregation. Consequently, the immotile gametes were unable to exflagellate.

Altogether, this thesis demonstrates how Alp1 influences actin filament stability in ookinetes and its absence inhibits gliding motility, as well as how Alp2b facilitates crucial steps of male gametogenesis while its function depends on specific residues of unique regions. In both cases, these Alps are essential for *Plasmodium* transmission and thus provide a firm basis for potential transmission-blocking drug development. Production of recombinant Alps, as pursued in this thesis, would be of great benefit in this context. Finally, this study offers the first insights into the roles of these unique members of the actin superfamily, which would also contribute to the advancement of current cytoskeleton research.

Zusammenfassung

Malaria, eine durch *Plasmodium*-Parasiten verursachte und von Anopheles-Mücken übertragene Krankheit, bleibt eine bedeutende globale Gesundheitsbedrohung, die verantwortlich für mehr als 600.000 Todesfälle jährlich ist. Die aktuellen Behandlungen sind durch Unwirksamkeit und die Ausbreitung von Wirkstoffresistenzen beeinträchtigt, was die Notwendigkeit alternativer Strategien zur Verhinderung der Parasitenübertragung unterstreicht. Die Actin-like proteins (Alps) Alp1 und Alp2b sind einzigartige Actin-related proteins und spezifisch für Apicomplexa. Sie spielen eine wesentliche Rolle bei der Übertragung von *Plasmodium*, ihre genauen Funktionen sind jedoch noch ungeklärt. Ziel dieser Arbeit war es daher, diese Alp-Proteine durch die Aufklärung ihrer spezifischen biologischen Funktionen zu charakterisieren, insbesondere während der Übertragungsphasen vom Säugetier- zum Insektenwirt.

Die Herstellung von rekombinantem *P. berghei* Alp1 und Alp2b wurde mittels *E. coli*-Zellsystem versucht, um *in vitro* biochemische Analysen zu ermöglichen. Trotz ausreichender Expressionsmengen erfordert die Reinigung und Solubilisierung von Alp1 bzw. Alp2b weitere technische Optimierungen.

Der teil- und vollständige Knock-out von Alp1 im Mausmodell *P. berghei* beweist die wesentliche Rolle dieses Proteins bei der Förderung der Gleitbewegung von Ookineten, wobei der C-Terminus weder auf das Wachstum noch auf die Motilität der Parasiten Einfluss hat. Bemerkenswerterweise konnte Alp1 aus der humanpathogenen Spezies *P. falciparum* die Beweglichkeit von *P. berghei* nicht wiederherstellen, wenn es als cDNA komplementiert wurde, was die mögliche Bedeutung der Introns unterstreicht. Die zelluläre Lokalisierung von Alp1 wurde durch die Generierung der Alp1-3xHA-Linie untersucht. Trotz der entscheidenden Rolle von Alp1 bei der Gleitbewegung wurde keine erwartete räumliche Verbindung mit dem Motorsystem des Zytoskeletts beobachtet. Der Actin-Chromobody wurde erfolgreich eingesetzt, um verschiedene Strukturen von Aktinfilamenten in Ookineten zu visualisieren. Außerdem zeigte sich, dass die Abwesenheit von Alp1 zu einer moderaten Stabilisierung der Aktinfilamente führt. Dies deutet darauf hin, dass Alp1 zum dynamischen Umsatz von Aktinfilamenten beiträgt, was sich letztlich auf die Funktion des Gleitmotors auswirkt.

Alp2b ist entscheidend für die Mikrogametogenese und die Exflagellation. Hier wurde ein quantitativer Assay etabliert, um die Exflagellationsaktivität verschiedener Alp2b-Mutanten präziser zu vergleichen. Während das strukturell ähnliche Alp2b von *P. falciparum* in *P. berghei* teilweise funktionsfähig war, wurde die Exflagellation durch den Austausch des D-Loops oder des H-Plugs von Alp2b gegen die entsprechenden Strukturen von Aktin

komplett unterbrochen. Dieses Ergebnis deutet darauf hin, dass der Alp2b-spezifische größere D-Loop und der H-Plug funktionell essenziell sind. Selektivere Mutationen in den jeweiligen Regionen identifizierten kritische Aminosäuren im D-Loop, während die konservierten Aminosäuren an der Spitze des H-Plugs mit der entsprechenden Aktin-Sequenz austauschbar sind. Insgesamt zeigt dies, dass die Funktion von Alp2b von bestimmten konservierten Aminosäuren innerhalb seiner spezifischen Regionen abhängt, während einige Aminosäuren auch zur strukturellen Integrität beitragen können. Die Deletion von Alp2b in *P. berghei* führte zu einer Verzögerung der axonemalen Entwicklung und zum Ausfall der Zellkernsegregation. Folglich waren die unbeweglichen Gameten nicht fähig, zu exflagellieren.

Insgesamt zeigt diese Arbeit, wie Alp1 die Stabilität der Aktinfilamente in Ookineten beeinflusst sowie dessen Abwesenheit die Gleitbewegung hemmt und wie Alp2b entscheidende Schritte der männlichen Gametogenese ermöglicht, während dessen Funktion von bestimmten Aminosäuren in spezifischen Regionen abhängt. In beiden Fällen sind diese Alps für die Übertragung von *Plasmodium* essentiell und bieten somit eine feste Grundlage für die Entwicklung potenzieller übertragungshemmender Medikamente. Die Herstellung von rekombinanten Alps, wie sie in dieser Arbeit verfolgt wurde, wäre in diesem Zusammenhang von großem Interesse. Schlussendlich bietet diese Studie erste Einblicke in die Rolle dieser einzigartigen Mitglieder der Aktin-Superfamilie, was auch zur Weiterentwicklung der aktuellen Zytoskelettforschung beiträgt.

Table of contents

List of figures

List of tables

List of supplementary data

List of abbreviations

Abbreviation	Full name
5FC	5-fluorocytosine
AA	Amino acid
ADD-H	Actin-depolymerising factor homology domain
ADF	Actin depolymerising factor
ADF-H	Actin-depolymerising factor homology domain
ADP	Adenosine diphosphate
Alp	Actin-like protein
APR	Apical polar ring
Arp	Actin-related protein
ATP	Adenosine triphosphate
bp	Base pair
cDNA	Complementary deoxyribonucleic acid
CHES	N-cyclohexyl-2-aminoethanesulfonic acid
CMA	Carboxylmethylaspartate
CMC	Critical micelle concentration
Co-CMA	Cobalt–carboxylmethylaspartate
CTRP	Surface adhesin circumsporozoite- and TRAP-related protein
Cyto D	Cytochalasin D
ddH2O	Double-distilled water
dNTP	Dideoxy-nucleotide triphosphate
DIC	Differential interference contrast
D-loop	DNase I binding loop
DMSO	Dimethyl sulfoxide
DNA	Deoxyribonucleic acid
DTT	Dithiothreitol
eEF1α	Eukaryotic translation elongation factor 1 alpha
EGFP	Enhanced green fluorescent protein
FBS	Fetal bovine serum
FBT	Fresh blood transfer
FC12	Fos-choline-12
GAP	Glideosome-associated protein
GDP	Guanosine diphosphate
GFP	Green fluorescent protein
GOI	Gene of interest
HA	Hemagglutinin
Halo	Haloalkane dehalogenase
hDHFR	Human dihydrofolate reductase
HEPES	4-(2-hydroxyethyl)-1-piperazineethanesulfonic acid
His tag	Histidine tag
H-plug	Hydrophobic plug
HRP	Horseradish peroxidase
IF	Immunofluorescence
IMAC	Immobilised metal affinity chromatography

IMC	Inner membrane complex
IP	Intraperitoneal
IPTG	Isopropyl ß-D-1-thiogalactopyranoside
ITNs	Insecticide-treated nets
IV	Intravenous
Jas	Jasplakinolide
Kb	Kilobase
kDa	Kilodalton
KO	Knock out (gene)
LDAO	Lauryldimethylamine oxide
LOBSTR	Low background strain (*Escherichia coli*)
LTD	Limiting dilution
MES	2-(N-morpholino) ethanesulfonic acid
mpa	Minutes post-activation
ms	Millisecond
MTIP	MyoA tail domain-interacting protein
MTOC	Microtubule organising centre
MyoA	Myosin A
Ni-NTA	Nickel-nitrilotriacetic acid
Ni-TED	Nickel-tris-carboxymethyl ethylene diamine
OD	Optical density
Pb	*Plasmodium berghei*
PbANKA	*Plasmodium berghei* ANKA strain
PBS	Phosphate-buffered saline
PCR	Polymerase chain reaction
Pf	*Plasmodium falciparum*
PFA	Paraformaldehyde
PI	Isoelectric point
PV	Parasitophorous vacuole
RNA	Ribonucleic acid
rpm	Rotation per minute
RT	Room temperature
SD	Subdomain
SDS-PAGE	Sodium dodecyl sulphate polyacrylamide gel electrophoresis
SPMT	Subpellicular microtubules
SUMO	Small ubiquitin-related modifier
TB	Terrific broth
TEM	Transmission electron microscopy
TRAP	Thrombospondin-related anonymous protein
TRIS	Tris(hydroxymethyl)aminomethane
tRNA	Transfer ribonucleic acid
US	Ultrasound
UTR	Untranslated region
WT	Wild-type
yFCU	Yeast cytosine deaminase-uracil phosphoribosyl transferase fusion gene

γTuRC	γ-Tubulin ring complex

Abbreviations of nucleotides and amino acids

Amino acid	3 letter code	1 letter code
Alanine	Ala	A
Arginine	Arg	R
Asparagine	Asn	N
Aspartic acid	Asp	D
Cysteine	Cys	C
Glutamic acid	Glu	E
Glutamine	Gln	Q
Glycine	Gly	G
Histidine	His	H
Isoleucine	Ile	I
Leucine	Leu	L
Lysine	Lys	K
Methionine	Met	M
Phenylalanine	Phe	F
Proline	Pro	P
Serine	Ser	S
Threonine	Thr	T
Tyrosine	Tyr	Y
Tryptophane	Trp	W
Valine	Val	V

Nucleotide	Abbreviation
Adenine	A
Thymine	T
Cytosine	C
Guanine	G

1 Introduction

1.1 Malaria – Epidemiology and control: in need of transmission blockers

Malaria has posed a significant health risk to humanity for millennia (Cox, 2010; Miller et al., 1994). Today, malaria still remains as one of the most lethal tropical diseases, accounting for over 600,000 deaths annually. The largest population at risk are young children in sub-Saharan Africa, who represent more than 70% of the global deaths (WHO, 2023). Furthermore, the susceptibility of pregnant women to malaria infection intensifies the health risks posed to children (Douamba et al., 2014; WHO, 2023). Malaria is a parasitic disease caused by *Plasmodium* spp.. Six species of *Plasmodium* are known to infect humans, including *P. falciparum*, *P. vivax*, *P. knowlesi*, *P. malariae*, *P. ovale curtisi* and *P. ovale wallikeri* (Ashley et al., 2018). While *P. falciparum* accounts for the highest mortality rate and is the dominant cause of infection in Africa, *P. vivax* and *P. knowlesi* are more prevalent in South America and South-East Asia, respectively. (WHO, 2023). The clinical presentation of malaria can range from asymptomatic, with only flu-like mild symptoms, to more severe conditions, including blood disorders and neurological complications (cerebral malaria), which can ultimately result in the death of the patient (Idro et al., 2010). Malaria can be treated with medications such as chloroquine, sulfadoxine-pyrimethamine (SP) and artemisinin (Arrow et al., 2004). Chloroquine was a traditional first-line treatment medication, used in tandem with pyrimethamine. The two were extensively employed in Africa as part of intermittent preventive therapy. However, they are no longer recommended for use due to the emergence of widespread resistance (Amimo et al., 2020; Skrzypek and Callaghan, 2017). Artemisinin is a more recent alternative to chloroquine and pyrimethamine in combination therapy. Its efficacy in the treatment of severe malaria has been demonstrated on account of its broad-spectrum targeting of the blood stage parasites and rapid onset of action. (Arrow et al., 2004; Dondorp et al., 2005). It is a matter of grave concern that artemisinin is now also facing the challenge of emerging drug resistance (Woodrow and White, 2017). The spread of drug resistance can be suppressed by reducing the rate of transmission, particularly in areas with low transmission rates, where the population is less immune to malaria infection (Klein, 2013). The key factor is the asymptomatic population, which may unknowingly serve as a reservoir for resistant parasites (Ibrahim et al., 2023; Legesse et al., 2024). Therefore, the fundamental approach to mitigating the risk of epidemic and emergence of drug resistance is the active treatment of asymptomatic patients, coupled with the prevention of *Plasmodium* transmission.

Thus far, the deployment of insecticide-treated nets (ITNs) and indoor residual spraying (IRS) has shown to be an effective method for lowering the prevalence of infection in endemic areas of Africa, with a reduction of over 68% (Bhatt et al., 2015). It is, however,

still some way off achieving the goal of eradication. Similarly, some commonly used classes of insecticides, including pyrethroids and organochlorines, appear to be susceptible to emerging resistance (Suh et al., 2023). This, in conjunction with antimalarial drug resistance, represents an additional challenge to the current malaria control measures.

The recent advancements in antimalarial vaccine development may offer a glimmer of hope in our long-term efforts to combat malaria (Duffy et al., 2024). The first WHO-recommended vaccine, RTS,S/AS01, targets the pre-erythrocytic stages (sporozoites) following immunisation by a truncated circumsporozoite protein (CSP) antigen fused with hepatitis B virus surface antigens as protein carriers (Laurens, 2019). The RTS,S vaccine has successfully completed the phase IV clinical trial, confirming its safety and demonstrating a minor contribution to the reduction of the incidence of severe malaria in young children (Wadman, 2023). The second and most recent development is the R21/Matrix-M vaccine, which also targets sporozoites utilising CSP antigen but with enhanced immunogenicity achieved by the universal display of CSP antigen fragment in every protein particle (Collins et al., 2017). In the phase III clinical trial, the R21 vaccine demonstrated a reduction in clinical malaria cases of over 68%, establishing itself as one of the most promising vaccines (Datoo et al., 2024).

In considering the most efficient means of eradicating malaria, the immunisation of vulnerable populations through vaccination and the control of vector mosquitoes are crucial aspects. A final potential avenue for disrupting the malaria infection cycle would be the development of transmission-blocking drugs. The only drug currently recommended for transmission-blocking is primaquine, which presents a health concern in the treatment of patients with glucose-6-phosphate dehydrogenase deficiency (G6PDd), a common occurrence in malaria-endemic regions (Pukrittayakamee et al., 2024). The necessity for new transmission-blocking drugs against *Plasmodium* is therefore clear, and their development is essential to facilitate the advent of a malaria-free future.

1.2 *Plasmodium* spp.

1.2.1 The phylum of Apicomplexa

Plasmodium belongs to the phylum of Apicomplexa (**Figure 1A**), which features unicellular obligate parasites that exhibit distinctive evolutionary traits within the eukaryotic diversity. In addition to *Plasmodium*, the phylum contains several genera of parasites that impose health risks on both humans and animals. These include *Toxoplasma* (toxoplasmosis) and *Babesia* (babesiosis), among others (Votýpka et al., 2017). Approximately 6,000 apicomplexan species are presently known, making Apicomplexa one of the main phyla of

Alveolata along with the ecologically important Dinoflagellata (phytoplankton) and Ciliophora (predatory protozoans) (Adl et al., 2007; Lin et al., 2024; Weisse, 2017).

The name 'Apicomplexa' is derived from the Latin terms *'apex'* (top) and *'complexus'* (infolds), as it refers to the group of phylum-specific organelles known as the 'apical complex', which are condensed at the anterior end of the parasite (Votýpka et al., 2017) (**Figure 1B**). The components of the apical complex, including micronemes, rhoptries, apical polar ring (APR) and conoid, serve essential roles in facilitating the motility and invasion of parasites (Haase et al., 2022; Sun et al., 2024). Micronemes secrete adhesins through exocytosis, which subsequently coats the parasite membrane and initiates migratory motility and host-cell engagement through interaction with host cell surface receptors (Heinzelman, 2015; Tham et al., 2015). Rhoptries are also integral to the host cell invasion, working in conjunction with micronemes (Carruthers and Sibley, 1997). In the case of *Toxoplasma gondii* tachyzoites, host cell adhesion is initiated by microneme proteins (MICs) and apical membrane antigen 1 (AMA1). This is followed by the rhoptry secretion of rhoptry neck proteins (RONs) through the APR, whereby a solid platform, known as a moving junction, is formed between the parasite and host cell membranes. This enables motility-driven penetration (Frénal et al., 2017; Straub et al., 2011). The conoid is a tubulin-based organelle that is attached to the microtubule organiser APR (Hu et al., 2002). It has been observed to extrude during the process of host cell invasion, in close temporal proximity to the secretion of MICs (Haase et al., 2022). Of note, despite the presence of conoid-associated spindle assembly abnormal 6 homolog-like (SAS6L) protein, *Plasmodium* is generally believed to lack conoid (Wall et al., 2016). However, a more recent study has indicated the existence of a conoid-like structure (Bertiaux et al., 2021; Koreny et al., 2021).

Besides the apical complex, the apicoplast is an evolutionally peculiar organelle that has its origin in a plastid derived from algae (McFadden and Yeh, 2017). Despite the apicoplast no longer being photosynthetic, it continues to facilitate vital metabolic pathways. These include the methylerythritol phosphate (MEP) pathway, which produces isoprenoid precursors that are required for tRNA regulation (Guggisberg et al., 2014; Imlay and Odom, 2014). The apicoplast also facilitates heme biosynthesis, which is crucial for cellular detoxification, growth and virulence (Bergmann et al., 2020; Ke et al., 2014).

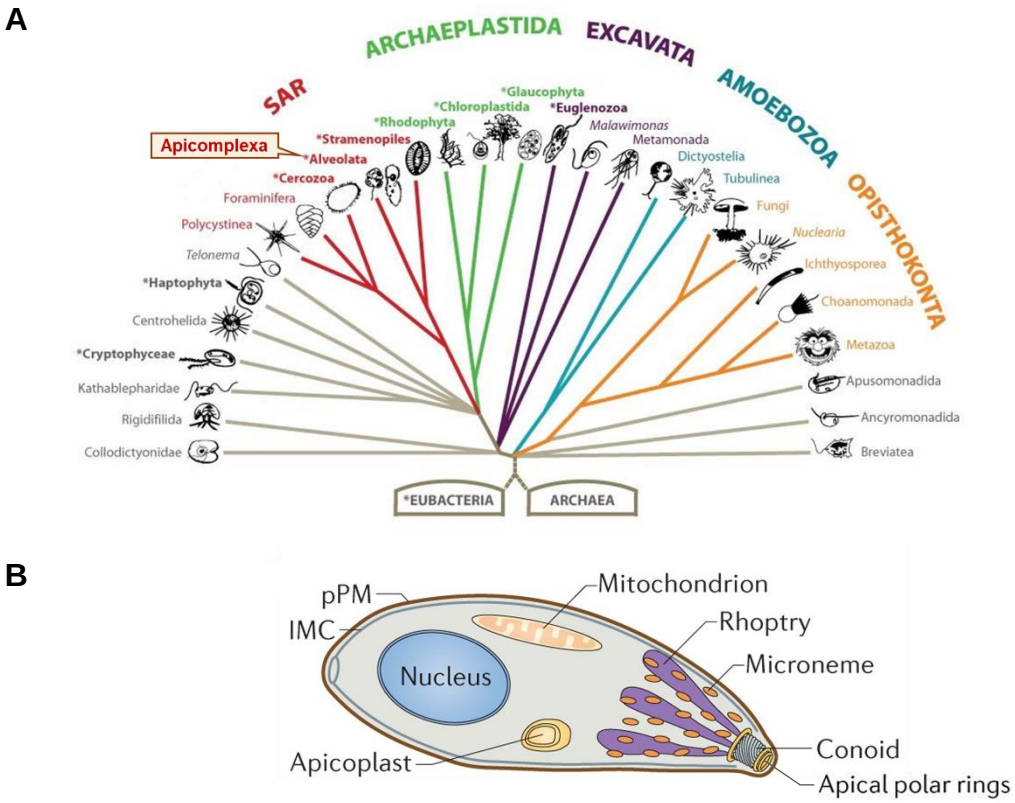

Figure 1: Evolutionary traits of the Apicomplexa. (A) A phylogenetic tree illustrating the evolutionary lineage of the Alveolata (indicated with the yellow arrow). The figure originated from Adl et al. (2012) modified by Ilana Gilg, adapted from https://ncma.bigelow.org/tree-of-life-search. **(B)** An illustration of *T. gondii* tachyzoites represents the apical complex organelles (conoid, apical polar rings (yellow), micronemes and rhoptries) as well as the apicoplast. pPM = parasite plasma membrane, IMC = inner membrane complex. The figure was adapted form Frénal et al. (2017).

1.2.2 Life cycle and biology of *Plasmodium*

As obligate parasites, *Plasmodium* is dependent on its respective hosts for both feeding and propagation. The life cycle of *Plasmodium* alternates between vertebrate hosts and blood-feeding insects, representing two markedly divergent living environments (Smith and Styczynski, 2018). In general, the human and primates-infecting species of *Plasmodium* are transmitted by female *Anopheles* mosquitoes during their blood meals (Ramasamy, 2014). Following the bite of a *Plasmodium*-infected mosquito, a small proportion of sporozoites are deposited into the dermis of the host (Frischknecht and Matuschewski, 2017) (**Figure 2 [1]**). At this point, approximately 75% of the ejected sporozoites actively migrate at an average speed of 1–2 µm/s, suggesting the necessity of powerful gliding motility to cross the dermis and reach blood vessels (Amino et al., 2006; Douglas et al., 2015). Ultimately, around half of the sporozoites are able to enter the blood vessels and are carried away by the bloodstream, while the remainder either persist in the dermis or become lost in the lymphatic system (Amino et al., 2006).

Upon reaching the liver, sporozoites traverse the sinusoidal barrier and some hepatocytes (Mota et al., 2001; Segireddy et al., 2024) (**Figure 2 [2]**), until they reach the final host hepatocytes, where they enter the cell through the rhoptry discharge and moving junction-mediated motility (**1.2.1**) (Baum et al., 2008a). The parasite undergoes a significant morphological transformation within its protective compartment called parasitophorous vacuole (PV), following the infection of hepatocytes, resulting in the formation of the liver stage trophozoite (Arredondo et al., 2021). Subsequently, the replication process described as exoerythrocytic schizogony (Goswami et al., 2022) generates approximately 10,000 blood-infective daughter parasites, known as merozoites (Yang et al., 2023). The release of mature merozoites from the hepatocyte is triggered by the destabilisation of the host cell actin cytoskeleton, whereby the merosomes containing merozoites bud off from the mother cell and enter the bloodstream by the surrounding shear forces (Burda et al., 2017; Sturm et al., 2006). It is noteworthy that during the liver stage, certain *Plasmodium* species, including *P. vivax* and *P. ovale*, are capable of entering a non-replicating latent state, known as a 'hypnozoite', which can result in relapse malaria (Venugopal et al., 2020).

Subsequent infection of erythrocytes by merozoites occurs when the parasite deploys its motility to deform the host cell membrane and internalise itself through pushing from the posterior end (Yahata et al., 2021) (**Figure 2 [3]**). In addition, the internalisation process involves AMA1, RON2 and RON4 to form a moving junction, indicating further involvement of motility-dependent invasion process (Srinivasan et al., 2011). During the intraerythrocytic phase, the parasite undergoes three distinct morphological stages, namely the ring stage, trophozoite and schizont within its PV. This is followed by a second asexual schizogony which gives rise to up to 32 merozoites for further erythrocyte infection (Venugopal et al., 2020). These stages are clinically important as they involve erythrocyte remodelling, which is associated with severe malaria symptoms (Idro et al., 2010). The formation of 'knobs' on *P. falciparum*-infected erythrocytes may be one of the most representative forms of cell remodelling, resulting in the blockage of microvasculature through endothelial cytoadherence, which is mediated by the *P. falciparum* erythrocyte membrane protein 1 (PfEMP1) (Moxon et al., 2011; Smith et al., 2013). The induction of cell remodelling is initiated by the exportation of parasite proteins into the host cell (Przyborski and Lanzer, 2004), with transcription peaking during the late ring to early trophozoite stages (Marti et al., 2004).

The mammalian blood stages are collectively referred to as the asexual stage. However, between 3 and 12% of the parasite develops into male and female gametocytes, which begin their sexual reproduction in the midgut of *Anopheles* mosquitoes shortly after being ingested with a blood meal (Kuehn and Pradel, 2010; Stewart et al., 2022) (**Figure 2 [4]**).

The transition from a mammalian host to an insect vector immediately initiates the sexual activation of gametocytes in response to environmental signals, including a decline in temperature (~20 °C), an increase in pH (~8.0), and the presence of mosquito-derived xanthurenic acid (Billker et al., 1997; Kuehn and Pradel, 2010). While sexually activated female gametocytes undergo a transformation into macrogametes, male gametocytes engage in three sets of rapid genome replication processes, resulting in the exflagellation (egress) of eight highly motile microgametes in less than 20 minutes. These microgametes eventually come into contact with a female counterpart for fertilisation (Dash et al., 2022).

The fusion of male and female gametes is followed by the formation of diploid zygotes, which subsequently develop into tetraploid ookinetes within approximately 20 hours (Bennink et al., 2016; Mzilahowa et al., 2007) (**Figure 2 [5]**). During this transition, zygotes synthesise the proteins required for motility and invasion, and as they mature, new apical complex organelles are formed to fully equip ookinetes for the forthcoming midgut colonisation stage (Sebastian et al., 2012). The invasion process commences with the penetration of the peritrophic matrix of the midgut lumen through the secretion of chitinases (Patra et al., 2021). This is followed by a traversal of the epithelial tissue through ligand-receptor interactions with the midgut surface proteins, allowing the parasite to reach the subepithelial basal space, where it forms the oocysts (Vega-Rodríguez et al., 2014).

An oocyst is an encapsulated cell that accommodates the asexual replication and development of sporozoites in the process known as sporogony (Frischknecht and Matuschewski, 2017) (**Figure 2 [6]**). It has been proposed that the egress of sporozoites from an oocyst occurs via a local rupture of the capsule, initiated by the active motility and the apical secretion of capsule-degrading enzymes (Klug and Frischknecht, 2017; Saeed et al., 2023). Consequently, hundreds of sporozoites are released into the open haemolymph circulation over the course of 10 to 14 days (Zhou et al., 2024).

The released sporozoites are transported passively by the circulation of haemolymph and eventually arrive in the salivary gland, where they initiate their final invasion before returning to the mammalian host (Douglas et al., 2015) (**Figure 2 [7]**). The sporozoites then attach themselves to the basal lamina of the salivary gland and penetrate their way through to the salivary cavity, utilising a gliding motility-associated mechanism (Ghosh and Jacobs-Lorena, 2009; Sultan et al., 1997). Ultimately, the parasite reaches the proboscis via the salivary duct and is expelled along with saliva as the *Anopheles* mosquito takes her blood meal (Frischknecht and Matuschewski, 2017), thereby completing the full life cycle.

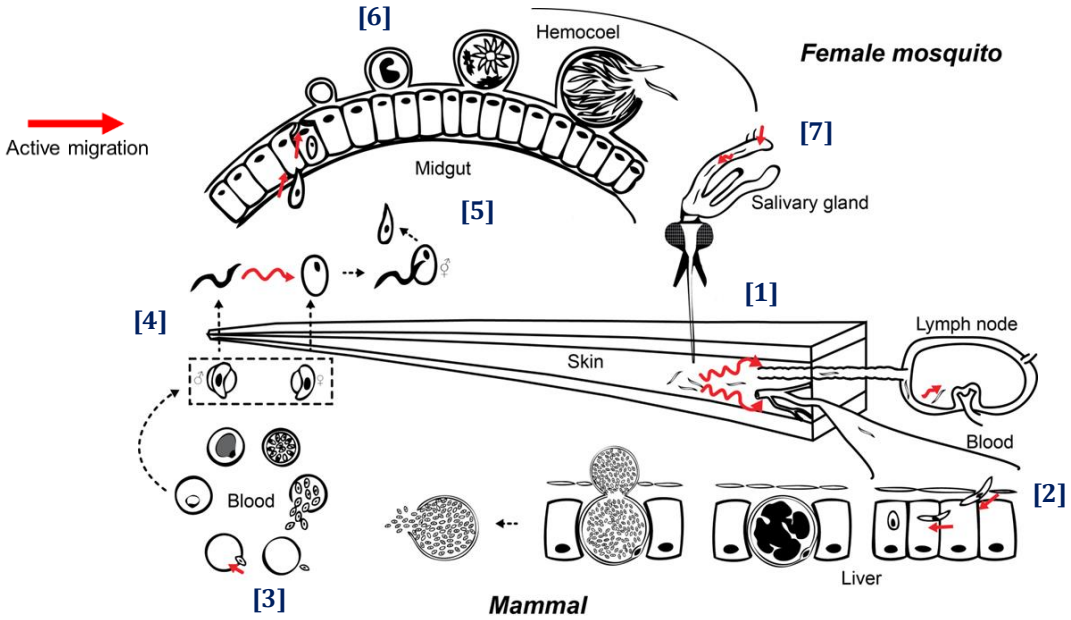

Figure 2: Life cycle of *Plasmodium* and its active motility. [1] The life cycle of *Plasmodium* commences with the transmission of sporozoites into a mammalian host via a bite from an infected female *Anopheles* mosquito. Following deposition, the sporozoites rapidly traverse the host dermis and enter the blood vessels, with some settling in the lymph nodes and being eliminated over time. [2] The parasites are transported passively through the bloodstream to the liver, where they invade hepatocytes and undergo asexual replication (schizogony), resulting in the production of approximately 10,000 merozoites. The mature merozoites, encased in their parasitophorous vacuole (PV), eventually bud off from the main merosome body and are swept away into the bloodstream. [3] The invasion of erythrocytes by free merozoites is once more an active process. Once within the erythrocyte, the parasite progresses through a series of stages, namely the ring stage, trophozoite and schizont stages. This process, known as second schizogony, results in the production of up to 32 merozoites, which then proceed to infect further erythrocytes. [4] Some parasites during the blood stage commit to sexual replication by differentiating into male and female gametocytes. Upon being ingested by an *Anopheles* mosquito during a subsequent blood meal, the parasites perceive the environmental changes (pH, temperature, and mosquito-derived molecules) and activate their fertilisation process. A sexually activated male gametocyte undergoes three rounds of rapid nuclear divisions and produces eight highly motile microgametes through a process called exflagellation, wherein the parasites actively seek female partners for fertilisation. [5] The fusion of male and female gametes results in the formation of an ookinete, a further invasive form that is specialised for colonisation of the mosquito midgut. Ookinetes are able to penetrate the peritrophic matrix and the epithelial layer of the midgut, subsequently forming oocysts beneath the basal lamina. [6] The oocysts facilitate the development of hundreds of sporozoites through asexual replication. Upon maturation, the sporozoites are released into the haemolymph circulation, where they are transported passively to the salivary gland. [7] The salivary gland represents the final bottleneck before the infection of the mammalian host. In order to reach the salivary cavity and be ejected at the next blood meal, the sporozoites must traverse the basal lamina and epithelial layers. The figure was adapted from Douglas et al. (2015).

1.2.3 Active motility is essential for *Plasmodium* survival

The success of the *Plasmodium* life cycle is inextricably linked to its capacity for active migration. As previously reviewed by Douglas et al. (2015) and illustrated in **Figure 2**, the active motility of *Plasmodium* is utilised not only for rapid translocation (Amino et al., 2006), but also for the overcoming of non-permissive biological barriers, such as hepatocytes (Silvie et al., 2004), erythrocytes (Yahata et al., 2021) and epithelial layers of different insect organs (Hirai et al., 2006; Sultan et al., 1997). Moreover, the sexual reproduction process is contingent upon actively motile male gametes, which exhibit disparate characteristics

compared to the remaining motile life stages (Wilson et al., 2013). The following sections will outline the molecular bases of two essential types of *Plasmodium* motility.

1.2.3.1 Ciliary motility

Ciliary motility represents a swimming-like flagellar beating that utilises hydrodynamic force to migrate (Walton et al., 2023). The axoneme is an essential cytoskeletal structure of motile eukaryotic flagella. It is canonically characterised by a "9+2" microtubule arrangement, comprising nine doublets of microtubules encircling two singlet microtubules (Grossman-Haham, 2023) (**Figure 3A**). This arrangement is conserved across eukaryotes, including *Plasmodium* (Sinden et al., 2010). In the axoneme, microtubule doublets are connected with inner and outer dynein arms. Dynein is an ATP-dependent motor protein that facilitates flagellar beating motion by sliding against neighbouring microtubules in a highly coordinated manner (Ishikawa, 2017).

A microtubule is constituted of α and β-tubulin heterodimer subunits, which collectively form a protofilament. Typically, 13 protofilaments are laterally associated to form a single microtubule, which takes on a cylindrical configuration (Goodson and Jonasson, 2018) (**Figure 3B**). The nucleation of a microtubule filament commences with the association of the γ-tubulin ring complex (γTuRC) with the microtubule organisation centres (MTOCs), also known as basal body. Here, the active polymerising side (+ end) of γ-tubulin is exposed, allowing the incorporation of αβ-tubulin subunits (Sulimenko et al., 2022). The minus (-) end, which is oriented towards the MTOC, is capped by the γTuRC proteins, thus modulating the depolymerisation dynamics (Wiese and Zheng, 2000). The process of incorporation and dissociation of αβ-tubulin subunits is regulated by the hydrolysis of the bound GTP in freshly incorporated subunits. Following incorporation into the filament, β-tubulin within the subunit hydrolyses the GTP to GDP (Goodson and Jonasson, 2018). This results in the release of phosphate and a change in the nucleotide state, which in turn causes a conformational change in the subunit, rendering it more susceptible to depolymerisation (Zhang et al., 2015)

In the life cycle of *Plasmodium*, ciliary motility is performed exclusively by microgametes, in order to initiate fertilisation (Sinden et al., 2010). The anatomy of the microgamete represents a highly simplified structure, with only axonemal microtubules attached to the basal body and a haploid nucleus (Wilson et al., 2013) (**Figure 3C**). The conserved '9+2' microtubule arrangement is also observed in the main axoneme, however, the basal body is comprised of nine singlet microtubules (Francia et al., 2016; Sinden et al., 2010). The basal body, or outer centriolar MTOC, is essential for flagellum assembly and also serves

as the origin of axoneme nucleation during microgametogenesis (Yahiya et al., 2022; Zeeshan et al., 2022). Once matured, microgametes are capable of swimming at a speed of up to five flagellar beats per second (Sinden and Croll, 1975). It is striking that a male gametocyte is able to produce eight such microgametes in less than ten minutes (Yahiya et al., 2022), reflecting the remarkable dynamics of *Plasmodium* biology.

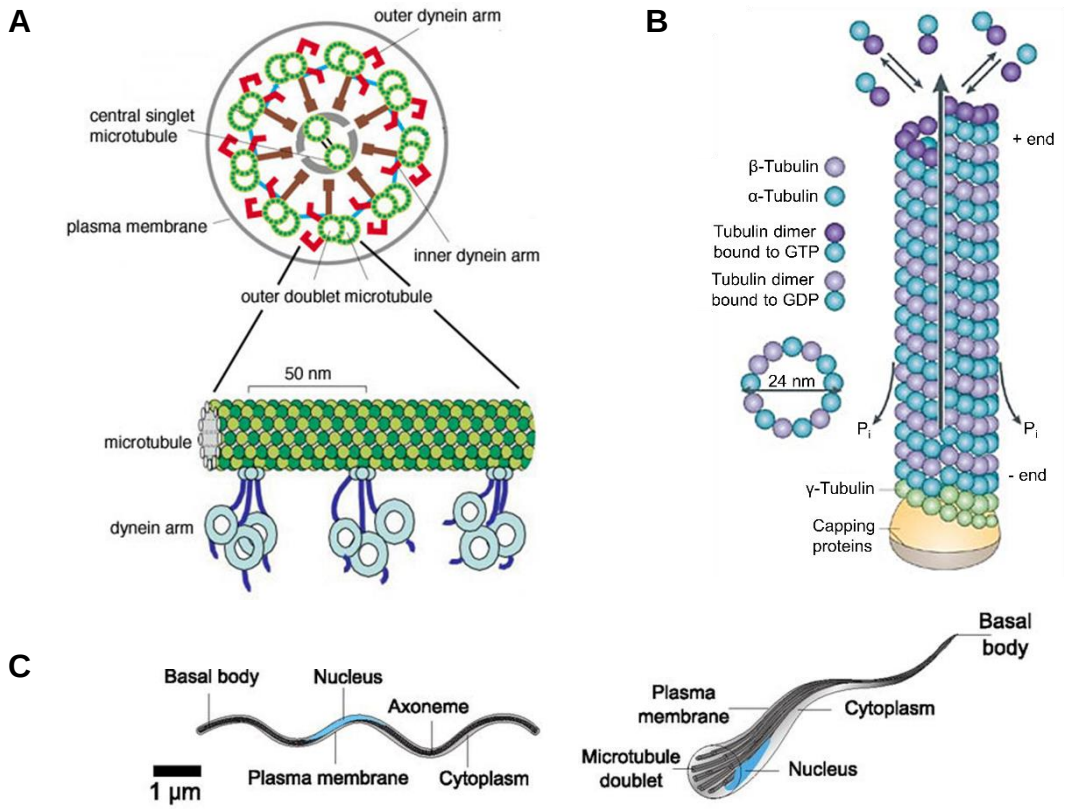

Figure 3: Axoneme structure and microtubule filament formation. (A) A cross-section of an axoneme illustrates the classical '9+2' structure, comprising nine doublets and two singlets of microtubules. The inner and outer dynein arms facilitate the beating motion of the flagellum by sliding the attached microtubules against the adjacent filaments. The figure was generated by Takeshi Ishikawa at Paul Scherrer Institute (date unknown). **(B)** The molecular mechanism of microtubule polymerisation. The nucleation of the filaments begins with the formation of the γ-tubulin ring complex (γTuRC). While the process of polymerisation occurs at the active site of the γ-tubulin (which becomes the plus end), the other side (the minus end) is capped by the γTuRC proteins, thereby hindering depolymerisation. The elongation of the filament is facilitated by the incorporation of α and β-tubulin heterodimer (αβ-tubulin) subunits. The polymerisation dynamics are contingent upon the state of the nucleotides that are bound to each subunit. Upon incorporation, the subunits are bound to a GTP molecule, which is subsequently hydrolysed to GDP by β-tubulin within the subunit. This results in a conformational destabilisation of the filament, which in turn promotes the dissociation of the subunits from the minus end. The figure was adapted from Nature Education (2014). **(C)** The anatomy of the *Plasmodium* microgamete illustrating an axonemal structure and an associated basal body along with the nucleus. The basal body is a microtubule organisation centre (MTOC) and facilitates flagellum assembly during the microgametogenesis. The figure was adapted from Wilson et al. (2013) and modified. GTP = guanosine-5'-triphosphate, GDP = guanosine-5'-diphosphate.

1.2.3.2 Gliding motility

The term 'gliding motility' refers to a type of cellular movement characterised by minimal alteration in cell shape and the capacity for high-speed migration on a solid surface (Lettermann et al., 2024). Gliding motility represents a distinctive mode of migration observed across the phylum of Apicomplexa, although not exclusive to this group. It is also known that certain bacteria, such as *Myxococcus xanthus*, perform gliding motility, albeit with different molecular machinery (Wartel et al., 2013). The apicomplexan gliding motility is facilitated by a conserved actin-myosin motor complex, collectively known as the glideosome (Opitz and Soldati, 2002) (**Figure 4**). The glideosome is situated in the interspace between the inner membrane complex (IMC) and the plasma membrane. The glideosome-associated proteins GAP40 and GAP50 securely anchor the complex to the IMC, thereby enabling the conduction of mechanical forces (Boucher et al., 2018; Bullen et al., 2009). On the outer IMC membrane, GAP45 is attached across the cellular compartment, where it serves as a protein scaffold (Frénal et al., 2017). The principal traction force of this motor complex is generated by the rearward stroking motion of the myosin heavy chain myosinA (MyoA) and its associated MyoA tail domain-interacting protein (MTIP), reinforced by the essential light chain (ELC) (Douse et al., 2012; Meissner et al., 2002; Pazicky et al., 2020).

The mechanical force is then converted into a locomotive force by the horizontally attached actin filament, which translocates the microneme-derived transmembrane adhesins of the thrombospondin-related anonymous protein (TRAP) family, enabling substrate-dependent gliding on the host cell surface (Kappe et al., 2004). The interaction between the TRAP adhesin and the host cell receptors is regulated by the conformational change of the TRAP protein, which influences the binding affinities of the TRAP adhesive domains (Braumann et al., 2023; Matuschewski et al., 2002). As the parasite continues to glide, the adhesins are eventually cleaved off by specialised proteases and replaced with fresh adhesins, which are secreted apically to bind to the new adhesion sites, thus initiating continuous movement (Baker et al., 2006; Münter et al., 2009). The dynamically elongating and shrinking actin filaments of *Plasmodium* contribute to the rapid turnover of adhesion sites (Schüler et al., 2005a). Conversely, stabilising actin filaments can have a detrimental impact on adhesion dynamics (Münter et al., 2009). It has been proposed that conoid regulates the distribution of glideosome-associated F-actin into the pellicular space (Dos Santos Pacheco et al., 2022). The discovery of a conoid-like structure in *Plasmodium* may indicate the presence of a comparable regulatory mechanism for F-actin (Bertiaux et al., 2021).

All three invasive zoites (sporozoite, merozoite and ookinete) of *Plasmodium* demonstrate helical gliding motility (Kan et al., 2014; Kelvin et al., 2012; Yahata et al., 2021). The

sporozoite is the fastest glider, with a migration speed of 1–2 µm/s (Amino et al., 2006). This is followed by the merozoites and ookinetes, with migration speeds of 0.59 µm/s and 0.1 µm/s, respectively (Kan et al., 2014; Yahata et al., 2021). Given that neutrophils migrate at approximately 0.3 µm/s (Hoang et al., 2013), it can be postulated that both sporozoite and merozoite outspeed the majority of immune cells in the mammalian host. It is beyond doubt that gliding motility represents a key competence of *Plasmodium*.

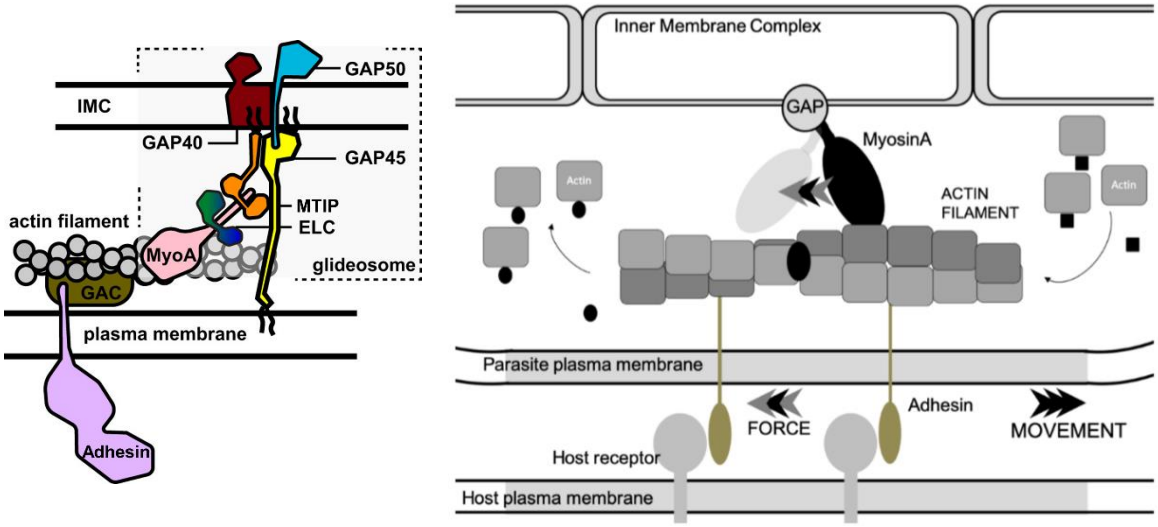

Figure 4: *Plasmodium* glideosome components and gliding mechanism. The glideosome lies between the inner membrane complex (IMC) and the plasma membrane. The complex is anchored to the IMC through the engagement of the GAP50 and GAP40 proteins. GAP45 functions as a scaffold to maintain cellular compartment integrity. The myosin A arm, which consists of MTIP and MyoA, serves as the primary force generator by executing a rearward power stroke, as illustrated in the second figure on the right. The dynamic actin filament serves to conduct the force generated by the myosin to the transmembrane adhesin (TRAP), which is connected to the actin filament via GAC. Upon adhesion of the parasite to the host cell surface receptor via TRAP, a rearward force propels the parasite forward. The dynamic actin filament is essential to facilitate rapid and flexible relocation of the parasite's adhesion sites. Left figure adapted from Pazicky et al. (2020). Right figure provided by Ross Douglas. GAP = glideosome-associated proteins, MyoA = myosin heavy chain myosinA, MTIP = MyoA tail domain-interacting protein, ELC = essential light chain, GAC = glideosome-associated connector, TRAP = thrombospondin-related anonymous protein.

1.3 Actin

Actin is a highly conserved and one of the most abundantly expressed proteins in eukaryotic cells (Bertola et al., 2008; Dominguez and Holmes, 2011; Gunning et al., 2015). Actin plays a vital role in numerous essential cellular processes, including cell motility (Moreau et al., 2020; Svitkina, 2018; Sweeney and Holzbaur, 2018), tissue integrity (Coravos et al., 2017), intracellular transport (Titus, 2018) and cell division (Kita et al., 2019). In general, actin exists in two major states, namely monomeric globular (G)-actin and polymeric filamentous (F)-actin. In many cellular activities, F-actin plays a direct role as part of the actin cytoskeleton (Svitkina, 2018), while monomeric G-actin serves as a building block for F-actin (Pollard, 1984). G-actin is, however, also known to participate in some chromatin-

regulating complexes (Kapoor et al., 2013; Mouilleron et al., 2011; Virtanen and Vartiainen, 2017) as well as in the dynactin complex (Schroer, 2004)

The protein structure of G-actin is traditionally divided into four subdomains (Kabsch et al., 1990) (**Figure 5A**) The right part is constituted by subdomains 1 and 2, while the left part is constituted by subdomains 3 and 4. These two structures are hinged by a helix and a loop. This results in the formation of two major clefts, which are regarded as the target-binding/hydrophobic cleft (between subdomains 1 and 3) and the nucleotide-binding cleft (between subdomains 2 and 4) (Dominguez and Holmes, 2011). Similar nucleotide-binding cleft structures have also been observed in certain ATPase proteins such as hexokinase and heat shock protein 70 (Hsp70) (Flaherty et al., 1991; Hurley, 1996). This specific conformation is referred to as the 'actin fold', which defines the central characteristics of the actin superfamily (Kabsch and Holmes, 1995). The hydrophobic cleft is a common interaction site for the majority of actin-binding proteins (ABPs) and a subset of polymerisation inhibiting toxins (Dominguez, 2007; Klenchin et al., 2003; Lee et al., 2007). The nucleotide-binding cleft binds ATP or ADP in a divalent cation (Ca^{2+}/Mg^{2+})-dependent manner, which also influences the nucleation and dynamics of F-actin by promoting the activity of selected ABPs (Kabsch et al., 1990; Ojala et al., 2002; Pollard, 1984). The DNase I-binding loop (D-loop) (Kabsch et al., 1990), situated in the outer corner of subdomain 2, is responsible for the stable longitudinal inter-subunit linkage in F-actin. Upon polymerisation, it securely docks into the hydrophobic cleft of the actin subunit above, interacting with both subdomains 1 and 3 (Chou and Pollard, 2019; Das et al., 2020; Dominguez, 2019; von der Ecken et al., 2015). While the D-loop has been shown to exist in several structural states during the transition from G to F-actin (Durer et al., 2012), the open conformation is the most favoured during the polymerisation process (Das et al., 2020). The hydrophobic plug (H-plug) between subdomains 3 and 4 (Holmes et al., 1990) also contributes to the stability of the actin filament through lateral contacts with the D-loop and subdomain 3 of the adjacent actin subunit (Dominguez and Holmes, 2011; von der Ecken et al., 2015).

The polymerisation of actin is a dynamic process, whereby G-actins undergo simultaneous association and dissociation to form filaments (Pollard, 2016) (**Figure 5B**). The nucleation of the actin filament is dependent upon the accumulation of G-actin above a critical concentration (Oosawa et al., 1959). The process initiates with the formation of unstable dimers and trimers, which then proceed to form more stable oligomers (Oda et al., 2016). The subsequent elongation of these oligomers is dependent on the concentration and nucleotide state of the available G-actin (Zsolnay et al., 2020). ATP-bound monomers incorporate at a faster rate at the growing 'barbed end' of the filament, whereas ADP-bound

monomers are predominantly found at the dissociating 'pointed end' (Pollard, 2016, 1984). The equilibrium between the net addition and loss of monomers at the barbed end and the pointed end, respectively, is referred to as steady-state 'treadmilling' (Neuhaus et al., 1983; Wegner, 1976). During the polymerisation process, the hydrolysis rate is increased due to a conformational change in monomer subunits (Oosterheert et al., 2023), whereby bound ATP is randomly hydrolysed to ADP through the slow release of the gamma phosphate (P_i) (Pollard, 2016). The ADP-P_i actin subunit is the most stable within the filament, and the dissociation of the phosphate occurs at a significantly faster rate on the pointed end subunits, leaving ADP-actin for rapid depolymerisation (Fujiwara et al., 2007). The dynamic turnover of the actin filament is a critical property for a number of cellular functions (Bugyi and Carlier, 2010; Chhabra and Higgs, 2007). It thus necessitates precise regulatory mechanisms, including a set of dedicated regulator proteins.

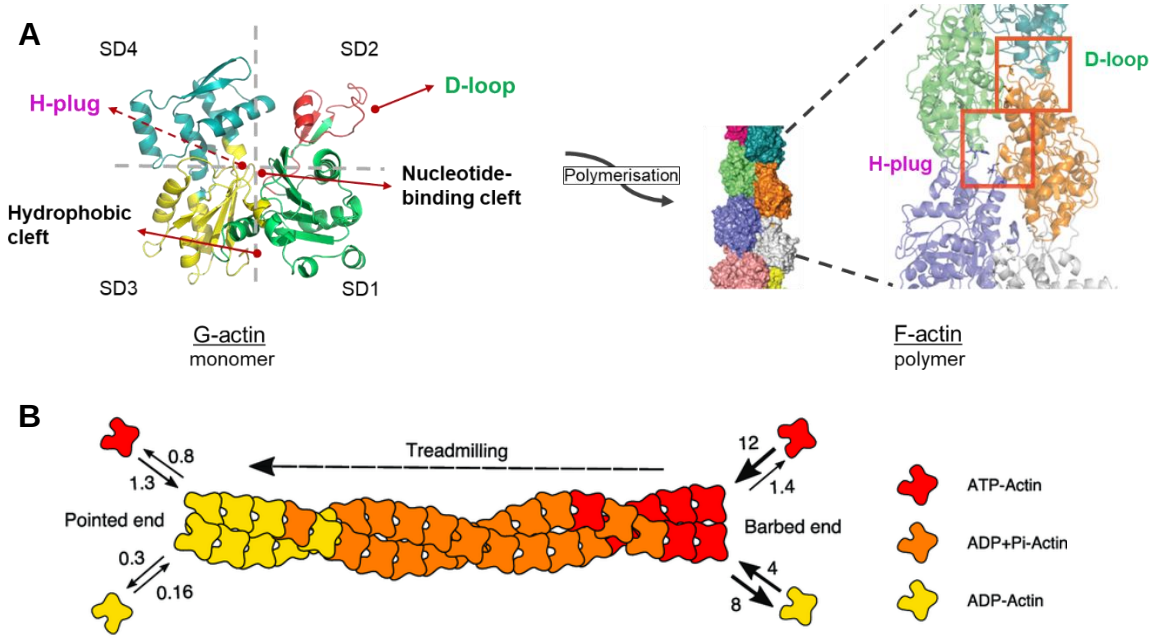

Figure 5: Actin structures and polymerisation process. (A) The protein structure of monomeric actin is typically divided into four subdomains (SDs). The nucleotide-binding cleft, which connects subdomains 1 and 2 and subdomains 3 and 4, represents a common structural feature known as the 'actin-fold'. This is a shared trait among other members of the actin superfamily, including hexokinase and heat shock protein 70. The hydrophobic cleft serves as a principal interaction point for numerous actin-regulating actin-binding proteins (ABPs). Actin exhibits a strong proclivity for polymerisation, wherein the D-loop and H-plug engage in longitudinal and lateral interactions with adjacent actin subunits, respectively, to stabilise the filament. The figure (polymer structure) was adapted from Douglas et al. (2018). **(B)** Actin polymerisation is a dynamic process whereby actin monomers incorporate and dissociate from both ends of the filament. The end of the filament that is actively elongating is referred to as the 'barbed end', whereas the end that is dissociating is known as the 'pointed end'. The equilibrium between the net addition and loss of monomers at the barbed end and the pointed end, respectively, is referred to as steady-state 'treadmilling'. The binding affinity of monomeric actin subunits is contingent upon the state of the bound nucleotide. In general, ATP-bound subunits polymerise at a faster rate than ADP-bound subunits. Within the filament, the bound ATP is hydrolysed into ADP through the release of phosphate (Pi). The intermediate ADP+P_i actin represents the most stable subunit state. The actin monomer association rate constants (μM^{-1} s^{-1}) are shown with the arrow pointing towards the filament, while the opposite arrows show the monomer dissociation rate constants (s^{-1}). The figure was adapted from Hakala (2020), generated based on Pollard et al. (2003). ATP = adenosine triphosphate, ADP = adenosine diphosphate, P_i = inorganic phosphate.

1.3.1 Classical regulators of actin

While actin concentration can influence its own polymerisation dynamics (Oosawa et al., 1959), the general architecture is largely dependent on the binding of regulator proteins, known as ABPs (Pollard, 2016). ABPs bind both monomeric and polymeric actins and regulate every aspect of actin assembly, including nucleation, elongation, filaments reorganisation, and depolymerisation (Dos Remedios et al., 2003).

In the canonical opisthokont system, actin monomer-binders, including thymosin-β4 and profilin, exert a profound influence on the assembly dynamics of monomeric actin. Thymosin-β4 sequesters monomers sterically, thereby preventing their incorporation into filaments at both barbed and pointed ends (Pollard, 2016). In contrast, profilin facilitates monomer incorporation at the barbed end by effectively removing ADP from actin monomers that have dissociated from the filament, enabling them to reload ATP (Mockrin and Korn, 1980; Selden et al., 1999). Additionally, profilin delivers actin monomers to the site of filament elongation (Ferron et al., 2007). It has been shown that thymosin-β4 and profilin exhibit functional competition (Xue et al., 2014).

Formins and enabled/vasodilator-stimulated phosphoprotein (Ena/VASP) family proteins promote actin filament elongation by not only recruiting profilin-bound actin monomers, but also by protecting barbed ends from being blocked by capping proteins (Goode and Eck, 2007; Svitkina et al., 2003; Yang et al., 2007). Capping protein binds to the barbed end of the growing filament, thereby preventing further incorporation of monomers (Edwards et al., 2014). It also regulates the construction of the actin network initiated by the Arp2/3 complex through the capping of daughter filaments (Iwasa and Mullins, 2007). While fascin bundles the actin filaments and adds rigidity (Jaiswal et al., 2013; Vignjevic et al., 2006), the Arp2/3 complex and its nucleation-promoting factors, such as Wiskott–Aldrich syndrome protein (WASP) family proteins, facilitate actin filament branching (Rotty et al., 2013). Coronin promotes the rapid expansion of the actin network by recruiting the Arp2/3 complex at nucleation sites (Gandhi and Goode, 2008). The Arp2/3 complex can also be inhibited by coronin, which in turn promotes filament severing by actin depolymerising factor (ADF)/cofilin at the ADP-rich pointed end (Mikati et al., 2015; Rodal et al., 2005).

Members of the ADF/cofilin family facilitate the disassembly of the actin network by promoting the dissociation of P_i from the bound ADP and severing the filaments (Blanchoin and Pollard, 1999). Furthermore, ADF/cofilin hinders the nucleotide exchange on monomeric actin, yet this process can be competitively compensated by profilin (Blanchoin and Pollard, 1998). Twinfilin, a member of the actin-depolymerising factor homology domain (ADF-H) superfamily, is another polymerisation suppressor with structurally distinct "twin"

ADF homology domains (Hilton et al., 2018). In addition to severing, gelsolin is capable of capping the barbed ends of exposed actin subunits owing to its stretching multi-domain structure (Burtnick et al., 1997; Harris and Weeds, 1984; Nag et al., 2013).

As briefly outlined, an array of ABPs participate in the intricate regulation of actin in the canonical opisthokont system, enabling its pleiotropic cellular functions.

1.3.2 Unusual properties of *Plasmodium* actin

Plasmodium has two distinct actin isoforms, actin1 and actin2, which are highly divergent from canonical opisthokont actins (76-83% protein sequence identity between opisthokont and *Plasmodium* actins) and even from each other (79% protein sequence identity between acitn1 and actin2) (Wesseling et al., 1988). Actin1 is expressed in all life stages of *Plasmodium* and plays a primary role in facilitating gliding motility, invasion and development (Das et al., 2017; Siden-Kiamos et al., 2006). The depletion of *actin1* in blood stage *P. falciparum* is lethal; however, the conditional knock-out approach demonstrated its essential functions ranging from daughter merozoite formation to host erythrocyte deformation (Das et al., 2017). The chemical disruption and mutagenesis of actin1 resulted in an impairment of gliding motility in sporozoites (Douglas et al., 2018; Münter et al., 2009; Yee et al., 2022). In contrast, actin2 is expressed during the sexual stage (gametocytes to zygote), where it is associated with the nucleus and plays a critical role in gametogenesis and oocyst development (Lopez et al., 2023). The depletion of *actin2* in *P. berghei* specifically inhibited the egress of microgametes at exflagellation, while female fertility remained unaffected (Deligianni et al., 2011). Moreover, the replacement of the *actin2* gene with *actin1* was unable to compensate for the function, indicating that these two actin isoforms are functionally distinct (Andreadaki et al., 2014).

Actin2 appears to form a more stable filament than actin1. Given that actin1 with the canonical actin D-loop forms longer filaments, which could compensate for the function of actin2, the stage-specific expression of actin2 might indicate the importance of stable filament structure during microgametogenesis (Vahokoski et al., 2014). A number of studies have indicated that the actin1 filament is dynamic and transient in nature, and plays an indispensable role in facilitating gliding motility (Lu et al., 2019; Münter et al., 2009; Schüler et al., 2005a; Skillman et al., 2011). Both actin1 and actin2 filaments have been observed to reach lengths of over 600 nm (Pražák et al., 2024; Vahokoski et al., 2014). However, they still remain considerably shorter than the canonical actin filaments, which can reach lengths of several microns (Schüler and Matuschewski, 2006; Vahokoski et al., 2014). This

represents a fundamental distinction in the functional requirements of actin in the canonical and *Plasmodium* systems.

1.3.3 Regulators of *Plasmodium* actin

In *Plasmodium*, only a limited set of actin-binding proteins appear to maintain such dynamic filament formation (Das et al., 2021). Profilin in *Plasmodium* is expressed abundantly during the invasive stages and structurally divergent from its canonical orthologues (Kursula et al., 2008). It is involved in the generation of gliding force through the *Plasmodium*-specific actin-binding motifs, although this effect does not necessarily depend on actin binding (Moreau et al., 2017, 2020). The formin family is the sole known actin filament nucleator in *Plasmodium* (Frénal et al., 2020). Two isoforms of formin, formin1 and formin2 have been identified as playing critical roles in parasite invasion and gametocyte development, respectively (Collier et al., 2023). Formin1 has been shown to be associated with moving junctions, while formin2 has been associated with centrin (Baum et al., 2008b; Collier et al., 2023). Coronin, which canonically regulates actin network formation by interacting with Arp2/3 complex and cofilin in opisthokont (Gandhi and Goode, 2008), instead serves to form parallel bundles of actin filaments (Olshina et al., 2015). The bundling activity of coronin may initiate the re-orientation of disordered actin filaments and contribute to the regulation of gliding motility directionality (Bane et al., 2016). The dynamic turnover of actin filaments is dependent on the capacity of ADF/cofilin family proteins to sever filaments (Mehta and Sibley, 2011). It is noteworthy that the *Plasmodium* ADF1 protein lacks the conventional actin filament-binding motif and exhibits a reduced binding affinity for the filament, despite retaining its ability to sever actin filaments (Wong et al., 2011).

In both opisthokonts and *Plasmodium*, ABPs are essential regulators of actin-associated cellular functions. It should be noted, however, that the interaction partners of actin are not limited to ABPs. Additionally, some proteins belonging to the actin superfamily serve as regulators or utilise actin as an integral component of their protein complexes.

1.3.4 Actin-related proteins (Arps)

Actin-related proteins (Arps) are members of the actin superfamily that have been identified based on their sequence similarities to conventional actin (Schroer et al., 1994). To date, 11 conventional Arps have been identified and named in accordance with their homology to actin (Arp1 – Arp10) (Muller et al., 2005) and the order of discovery (Arp11) (Eckley et al., 1999). Notwithstanding the conserved actin-fold core structure, the sequence similarity between conventional actin and the closest Arp (Arp1) is less than 70% (Oma and Harata,

2011; Schroer et al., 1994). Arps are typically larger than conventional actin due to multiple insertions, which appear to alter the major surface structures of subdomains 2, 3 and 4 (Muller et al., 2005; Schafer and Schroer, 1999). Such modifications are necessary to facilitate interactions with protein complex subunits (Eustermann et al., 2018; Knoll et al., 2018; Yao et al., 2015) and may also inhibit classical actin properties, including polymerisation and binding of ABPs (Fenn et al., 2011).

1.3.4.1 Function of classical Arps

In opisthokont systems, Arp1, Arp10 and Arp11 function as cytoplasmic Arps, whereas Arp4-Arp9 are localised to the nucleus (Eckley et al., 1999; Oma and Harata, 2011). Arp2 and Arp3 are both cytoplasmic and nuclear (Yoo et al., 2007). In contrast to actin, the majority of Arps do not appear to form filaments and instead serve a specific function as a subunit of a larger complex (Chen et al., 2024; Eustermann et al., 2018; Goley and Welch, 2006). Arp1 is an exception that has been demonstrated to form a microfilament within the dynactin complex, which serves as a cofactor for the dynein-mediated intracellular vesicle transport (Schafer et al., 1994). In addition, the dynactin complex comprises monomeric Arp11, which is bound at the pointed end of the Arp1 microfilament (Urnavicius et al., 2015). Arp10 is the yeast orthologue of Arp11 and is also associated with the pointed end of Arp1 (Hammesfahr and Kollmar, 2012). Arp2 and Arp3 collectively constitute an actin nucleator complex, known as the Arp2/3 complex. This complex is indispensable for actin filament branching, thus facilitating cell motility, phagocytosis, intracellular trafficking, and numerous other vital cellular processes (Goley and Welch, 2006; Rotty et al., 2013). It has been shown that Arp4 also binds to actin in some histone acetylation complexes, including NuA4 and Tip60 (Chen et al., 2024; Qu et al., 2022). The ATP-dependent chromatin remodeller INO80 contains Arp4, Arp5, Arp8, and actin (Eustermann et al., 2018). In the yeast, an additional set of Arps, Arp7 and Arp9, are involved in the formation of SWI/SNF and RSC, which are ATP-dependent chromatin remodelling complexes (Muller et al., 2005; Oma and Harata, 2011).

1.3.4.2 Arps in Apicomplexa

The apicomplexan parasites including *Plasmodium* and *Toxoplasma* are known to possess orthologues of conventional Arp1, Arp4 and Arp6 (Muller et al., 2005). Additionally, a recent study by Hentzschel et al. (2023) has identified potential orthologues of Arp2 and Arp3 in *P. berghei*. Arp1 in *P. berghei* has been shown to be essential for the survival of asexual stage parasites and is localised around the nucleus in ookinetes (Siden-Kiamos et al., 2010).

The observed localisation pattern may indicate the involvement of this protein in vesicular transport. However, it should be noted that apicomplexans are also missing Arp11 of the dynactin complex (Muller et al., 2005; Siden-Kiamos et al., 2010; Urnavicius et al., 2015). This may signify an unconventional cellular role of *Plasmodium* Arp1, as well as the potential existence of a *Plasmodium*-specific Arp11-like protein. Arp2 and Arp3, which canonically constitute the Arp2/3 complex, were identified through a pull-down assay of the *Plasmodium* orthologue of actin-related protein 2/3 complex subunit 1 (ARPC1) (Hentzschel et al., 2023). They appear to interact with F-actin in the form of a protein complex, and maintain mitosis during microgametogenesis (Hentzschel et al., 2023). The presence of the *Plasmodium* Arp2 orthologue in *Toxoplasma* (Kissinger et al., 2003) may also suggest the existence of a comparable Arp2/3-like complex in this genus. Both Arp4 and Arp6 of *P. falciparum* have been observed to be localised in the nucleus, suggesting the potential involvement of these proteins as subunits of chromatin remodelling complexes. (Liu et al., 2020; Oma and Harata, 2011). Arp4 was specifically identified as a transcription factor that promotes the expression of H2A.Z-dependent euchromatic genes and is also associated with centromere biology, particularly important for the cell proliferation during schizogony (Liu et al., 2020).

To date, only a subset of Arps has been annotated in Apicomplexa (Muller et al., 2005). However, within the family of Arps, there are several additional proteins that remain uncharacterised due to the absence of canonical orthologues (Goodson and Hawse, 2002; Muller et al., 2005).

1.3.5 Actin-like proteins (Alps)

Following the identification of 11 apicomplexan-specific Arps which do not share direct sequence homology with canonical Arps, Gordon and Sibley (2005) proposed the designation 'actin-like proteins' (Alps) for this distinct protein group (**Figure 6**). Some of these Apicomplexa Alps are conserved across the genera (Alp1, Alp2a, Alp3 and Alp5), while some are genus-specific (Alp8 and Alp9 of *Toxoplasma* and Alp2b and Alp5b of *Plasmodium*, for instance) (Gordon and Sibley, 2005; Kissinger et al., 2003). In the case of *Plasmodium* Alps, the amino acid sequence identity to actin1 is between 19 and 34%. Considering actin shares approximately 23% sequence identity with functionally divergent hexokinase and heat-shock proteins of the same actin superfamily, Alps represent a significantly divergent actin-related subgroup. Gordon and Sibley (2005) further highlighted that some Alps may be fulfilling the functions of certain Arps that are absent in Apicomplexa (Muller et al., 2005). For example, orthologues of all the subunits of the dynactin Arp1 rod,

with the exception of Arp11, have been identified in apicomplexans (Gordon and Sibley, 2005). This suggests the existence of a dynactin-like system in this phylum, but with an alternative capping system that replaces the conventional Arp11. Based on the sequence similarity, Alp3 may be considered as a potential orthologue candidate (Gordon and Sibley, 2005). Furthermore, *Plasmodium* Alp5a and Alp5b have been identified as being associated with a selected orthologue of the Arp2/3 complex subunit, potentially replacing Arp2 and Arp3, respectively (Gordon and Sibley, 2005; Hentzschel et al., 2023). In *Toxoplasma*, Alp1 has been demonstrated to be indispensable for the viability of the parasite. Its overexpression resulted in the failure of inner membrane complex formation in daughter cells during cytokinesis (Gordon et al., 2008). Additionally, it was proposed that Alp1 might be part of a larger protein complex (Gordon et al., 2009).

Although the identification of the Alps has opened up a new avenue for apicomplexan actin research, there is still little known about the functions of these distinctive proteins. Some Alps may represent unconventional counterparts of known Arps, while others may introduce highly specialised cellular functions.

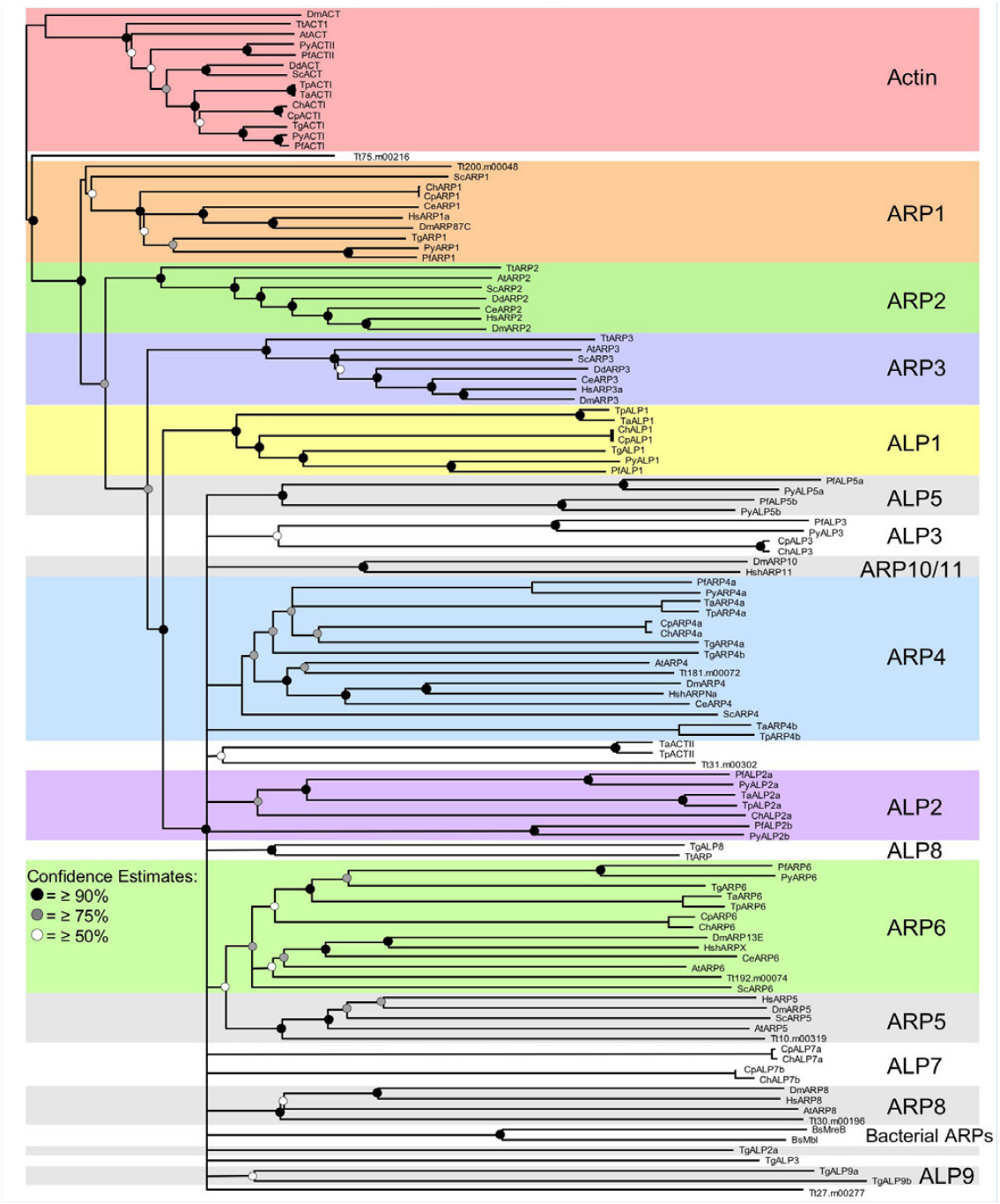

Figure 6: Phylogenetic comparisons of actin and actin-related proteins in apicomplexans and model organisms by Gordon and Sibley (2005). A comparative genomic analysis of undefined actin-related proteins (Arps) identified seven conserved groups of proteins across the Apicomplexa, which were subsequently classified as actin-like proteins (Alps). In total, 11 Alps were identified, including the paralogues of Alp2, Alp5, Alp7 and Alp9. Some Alps are conserved across the genera (Alp1, Alp2a, Alp3 and Alp5), while others are genus-specific (Alp8 and Alp9 of *Toxoplasma* and Alp2b and Alp5b of *Plasmodium*). The phylogenetic tree is constructed according to the 50% majority rule. The figure was adapted from Gordon and Sibley (2005). At = *Arabidopsis thaliana*, Bs = *Bacillus subtilis*, Ce = *Caenorhabditis elegans*, Cp = *Cryptosporidium parvum*, Dd = *Dictyostelium discodium*, Dm = *Drosophila melanogaster*, Hs = *Homo sapiens*, Pf = *Plasmodium falciparum*, Sc = *Saccharomyces cerevisiae*, Tg = *Toxoplasma gondii*, Tp = *Theileria parva*, Tt = *Tetrahymena thermophila*.

1.3.5.1 *Plasmodium* Alp1 and Alp2b

Alp1 is one of the most widely expressed and conserved Alps in Apicomplexa (Gordon and Sibley, 2005). In contrast, Alp2b is exclusive to the genus of *Plasmodium*, while its paralogue Alp2a is shared across other genera (Gordon and Sibley, 2005). Despite being members of the actin superfamily, both Alps exhibit considerably low amino acid (AA) sequence identities to *Plasmodium* actin1 and actin2, with less than 35% for Alp1 and 27% for Alp2b. With respect to Arps, Alp1 shares the highest sequence identity with Arp1 at 35%, whereas Alp2b shares 27% with Arp4. The comparatively low sequence identities to both actins and Arps underline the divergence of Alp1 and Alp2b within the actin superfamily. The conservation of Alp1 with other *Plasmodium* species (*P. berghei* vs. *P. falciparum* and *P. vivax*) is 76-78%, whereas Alp2b exhibits 64% conservation. The interspecies variance may be reflective of species-specific adaptations, suggesting specialized functions of these proteins.

The protein sequence alignments of *P. berghei* Alp1 (378 AA) and Alp2b (556 AA) against actin1 (376 AA) using Clustal Omega revealed the presence of several unique insertions and deletions (InDels) (**Figure 7A, Supplement 1, Supplement 2**). While the InDels in Alp1 are relatively small, those in Alp2b are considerable, particularly in SD2, expanding the respective region almost twice the size of that of actin1. In the predicted protein structures of Alp1 and Alp2b, these unique InDels constitute distinctive structures surrounding the conserved actin-fold core (**Figure 7B**). In Alp1, the loop structure (D-loop) in SD2 is reduced in size as a consequence of the sequence deletion. Similarly, the left-side loop in SD4 displays a shortened alpha helix, while the insertion at the top part results in the addition of an extra loop. A further insertion at the left-hand corner of SD3 introduces an extra helical structure. Strikingly, many of the InDel sites of Alp1 are explicitly exposed to the surface of the protein. It is tempting to hypothesise that these sites serve as interaction points with different proteins and compounds, as well as rendering Alp1 an adaptable subunit of protein complexes that is similar to actin. The structural resemblance to actin may further imply Alp1's capacity to polymerise, with the reduced D-loop structure potentially leading to the formation of non-canonical filaments.

Conversely, the substantial insertions of Alp2b may represent distinctly different properties of this protein from Alp1. The particularly prominent insertions result in a considerable expansion of the D-loop in SD2 and the hook (H-plug) structures at the interface of SD3 and SD4. Given that in actin, both D-loop and H-plug facilitate polymerisation by incorporating into the neighbouring subunits, it seems likely that these enlarged structures are rather obstructive for polymerisation. It can therefore be hypothesised that the potential

function of Alp2b may be divergent from actin, and that it may substitute for missing Arps or play a specialised role in *Plasmodium*.

Thus far, no studies have been published that describe the functions of *Plasmodium* Alp1 and Alp2b. Preliminary studies of *alp1* and *alp2b* in *P. berghei* using PlasmoGem vectors have indicated that these proteins play critical roles during transmission stages to mosquitoes (Binder, 2020; Mikus, 2020). However, the precise cellular functions of Alp1 and Alp2b remain to be elucidated, as do the functional contribution of the distinctive InDel regions. Furthermore, the role of Alp1 in *Plasmodium* appears to differ from that observed in *Toxoplasma* (Gordon et al., 2009, 2008), suggesting that Alps are not only divergent from actin, but may also be involved in genus-specific functions.

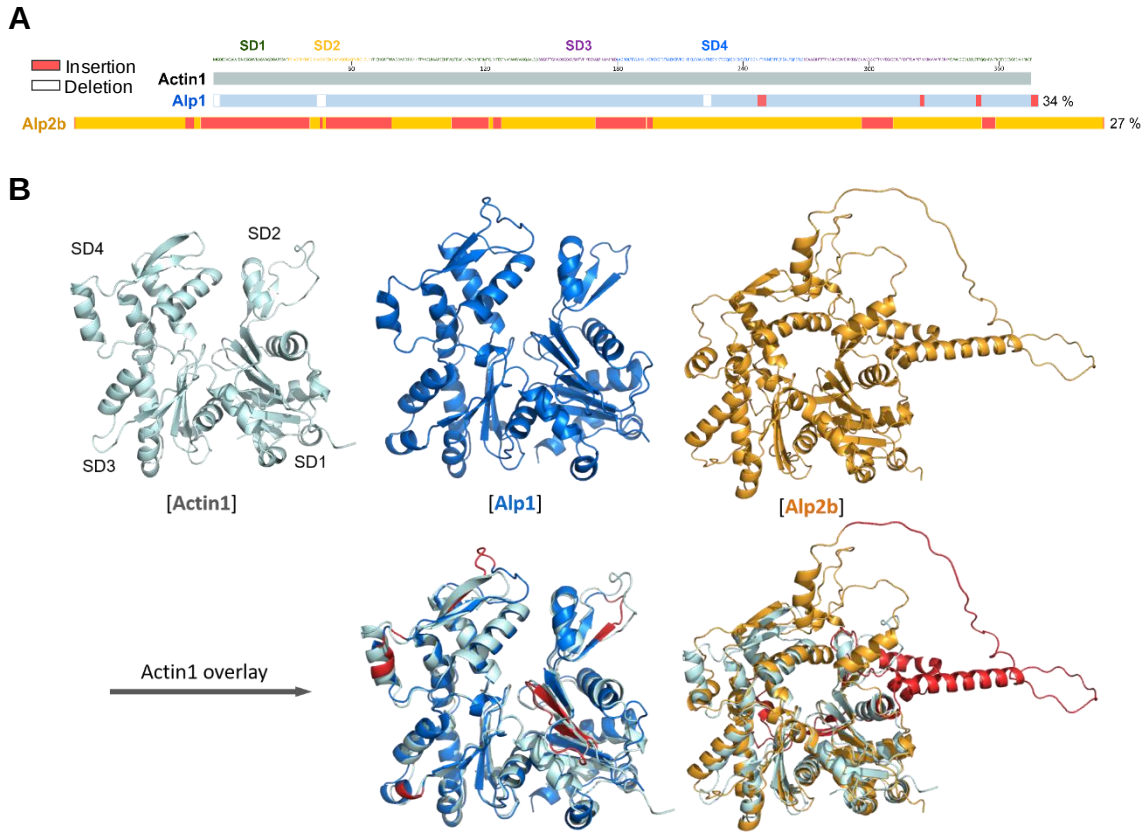

Figure 7: Unique insertions and deletions of Alp1 and Alp2b and predicted protein structures. (A) Insertion and deletion (InDel) scheme of *P. berghei* Alp1 and Alp2b presented relative to actin1. The percentage indicates the degree of amino acid sequence identity to actin1, as determined by the Clustal Omega multiple sequence alignment (EMBL). **(B)** The AlphaFold-predicted structures of *P. berghei* Alp1 and Alp2b are shown in overlay with actin1, illustrating the presence of the conserved actin-fold core, as well as distinct protein structures derived from the unique InDels shown in (A). The InDel regions in Alp1 are relatively smaller and are mainly situated within the outer loops and helices. In contrast, Alp2b has significantly larger insertions, which result in a marked expansion of the D-loop structure in SD2 and the H-plug hook between SD3 and SD4. The red-highlighted regions indicate Alps-unique InDel structures. SD = subdomain.

1.4 Aim of this thesis

The apicomplexan-specific proteins Alp1 and Alp2b play vital roles during the transmission of *Plasmodium* to mosquitoes; yet, their exact cellular functions are still not known. This thesis thus aims to elucidate the functional contribution of Alp1 and Alp2b to the specific transmission stages, as well as to identify the significance of the unique insertion and deletion regions of Alps for their functional properties. Specifically, the investigation addresses the following questions:

1. What are the protein structures and biochemical properties of Alp1 and Alp2b?
2. What are the biological roles of Alp1 and Alp2b in *Plasmodium*?
3. How do the unique InDel regions contribute to the functions of Alp2b?
4. Where are Alp1 and Alp2b localised?
5. In which stages of *Plasmodium* transmission are Alp1 and Alp2b important?

The first question pertains to the production of recombinant Alp1 and Alp2b in *E. coli*. The ultimate objective is to obtain their crystal structures and conduct *in vitro* assays to study various biochemical properties, including polymerisation, ATP-binding and protein interactions. The second and third questions are tackled through a reverse genetic approach, which encompasses gene knock-out, cross-species complementation and targeted mutagenesis. The phenotypic impacts of the gene manipulations are observed using a mouse model and quantitatively analysed in order to elucidate the precise involvement of the target proteins and sequences. The last two questions make use of fluorescence microscopy. This involves the tagging of Alps and the immunostaining of tubulin, as well as the expression of actin chromobody (an actin-specific fluorescent nanobody), which collectively allow the localisation of target proteins and specific cellular processes to be visualised.

Finally, this work uncovers the critical involvement of Alp1 and Alp2b in *Plasmodium* transmission. The detailed characterisation of these unique members of the actin superfamily will not only provide fresh insights into the present *Plasmodium* research, but will also highlight new potential transmission-blocking drug targets to strengthen our ongoing efforts to combat malaria.

2 Materials and methods

2.1 Materials

2.1.1 Organisms and cell lines

Escherichia coli

Strain	Genotype	Source
BL21 (DE3)	F– ompT gal dcm lon hsdSB(rB- mB-) λ(DE3 [lacI lacUV5-T7 gene 1 ind1 sam7 nin5]	Qiagen, Hilden, Germany
C41 (DE3)	F – ompT hsdSB (rB- mB-) gal dcm (DE3)	Sigma-Aldrich, Taufkirchen, Germany
C43 (DE3)	F – ompT hsdSB (rB- mB-) gal dcm (DE3)	Sigma-Aldrich, Taufkirchen, Germany
KRX	F´, traD36, ΔompP, proA+B+, lacIq , Δ(lacZ)M15] ΔompT, endA1, recA1, gyrA96 (Nalr), thi-1, hsdR17 (rK –, mK +), e14– (McrA–), relA1, supE44, Δ(lac-proAB), Δ(rhaBAD)::T7 RNA polymerase	Promega, Mannheim, Germany
LOBSTR	N/A. See Andersen et al. (2013)	Kerafast, MA, USA
DH5-α	F– *endA1 glnV44 thi-1 recA1 relA1 gyrA96 deoR nupG purB20* φ80d*lac Z*ΔM15 Δ(*lacZYA-argF*)U169, hsd R17(*rK–mK*+), λ–	Agilent Technologies, Inc., Santa Clara, CA, USA
XL1-Blue	recA1, endA1, gyrA96, thi-1, hsd-r17,supE44, relA1, lac, [F' pro AB, laclqZ M15, Tn10, (Tetr)]	Stratagene, Amsterdam, Netherland

Plasmodium berghei

Strain/ cell line	Genotype	Source
ANKA	Wild-type	AG Frischknecht, Heidelberg, Germany

Mice

Strain	Genotype/ Sex/ Age	Source
RjOrl:SWISS	Tyrc/Tyrc, Female, >5 weeks	Janvier Labs, Le Genest-Saint-Isle, France

2.1.2 Gene IDs

Gene ID	Organism/ Strain	Annotation
PBANKA_0936900	*Plasmodium berghei*/ ANKA	Actin-like proteins 1 (Alp1)
PF3D7_1110700	*Plasmodium falciparum*/ 3D7	Actin-like proteins 1 (Alp1)
PBANKA_1104800	*Plasmodium berghei*/ ANKA	Actin-like proteins 2b (Alp2b)
PF3D7_0505200	*Plasmodium falciparum*/ 3D7	Actin-like proteins 2b (Alp2b)
PBANKA_1459300	*Plasmodium berghei*/ ANKA	Actin1

2.1.3 Plasmids

Heterologous expression in *E. coli*

Plasmid	Selection marker	Source
pET28a(+)-PbAlp1 (codon optimised)	KanR*	Custom synthesis by BioCat, Heidelberg, Germany
pSUMO-YHRC	KanR	Dr. Isabell Berneburg/ AG Przyborski, Giessen, Germany
pRAREII	ChlR**	Novagen, Darmstadt, Germany
pG-KJE8_dnaK-dnaJ-grpE-groES-groEL	ChlR	Takara Bio Europe, Saint-Germain-en-Laye, France
pGro7_ groES-groEL	ChlR	Takara Bio Europe, Saint-Germain-en-Laye, France
pG-Tf2_ groES-groEL-tig	ChlR	Takara Bio Europe, Saint-Germain-en-Laye, France
pTf16_tig	ChlR	Takara Bio Europe, Saint-Germain-en-Laye, France

P. berghei mutagenesis

Plasmid	Selection marker		Source
	E. coli	***P. berghei***	
Pb238	AmpR***	hDHFR	Douglas et al. (2018)
Pb262	AmpR	hDHFR, yFCU	Dr. Ross Douglas/ AG Frischknecht, Heidelberg, Germany
pJAZZ-OK-PbAlp1 KO	AmpR	hDHFR, yFCU	PlasmoGEM (Gomes et al., 2015)
pJAZZ-OK-PbAlp2b KO	AmpR	hDHFR, yFCU	PlasmoGEM (Gomes et al., 2015)
Pb238_PbAlp1 complementation	AmpR	hDHFR	Binder (2020)
Pb238_Cb-Em	AmpR	hDHFR	Yee et al. (2022)
Pb262_PbAlp2b Actin-H-plug	AmpR	hDHFR, yFCU	Mikus (2020)

*KanR = kanamycin resistance, **ChlR = Chloramphenicol resistance, ***AmpR = ampicillin resistance

2.1.4 Oligonucleotides

The oligonucleotides used in this study were synthesised by Thermo Fisher Scientific (Dreieich, Germany).

Cloning: heterologous expression in *E. coli*

Construct	Primer sequence (5' - 3')	Amplification of
pET28a(+)-PbAlp1-6xHis	GATCCCATGGATGGATAACAACACCATTGTTATCGATAAC	*pbalp1* ORF
	GATCCTCGAGGGTCAGTTTCAGGGTTGC	
pET28a(+)-PbAlp1-5xAla-6xHis	GATCCCATGGATGGATAACAACACCATTGTTATCGATAAC	*pbalp1* ORF + 5xAla linker
	GATCCTCGAGCGCCGCCGCCGCCGCGGTCAGTTTCAGGGTTGC	
pSUMO-YHRC-PbAlp2b	GATCGGATCCGATGGCTCAATACAACGACG	*pbalp2b* ORF
	ATATCTCGAGTTAGCATTTTCTATTTACAATCTC	

Sequencing: heterologous expression in *E. coli*

Region	Primer sequence (5' - 3')
pET28a(+) backbone	ATATAGGCGCCAGCAACC
	ATAGTTCCTCCTTTCAGC
pbalp2b	ATATCTCGAGTTAGCATTTTCTATTTACAATCTC
	GATCGGATCCGATGGCTCAATACAACGACG
	CCATTCTTTTAAAGTAGACG
	GTAGATATGTTTTTAGAGGAG

Cloning: *P. berghei* mutagenesis

Construct	Primer sequence (5' - 3')	Amplification of
Pb262_PbAlp1 full KO	GATCGCGGCCGCTATGTGCAACTTTACCTAAAGG	*pbalp1* 5' UTR
	GATCGATATCTCGTATAAGGTTATGTATGTTTAGTTATTTAATATTATG	
	GCTAGGGCCCTTCAATTTATCTTTCCCGTTTTTTTTTC	*pbalp1* 3' UTR
	ATGCGTTTAAACCGTACACACAAATATATGTGTATAC	
Pb262_PfAlp1 complementation	GATCGAATTCTTCAATTTATCTTTCCCGTTTTTTTTTC	*pbalp1* inner 3' UTR
	CGATGATATCGTGAGAATAATCAAACTAGTGC	
	CAGTGCGGCCGCATGGAGAACAAGACAATAGTAATTGATAAC	*pfalp1* cDNA ORF
	CAGTGAATTCTTAAGTAAGTTTTAGAGATGCCTTTG	
	GCATGCGCGCTATGTGCAACTTTACCTAAAGG	*pbalp1* 5' UTR

	ATATGCGGCCGCTCGTATAAGGTTATGTATGTTTAGTTATTTAATATTATG	
	ATGCGTTTAAACCGTACACACAAATATATGTGTATAC	*pbalp1* outer 3' UTR
	GCATGGCCGGCCTTCAATTTATCTTTCCCGTTTTTTTTC	
Pb262_EGFP-PbAlp1 endogenous tag and Pb262_EGFP-PbAlp1 additional copy	CGATGAATTCGCTGCAGCAGCTATGGATAATAACACAATTGTAATTGAC	*pbalp1* ORF + 3' UTR
	CGATGATATCGTGAGAATAATCAAACTAGTGC	
	ATATGCGGCCGCATGGTGAGCAAGGGCGAG	*egfp* + 4xAla linker
	CAGCGAATTCAGCTGCTG	
	GCATGCGCGCTATGTGCAACTTTACCTAAAGG	*pbalp1* 5' UTR
	ATATGCGGCCGCTCGTATAAGGTTATGTATGTTTAGTTATTTAATATTATG	
	GCATCTCGAGGAGAAAAGTTAGGAGACCAACG	*pbalp1* outer 3' UTR
	GCATGGCCGGCCTTCAATTTATCTTTCCCGTTTTTTTTC	
Pb238_PbAlp1-3xHA additional copy	GCTAAAATTGGAAGTGGAGGATACCCGTACGACGTCCCG	Linker + 3x*ha* tag (Overlapping PCR)
	GCATGGATCCTTAGGCATAATCTGGAACATCGTAAG	
	GCATGCGCGCTATGTGCAACTTTACCTAAAGG	*pbalp1* ORF no stop
	CCTCCACTTCCAATTTTAGCAGTTAGCTTTAGAGTTGCCTATAAAAAAAATATTAAAATAAC	
Pb238_PfAlp2b complementation	CTAGCATATGTATTAAAAAAAGTACAGATTCGTATATATGAATAAATGGATACATACAACGACATATTAAG	*pfalp2b* ORF
	CAGTGGATCCTCAACACTTTCTATTAATAATTTCAAAACCATAC	
Pb238_PbAlp2b D-loop$^{Y52\text{-}K59}$ alanine substitution	GATCCATATGTATTAAAAAAAGTACAGATTCGTATATATG	*pbalp2b* D-loop Ala ORF 1 (Overlapping PCR)
	TGCAGCTGCAGCTGCTGCAGCAGCTACTTCATTTTTTATTTTTTCATCCAAATCTAAAG	
	GCAGCAGCTGCAGCTGCAGATGAATTTTATAAGTTTAATTTAATATATCCCC	*pbalp2b* D-loop Ala ORF 2 (Overlapping PCR)
	GCAGGATCCTTAGCATTTTCTATTTACAATCTCAAAACC	
Pb238_PbAlp2b H-plug$^{N438\text{-}K442}$ actin sequence substitution	GATCCATATGTATTAAAAAAAGTACAGATTCGTATATATG	*pbalp2b* H-plug Act ORF 1 (Overlapping PCR)
	TTTATCTGCTGCTTCTTTTCCATTTAAATGGCTATTTATGGTTGTATC	
	GGAAAAGAAGCAGCAGATAAAACTTTTGAAGGTATTCCTATTAC	*pbalp2b* H-plug Act ORF2 (Overlapping PCR)
	GCAGGATCCTTAGCATTTTCTATTTACAATCTCAAAACC	
Pb262_EGFP-PbAlp2b additional copy	GCATGCGCGCCCAATTATCCCTTAATTTATTCCCC	*pbalp2b* 5' UTR
	AATACATATGGGGAAGGGAAAG	

Sequencing: *P. berghei* mutagenesis

Region	**Primer sequence (5' - 3')**
Chr.12 5' UTR	TTCCCATCTGTTGCTAGTT
Chr.12 3' UTR	GCAACTGCTCCTTTACAG

pbalp1 5' UTR	GTTGCCATATTATGAATGTAC
pbalp1 ORF	TATTGGACATTTGGGGGG
	CCACCATTATGTTCTATATCTC
	CTGAAAATGCCAGATCTGC
	GGCAACTCTAAAGCTAACTTAG
pbalp1 3' UTR	ACCGAAAGTTTACCATAATG
	TCGAATAAAATCCACGAAATC
pfalp1 ORF	GTTCAGATTTCGGTGGAGAAG
pbalp2b 5' UTR	ACAGCCAATTTAAAATGGC
	ACACGCTTTCCCTTCCCCAT
pbalp2b ORF	GAATATAAATGGGGATAGATCAG
	GAATTTGGTTTTGAGATTG
	GTAGATATGTTTTTAGAGGAG
pfalp2b ORF	GAGGACAATGGTGACATTACAA
	ATCATCATGTGTACAATCGGG
	ACACAATATTGTTCTCCATATTATGAAC
	GGAAAGGTGGAAGTATTCTTG
yfcu	CCAACCCTGGAACTAGATAC
	GAGAGGTGTTAAGCCAGAG
	CCTCGTGACCTCTAGTTTG
hDHFR	GTGGAGGTTCCTTGAGTTC
eEF1α	GGGGTGAGCATTTAAAGC
egfp	CACAACATCGAGGACGGC
	GTGAACCGCATCGAGCTG
	GCGGATCTTGAAGTTCAC
Plasmid Pb238/Pb262 backbone	TCCTTCAATTTCGATGGGTAC
	AGCACTAAATCGGAACCC
	GCTGGCCTTTTGCTCACATG

Genotyping: *P. berghei* mutagenesis Alp1

Primer pair no.	**Direction**	**Primer sequence (5' - 3')**
1	Forward	GTTCTAGTGTAACTTGAATTGGAAC
	Reverse	GCTACAATGCATAAAGGATACG
2	Forward	GTTCTAGTGTAACTTGAATTGGAAC
	Reverse	GAGAGGTGTTAAGCCAGAG
3	Forward	GGGGTGAGCATTTAAAGC
	Reverse	GCTACAATGCATAAAGGATACG
4	Forward	TATTGGACATTTGGGGGG
	Reverse	TAATTCAAAGGGACGAGG
5	Forward	TTCTTTGATATGCTTTTTGTTCTTTC
	Reverse	TCCTTCAATTTCGATGGGTAC
6	Forward	TATTGGACATTTGGGGGG
	Reverse	ATCTCTATGACATAAAAGTGG

7	Forward	GTTCTAGTGTAACTTGAATTGGAAC
	Reverse	ACTTATTTGCCTGCACATGC
8	Forward	TATTGGACATTTGGGGGG
	Reverse	CTTCGTCGCCCACATATG
9	Forward	GTTCAGATTTCGGTGGAGAAG
	Reverse	GAGAGGTGTTAAGCCAGAG
10	Forward	GTTCTAGTGTAACTTGAATTGGAAC
	Reverse	GCGGATCTTGAAGTTCAC
11	Forward	CCTCGTGACCTCTAGTTTG
	Reverse	GCGGCTAGCTGCACTAGTGA
12	Forward	GTGAACCGCATCGAGCTG
	Reverse	GAGAGGTGTTAAGCCAGAG
13	Forward	AGGATTGGCGCTTAATCG
	Reverse	CAGGGATACGGTATATATGTTTCG
14	Forward	GAGCATACAAAAATACATGCACAC
	Reverse	CCATTCTTTTAAAGTAGACG
15	Forward	CCTCGTGACCTCTAGTTTG
	Reverse	TGATTTACTTCCATCATTTTGCCC
16	Forward	GAAGACAACCAAGACGATCTTG
	Reverse	GTAGCTCGAGGATGATTTAGAATCTTTATATGCACCTATGC
17	Forward	GAAGACAACCAAGACGATCTTG
	Reverse	GCTCTAGATTTAATTTTTTTTTTAAGTATATGAGTATATATATGTG TGTAAAAATTTATATTAAATATGC
18	Forward	CACAACATCGAGGACGGC
	Reverse	GTAGCTCGAGGATGATTTAGAATCTTTATATGCACCTATGC
19	Forward	ATATGCGGCCGCATGGTGAGCAAGGGCGAG
	Reverse	AGCCCTAGGTTACTTGTACAGCTCGTCC
20	Forward	CGATGTCGACATCGATGGCACGCACTTC
	Reverse	CTTCGTCGCCCACATATG
21	Forward	GAAATATAAATAATTACGCCTAGTTAATAAAGGGCAC
	Reverse	GTAGCTCGAGGATGATTTAGAATCTTTATATGCACCTATGC
22	Forward	TATTGGACATTTGGGGGG
	Reverse	GCATGGATCCTTAGGCATAATCTGGAACATCGTAAG
23	Forward	CCTCGTGACCTCTAGTTTG
	Reverse	GCTACAATGCATAAAGGATACG

Genotyping: *P. berghei* mutagenesis Alp2b

Primer pair no.	**Direction**	**Primer sequence (5' - 3')**
1	Forward	ACCAATAGAAAAGGGCAAGGA
	Reverse	ATAGAGCTTCACTCTGAATTCG
2	Forward	ACCAATAGAAAAGGGCAAGGA
	Reverse	ATCATCATGTGTACAATCGGG

3	Forward	GAAATATAAATAATTACGCCTAGTTAATAAAGGGCAC
	Reverse	ATAGAGCTTCACTCTGAATTCG
4	Forward	ACACAATATTGTTCTCCATATTATGAAC
	Reverse	ATAGAGCTTCACTCTGAATTCG
5	Forward	ACCAATAGAAAAGGGCAAGGA
	Reverse	CCATTCTTTTAAAGTAGACG
6	Forward	CCTCGTGACCTCTAGTTTG
	Reverse	ATAGAGCTTCACTCTGAATTCG
7	Forward	ACACGCTTTCCCTTCCCCAT
	Reverse	GAGAGGTGTTAAGCCAGAG
8	Forward	TCCTAACTATAGTCCGCC
	Reverse	ATAGAGCTTCACTCTGAATTCG
9	Forward	TCCTAACTATAGTCCGCC
	Reverse	ATCTGCTGTATAAGCTGCATTTAAATGGCTATTTATGGTTGTATC
10	Forward	GGGGTGAGCATTTAAAGC
	Reverse	ATAGAGCTTCACTCTGAATTCG
11	Forward	GCAGCAGCTGCAGCTGCAGATGAATTTTATAAGTTTAATTTAATATATCCCC
	Reverse	GCAGGATCCTTAGCATTTTCTATTTACAATCTCAAAACC
12	Forward	TCCTAACTATAGTCCGCC
	Reverse	TGCAGCTGCAGCTGCTGCAGCAGCTACTTCATTTTTTATTTTTTCATCCAAATCTAAAG
13	Forward	ACACGCTTTCCCTTCCCCAT
	Reverse	TTTATCTGCTGCTTCTTTTCCATTTAAATGGCTATTTATGGTTGTATC
14	Forward	AGGATTGGCGCTTAATCG
	Reverse	CAGGGATACGGTATATATGTTTCG
15	Forward	GAGCATACAAAAATACATGCACAC
	Reverse	CCATTCTTTTAAAGTAGACG
16	Forward	CCTCGTGACCTCTAGTTTG
	Reverse	TGATTTACTTCCATCATTTTGCCC
17	Forward	GTGAACCGCATCGAGCTG
	Reverse	GAGAGGTGTTAAGCCAGAG

2.1.5 Chemicals

Chemical	**Supplier**
1,2-Di-(Dimethylamino)-ethan (TEMED)	AppliChem, Darmstadt, Germany
3-{Dimethyl[3-(3α,7α,12α-trihydroxy-5β-cholan-24amido)propyl]azaniumyl} propane-1-sulfonate (CHAPs)	Thermo Fisher Scientific, Dreieich, Germany
5-Fluorocytosine (5FC)	Sigma Aldrich, Steinheim, Germany
Acetic acid ($C_2H_4O_2$)	Roth, Karlsruhe, Germany
Acrylamide 30%	Roth, Karlsruhe, Germany
Agar-agar	Roth, Karlsruhe, Germany

Agarose universal	VWR International, Darmstadt, Germany
Albumin Fraction V (BSA)	Roth, Karlsruhe, Germany
Alsever's solution	Sigma Aldrich, Steinheim, Germany
Ammonium peroxydisulfate (APS)	Roth, Karlsruhe, Germany
ATP-Mg	Sigma Aldrich, Steinheim, Germany
Blueray pre-stained protein marker	Jena Bioscience, Jena, Germany
Bovine serum albumin (BSA)	Roth, Karlsruhe, Germany
Bromophenol blue	Thermo Fisher Scientific, Dreieich, Germany
Cobalt Resin HisPur	Thermo Fisher Scientific, Dreieich, Germany
Coomassie brilliant blue	AppliChem, Darmstadt, Germany
Coumaric acid	Sigma Aldrich, Steinheim, Germany
Cystatin	Sigma Aldrich, Steinheim, Germany
Cytochalasin D	Sigma Aldrich, Steinheim, Germany
Decylmaltoside (DM)	Cube Biotech, Monheim am Rhein, Germany
D-Glucose	Roth, Karlsruhe, Germany
Dimethyl sulfoxide (DMSO)	Thermo Fisher Scientific, Dreieich, Germany
Dipotassium hydrogen phosphate (K_2HPO_4)	Roth, Karlsruhe, Germany
Disodium hydrogen phosphate (Na_2HPO_4)	Roth, Karlsruhe, Germany
Dithiothreitol (DTT)	Roth, Karlsruhe, Germany
DNA-dye NonTox	AppliChem, Darmstadt, Germany
dNTP Mix	Thermo Fisher Scientific, Dreieich, Germany
EDTA	AppliChem, Darmstadt, Germany
Ethanol 70%	Roth, Karlsruhe, Germany
Ethanol 99.9%	Roth, Karlsruhe, Germany
Foetal Bovine Serum (FBS)	Gibco Thermo Fisher Scientific, Dreieich, Germany
Fos-choline-12 (FC12)	Cube Biotech, Monheim am Rhein, Germany
Gas mixture for *P. berghei* (5% CO_2, 5% O_2, and 90% N_2)	Nippon Gases, Oevel, Belgium
Gene Ruler 1 kb plus DNA ladder	Thermo Fisher Scientific, Dreieich, Germany
Gene Ruler 100 bp plus DNA ladder	Thermo Fisher Scientific, Dreieich, Germany
Giemsa dye Hemacolor rapid staining solution 2 and 3	Sigma Aldrich, Steinheim, Germany
Glutardialdehyde 25%	Roth, Karlsruhe, Germany
Glycerol	Sigma Aldrich, Steinheim, Germany
Glycine	Roth, Karlsruhe, Germany
Heparin sodium	Sigma Aldrich, Steinheim, Germany
HEPES	Sigma Aldrich, Steinheim, Germany
Histodenz	Sigma Aldrich, Steinheim, Germany
Hoechst 33342	Thermo Fisher Scientific, Dreieich, Germany
Hydrochloric acid (HCl)	Roth, Karlsruhe, Germany
Hydrogen peroxide (H_2O_2)	Roth, Karlsruhe, Germany
Hypoxanthine	C.C.pro, Oberdorla, Germany
Imidazole	AppliChem, Darmstadt, Germany

Immersion oil 518F	Carl Zeiss AG, Oberkochen, Germany
Isopropanol	Karl-Josef Kost, Koblenz, Germany
Isopropyl-β-D-1-thiogalactopyranoside (IPTG)	Roth, Karlsruhe, Germany
Jasplakinolide	Invitrogen Thermo Fisher Scientific, Dreieich, Germany
Ketamine hydrochloride solution	Serumwerk, Bernburg, Germany
L-(+)-Arabinose	Sigma Aldrich, Steinheim, Germany
Lanolin	Roth, Karlsruhe, Germany
Lauryldimethylamine oxide (LDAO)	Cube Biotech, Monheim am Rhein, Germany
Luminol	Roth, Karlsruhe, Germany
Lysozyme	Sigma Aldrich, Steinheim, Germany
Magnesium chloride ($MgCl_2$)	Sigma Aldrich, Steinheim, Germany
MES	Roth, Karlsruhe, Germany
Methanol	Roth, Karlsruhe, Germany
Milk powder	Roth, Karlsruhe, Germany
NaCl 0.9 % injection solution	B.Braun, Melsungen, Germany
Ni-NTA agarose	Invitrogen Thermo Fisher Scientific, Dreieich, Germany
Ni-TED resin Protino	Macherey-Nagel Thermo Fisher Scientific, Dreieich, Germany
Nycodenz	Progen, Heidelberg, Germany
Octyl-beta-glucoside (OG)	Cube Biotech, Monheim am Rhein, Germany
Paraffin	Roth, Karlsruhe, Germany
Paraformaldehyde	Roth, Karlsruhe, Germany
Pepstatin A	Sigma Aldrich, Steinheim, Germany
Peptone	Roth, Karlsruhe, Germany
Phenylmethylsulfonylfluorid (PMSF)	Sigma Aldrich, Steinheim, Germany
Phosphate buffered saline (PBS) pH7.2	Gibco Thermo Fisher Scientific, Dreieich, Germany
Phosphate buffered saline (PBS) tablet	Sigma Aldrich, Steinheim, Germany
Ponceau S	Roth, Karlsruhe, Germany
Potassium chloride (KCl)	Roth, Karlsruhe, Germany
Potassium phosphate (KH_2PO_4)	Roth, Karlsruhe, Germany
Pyrimethamine	MP Biomedicals LLC, OH, USA
Rhamnose	Becton Dickinson GmbH, Heidelberg, Germany
RPMI-1640 + L-Glutamine – Phenol Red	Gibco Thermo Fisher Scientific, Dreieich, Germany
Saponin	Sigma Aldrich, Steinheim, Germany
Sodium bicarbonate ($NaHCO_3$)	Roth, Karlsruhe, Germany
Sodium chloride (NaCl)	Roth, Karlsruhe, Germany
Sodium dodecyl sulfate (SDS)	AppliChem, Darmstadt, Germany
Sodium dihydrogen phosphate (NaH_2PO_4)	AppliChem, Darmstadt, Germany
Sodium phosphate (Na_2PO_4)	Sigma Aldrich, Steinheim, Germany
Tetracycline	Sigma Aldrich, Steinheim, Germany

Trichloroacetic acid (TCA)	Sigma Aldrich, Steinheim, Germany
TRIS (C_4H11NO_3)	Roth, Karlsruhe, Germany
TRIS-HCl	Roth, Karlsruhe, Germany
Triton-X-100	Roth, Karlsruhe, Germany
Tryptone	Roth, Karlsruhe, Germany
Tween 20	Roth, Karlsruhe, Germany
Unstained protein marker (14.4 - 116 kDa)	Thermo Fisher Scientific, Dreieich, Germany
Vaseline	Roth, Karlsruhe, Germany
Western-Ready ECL Substrate Premium	BioLegend/Biozol, Eching, Germany
Xanthurenic acid	Roth, Karlsruhe, Germany
Xylazine hypochlorite solution	CP-Pharma GmbH, Burgdorf, Germany
Yeast extract	Roth, Karlsruhe, Germany
β-Mercaptoethanol	Sigma Aldrich, Steinheim, Germany

2.1.6 Buffers and solutions

Buffer/solution	**Composition**
5-FC drinking water	1 mg/mL 5-FC in H_2O, kept in the dark
Agarose gel	0.7-1.2% (w/v) Agarose in TAE buffer
Alps solubilisation buffer	50 mM HEPES, 200 mM NaCl, pH 8.0
Ammonium peroxodisulfate (APS)	10% (w/v) APS in ddH_2O
ATP-Mg solution	5 mM ATP-Mg in Alps solubilisation buffer
Chemiluminescence solution	1 mL Luminol, 10 µL Coumaric acid solution, 1 µL 30% H_2O_2 (added before application)
CHES buffer	60 mM MES in ddH_2O, pH9.0
Coomassie staining solution	6 % (w/v) Coomassie Brilliant Blue in 0.3 % HCL (fuming 37%)
Coumaric acid solution	0.11% (w/v) Coumaric acid in DMSO
Freezing solution	10 % Glycerol in Alsever's solution
Heparin solution	10 mg/mL Heparin in PBS
Histodenz stock solution (100 %) 400 mL	5 mM Tris (pH7.5), 3 mM KCl, 0.3 mM EDTA, 110.4g Histodenz, autoclaved, kept in the dark
Histodenz working solution (55 %/ 63 %)	55%/63% (v/v) 100% Histodenz solution in PBS
Ketamine/Xylazine	200 mg/kg (mouse body weight) Ketamine and16 mg/kg (mouse body weight) Xylazine in 0.9 % NaCl injection solution
Luminol solution	1.25 mM Luminol, 0.0093% (v/v) H_2O_2, 0.1 M Tris-HCl, pH 8.6, kept in dark
MES buffer	60 mM MES in ddH_2O, pH5.0
PFA fixing solution	4% (w/v) Paraformaldehyde, 0.05% (v/v) 25% Glutardialdehyde
Pyrimethamine drinking water	70 mg Pyrimethamine (in 10 mL DMSO) in 1 L H_2O (pH3.5 ~ 5.0), kept in dark

Saponine lysis solution	0.03% (w/v) Saponin in PBS
SDS Electrophoresis Buffer	25 mM Tris, 192 mM Glycerol, 0.1% (w/v) SDS, pH8.3
SDS Sample buffer (4x)	250 mM Tris-HCl, pH 6.8, 8% (w/v) SDS, 40% (v/v) Glycerol, 0.03% (w/v) Bromophenol blue, 200 mM DTT
SDS-PAGE separating gel (12%)	5.1 ml ddH_2O, 3.75 ml separating gel buffer, 6 ml Acrylamide (30%), 0.15 ml SDS (10%), 75 µl APS (10%), 7.5 µl TEMED
SDS-PAGE stacking gel (4%)	3.05 ml ddH_2O, 1.25 ml stacking gel buffer, 0.65 ml Acrylamide (30%), 0.05 ml SDS (10%), 25 µl APS (10%), 5 µl TEMED
Separating gel buffer	1.5 M Tris, pH 8.8
Stacking gel buffer	0.5 M Tris, pH 6.8
Stripping buffer	62.5 mM Tris/HCl (pH 6.8), 100 mM β-Mercaptoethanol, 2 % (w/v) SDS
TAE buffer (50x)	2 M Tris, 1 M Acetic acid, 50 mM EDTA (pH 8.0)
Transfer buffer	25 mM Tris, 192 mM Glycine, 10% (v/v) EtOH, pH 8.3
TBS buffer	10 mM Tris, 155 mM NaCl, pH 8.0
TBST buffer	0.05% (v/v) Tween 20 in TBS buffer
US buffer	6.97 mM Sodium phosphate, 43.02 mM Sodium dihydrogen phosphate, Sodium chloride 300 mM, pH8.0
Valap coverslip sealant	Vaseline 10g, Paraffin 10g, Lanolin 10g

2.1.7 Media

Medium	**Composition**
Lysogeny broth medium (LB)	5 g/L Tryptone, 10 g/L yeast extract, 5 g/L NaCl
Lysogeny broth medium (LB) Agar plate	1.5% (w/v) Agar-agar in LB medium
Ookinete medium	250 mL RPMI1640 + HEPES + Glutamine, 12.5 mg Hypoxanthine, 2.5 ml Penicillin/streptomycin (100x), 0.5 g Sodium bicarbonate, 5.12 mg Xanthurenic acid (100 µM), pH7.8, sterile filtered, kept in the dark
Ookinete medium complete	16% (v/v) FBS in ookinete medium
Terrific broth medium (TB)	12 g/L Tryptone, 24 g/L Yeast extract, 9.4 g/L Potassium phosphate, 2.2 g/L Dipotassium hydrogen phosphate, 4 mL/l Glycerol
Transfection medium	60 mL RPMI1640 + HEPES + Glutamine, 15 mL FBS , 22.5 mL Gentamycin (10 mg/mL) Sterile filtered

2.1.8 Antibiotics

Antibiotic	Stock	Working concentration	Supplier
Ampicillin	100 mg/mL in 100% EtOH	100 µg/mL	Sigma Aldrich, Steinheim, Germany
Chloramphenicol	17 mg/mL in 100% EtOH	17 µg/mL	Roth, Karlsruhe, Germany
Gentamycin	7 mg/mL in ddH_2O	7 µg/mL	Gibco Thermo Fisher Scientific, Dreieich, Germany
Kanamycin	50 mg/mL in ddH_2O	50 µg/mL	Sigma Aldrich, Steinheim, Germany

2.1.9 Antibodies

Primary antibodies

Antibody	Supplier
Mouse α- alpha Tubulin	Sigma Aldrich, Steinheim, Germany
Mouse α-GFP	Cell Biolans, Eching, Germany
Mouse α-Histidine	Dianova, Hamburg, Germany
Rabbit α-*P. berghei* Alp1	Custom generation by Eurogentec, Seraing, Belgium
Rabbit α-*P. berghei* Alp2b	Custom generation by Eurogentec, Seraing, Belgium
Rabbit α-*Plasmodium* Aldolase	Thermo Fisher Scientific, Dreieich, Germany
Rat α-Haemagglutinin (HA)	Roche, Basel, Switzerland

Secondary antibodies

Antibody	Supplier
α-Mouse IgG (HRP)	Sigma Aldrich, Steinheim, Germany
α-Mouse IgG Alexa Fluor Readyprobes 594	Invitrogen Thermo Fisher Scientific, Dreieich, Germany
α-Rabbit IgG (HRP)	Dianova, Hamburg, Germany
α-Rat IgG (HRP)	Sigma Aldrich, Steinheim, Germany
α-Rat IgG Alexa Fluor 594	Invitrogen Thermo Fisher Scientific, Dreieich, Germany

2.1.10 Enzymes and buffers

Enzyme and buffer	Supplier
Lysozyme	Sigma Aldrich, Steinheim, Germany
ALLin HiFI DNA polymerase	HighQu, Kraichtal, Germany
ALLin buffer (5x)	HighQu, Kraichtal, Germany
DNaseI	Sigma Aldrich, Steinheim, Germany
Taq polymerase	New England Biolabs, Frankfurt, Germany
Taq Standard buffer (10x)	New England Biolabs, Frankfurt, Germany

T4 DNA ligase	Invitrogen Thermo Fisher Scientific, Dreieich, Germany
T4 DNA ligase buffer (5x)	Invitrogen Thermo Fisher Scientific, Dreieich, Germany
NotI-HF	New England Biolabs, Frankfurt, Germany
EcoRV-HF	New England Biolabs, Frankfurt, Germany
ApaI	New England Biolabs, Frankfurt, Germany
PmeI	New England Biolabs, Frankfurt, Germany
EcoRI-HF	New England Biolabs, Frankfurt, Germany
BssHI	New England Biolabs, Frankfurt, Germany
FseI	New England Biolabs, Frankfurt, Germany
XhoI	New England Biolabs, Frankfurt, Germany
BamHI-HF	New England Biolabs, Frankfurt, Germany
NdeI	New England Biolabs, Frankfurt, Germany
KpnI-HF	New England Biolabs, Frankfurt, Germany
SapI	New England Biolabs, Frankfurt, Germany
SalI-HF	New England Biolabs, Frankfurt, Germany
NcoI-HF	New England Biolabs, Frankfurt, Germany
rCutSmart buffer (10x)	New England Biolabs, Frankfurt, Germany

2.1.11 Kits

Kit	**Supplier**
Amaxa Human T Cell Nucleofector Kit	Lonza, Cologne, Germany
DNeasy Blood & Tissue Kit	Qiagen, Hilden, Germany
FastGene Plasmid Mini Kit	Nippon Genetics Europe, Düren, Germany
peqGOLD Cycle-Pure PCR Clean-up Kit	VWR International, Darmstadt, Germany
peqGOLD Gel Extraction Kit	VWR International, Darmstadt, Germany
QIAprep Spin Miniprep Kit	Qiagen, Hilden, Germany

2.1.12 Equipment

Equipment	**Supplier**
Amaxa Nucleofector 2b	Lonza, Cologne, Germany
Autoclaving machine VX-95	Systec, Linden, Germany
Axio Lab.A1	Carl Zeiss AG, Oberkochen, Germany
Axio Observer Z1	Carl Zeiss AG, Oberkochen, Germany
Axiocam 208 colour	Carl Zeiss AG, Oberkochen, Germany
Axiocam 506	Carl Zeiss AG, Oberkochen, Germany
Axioskop 2 MOT	Carl Zeiss AG, Oberkochen, Germany
Beakers	DWK Life Sciences, Wertheim, Germany
Bunsen burner Fireboy eco	Integra Biosciences, Zizers, Switzerland
Centrifuge Mega Star 1.6R.	VWR International, Darmstadt, Germany
Certomat H 886342/3 incubator shaker	B. Braun, Melsungen, Germany

ChemiDoc imaging system	Bio-Rad, Munich, Germany
Digital heat block	VWR International, Darmstadt, Germany
Dry Block Heater 2	IKA, Staufen, Germany
Duran bottles	DWK Life Sciences, Wertheim, Germany
Electrophoresis chamber Mini PROTEAN Tetra System	BioRad, Munich, Germany
Electrophoresis Power Supply EPS 301	Amersham pharmacia biotech, Little Chalfont, UK
Electrophoresis PowerPac 300 and 1000	Bio-Rad, Munich, Germany
Erlenmeyer flasks	DWK Life Sciences, Wertheim, Germany
Excella E24 incubator shaker	New Brunswick Scientific, NJ, USA
FAS-Digi Gel Documatation System	Nippon Genetics Europe, Düren, Germany
FastGene NanoView	Nippon Genetics Europe, Duren, Germany
FastGene Ultra Cycler Gradient (G-TC01)	Nippon Genetics Europe, Düren, Germany
Hamilton injector	Hamilton Bonaduz AG, Bonaduz, Switzerland
HERAsafe KS	Thermo Fisher Scientific, Dreieich, Germany
Heratherm incubator	Thermo Fisher Scientific, Dreieich, Germany
Incubator shaker KS500	IKA-Werke, Staufen, Germany
Intas ECL ChemoStar	Onzas Science Imaging Instruments GmbH, Göttingen, Germany
KERN Transmitted light microscope OBF 121	Kern & Sohn, Balingen, Germany
Magnetic stirrer RCT basic	IKA, Staufen, Germany
MaxQ 6000 incubating shaker	Thermo Fisher Scientific, Dreieich, Germany
Measuring cylinder	VitaLab GmbH, Pinneberg, Germany
Micro Star 17 centrifuge	VWR International, Darmstadt, Germany
Micro Star 17R centrifuge	VWR International, Darmstadt, Germany
Microcentrifuge 220R	Hettich, Tuttlingen, Germany
Microwave OK. OMW 1213 W	Imtron GmbH, Ingolstadt, Germany
Mini-PROTEAN Tetra Handcast Systems	BioRad, Munich, Germany
Mouse restrainer	G&P Kunststofftechnik GbR, Kassel, Germany
MSC-Advantage sterile bench	Thermo Fisher Scientific, Dreieich, Germany
NeoBlock II	neoLab Migge, Heidelberg, Germany
Neubauer improved counting chamber	Brand GMBH & Co, Wertheim, Germany
New Brunswick Innova 44	Eppendorf, Hamburg, Germany
Owl horizontal electrophoresis systems	Thermo Fisher Scientific, Dreieich, Germany
Panasonic Lumix DMC-GF7 digital camera	Panasonic Corporation, Ōsaka, Japan
pH Meter MU6100L	VWR International, Darmstadt, Germany
Pipette boy	Integra Biosciences, Zizers, Switzerland
Piston pipette (1 µL, 10 µL, 20 µL, 200 µL, 1000 µL)	Gilson, Limburg an der Lahn, Germany
Rocking platform	VWR International, Darmstadt, Germany

Scales ADJ 100-4 and PCB 1000-2	Kern & Sohn, Balingen, Germany
Sorvall RC 6+ (Rotor SS-34, Rotor SLA-300, Rotor F9S-4x1000y)	Thermo Fisher Scientific, Dreieich, Germany
Spectrophotometer U-2001	Hitachi, Schwäbisch Gmünd, Germany
Tabletop spin	Roth, Karlsruhe, Germany
Thermometer	Roth, Karlsruhe, Germany
Trans-Blot SD Semi-Dry Transfer Cell	Bio-Rad, Munich, Germany
Trans-Blot Turbo transfer system	Bio-Rad, Munich, Germany
Ultrasonic wand Sonoplus HD 2070	Bandelin, Berlin, Germany
Water bath	VWR International, Darmstadt, Germany

2.1.13 Consumables

Consumable	**Supplier**
Blotting paper	MAGV, Rabenau, Germany
Amersham Protran nitrocellulose blotting membrane (0.45 µm)	Cytiva Marlborough, MA, USA
BD Microlance 3, 27G injection needle	Becton Dickinson GmbH, Heidelberg, Germany
Cell culture flasks (T75, T175)	Sarstedt AG & Co. KG, Nümbrecht, Germany
Cellstar falcon tubes (15 ml, 50 ml)	Greiner Bio-One, Kremsmünster, Austria
Cellstar serological pipettes	Greiner Bio-One, Kremsmünster, Austria
Cover glass 22×40 mm	VWR International, Darmstadt, Germany
CryoPure Tube 1.6 ml	Sarstedt AG & Co. KG, Nümbrecht, Germany
Cuvettes for OD measurement	Sarstedt AG & Co. KG, Nümbrecht, Germany
Glass Pasteur pipettes	Brand GMBH & Co, Wertheim, Germany
Glass slides Epredia SuperFrost Plus	Thermo Fisher Scientific, Dreieich, Germany
Gloves	Unigloves, Troisdorf, Germany
Inoculation loops	Sarstedt AG & Co. KG, Nümbrecht, Germany
Kimtech Science precision wipes	Kimberly-Clark Professional, Koblenz Rheinhafen, Germany
Parafilm	Th. Geyer, Warsaw, Poland
PCR reaction tubes	Nippon Genetics Europe, Düren, Germany
Petri dish (100 mm)	Greiner Bio-One, Frickenhausen, Germany
Pipette tips	Nerbe plus, Winsen (Luhe), Germany
Plastic syringes	B. Braun, Melsungen, Germany
Reaction tubes (0.5 mL, 1 mL, 2 mL)	Sarstedt, Nürnbrecht, Germany
Stericup filter bottle 0.22 µm	Millipore Sigma Aldrich, Steinheim, Germany
Syringe filter 0.2 µm	Whatman plc, Maidstone, UK

Syringe Micro-Fine + U-100 Insulin (0.5 mL)	Becton Dickinson GmbH, Heidelberg, Germany
Syringe Plastipak (1 mL)	Becton Dickinson GmbH, Heidelberg, Germany
Weighing dishes	BRAND GmbH & Co. KG, Wertheim, Germany

2.1.14 Software and online tools

Software

Software	**Provider**
ChemoStar TS software	Intas Science Imaging Instruments GmbH, Göttingen, Germany
Fiji ImageJ 1.8.0	Schindelin et al. (2012) https://imagej.net/software/fiji/downloads
GraphPad Prism 9.5.1	GraphPad Software, CA, USA
LabScope (for Axioskop 2 MOT)	Carl Zeiss AG, Oberkochen, Germany
PyMOL 4.6. (opensource)	Schrodinger, LLC. 2010. The PyMOL Molecular Graphics System
SnapGene 5.0.8	GSL Biotech, IL, USA
Zeiss ZEN (for Axio Observer Z1)	Carl Zeiss, Oberkochen, Germany

Online tools

Online tool	**Source**
AlphaFold 2	European bioinformatics institute, Hinxton, UK, Google DeepMind https://alphafold.ebi.ac.uk/ Jumper et al. (2021)
BioRender	BioRender Computer-Software, ON, Canada https://www.biorender.com/
ClustalOmega 1.2.4	European bioinformatics institute, Hinxton, UK https://www.ebi.ac.uk/jdispatcher/msa/clustalo
Malaria Cell Atlas	Lawniczak lab, Wellcome Sanger Institute, Hinxton, UK https://www.malariacellatlas.org/ Howick et al. (2019)
Plasmo DB	VEuPathDB Bioinformatics Resource Center https://plasmodb.org/plasmo/app/ Bahl et al. (2003)
PTMGPT2	https://nsclbio.jbnu.ac.kr/tools/ptmgpt2/ Shrestha et al. (2024)
SPOT	https://frischknechtlab.shinyapps.io/SPOT/ Ferr et al. (2022)
VADAR Ver. 1.8	http://redpoll.pharmacy.ualberta.ca/vadar Willard et al. (2003)

2.2 Methods

2.2.1 Molecular biology methods

Polymerase chain reaction (PCR)

Polymerase chain reaction (PCR) is a technique that enables the amplification of a specific DNA sequence. This is achieved by utilising a thermostable polymerase and target-specific oligonucleotides (primers). In this study, all molecular cloning was conducted using the HighQ high-fidelity polymerase (HighQu, Kraichtal, Germany), as detailed below. The standard amplification programme was employed for the majority of the constructs, except for [Pb238_PbAlp1-3xHA additional copy], [Pb238_PbAlp2b D-loop$^{Y52\text{-}K59}$ alanine substitution] and [Pb238_PbAlp2b H-plug $^{N438\text{-}K442}$ actin sequence substitution], which were subjected to the overlapping amplification programme.

Standard programme

PCR reaction mix

Volume [µL]	Reagents
1	Template (~500 ng/µL)
2	Forward primer (10 µM)
2	Reverse primer (10 µM)
10	5x polymerase buffer (includes dNTPs)
0.5	HighQ polymerase (2 U/µL)
34.5	Autoclaved ddH_2O
50	

PCR programme

Temperature/Time	Programme
95°C / 1 min	Initial denaturation
95°C / 15 sec	Denaturation
Tm*°C / 15 sec	Annealing
60°C / 30 sec/kb	Extension
>35x cycles repeat	
60°C / 10 min	Final extension
4°C / infinite	Hold

*Tm = melting temperature of the primer pair used in the reaction

Overlapping amplification programme

This amplification process makes use of two overlapping DNA templates as primers, thereby enabling the seamless connection and amplification of the templates. In the first PCR reaction, the two template DNA fragments (generated prior to this step through the standard PCR) were annealed and amplified. Subsequently, the merged fragment was amplified again using a primer pair flanking the 5' and 3' ends, in order to increase the copy number. The protocol was optimised based on the methodology outlined by Busse (2023).

PCR reaction mixture

Volume [µL]	Reagents
2	Fragment 1 (~100 ng/µL)
2	Fragment 2 (~100 ng/µL)
1 (each)	Primers for 5' and 3' end (10 µM each) *to be added at the end of 1st reaction
10	5x polymerase buffer (includes dNTPs)
0.5	HighQ polymerase (2 U/µL)
33.5	Autoclaved ddH_2O
50	

PCR programme (reaction 1)

Temperature/Time	Programme
95°C / 1 min	Initial denaturation
95°C / 15 sec	Denaturation
65-50°C / 30 sec	Annealing
65°C / 1 min/kb	Extension
10x cycles (-1.5 °C at each cycle)	
65°C / 10 min	Final extension
4°C / infinite	Hold

PCR programme (reaction 2)

Temperature/Time	Programme
Addition of 5' and 3' end primers	
95°C / 1 min	Initial denaturation
95°C / 15 sec	Denaturation
Tm*°C / 30 sec	Annealing
65°C / 1 min/kb	Extension
25x cycles repeat	
65°C / 10 min	Final extension
4°C / infinite	Hold

*Tm = melting temperature of the primer pair used in the reaction

Agarose gel electrophoresis

Agarose gel electrophoresis provides a means of separating DNA fragments on the basis of size, utilising an electric field. The PCR products or isolated DNA samples were combined with the 6x DNA-dye NonTox (AppliChem, Darmstadt, Germany), which enables the visualisation of DNA through exposure to light with a wavelength of 470 nm. The prepared samples were loaded onto a 0.7-1.2% agarose gel alongside the Gene Ruler 1 kb or 100 bp plus DNA ladder (Thermo Fisher Scientific, Dreieich, Germany), according to the target DNA size. The DNA separation was executed at 80-120V for 30-60 minutes in 1x TAE buffer, thereby ensuring clear separation. To confirm the presence of the target DNA fragments, the agarose gel was visualised in the FAS-Digi gel documentation LED chamber (Nippon Genetics Europe, Düren, Germany).

Purification of DNA

The DNA samples that were subjected to downstream processing (e.g. cloning, sequencing, or transfection) were purified using the peqGOLD Cycle-Pure PCR Clean-up kit (VWR International, Darmstadt, Germany) in accordance with the protocol provided by the

respective manufacturer. The DNA that had been isolated from an agarose gel following electrophoresis was purified using the peqGOLD Gel Extraction kit (VWR International, Darmstadt, Germany). In order to reduce the risk of chemical contamination in subsequent experiments, the final elution was conducted using 30-200 µL of nuclease-free water.

Photometric measurements of DNA

The absorbencies at 260 nm and 280 nm serve to quantify the amount of nucleic acid and protein present in the specified sample, respectively. These parameters are important in determining the DNA concentration and purity of the sample, which can play a significant role in the subsequent Sanger sequencing process. The 260/280 absorbency ratio of 1.8 was typically sought as a target for a pure DNA sample. The measurement was conducted using FastGene NanoView spectrophotometer (Nippon Genetics Europe, Duren, Germany), with 2 µL of the DNA sample mounted for analysis.

Restriction digest of vectors and DNA fragments

Restriction enzymes are endonucleases that are capable of making a specific double-stranded DNA cleavage at a defined site. The use of the same or compatible restriction enzymes to treat DNA fragments and cloning vectors allows them to be ligated through the activity of a DNA ligase. All of the restriction enzymes employed in this study were sourced from New England Biolabs (Frankfurt, Germany). The restriction digest reaction was set up as detailed below and incubated at 37-50°C for >4 hours (DNA fragments) and >6 hours (vector plasmids), in accordance with the recommended protocol by the manufacturer. Unless otherwise specified, the restriction enzymes were heat-inactivated at 65-80°C for 10 minutes. Alternatively, the peqGOLD Cycle-Pure PCR Clean-up kit (VWR International, Darmstadt, Germany) was used to remove residual enzymes and chemicals prior to ligation. To confirm the correct linearisation of the treated vector and isolate only the desired cloning backbone, an agarose gel electrophoresis was conducted on the entire sample. Thereafter, the target DNA fragment was excised from the gel and purified using the peqGOLD Gel Extraction Kit (VWR International, Darmstadt, Germany).

Restriction digest reaction mix

Volume [µL]	Reagents
X	DNA (1 µg)
5	10x rCutSmart buffer
1	Restriction enzyme 1 (20 U/µL)
1	Restriction enzyme 2 (20 U/µL)
to 50	Autoclaved ddH_2O

Performed restriction digests for heterologous expression in *E. coli*

Vector/ Construct	Digested fragment	Enzyme
pET28a(+)-PbAlp1-6xHis	*pbalp1* ORF	*Nco*I, *Xho*I
pET28a(+)-PbAlp1-5xAla-6xHis	*pbalp1* ORF + 5xAla linker	*Nco*I, *Xho*I
pSUMO-YHRC-PbAlp2b	*Pbalp2b* ORF	*Xho*I, *Bum*HI

Performed restriction digests for *P. berghei* mutagenesis

Vector/ Construct	Digested fragment	Enzyme
Pb262_PbAlp1 full KO	*pbalp1* 5' UTR	*Not*I, *Eco*RV
	pbalp1 3' UTR	*Apa*I, *Pme*I
Pb262_PfAlp1 complementation	*pbalp1* inner 3' UTR	*Eco*RI, *Eco*RV
	pfalp1 ORF	*Not*I, *Eco*RI
	pbalp1 5' UTR	*Bss*HII, *Not*I
	pbalp1 outer 3' UTR	*Pme*I, *Fse*I
Pb262_EGFP-PbAlp1 endogenous tag	*pbalp1* ORF + 3' UTR	*Eco*RI, *Eco*RV
	egfp + 4xAla linker	*Not*I, *Eco*RI
Pb262_EGFP-PbAlp1 additional copy	*pbalp1* 5' UTR	*Not*I, *Bss*HII
	pbalp1 outer 3' UTR	*Fse*I, *Xho*I
Pb238_PbAlp1-3xHA additional copy	Linker + 3x*ha* tag	*Bam*HI
	pbalp1 ORF no stop	*Bss*HII
Pb238_PfAlp2b complementation	*pfalp2b* ORF	*Nde*I, *Bam*HI
Pb238_PbAlp2b D-loop$^{Y52\text{-}K59}$ alanine substitution	*pbalp2b* D-loop Ala ORF 1	*Nde*I
	pbalp2b D-loop Ala ORF 2	*Bam*HI
Pb238_PbAlp2b H-plug $^{N438\text{-}K442}$ actin sequence substitution	*pbalp2b* H-plug Act ORF 1	*Nde*I
	pbalp2b H-plug Act ORF 2	*Bam*HI
Pb262_EGFP-PbAlp2b additional copy	*pbalp1* 5' UTR	*Bss*HII, *Nde*I

Ligation of DNA fragments

The digested DNA fragment and vector with compatible ends were joined into a single plasmid through the application of T4 DNA ligase (Invitrogen Thermo Fisher Scientific, Dreieich, Germany), which connects the 3’ hydroxyl and 5’ phosphate of each end. The reaction was then incubated for at least 16 hours at 8°C. Prior to ligation, both DNA products were analysed by agarose gel electrophoresis to confirm their correct size and purity. Furthermore, the precise DNA concentration was determined using a spectrophotometer, in order to set an appropriate reaction ratio of 1:4 vector to DNA fragment, which is optimal for ligation.

$$\text{DNA fragment (ng)} = \frac{\text{Vector DNA (ng)} \times \text{DNA fragment (bp)}}{\text{Vector DNA (bp)}} \times 4$$

Ligation reaction mix

Volume [µL]	Reagents
X	Vector (~100 ng)
X	DNA fragment (see the formula)
4	5x T4 ligase buffer
1	T4 ligase (1 U/µL)
to 20	Autoclaved ddH_2O

Isolation of plasmid DNA from *E. coli*

Plasmid DNA was extracted from the *E. coli* cells, which were cultured overnight at 37°C in a shaking incubator at 130 rpm in LB medium supplemented with the appropriate antibiotics. Subsequently, the *E. coli* pellet was harvested via centrifugation for two minutes at 13,000 rpm, and the plasmid was isolated using the FastGene Plasmid Mini kit (Nippon Genetics Europe, Düren, Germany) or the QIAprep Spin Miniprep kit (Qiagen, Hilden, Germany), in accordance with the manufacturers' protocols. The isolated plasmids were finally eluted with 30–50 µL of nuclease-free ddH_2O.

Post-cloning screening of *E. coli*

Once the molecular cloning steps were complete, the transformed *E. coli* cells were screened for the possession of the target plasmid. This was achieved through either a small-scale test digestion of the isolated plasmid DNA or a PCR using a single colony as a template. The test digestion was set up in a 25 µL volume using the corresponding restriction enzymes (New England Biolabs, Frankfurt, Germany) and incubated for at least two hours at 37-50°C, according to the manufacturer's recommended protocol. The colony PCR was conducted by directly adding a trace amount of a single transformed *E. coli* colony into a 10 µL PCR reaction mixture containing a standard Taq polymerase (New England Biolabs, Frankfurt, Germany) and a target gene-specific primer pair. Both the digested and the colony PCR samples were subsequently analysed on an agarose gel electrophoresis. Colony PCR enables rapid, mass screening of *E. coli* colonies, while test digestion verifies the accurate integration of the target DNA fragment into the vector plasmid.

Test digestion reaction mix

Volume [µL]	Reagents
X	Isolated plasmid DNA (~500 ng)
2.5	10x rCutSmart buffer
0.5	Restriction enzyme 1 (20 U/µL)
0.5	Restriction enzyme 2 (20 U/µL)
to 25	Autoclaved ddH_2O

Colony PCR reaction mixture

Volume [µL]	Reagents
0.2	Forward primer (10 µM)
0.2	Reverse primer (10 µM)
1	10x Taq polymerase buffer
0.2	dNTPs (2mM each)
0.05	Taq polymerase (5 U/mL)
8.35	Autoclaved ddH_2O
10	+ single *E. coli* colony

Colony PCR programme

Temperature/Time	Programme
95 °C / 30 sec	Initial denaturation (x1)
95 °C / 30 sec	Denaturation
55 °C / 1 min	Annealing
60 °C / 1 min/kb	Extension
30x cycles repeat	
60 °C / 10 min	Final extension
10 °C / infinite	Hold

DNA sequencing

The nucleotide sequence of the target DNA was determined using the Sanger sequencing service, which is provided by Eurofins Genomics (Konstanz, Germany). The Sanger sequencing method allows the identification of individual nucleotides through the synthesis of the complementary strand of the target template DNA. During the elongation phase, both the normal dNTPs and the fluorescently labelled dideoxynucleoside triphosphates (ddNTPs) are incorporated into the strand. The molecular structure of ddNTP inhibits the formation of a phosphodiester bond, which results in the termination of the elongation process by DNA polymerase. The resulting mixture of the normal dNTPs fragments and the prematurely terminated ddNTPs fragments is subjected to capillary electrophoresis, whereby the fluorescent signals of the ddNTPs are detected in order to identify the original target DNA sequence. The DNA samples were prepared in nuclease-free ddH_2O at a concentration as recommended by the company, and sent together with primers specific to the target sequencing region. The completed sequence data were analysed using the SnapGene software (GSL Biotech, IL, USA).

2.2.2 Microbiology methods

Transformation of chemically competent *E. coli* cells

The introduction of plasmids into *E. coli* was achieved through the heat shock-based transformation, with the objective of selecting the cloned plasmids and expressing the recombinant Alp1 and Alp2b proteins. For the cloning purpose, the DH5-α and XL1-Blue strains of *E. coli* were employed, whereas for the protein expression, the BL21, C41, C43, KRX and LOBSTR strains were used. Prior to transformation, 125 µL of the chemically competent *E. coli* cells were thawed on ice. 1–10 ng of the plasmid DNA (2-4 µL for ligated plasmids) was added to the cells and incubated for 30 minutes on ice. Subsequently, the cells were exposed to a heat shock at 42°C for 90 seconds, immediately followed by a two-

minute incubation on ice. The cells were then supplemented gently with 400 µL of pre-warmed LB medium (37°C, no antibiotics) and incubated for at least an hour at 37°C, 130 rpm to promote cell recovery. Following the recovery period, 100 µL of the cells were plated on an LB agar plate supplemented with the appropriate antibiotics, and incubated overnight at 37°C. The remaining cells were also plated after a pulse centrifugation and the removal of approximately 200 µL of the excess medium. The antibiotics present in the agar plate act as a selection marker, allowing the growth of only those *E. coli* cells that possess the target plasmids.

Codon optimisation of *P. berghei* Alp1 for the expression in *E. coli*

The codon usage of *E. coli* differs significantly from that of *Plasmodium* (Baca and Hol, 2000). In order to optimise the expression of *P. berghei* Alp1 in *E. coli*, the cDNA sequence of *pbalp1* was modified based on the *E. coli* codon bias and synthesised and integrated into the pET28a(+) vector by Biocat (Heidelberg, Germany).

Heterologous overexpression in *E. coli* cells

The *P. berghei* Alp1 and Alp2b proteins were heterologously expressed in *E. coli* using the pET28a(+) and the pSUMO-YHRC vectors, which operate under the T7 RNA polymerase/promoter system. The T7 system is a well-established *E. coli* overexpression system that is based on the transcription machinery of the T7 bacteriophage (Tabor, 1990). The expression of the target protein, placed downstream of the T7 promoter in the vector, is specifically initiated by the highly active T7 RNA polymerase, which is expressed by genetically modified *E. coli* strains, such as DE3 (Tabor, 1990). In the normal state, the T7 RNA polymerase activity is inhibited by the lacI repressor in order to maintain an optimal balance between the growth of the host *E. coli* cells and the overexpression of the target gene. The transcription of the gene can be activated by the addition of an inducer, such as isopropyl β-d-1-thiogalactopyranoside (IPTG), which binds to the lacI repressor, preventing its binding to the inhibitory site (Marbach and Bettenbrock, 2012). In this study, five T7 RNA polymerase-expressing *E. coli* strains (BL21, C41, C43, KRX and LOBSTR) were employed to express recombinant PbAlp1 and Alp2b following the standardised protocol outlined below:

1. Pre-culture

   3 mL of the sterile *E. coli* growth medium (LB or TB), supplemented with kanamycin (50 µg/ml), was inoculated with the target *E. coli* line and incubated in the shaker New Brunswick Innova 44 (Eppendorf, Hamburg, Germany) for five hours at 37°C, 130 rpm.

2. Overnight culture
   The whole pre-culture was added to 250 mL sterile *E. coli* growth medium supplemented with kanamycin (50 µg/ml). The subsequent culture was then Incubated in the shaker overnight at 37°C, 130 rpm.
3. Main culture: setup
   The OD_{600} of the overnight culture was determined using a spectrophotometer U-2001 (Hitachi, Schwäbisch Gmünd, Germany) and added to the 1L main culture (sterile, with 50 µg/ml kanamycin) to set the initial OD_{600} to 0.1. The main culture was then shaken and incubated at 37°C, 130 rpm, until the OD_{600} reached 0.6.
4. Main culture: induction
   Once the OD_{600} reached 0.6, the culture was induced with 0.1-1 mM IPTG to facilitate the expression of the target protein. With the exception of KRX cells, which were induced with 0.1% rhamnose. Subsequently, the main culture was subjected to further shaking and incubation for four hours at 37°C, or for overnight duration at room temperature or at 16°C.
5. Main culture: harvesting
   Following the completion of the full cultivation period, the entire 1 L culture was centrifuged for 15 minutes at 4°C with 8,000 rpm using a Sorvall RC 6+ centrifuge (Thermo Fisher Scientific, Dreieich, Germany) in order to harvest the bacterial pellet. Subsequently, the dry pellet was supplemented with a mixture of protease inhibitors, comprising 150 nM pepstatin, 40 nM cystatin and 100 µM PMSF, and stored at -20°C for subsequent use.

To monitor the expression level of the target protein, 1 mL of culture samples were taken before the induction and after the full cultivation period. The samples were immediately spun down for two minutes at 13,000 rpm, after which the *E. coli* pellet was resuspended with 60 µL 1x SDS sample buffer. This was followed by a 10-minute boiling at 95°C and storage at -20°C.

Co-expression of pRAREII and chaperons in *E. coli*

In order to enhance the expression and solubility of the target protein, the pRAREII (Novagen, Darmstadt, Germany) and the *E. coli*-derived chaperone set (Takara Bio Europe, Saint-Germain-en-Laye, France) plasmids were co-expressed during the expression of PbAlp1 and PbAlp2b in *E. coli*. The co-expressed plasmids were transformed into the host *E. coli* cells concurrently with the PbAlp1/PbAlp2b-expressing plasmid with the specific antibiotics, thereby adjusting the total plasmid DNA amount to 1-10 ng/plasmid. The expression with pRAREII was conducted following the standard expression protocol with 0.1-1 mM IPTG induction. The chaperone set plasmids, in contrast, required specific

inducers, as detailed in the following list. Given that the chaperone activity is essential for the folding of the target protein, the expression of these chaperones was induced at the same time as the main culture was set up. Subsequently, the target protein expression was induced with 0.1-1 mM IPTG at 0.6 OD_{600}.

Takara chaperone set plasmids

Plasmid	Chaperone	Inducer
pG-KJE8	DnaK, DnaJ, GrpE, GroES, GroEL	L-arabinose (0.5 mg/mL) Tetracycline (5 ng/mL)
pGro7	GroES, GroEL	L-arabinose (0.5 mg/mL)
pG-Tf2	GroES, GroEL, Tig	L-arabinose (0.5 mg/mL)
pTf16	Tig	L-arabinose (0.5 mg/mL)

2.2.3 Protein biochemistry methods

Recombinant protein solubilisation

Prior to the purification process, the target proteins were extracted from the *E. coli* pellet via chemical and physical means and solubilised in a buffer with controlled pH and ionic strength. The *E. coli* pellet harvested from a 1 L culture containing recombinant PbAlp1 or PbAlp2b was resuspended in 40-60 mL Alps solubilisation buffer and supplemented with a small amount of DNase I (Sigma Aldrich, Steinheim, Germany) and 16 mg/L lysozyme (Sigma Aldrich, Steinheim, Germany), as well as protease inhibitors (150 nM pepstatin, 40 nM cystatin and 100 µM PMSF). Subsequently, the mixture was vigorously stirred for two hours to overnight at 4°C, and sonicated three times for 30 seconds each with an ultrasonic wand Sonoplus HD 2070 (Bandelin, Berlin, Germany) at 60% maximum power. The resulting cell lysate was then subjected to centrifugation in a Sorvall RC 6+ centrifuge (Thermo Fisher Scientific, Dreieich, Germany) for 30 minutes at 4°C with 18,000 rpm. Upon completion of the solubilisation process, the lysate was separated into a pellet and a supernatant (soluble fraction), and stored at -20°C until the subsequent purification process. In this study, various solubilisation buffer conditions were explored to identify the optimal solubilisation outcome (**Table 1**). The buffers contained varying concentrations of mono- or divalent salts, ranging from 0 to 1000 mM. In some cases, additional components were introduced, such as glycerol (a protein stabiliser), Triton X-100 and Tween 20 (detergents to dissociate protein from the membrane), and DTT (a reducing agent to prevent oxidative damage). The pH range of 5.0 to 9.0 was selected based on the theoretical isoelectric point (pI) of PbAlp1 (= 5.02) and PbAlp2b (= 5.46).

Table 1: List of tested solubilisation buffer conditions. US= Ultrasound/phosphate buffer, HEPES= 4-(2-hydroxyethyl)-1-piperazineethanesulfonic acid buffer, Tris-HCl= tris(hydroxymethyl)aminomethane-hydrogen chloride buffer, MES= 2-(N-morpholino)ethanesulfonic acid, CHES= N-cyclohexyl-2-aminoethanesulfonic acid, DTT= dithiothreitol.

Buffer	Volume (mL/1L pellet)	Concentration (mM)	pH	Salt (mM)	Glycerol (%)	Triton X-100 (%)	Tween 20 (%)	DTT (mM)
US	50	50	8.0	300/NaCl	–	–		–
HEPES	40 - 60	50	5.0	500/$MgCl_2$	20	2	–	5
			7.5	—	—	—	—	—
			8.0	200/NaCl	10	—	—	—
						1		
						—	1	
						1	1	
					20	2	–	5
				300/NaCl	–	2	–	–
								5
						–		–
					10	–		–
								5
				300/KCl	20	2		5
				600/NaCl				
				1000/NaCl				
				1000/KCl	30	3		10
Tris-HCl	60	50	8.0	300/NaCl	–	2	–	5
								–
						–		5
								–
					10	2		5
								–
						–		5
								–
				1000/NaCl	20	2		5
					30	3		10
			9.0	500/$MgCl_2$	20	2		5
MES	60	50	5.0	300/NaCl	20	2	–	5
				500/$MgCl_2$				
CHES	60	50	9.0	300/NaCl	20	2	–	5
				500/$MgCl_2$				

Solubilisation with detergent

In the context of protein solubilisation, detergents refer to amphiphilic agents that increase the solubility of the target protein by incorporating it into a hydrophilic micelle (Ratkeviciute et al., 2021). The formation of micelles occurs when the concentration of the detergent exceeds a specific critical micelle concentration (CMC). The extent of the interaction between the detergent and the target protein is dependent upon the ionic properties of the head group. Ionic detergents are characterised by a head with either cationic or anionic properties, whereas non-ionic detergents lack any charge. Zwitterionic detergents exhibit both ionic and non-ionic properties, which enables disruption of protein-protein interactions, thereby enhancing protein solubilisation efficacy (Soulié et al., 2023). In this study, 3-{Dimethyl [3-(3α,7α,12α-trihydroxy-5β-cholan-24-amido) propyl] azaniumyl} propane-1-sulfonate (CHAPs), Decylmaltoside (DM), Fos-choline-12 (FC12), Lauryldimethylamine oxide (LDAO) and Octyl-beta-glucoside (OG) (Cube Biotech, Monheim am Rhein, Germany) were tested. Each detergent was added to the solubilisation buffer at the specified concentration and stirred for 20 minutes to overnight at 4°C. Subsequently, the

resulting lysate was sonicated, centrifuged and stored in accordance with the standard protocol.

Detergent	CMC in H_20 (mM)	Type	Concentration (mM)
CHAPs	8	Zwitterionic	33
DM	1.6	Non-ionic	20
FC12	1.5	Zwitterionic	5-32
LDAO	2	Zwitterionic	30
OG	20	Non-ionic	50

Immobilised metal affinity chromatography (IMAC)

IMAC is an affinity tag-based protein purification process. In this study, recombinant PbAlp1 and PbAlp2b were N- or C-terminally tagged with a 6x histidine (HHHHHH) sequence, which binds to the metal ions immobilised to the resin matrix in the purification column. Following the removal of non-specific proteins and molecules through washing steps, the bound PbAlp1 or PbAlp2b in the purification column was eluted with imidazole solutions of increasing concentration. Given the higher binding affinity of imidazole to the metal ions, the histidine-tagged PbAlp1 and PbAlp2b were released from the purification column. Precisely, the soluble fraction (supernatant) of PbAlp1 or PbAlp2b was introduced to a glass purification column containing a layer of 1-2 mL Ni-NTA (Invitrogen Thermo Fisher Scientific, Dreieich, Germany), Ni-TED (Macherey-Nagel Thermo Fisher Scientific, Dreieich, Germany) or Co-CMA (Thermo Fisher Scientific, Dreieich, Germany) resin to allow binding of the protein to the metal ions, while slowly running down the column (flow-through fraction). As an optional step, the protein-bound column was incubated with 4 mL of 5 mM Mg-ATP solution for 40 minutes to stimulate the release of molecular chaperones. Subsequently, the column was washed with 10 mL Alps solubilisation buffer containing 10 mM imidazole by similarly dripping the solution through (wash fraction). Finally, the target protein was eluted by slowly dripping 1 mL each of 20 mM, 50 mM, 100 mM, 200 mM, 300 mM and 500 mM imidazole solution in that order.

Sodium dodecyl-sulfate polyacrylamide gel electrophoresis (SDS-PAGE)

SDS-PAGE is a gel electrophoresis-based method that is used to separate proteins based on their molecular weights (kDa). The polyacrylamide gels were manually cast using the Mini-PROTEAN Tetra Handcast Systems (BioRad, Munich, Germany) with the layers comprising 4% stacking gel and 12% separating gel. The target samples were mixed with 1x SDS sample buffer containing dithiothreitol (DTT) and boiled for 10 minutes at 95°C to denature the protein. The samples obtained from the preceding protein solubilisation and IMAC purification were prepared as follows:

Protein sample and amount		Sample buffer (µL)
Solubilisation: pellet	A pipet-tip amount of pellet	60
Solubilisation: supernatant	20 µL	30
IMAC: flow through	20 µL	30
IMAC: wash	20 µL	30
IMAC: eluants 20-500 mM	20 µL	30

10 µL of each sample was loaded onto the SDS gel alongside 8 µL of protein marker (Thermo Fisher Scientific, Dreieich, Germany) and subjected to electrophoresis in a Mini PROTEAN Tetra System electrophoresis chamber (BioRad, Munich, Germany) using 1x SDS electrophoresis buffer at 200 V for 30-40 minutes. The subsequent polyacrylamide gel was washed twice with H_2O and stained with Coomassie brilliant blue staining solution for 10 minutes, followed by further washing with H_2O to remove any residual staining. At each step, the gel was heated in a microwave for 40 seconds at 700 W, in order to enhance the staining efficiency.

Western blot

The western blot technique enables the detection of specific proteins based on the binding of an antibody conjugated with horseradish peroxidase (HRP) (chemiluminescence). To identify the recombinant PbAlp1 and PbAlp2b in the solubilised and IMAC-purified fractions, a western blot was conducted using an antibody directed against the 6x histidine-tag sequence. After the SDS-PAGE of the samples, the unstained gel was soaked in the transfer buffer, along with blotting paper and an Amersham nitrocellulose blotting membrane (Cytiva Marlborough, MA, USA) for at least 10 minutes to equilibrate. Subsequently, the SDS gel, membrane and paper were layered onto a cathode graphite tray without air bubbles and set into the Trans-Blot Turbo transfer machine (Bio-Rad, Munich, Germany) for 30 minutes at 13 V, thereby allowing the migration of the sample proteins from the gel to the nitrocellulose membrane. To ascertain the efficacy of the protein transfer, the membrane was briefly stained with Ponceau S stain (Roth, Karlsruhe, Germany). The stain was then removed by washing with a 1% acetic acid solution, followed by three washes (10 minutes each) with TBST. Once the complete removal of the Ponceau stain had been confirmed, the membrane was soaked in a 5% milk powder-TBST solution for one hour at room temperature (RT) in order to block non-specific proteins from cross-reacting with the antibody. Subsequently, the membrane was washed three times with TBST and incubated with the first antibody solution, comprising 1:1000 mouse α-histidine antibody (Dianova, Hamburg, Germany) in 3% BSA in TBST, for one hour at RT on a rocking platform (VWR International, Darmstadt, Germany). Following the removal of the primary antibody through the three-time wash step, the secondary antibody solution,

comprising 1:10,000 α-Mouse IgG (HRP) antibody (Sigma Aldrich, Steinheim, Germany) in 5% milk in TBST, was applied to the membrane and incubated for one hour at RT. Ultimately, the membrane was washed three times with TBST and covered with the chemiluminescence solution shortly before imaging with the Intas ECL ChemoStar (Onzas Science Imaging Instruments GmbH, Göttingen, Germany).

2.2.4 Parasitology methods

Overview of genetic modification strategies

The *P. berghei* knock-out (KO), complementation and mutant lines presented in this study were generated through the introduction or replacement of the gene of interest (GOI) via homologous recombination of the 5' and 3' untranslated region (UTR) homology arms (**Figure 8**). The KO construct was designed to replace the GOI with the drug selection cassette, which carries the human dihydrofolate reductase (*hDHFR*) and the yeast cytosine deaminase-uracil phosphoribosyl transferase (*yfcu*) genes under the control of the eukaryotic translation elongation factor 1 alpha (eEF1α) promoter and the 3' UTR of the *P. berghei* dihydrofolate reductase (*pbdhfr*) gene. The second 3' *pbdhfr*, located at the 3' end of the selection cassette, serves as the recombination site during the negative selection process. The *hDHFR* gene confers resistance to the anti-folate drug pyrimethamine in *P. berghei* and serves as a positive selection marker (de Koning-Ward et al., 2000). In contrast, the *yfcu* gene confers sensitivity to the prodrug 5-fluorocytosine (5FC) by converting it into the active 5-fluorouracil (5FU) (Braks et al., 2006). Consequently, parasites that have the *yfcu* gene will be negatively selected. The removal of the selection cassette through negative selection allows the generation of a marker-free mutant parasite line, which can then be further transfected by reusing the same selection cassette.

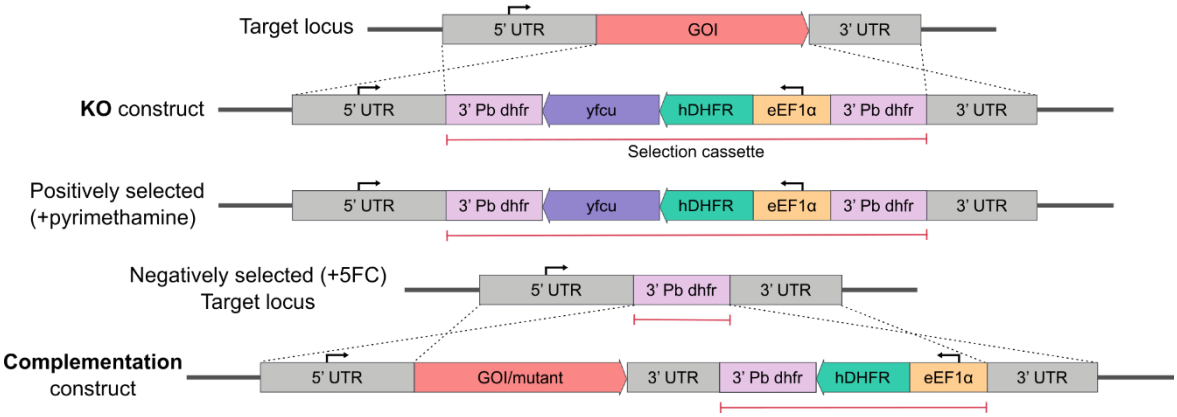

Figure 8: Overview of the genetic modification strategies employed in this study. The gene of interest (GOI) was replaced or introduced via homologous recombination of the 5' and 3' end homology regions. To perform a KO, the target gene was replaced with a selection cassette, which carries *hDHFR* and *yfcu* under the control of the eEF1α promoter and 3' *pbdhfr*. *hDHFR* conveys resistance to the pyrimethamine and serves as a positive selection marker, whereas *yfcu* increases the sensitivity of the parasite to 5FC, thus negatively selecting the parasites lacking the selection cassette. The marker-free mutant parasite line permits the reuse of the same selection cassette in subsequent transfection. UTR (untranslated region); GOI (gene of interest); 3' Pb *dhfr* (3' untranslated region of *P. berghei* dihydrofolate reductase); *hDHFR* (human dihydrofolate reductase); *yfcu* (yeast cytosine deaminase-uracil phosphoribosyl transferase); eEF1α (eukaryotic translation elongation factor 1 alpha); 5FC (5-fluorocytosine).

Transfection of *P. berghei*

DNA construct preparation

The target DNA construct was linearised and ethanol precipitated prior to transfection. The *E. coli* cells carrying the construct plasmid were cultured in 6 mL LB medium with ampicillin (100 µg/ml) overnight at 37°C at 130 rpm in a MaxQ 6000 incubating shaker (Thermo Fisher Scientific, Dreieich, Germany). The plasmids were isolated using the QIAprep Spin Miniprep kit (Qiagen, Hilden, Germany) and eluted with 50 µL of nuclease-free ddH_2O. The plasmid was subsequently digested with specific restriction enzymes for at least six hours, thus obtaining a linearised construct. A 3 µL sample of the post-digestion product was run on an agarose gel in order to confirm the quality of the product. The entire construct DNA was then precipitated with ethanol according to the following procedure: 0.1 volume of 3 M sodium acetate (pH 5.3) and 2.5 volume of 100% ethanol were added and incubated on ice for one hour, followed by a 10-minute centrifugation at 4°C, 13,500 rpm. After carefully removing the supernatant, the pellet was resuspended in 1 mL of 70% ethanol and centrifuged for 10 minutes at 4°C, 13,500 rpm. Once more, the supernatant was removed and the DNA pellet was allowed to air-dry under sterile conditions until it appeared transparent. Once no residual ethanol was apparent, the DNA was resuspended in 30 µL of nuclease-free ddH_20.

DNA construct digestion

Volume [µL]	Reagents
50	Isolated plasmid DNA
20	10x rCutSmart buffer
1.5	Restriction enzyme 1 (20 U/µL)
1.5	Restriction enzyme 2 (20 U/µL)
127	Autoclaved ddH_2O
200	

Used restriction enzymes for each transfection construct

Construct	**Enzyme**
Pb262_PbAlp1 full KO	*Not*I, *Pme*I
Pb262_PfAlp1 complementation	*Bss*HII, *Pme*I
Pb262_EGFP-PbAlp1 endogenous tag	*Bss*HII, *Pme*I
Pb262_EGFP-PbAlp1 additional copy	*Sap*I, *Sal*I
Pb238_PbAlp1-3xHA additional copy	*Sap*I, *Sal*I
Pb238_PfAlp2b complementation	*BssH*II, *Pme*I
Pb238_PbAlp2b D-loop$^{Y52\text{-}K59}$ alanine substitution	*BssH*II, *Kpn*I
Pb262_PbAlp2b Actin-H-plug	*BssH*II, *Pme*I
Pb238_PbAlp2b H-plug $^{N438\text{-}K442}$ actin sequence substitution	*BssH*II, *Kpn*I
Pb262_EGFP-PbAlp2b additional copy	*Sap*I, *Sal*I

Schizont culture and purification

The transfection of the DNA construct was performed exclusively on blood stage schizonts of *P. berghei*, as previously described (Janse et al., 2006), to achieve maximum transfection efficiency. In order to set up a schizont culture, a naïve Swiss mouse was infected with a background *P. berghei* line via intraperitoneal (IP) injection of a cryo-preserved stabilate. From the fourth day post-infection, the parasitaemia was counted on a daily basis. When it reached approximately 2%, the blood was drawn into a heparin-primed syringe via cardiac puncture. The blood was immediately transferred into 10 mL transfection medium (37°C), supplemented with 0.1 mg heparin. Subsequently, the mixture was centrifuged for eight minutes at RT, 1,000 rpm, after which the pellet containing the parasites was gently resuspended with 10 mL of fresh transfection medium (37°C). The entire volume was then carefully (drop by drop) added to a T175 flask with a vent cap (Sarstedt AG & Co. KG, Nümbrecht, Germany), which had been filled with 20 mL of transfection medium and pre-warmed at 37°C. The remaining pellet was resuspended with an additional 8 mL of transfection medium and added to the same flask, thus setting up a culture with a total volume of approximately 38 mL. The culture flask was placed in a gas chamber filled with a mixture of 5% CO_2, 5% O_2, and 90% N_2 (Nippon Gases, Oevel, Belgium) and incubated

for 18–20 hours at 37°C in a Heratherm incubator (Thermo Fisher Scientific, Dreieich, Germany).

Prior to the purification of schizonts, 1 mL of the culture was centrifuged for two minutes at RT, 7,000 rpm. Thereafter, the pellet was examined via histological staining with Giemsa dye Hemacolor rapid staining (Sigma Aldrich, Steinheim, Germany) to assess the developmental state of the schizonts. Once the sufficient number of schizonts had been confirmed, 35 mL of the culture was transferred into a 50 mL falcon tube and underlaid with 10 mL of a pre-warmed (37°C) 55% Histodenz solution (Sigma Aldrich, Steinheim, Germany), using a glass Pasteur pipette. The Falcon tube was then carefully placed in a Mega Star 1.6R centrifuge (VWR International, Darmstadt, Germany) and spun for 25 minutes at RT, 1,000 rpm without brake. Subsequent to the separation of schizonts through density gradients, the target layer (containing schizonts) was extracted using a Pasteur pipette and placed into a 15 mL Falcon tube. The isolated schizonts were then centrifuged for 10 minutes at RT, 1,000 rpm with brake, and resuspended in 1 mL of transfection medium (RT) for the subsequent transfection.

Transfection via electroporation

For the transfection using the Amaxa Nucleofector 2b (Lonza, Cologne, Germany), the previously purified DNA construct (35 µL) was mixed with 100 µL of nucleofector solution from the Amaxa Human T Cell Nucleofector kit (Lonza, Cologne, Germany). Meanwhile, the collected schizonts were pelleted by centrifugation at 13,000 rpm for 15 seconds at RT, after which they were resuspended in the DNA-nucleofector solution. Subsequently, the entire mixture was carefully transferred into a cuvette without creating any air bubbles and electroporated using the U33 programme. Immediately following the completion, the schizonts were supplemented with 50 µL of transfection medium and intravenously (IV) injected into a recipient naïve Swiss mouse with a Micro-Fine + U-100 Insulin syringe (Becton Dickinson GmbH, Heidelberg, Germany). Upon IV injection, the mouse was placed in a restrainer (G&P Kunststofftechnik GbR, Kassel, Germany) and its tail was pre-warmed with warm water (≤37°C) to optimise the injection process.

Approximately 24 hours post-infection, the mouse was administered pyrimethamine-supplemented drinking water (70 µg/mL) for positive drug selection. The parasitaemia was quantified from the seventh day post-infection until it reached approximately 2%. At this point, the mouse blood was harvested for genotyping and cryo-preserved stabilate generation. Cryo-preservation was achieved by mixing 100 µL of fresh blood with 200 µL of freezing solution in a screw cap cryo-tube (Sarstedt AG & Co. KG, Nümbrecht, Germany). The sample was then stored in liquid nitrogen for further use.

Parasitaemia determination

The parasitaemia of *P. berghei*-infected mice was determined by quantifying the infected erythrocytes under a light microscope. A drop of tail blood from the infected mouse was collected and smeared onto a glass slide. The smear was then fixed with 100% methanol for five seconds and subsequently stained in Giemsa dye Hemacolor rapid staining (Sigma Aldrich, Steinheim, Germany) solution 2 for three seconds and in solution 3 for two minutes, with a washing step with tap water in between and at the end. Once the stained slide had been thoroughly dried, the parasitaemia was quantified under a KERN OBF 121 transmitted light microscope (Kern & Sohn, Balingen, Germany) with 100x magnification. Firstly, the total number of erythrocytes per microscopy field was counted and documented. Subsequently, the number of infected erythrocytes in a field with a comparable erythrocyte density was quantified, and this was repeated for 20-50 fields. Finally, the parasitaemia was calculated using the following formula:

$$\text{Parasitaemia (\%)} = \frac{\text{Erythrocyte}_{\text{infected}} \times 100}{\text{Erythrocyte}_{\text{total}} \times \text{number of counted fields}}$$

Cardiac puncture

In order to obtain a blood sample from an infected mouse, anaesthesia was induced via IP injection with a narcotic agent containing 200 mg/kg ketamine and 16 mg/kg xylazine. Subsequently, the blood was extracted via direct puncture of the heart with a heparin-primed BD 27G injection needle and 1 mL syringe (Becton Dickinson GmbH, Heidelberg, Germany). At the end of the procedure, the mouse was euthanised via cervical dislocation.

Genomic DNA extraction and genotyping PCR

Genotyping was performed to examine the correct integration of the target gene into the parasite locus following a transfection and a limiting dilution. Once parasitaemia exceeded 2%, infected blood was harvested from the mouse via cardiac puncture and lysed in 13 mL of 0.03% saponin lysis solution, thereby releasing the blood-stage parasite from the erythrocytes. Subsequently, the blood sample was centrifuged for eight minutes at RT, 2,800 rpm, and the pellet was resuspended in 1 mL PBS in a fresh tube. Following a two-minute centrifugation at RT, 7,000 rpm, the final parasite pellet was resuspended in 200 µL PBS. This suspension was then either stored at -20°C for future use or directly subjected to genomic DNA extraction with the DNeasy Blood & Tissue Kit (Qiagen, Hilden, Germany). The extracted genomic DNA was finally eluted with 200 µL of nuclease-free ddH2O. For the genotyping PCR, specific primer pairs targeting the following regions were employed: 1) the whole integration locus (including the upstream and downstream genomic regions of

the integration sites), 2) the 5' integration site, 3) the 3' integration site and 4) the mutant-specific region (e.g. mutation site or selection cassette). With these primer pairs, the parasite with the correctly integrated genomic locus could be specifically distinguished. Additionally, the genomic DNA of the untransfected parasite line was included as a template to serve as a negative control. The subsequent PCR results were evaluated using agarose gel electrophoresis.

Genotyping PCR reaction mixture

Volume [µL]	Reagents
1	*P. berghei* genomic DNA
0.5	Forward primer (10 µM)
0.5	Reverse primer (10 µM)
2.5	10x Taq polymerase buffer
0.5	dNTPs (2mM each)
0.125	Taq polymerase (5 U/µL)
19.875	Autoclaved ddH_2O
25	

Genotyping PCR programme

Temperature/Time	Programme
95 °C / 30 sec	Initial denaturation (x1)
95 °C / 30 sec	Denaturation
55 °C / 1 min	Annealing
60 °C / 1 min/kb	Extension
30x cycles repeat	
60 °C / 10 min	Final extension
10 °C / infinite	Hold

Limiting dilution (LTD) and asexual growth rate determination

Following transfection, the parasites were subjected to positive selection under pyrimethamine treatment. However, it was frequently observed that some parasites developed resistance to the drug, resulting in a population comprising a mixture of transfected and untransfected parasites. Limiting dilution is a method of isolating a target parasite line by introducing a single parasite into a mouse to establish an isogenic population. To proceed, a cryo-stabilate of post-transfection parasites was injected into a naïve Swiss mouse through an IP injection. Approximately 24 hours post-infection, the mouse was administered drinking water supplemented with pyrimethamine (70 µg/mL) for positive drug selection. Once the parasitaemia reached around 0.5%, the blood was drawn via cardiac puncture and diluted in PBS to obtain an injection solution containing approximately one parasite per 100 µL. Subsequently, each of the eight recipient Swiss mice was IV injected with 100 µL of the solution, resulting in the introduction of one parasite per mouse. Parasitaemia progression was monitored from the seventh day post-infection without drug selection until it reached 2%. Thereafter, a blood sample was collected for genotyping and cryo-stabilate generation. The dilution for the injection solution was calculated as follows:

$$\text{Parasites per } 100\ \mu\text{L} = \frac{\text{Parasitaemia (\%)} \times \text{Erythrocytes per } \mu\text{L blood}}{100^{2\ dilution}}$$

$$\text{Diluted blood } (\mu\text{L}) = \frac{\left(\frac{n-1}{n}\right) \times 2000\ \mu\text{L}}{\text{Parasites per } 100\ \mu\text{L}}$$

Erythrocytes per µL blood = 7 x 10^6 (theoretical value)
n = number of infected mice
Diluted blood = fresh blood diluted twice by a factor of 100
2000 µL = final volume of the injection solution (diluted blood + PBS)

Since limiting dilution infects mice with a known number of parasites, this method allows for a more accurate observation of the blood stage growth. The asexual growth rate was determined by calculating the fold increase in parasite numbers over a 24-hour period:

$$\text{Asexual growth rate } \left(\frac{\text{Fold}}{24\text{h}}\right) = \left(\frac{\left(\frac{\text{Parasitaemia } (\%)}{100}\right) \times (7 \times 10^6) \times 2000_{\mu\text{L whole blood}}}{\text{Number of parasites injected}}\right)^{\frac{1}{\text{Days post infection}}}$$

For the comparisons of asexual growth rate, the values were calculated based on the parasitaemia from one day before it reached 1%. In the event that the parasite line did not reach 1% parasitaemia, the first countable parasitaemia value was used. All values presented in this study were obtained between day 7 and 14 post-infection.

Negative selection

The negative selection was conducted for the purpose of removing the selection cassette from the transfected parasites. This approach is advantageous when two or more genetic modifications are introduced sequentially to a parasite line. For example, complementation of mutant Alps into a knock-out locus was achieved using this method. The procedure was conducted in accordance with the standard LTD protocol. Following infection of a naïve Swiss mouse with the target parasite line, the mouse was given 1 mg/mL 5-FC-containing drinking water from 24 hours. Once the parasitaemia reached approximately 0.5%, the parasites were subjected to limiting dilution, in order to isolate the correctly selected parasite clones. The genotyping PCR was conducted using primer pairs targeting the whole locus and the selection cassette.

Ookinete culture and purification

A naïve Swiss mouse was IP injected with a cryo-stabilate of an isogenic parasite line, and the progression of parasitaemia was monitored on a daily basis from the fourth day post-infection. Once the parasitaemia reached >1.5%, the blood was harvested via cardiac

puncture and subjected to fresh blood transfer (FBT). FBT describes the direct transfer of infected blood to another animal, thereby allowing the parasites to fully restore their biological functions, which may have been compromised due to cryo-preservation. Following the collection of infected blood, 20 x 10^6 parasites were diluted in PBS or directly IP injected into a recipient naïve Swiss mouse.

$$\text{Fresh blood } (\mu\text{L}) = \frac{20 \times 10^6}{\left(\frac{\text{Parasitaemia } (\%)}{100}\right) \times (7 \times 10^6)}$$

On the third day post FBT, the exflagellation activity of the parasites was examined. A drop of tail blood from the infected mouse was applied to a glass slide and pressed tightly with a coverslip. Subsequently, the slide was incubated in the dark for nine minutes at RT. The exflagellation activity was observed using a ZEISS Axio Lab.A1 microscope (Carl Zeiss AG, Oberkochen, Germany) at 40x magnification with phase contrast. Once the exflagellation activity had been confirmed, the infected mouse was bled through cardiac puncture, and the entire blood volume was used to inoculate 10 mL of complete ookinete medium in a T75 flask (Sarstedt AG & Co. KG, Nümbrecht, Germany), which had been equilibrated for at least one hour at 19°C. The T75 flask containing the ookinete culture was wrapped in aluminium foil to prevent light exposure and incubated in an Excella E24 incubator (New Brunswick Scientific, NJ, USA) for 21 hours at 19°C. On the following day, 1 mL of the culture was drawn out of the flask and centrifuged for two minutes at RT, 7,000 rpm in order to obtain the pellet for Giemsa staining, as described in the schizont culture protocol. Once the presence of ookinetes in the pellet had been confirmed, 10 mL of the culture was carefully transferred into a 50 mL Falcon tube and underlaid with 63% Histodenz by pipetting through a glass Pasteur pipette. Without disturbing the layers, the Falcon tube was carefully placed into a centrifuge and spun for 25 minutes at RT, 1,000 rpm without brake. Subsequently, the ookinete layer was isolated using a Pasteur pipette and centrifuged for eight minutes at RT, 1,000 rpm with brake. The resulting ookinete pellet was gently resuspended in 1 mL ookinete medium and kept in the dark at 19°C for subsequent analysis.

Ookinete motility assay

The ookinete motility was evaluated in a two-dimensional setup using two glass slides sealed together. 100-300 µL of the purified ookinetes (in 1 mL ookinete medium) was pulse centrifuged for 10 seconds and the supernatant was removed almost completely, leaving a slightly wet pellet. 2 µL of the pellet was applied to a glass slide (Thermo Fisher Scientific, Dreieich, Germany) and pressed with a cover glass (VWR International, Darmstadt, Germany) with sufficient force to ensure full contact between the two surfaces. The glass

slides were then sealed with Valap sealant to ensure an airtight seal. Subsequently, the ookinetes were filmed with or without fluorescence using a microscope either Axio Observer Z1 with Axiocam 506 or Axioskop 2 MOT with the Axiocam 208 colour camera (all from Carl Zeiss AG, Oberkochen, Germany) at 40x magnification for 15 minutes with one frame captured every 30 seconds. Two or three films were obtained from a single slide. The analysis of the acquired films was conducted using Fiji, as detailed in the subsequent section.

Live quantification of exflagellation events

The ability of the parasites to exflagellate was evaluated by quantifying the number of exflagellating male gametocytes (exflagellation centres) within the specified time frame following activation. The value was normalised to gametocytaemia and presented as the number of exflagellation events per 100 gametes. To perform the exflagellation assay, a naïve Swiss mouse was infected with the target parasite line and subjected to FBT upon reaching 1.5% parasitaemia, as detailed in the ookinete culture protocol. Once the mouse had reached a parasitaemia of over 2%, the gametocytaemia was determined from the same blood smear by calculating the number of mature gametocytes per 100 erythrocytes. To quantify the exflagellation events in real time, a drop of tail blood from the infected mouse was applied to a glass slide and pressed tightly with a coverslip. Subsequently, the slide was incubated in the dark to allow for the activation of male gametocytes, which were then quantified as outlined below. The assay was conducted using a ZEISS Axio Lab.A1 microscope (Carl Zeiss AG, Oberkochen, Germany) at 40x magnification with phase contrast.

$$\text{Gametocytaemia (\%)} = \frac{\text{Gametocyte} \times 100}{\text{Erythrocyte}_{\text{total}} \times \text{number of counted fields } (> 150)}$$

$$\text{Exflagllation (\%)} = \frac{\text{Gametocyte}_{\text{exflagellating}} \times 100}{\text{Erythrocyte}_{\text{total}} \times \text{number of counted fields}}$$

$$\text{Exflagellation event/100 gametocytes} = \frac{\text{Exflagellation (\%)} \times 100}{\text{Gametocytaemia (\%)}}$$

Exflagellation assay procedure

Action	Time (min)	Description
Collection of tail blood	0~ 8	Incubate in the dark, RT
Erythrocyte quantification	8 ~ 10	Count the total erythrocytes/field
Exflagellation centre quantification	10 ~ 13	Count the exflagellation centres/field, continue counting until 13 minutes. Ideally > 25 fields
Extra observation	13 ~	Extra time for any late observation. Excluded from the evaluation

Fixation of activated gametocytes in exflagellation process

In order to visualise the exflagellation process using immunofluorescence, male gametocytes were chemically fixed at 0, 2, 4, 8, 10, 12, 14, 16 and 20 minutes post-activation during the course of gametogenesis. Prior to the experiment, eight Eppendorf tubes, each containing 450 µL of ookinete medium, were prepared and stored at 19°C in the dark. In addition, one tube containing 1 mL of paraformaldehyde (PFA) fixing solution was prepared for the 0 minute sample. The infected blood, with a parasitaemia of over 2%, was harvested from a post-FBT mouse according to the standard protocol. Immediately following the collection of the fresh blood, a volume of 50 µL was transferred to each of the prepared PFA and ookinete medium Eppendorf tubes (**Figure 9**). These were then incubated at 19°C in the dark. At 1 minute 20 seconds (1:20), the first ookinete medium sample was taken out and centrifuged for 30 seconds at RT, 12,000 rpm in order to remove the ookinete medium. The parasite pellet was promptly resuspended in the 1 mL fixing solution and fixed for 40-60 minutes at RT. The same fixation step was repeated for the remaining time points, whereby the sample was always subjected to a centrifugation 40 seconds prior to the designated fixation time.

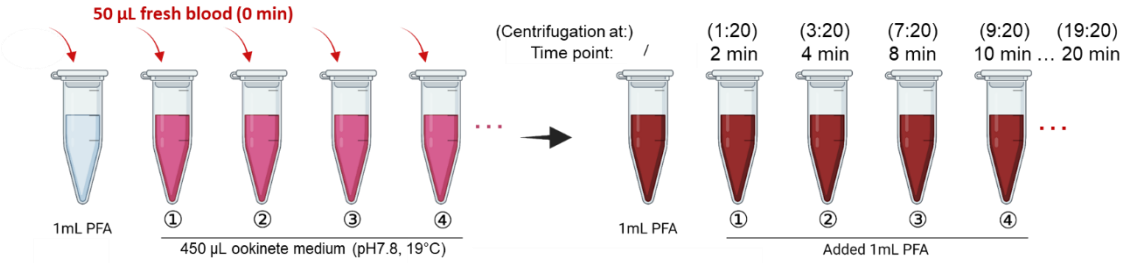

Figure 9: Fixation scheme of activated gametocytes in exflagellation process. The infected blood was added to the pre-conditioned ookinete medium (19°C, pH 7.8) to facilitate the activation of microgametogenesis. 40 seconds prior to the designated fixation time, the sample was centrifuged for 30 seconds at RT, 12,000 rpm. The supernatant ookinete medium was removed, and the pellet was then carefully resuspended with 1 mL of PFA fixing solution.

Following the fixation, the sample was centrifuged for five minutes at RT, 1,800 rpm in order to remove the fixing solution. The resulting pellet was then washed three times with 1 mL

PBS, with centrifugation for five minutes at RT, 1,800 rpm taking place between each wash. Subsequently, the sample was resuspended in 500 µL PBS and stored at 4°C in the dark until further use.

Jasplakinolide and cytochalasin D treatment and imaging of actin chromobody ookinetes

The actin chromobody-expressing ookinetes were chemically fixed prior to fluorescence microscopy imaging. For the non-treated sample, 100-300 µL of the purified ookinetes (in 1 mL ookinete medium, as detailed in the ookinete protocol) were subjected to a pulse centrifugation for 20 seconds and subsequently resuspended in 500 mL PFA fixing solution. For the jasplakinolide and cytochalasin D treatment, 198 µL of purified ookinetes were supplemented with 2 µL of 50 nM or 500 nM jasplakinolide in dimethyl sulfoxide (DMSO) (for a final concentration of 0.5 nM and 5 nM, respectively) or 2 µL of 1 µM or 10 µM cytochalasin D in DMSO (for a final concentration of 0.01 µM and 0.1 µM, respectively). Following a three-minute incubation period with the compounds, the samples were pulse-centrifuged for 20 seconds and subsequently resuspended in 500 µL of PFA fixing solution. All ookinete samples were fixed for a minimum of 60 minutes at RT, followed by a two-minute centrifugation at RT, 7,000 rpm. Subsequently, the samples were washed three times with 1 mL PBS, with the same centrifugation step taking place between each wash. The sample was then resuspended in 100 µL PBS supplemented with 5 µg/mL Hoechst dye. Following a 20-minute incubation period, the sample was washed with 1 mL of PBS once more, and the supernatant was removed, leaving approximately 10-30 µL of liquid with the pellet. For imaging, 2 µL of the pellet was applied to a glass slide with a cover glass. Fluorescence images were obtained using an Axio Observer Z1 microscope and an Axiocam 506 camera, with a 63x oil objective (all from Carl Zeiss AG, Oberkochen, Germany). The actin-chromobody and Hoechst signals were imaged with the EGFP (150 ms exposure time) and H3258 (25 ms exposure time) filters, respectively.

Immunofluorescence assay (IFA)

IFA refers to the fluorescence microscopy-based detection of a target protein or epitope peptide using a specific antibody conjugated with a fluorophore. In this study, alpha-tubulins in male gametocytes and microgametes, as well as the haemagglutinin (HA) epitope-tagged PbAlp1 in ookinetes, were detected as detailed below:

Detection of	Primary antibody	Secondary antibody
Alpha-tubulin	Mouse α- alpha-Tubulin, 1:1000 in 2% BSA in PBS	α-Mouse IgG Alexa Fluor R.p. 594, 1 drop/500 µL 5% milk in PBS
3x HA tag	Rat α-Haemagglutinin (HA), 1:30 in 2% BSA in PBS	α-Rat IgG Alexa Fluor 594, 1:500 in 5% milk in PBS

In the following IFA protocol, all centrifugation steps for the gametocyte samples were performed for five minutes at RT, 1,800 rpm, whereas for the ookinete samples, the condition of two minutes at RT, 7,000 rpm was employed.

To initiate the process, 100 µL of the fixed gametocyte or ookinete sample was pelletted by centrifugation and permeabilised for 10 minutes at RT in 100 µL of 0.1% Triton-X-PBS solution. The pellet was then washed twice with 1 mL of PBS and blocked for a period of two hours at RT in 2% BSA-PBS solution. Following the blocking step, the solution was removed by centrifugation and 60-100 µL of the specific primary antibody solution was added, after which the samples were incubated at RT for one hour. Subsequently, the samples were washed twice with 1 mL PBS and incubated in 100 µL of the corresponding secondary antibody solution, supplemented with 5 µg/mL Hoechst dye, for one hour at RT in the dark. Lastly, the sample was washed twice for the final time and resuspended in 10-50 µL of PBS, according to the desired sample cell density. For fluorescence microscopy analysis, 1.5-2 µL of the cell suspension was loaded onto a glass slide and overlaid with a cover glass. All fluorescence imaging was conducted using an Axio Observer Z1 microscope with Axiocam 506 and a 63x oil objective (Carl Zeiss AG, Oberkochen, Germany). For the imaging of both alpha-tubulin and HA, the AF594 filter was employed with an exposure time of 200 ms, whereas for Hoechst, the H3258 filter was applied with an exposure time of 25 ms.

Western blot of *P. berghei* protein

Western blot analysis was conducted on blood stage and ookinetes of *P. berghei* to ascertain the expression of epitope-tagged Alp1 and Alp2b, as well as the target specificity of the synthesised α-PbAlp1 and α-PbAlp2b antibodies (Eurogentec, Seraing, Belgium). The blood stage parasite sample, including gametocytes, was prepared by treating the infected blood with a 0.03% saponin lysis solution in order to extract the intraerythrocytic parasites. Following the washing of the parasite pellet twice with PBS and centrifugation for two minutes at RT, 7,000 rpm, it was resuspended in PBS supplemented with 1 mM PMSF and stored at -20°C, unless prepared directly for SDS-PAGE. In contrast, the ookinete sample was prepared directly from the purified ookinetes, which had been quantified using a Neubauer chamber (Brand GMBH & Co, Wertheim, Germany). All samples were mixed

with 1x or 4x SDS sample buffer to the desired concentration and denatured for 10 minutes at 95°C. Approximately 10^6 blood stage parasites and 5×10^5 ookinetes were loaded into a single of an SDS gel. The SDS-PAGE and western blot were performed according to the standard protocol outlined in the protein biochemistry methodology section. For the chemiluminescent detection of the target proteins, Western-Ready ECL Substrate Premium solution (BioLegend/Biozol, Eching, Germany) and ChemiDoc imaging system (Bio-Rad, Munich, Germany) were employed.

Detection of	**Primary antibody**	**Secondary antibody**
EGFP-tagged PbAlp1 and PbAlp2b	Mouse α- GFP, 1:1000 in 3% BSA in TBST	α-Mouse IgG (HRP), 1:10,000 in 5% milk in TBST
HA-tagged PbAlp1	Rat α-Haemagglutinin (HA), 1:1000 in 3% BSA in TBST	α-Rat IgG (HRP), 1:10,000 in 5% milk in TBST
PbAlp1	Rabbit α- PbAlp1, 1:2000-5000 in 3% BSA in TBST	α-Rabbit IgG (HRP), 1:2000 in 5% milk in TBST
PbAlp2b	Rabbit α- PbAlp2b, 1:2000-5000 in 3% BSA in TBST	α-Rabbit IgG (HRP), 1:2000 in 5% milk in TBST
Plasmodium Aldolase	Rabbit α-Aldolase, 1:5000 in 3% BSA in TBST	α-Rabbit IgG (HRP), 1:2000 in 5% milk in TBST

Stripping

Subsequent to the detection of the target protein, the same membrane was subjected to a second blotting procedure for the purpose of quality control of the parasite sample, utilising the aldolase protein as the target. The ECL solution was removed through three 10-minute wash steps with TBST, after which the membrane was incubated in stripping buffer for 30 minutes at 56°C. Subsequently, the membrane was washed with TBST at least four times, then blocked in 5% milk-TBST for one hour. The subsequent procedure was conducted in accordance with the established standard protocol.

Mouse handling and ethics statement

All experimental procedures involving mice were conducted in accordance with the FELASA B rodent animal guidelines and the guidelines approved by the Regierungspräsidium Giessen.

2.2.5 Computer-based analysis

AlphaFold2 protein structure prediction

The predicted structures of *P. berghei* and *P. falciparum* Alp1 and Alp2b were generated using the AlphaFold2 online tool (Jumper et al., 2021). In order to generate predictions for the mutated versions of PbAlp1 and PbAlp2b, the corresponding amino acid sequences were provided to the programme. The protein model with the highest prediction confidence was ultimately selected for use in the experimental planning. The protein structures were subsequently coloured, highlighted and overlapped using PyMOL 4.6.

Fiji imageJ image and movie analysis

The Fiji ImageJ 1.8.0 software was employed to extract fluorescent parasite images from the multi-channel raw microscopy data, using the following macro script:

```
inputDir = getDirectory("Select A folder");fileList = getFileList(inputDir);
outputDirName = inputDir + File.separator + "Output image" + File.separator;
File.makeDirectory(outputDirName);
outputDirPath = outputDirName + File.separator;
waitForUser("Action required", "Select the crop area and press OK");
run("Crop");
setOption("ScaleConversions", true);
run("Brightness/Contrast...");
resetMinAndMax();
run("8-bit");
title = getTitle();
run("Split Channels");
three = "C3-" +title;
two = "C2-" +title;
one = "C1-" +title;
run("Merge Channels...", "c2=["+two+"] c3=["+three+"] create keep");
run("RGB Color");
selectWindow(one);
run("Grays");
save(outputDirPath + File.getNameWithoutExtension(one) + ".tif");
selectWindow(two);
run("Grays");
run("Invert");
save(outputDirPath + File.getNameWithoutExtension(two) + ".tif");
selectWindow(three);
run("Grays");
run("Invert");
save(outputDirPath + File.getNameWithoutExtension(three) + ".tif");
selectWindow("Composite (RGB)");
save(outputDirPath + File.getNameWithoutExtension("Composite (RGB)" +title) +
".tif");
close("*");
```

To analyse the motility of ookinetes, the manual tracking function was utilised with an interval of 30 seconds, x/y calibration of 0.1134 pixel/µm, and z calibration of 0.0. This tracking was continued for the entire 15-minute period.

3 Results

3.1 Heterologous overexpression of PbAlp1 and PbAlp2b in *E. coli*

The production of recombinant target proteins enables structural determination and *in vitro* biochemical assays to analyse their physical and biochemical properties at molecular level. In order to obtain sufficient amount of pure recombinant *Plasmodium berghei* Alp1 (PbAlp1) and Alp2b (PbAlp2b), an *Escherichia coli*-based expression system was selected on the grounds of its accessibility and the extensive range of established methodologies. The subsequent purification of the target proteins was conducted through chemical and physical solubilisation, followed by immobilised metal affinity chromatography (IMAC) (**Figure 10**).

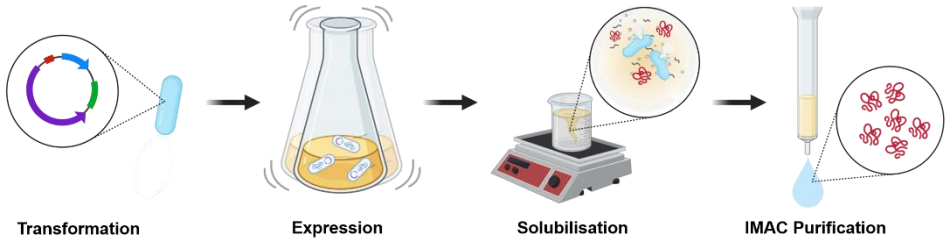

Figure 10: Simplified overview of the recombinant protein production with *E. coli*. After transformation of the overexpression vector carrying the target protein gene, *E. coli* cells were cultured under optimal conditions to promote expression of the target protein. The cells were then lysed and the target protein was released into a soluble fraction conditioned with a suitable buffer. The IMAC purification method was used to separate the target protein based on its binding affinity to the purification column material.

3.1.1 Overexpression and purification of PbAlp1

The cDNA sequence of *Plasmodium berghei alp1* (*pbalp1*) was codon optimised for *E. coli* expression and synthesised (BioCat). The DNA was integrated downstream of the T7 promoter and a 6x histidine tag (polyhistidine tag) in a pET28a vector (BioCat) (**Figure 11A**). Optimal expression conditions were identified by testing different T7 expressing host *E.coli* strains, media, expression temperature and culture durations after induction with 0.1 mM IPTG. As a result, *E. coli* strain BL21 (DE3) cultured overnight at 16°C with TB medium produced the best amount of PbAlp1 (**Figure 11B**). This culture condition was used consistently for further experiments described in this section, unless otherwise specified. Various sets of *E. coli* chaperones (Takara Bio) were co-expressed with PbAlp1 to assist its correct folding and anti-aggregation.

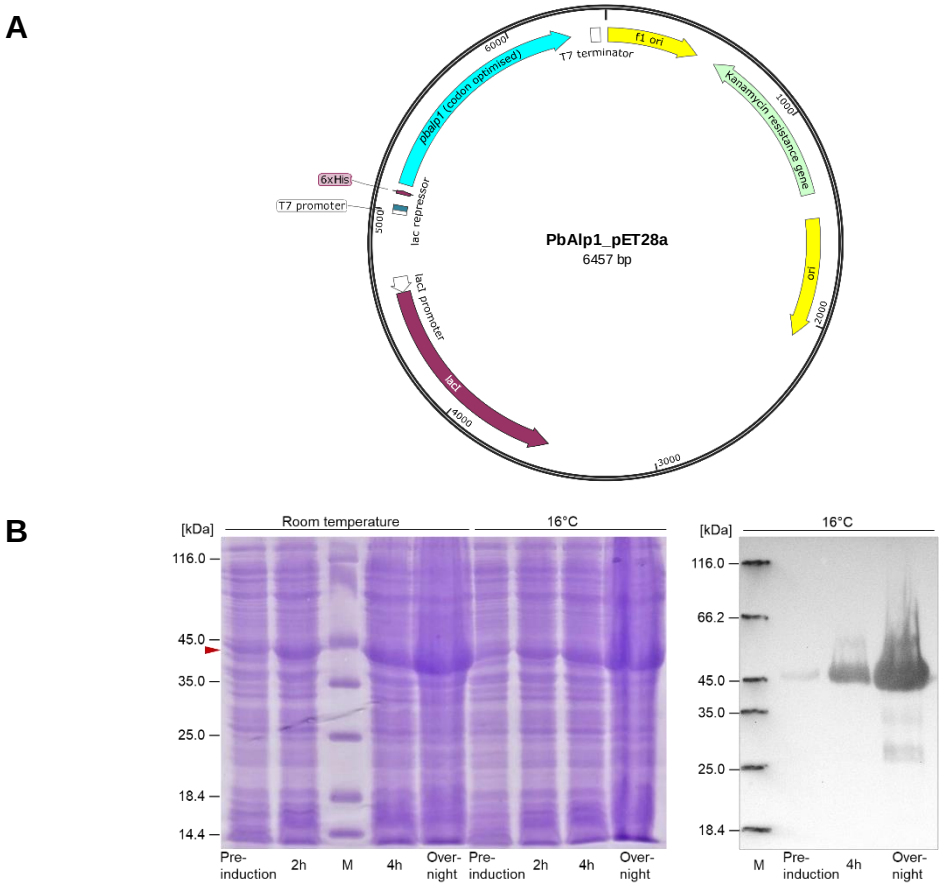

Figure 11: Plasmid map of PbAlp1_pET28a expression vector and expression test of PbAlp1. (A) Codon-optimised pbalp*1* cDNA sequence attached with a 6x histidine tag at the 5'-end is located downstream of the T7 promoter. The plasmid carries a kanamycin resistance gene for drug selection and a *lacI* gene encoding the lac repressor protein to regulate target gene expression. **(B)** SDS-PAGE gel (left) showing overexpressed PbAlp1 (43 kDa) under different culture conditions with terrific broth (TB) medium (no chaperone co-expression). α-his tag western blot (right) confirms intact expression of polyhis-PbAlp1, which is particularly abundant in the overnight culture at 16°C. M = marker, h= hours after IPTG induction. Red arrow indicates the target size (43 kDa) of PbAlp1.

Subsequently, PbAlp1 was released from the *E. coli* cells through a lysozyme treatment and ultra-sonication. The lysis process was conducted in a conditioned solubilisation buffer, which typically contains salt to regulate the ionic strength of the solvent and other additives to promote the solubility of the target protein (**Table 1**). Once the solubilisation process was complete, the lysate was separated into a pellet and a supernatant (soluble fraction). The target protein contents of these fractions were then determined using a western blot (**Figure 12**). The comparison revealed that the 50 mM HEPES buffer at pH 8.0 with 200 mM NaCl (with/without additives) was the only tested buffer condition that was able to successfully solubilise PbAlp1. It is noteworthy that the CHES buffer (pH 9.0, 300 mM NaCl) and the MES buffer (pH 5.0, 300 mM NaCl) also demonstrated moderate solubilisation of the protein. In comparison, the identical HEPES buffer (pH 8.0) with an increased NaCl concentration (600 mM) lacked the capacity to solubilise the protein, suggesting that the solubilisation process of PbAlp1 is influenced by the ionic strength of the solvent. Nevertheless, the 50

mM HEPES buffer (pH 8.0) with 200 mM NaCl was taken as the standard solubilisation buffer for all the following experiments in this section.

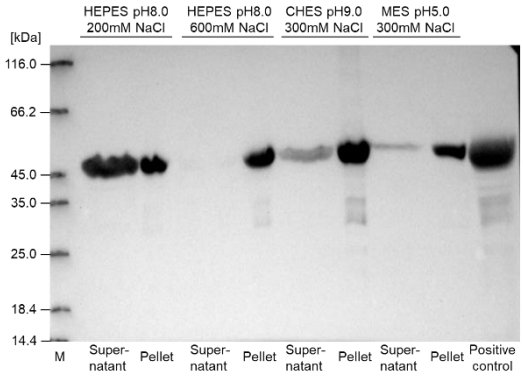

Figure 12: Representative western blot of successfully solubilised PbAlp1. An α-his tag western blot visualises the presence of PbAlp1 (43 kDa) in the soluble fraction (supernatant) of the lysate treated with 50 mM HEPES buffer pH 8.0, 200 mM NaCl, supplemented with 20% glycerol, 2% Triton X-100, 5 mM DTT. At a concentration of 600 mM NaCl, solubilisation was prevented. In contrast, a concentration of 300 mM NaCl in CHES and MES buffer allowed for moderate solubilisation of the protein, indicating that salt concentration has an effect on PbAlp1 solubilisation.

The purification of the successfully solubilised PbAlp1 was conducted using immobilised metal affinity chromatography (IMAC) with Ni-NTA resin. On the SDS-PAGE gel (**Figure 13**), the bands corresponding to PbAlp1 (43 kDa) were barely visible in the eluted fractions. Moreover, several impurities remained after the elution steps, almost masking the target protein. Although intact PbAlp1 was detected on the western blot performed post-IMAC purification, the total yield was clearly insufficient for an additional purification process to remove the observed impurities. The result thus underscores the necessity for either an increased solubilisation volume or an improvement in the purity of the eluted product.

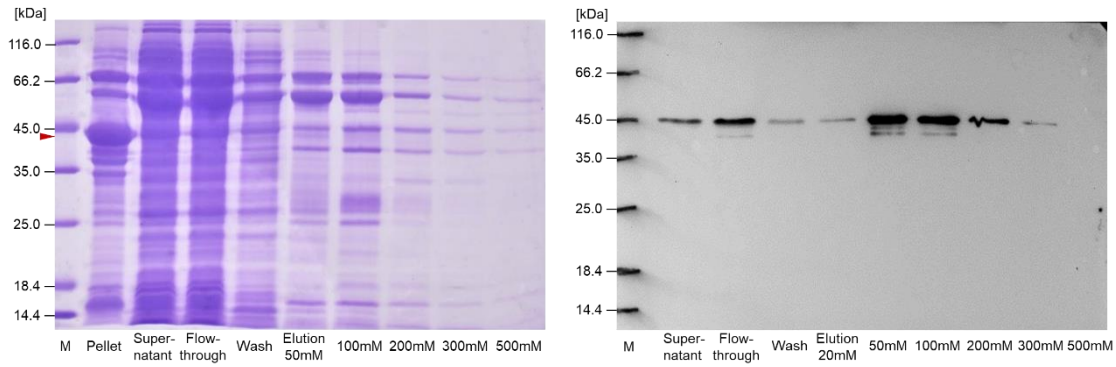

Figure 13: 6x histidine tag-PbAlp1 purified with Ni-NTA IMAC. The eluted fractions with 50–500 mM imidazole on the SDS gel (left) still contain several nonspecific proteins and the target PbAlp1 was not visibly enriched. The presence of PbAlp1 was confirmed through an α-his tag western blot (right), although the quantity was low. M = marker. The red arrow indicates the target size (43 kDa) of PbAlp1.

3.1.1.1 Ni-TED and Co-CMA purification resins did not enhance PbAlp1 purity

One potential cause of impurities following elution is the nonspecific binding of histidine-rich proteins to the Ni-NTA column. In order to enhance the specificity of the IMAC purification, the efficacy of Ni-TED and Co-CMA resins was evaluated (**Figure 14**). Due to an error in the experimental procedure, the Ni-TED elution was conducted initially with 500 mM imidazole, followed by a second wash and then 100 mM and 200 mM imidazole. However, this would not affect the ultimate assessment of the Ni-TED purification capacity, as the 100 mM and 200 mM elution steps also yielded distinct impurity bands even after an additional wash step. In comparison to the Ni-NTA purification, there was a notable reduction of minor background bands in the 50–200 mM imidazole eluted fractions in both Ni-TED and Co-CMA. Despite this, no substantial enhancement in purity was discerned with either purification approach, and the target bands of PbAlp1 (43 kDa) remained faint.

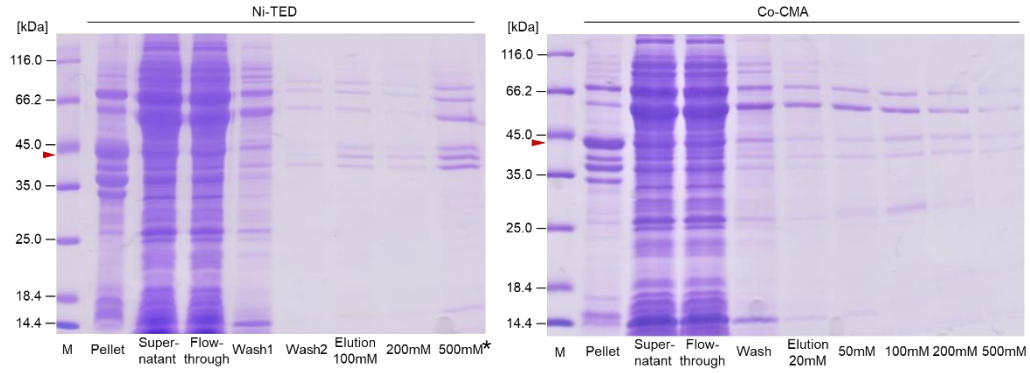

Figure 14: 6x histidine tag-PbAlp1 purified with Ni-TED and Co-CMA IMAC. The SDS gels of both Ni-TED (left) and Co-CMA (right) –purified products show a noticeable reduction in background contaminants compared to the Ni-NTA. However, some undesirable bands still remain. No enrichment of PbAlp1 was indicated through the target bands at 43 kDa. *Due to a procedural error, Ni-TED was initially eluted with 500 mM imidazole, followed by a second wash and then 100 mM and 200 mM. M = marker. The red arrow indicates the target size (43 kDa) of PbAlp1.

3.1.1.2 *E. coli* LOBSTR strain expressed PbAlp1 abundantly, but could not solubilise

As the application of different IMAC resins did not result in enhanced product purity, a low-background strain of *E. coli* was employed to minimise the expression of contaminant proteins. LOBSTR *E. coli* (kindly provided by AG Grevelding) is a genetically modified strain that expresses less histidine-rich proteins. (Andersen et al., 2013). The expression of PbAlp1 in LOBSTR was successful. However, solubilisation was not achieved even after an overnight treatment (**Figure 15**), and thus subsequent IMAC purification was not performed. Based on the solubilisation tests previously conducted on BL21 cells, it can be speculated that LOBSTR cells may also require the co-expression of chaperones to produce soluble PbAlp1. This was not conducted in this study, as the LOBSTR cells and chaperone plasmids both contained the same resistance marker. In order to fully exploit the

potential of the LOBSTR strain, further investigation into chaperone co-expression strategies is required.

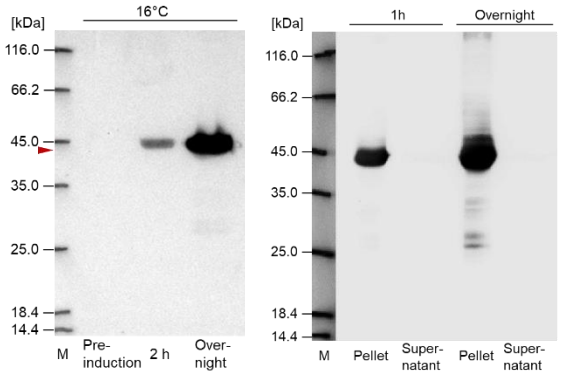

Figure 15: Expression and solubilisation of PbAlp1 in *E. coli* LOBSTR strain. α-his western blot analysis revealed a satisfactory expression of PbAlp1 in the overnight culture (left). Despite the favourable expression levels, PbAlp1 remained insoluble even after an overnight treatment (right), which is likely attributable to the absence of the chaperones that are essential for the production of soluble PbAlp1 in BL21 cells. M = marker (the marker bands on the right membrane were overlaid using a different setting inadvertently). The red arrow indicates the target size (43 kDa) of PbAlp1.

3.1.1.3 Co-expressed chaperones likely caused contaminations in IMAC purification

The *E. coli* chaperon set KJE8 (Takara Bio) comprising GroEL, GroES, DnaK, DnaJ and GrpE, has been consistently co-expressed in order to facilitate the production of soluble PbAlp1. These chaperones were required to enhance solubility while also causing impurities during IMAC purification. They have a natural affinity for binding to their substrates, including the target protein, which may be co-purified during elution. One possible measure to counteract this undesired activity is to wash the purification column with Mg-ATP prior to elution. The activity of major contaminating chaperones such as DnaK and GroEL is dependent on ATP hydrolysis, and their ATP-bound state exhibits a reduced binding affinity for the substrate, which leads to their detachment from the target protein. In the no ATP-wash control fractions, there are particularly prominent bands at around 60 kDa and 70 kDa (**Figure 16A**). In comparison, the ATP-washed fractions exhibited a notable reduction of these bands, suggesting that they may be DnaK (70 kDa) and GroEL (60 kDa) chaperones based on their estimated molecular weights. In conclusion, while Mg-ATP did lead to a reduction of some contaminants, the overall purification quality did not improve markedly and no enrichment of PbAlp1 in the eluted fraction was observed. Alternatively, the composition of the *E. coli* chaperones used to solubilise PbAlp1 was reassessed in order to identify effective combinations with reduced numbers of chaperones. A series of co-expression and solubilisation trials revealed that a chaperone set pGro7 (Takara Bio), consisting of GroEL and GroES, was also capable of producing soluble PbAlp1 (**Figure 16B**). The purity of the eluted product was considerably improved, and the persistent contaminants at 40 kDa and 70 kDa were no longer present. The quantity of solubilised

PbAlp1 appeared to have diminished slightly, yet no practical distinction was discerned in comparison to the more expansive chaperon set KJE8. This experiment, however, also highlighted a further issue that the concentration of purified PbAlp1 needs to be increased in order to enable additional purification processes.

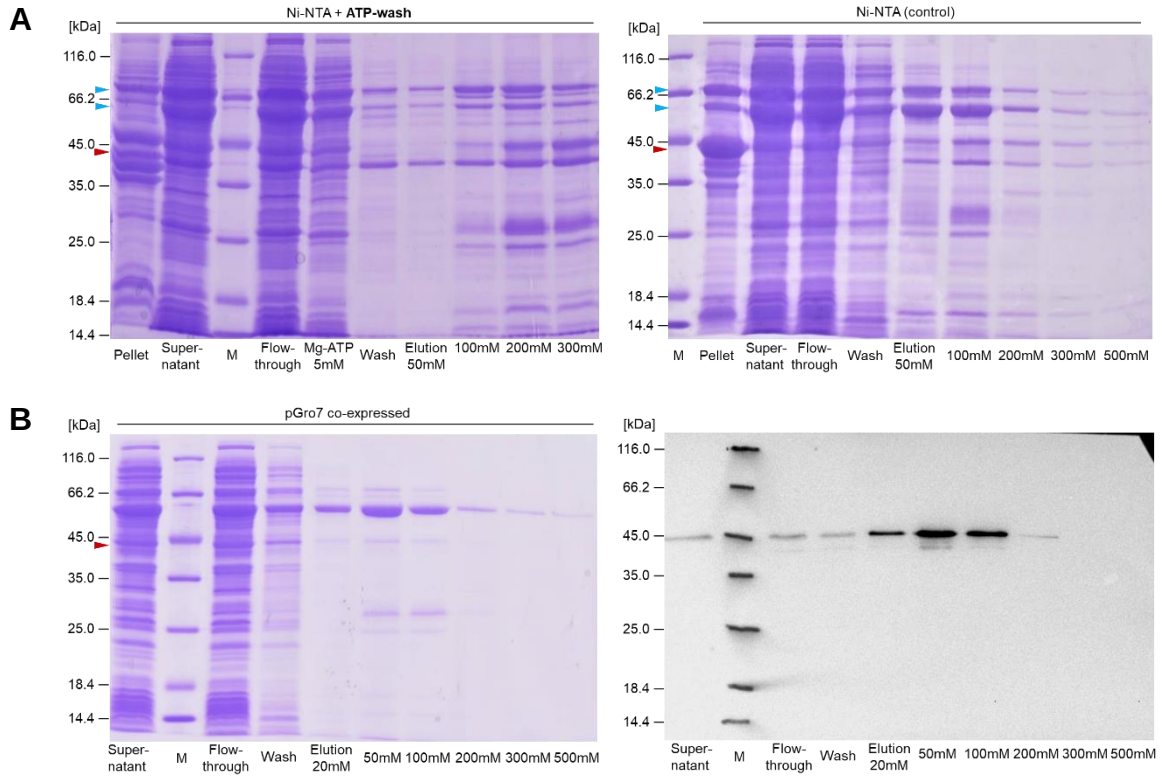

Figure 16: Effects of ATP-wash treatment and smaller chaperon set co-expression on PbAlp1 IMAC purification. (A) Application of a 5 mM Mg-ATP solution to the Ni-NTA purification column prior to elution resulted in the reduction of certain contaminants, presumed to be DnaK and GroEL chaperones, of 60 kDa and 70 kDa (blue arrows). **(B)** The smaller chaperonin set pGro7, comprising *E. coli* GroEL and GroES, was sufficient to produce soluble PbAlp1. The reduction of chaperones also resulted in a decrease in contaminants present in the eluted fractions. M = marker. The red arrow indicates the target size (43 kDa) of PbAlp1.

3.1.1.4 C-terminus polyhistidine tag caused degradation of PbAlp1

One of the fundamental prerequisites for a successful IMAC purification is the effective binding of the target protein to the purification resin. Another issue that must be addressed during the purification of PbAlp1 is the relatively high loss of PbAlp1 in the flow-through and wash fractions, which failed to bind to the purification resin. Previously, it was shown that different purification resin capacities did not influence the quantity of eluted PbAlp1 (**Figure 14**). Therefore, it can be hypothesised that the issue lies in the solubilised PbAlp1 struggling to bind to the purification column through their polyhistidine tag. The native structure of PbAlp1 is yet to be determined, and it is possible that the N-terminus polyhistidine tag was not exposed correctly for optimal interaction with the metal ions present in the purification resin (Bornhorst and Falke, 2000). Furthermore, given the essential role of chaperone

activity in solubilisation, it can be postulated that PbAlp1 is prone to misfolding or aggregation, which might hinder the polyhistidine interaction with the purification column. In order to investigate the potential positional effects of a polyhistidine tag on the purification of PbAlp1, the codon-optimised cDNA of *pbalp1* was tagged with a 6x histidine at the 3'-end (C-terminus) and cloned into a pET28a vector (**Figure 17A**). An additional construct was generated with a 5x alanine linker sequence inserted between *pbalp1* and the 6x histidine tag to observe whether the polyhistidine tag would function advantageously in this extended configuration. Both plasmids were expressed with and without the chaperone set (KJE8) and solubilised using Alps solubilisation buffer, as previously described. Unexpectedly, C-terminally tagged PbAlp1 showed strong degradation regardless of the presence of a linker sequence or co-expression of chaperones (**Figure 17B**). Together with the generally suboptimal expression, the outcome demonstrates that C-terminus tagging of PbAlp1 is not a viable approach for this *E. coli* expression system.

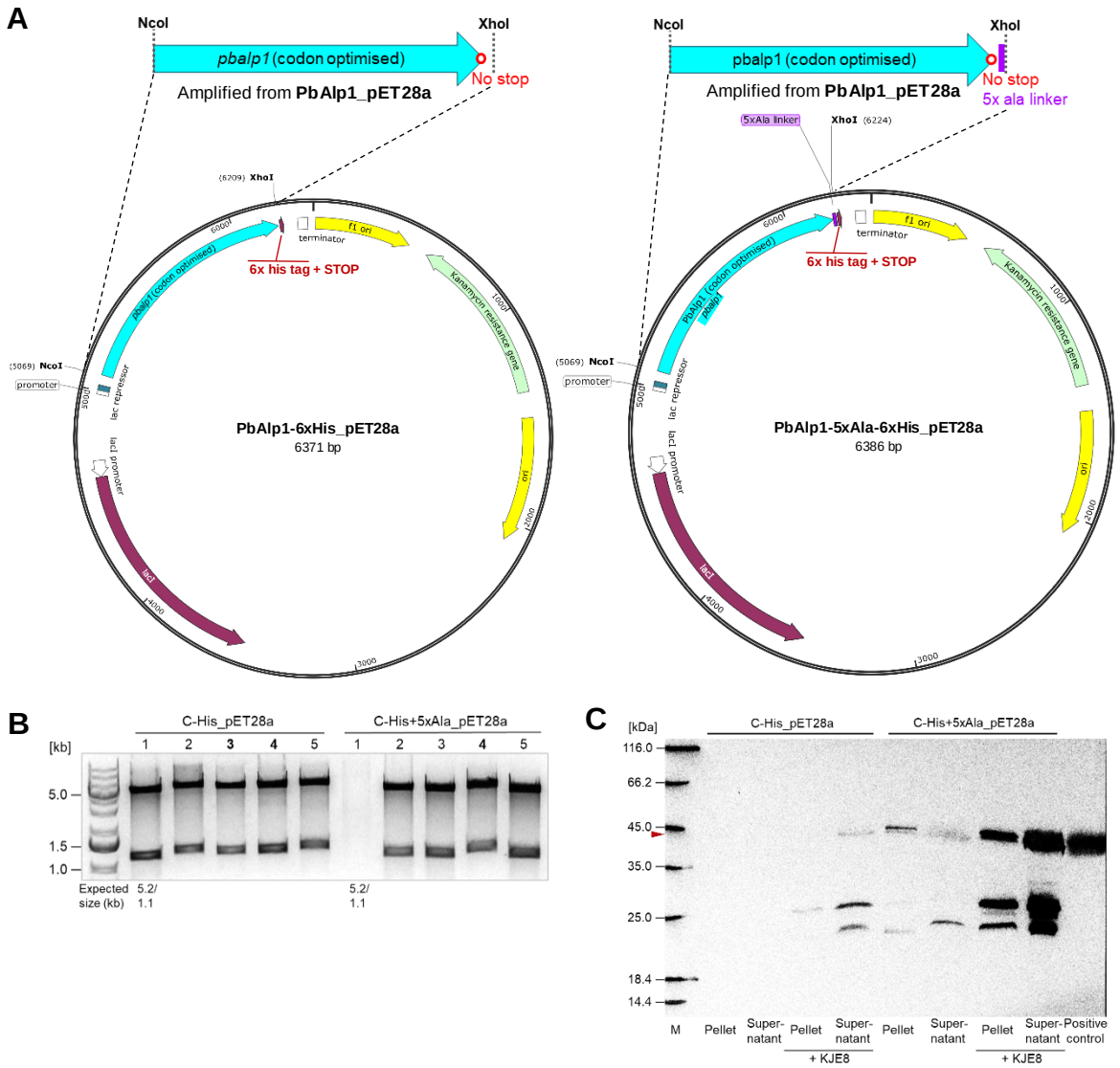

Figure 17: Plasmid maps and cloning test digestion of PbAlp1 C-terminus 6x histidine tag with/without linker and solubilisation test results. (A) Codon-optimised *pbalp1* cDNA (without stop codon) was amplified via PCR from the PbAlp1_pET28a vector (**Figure 11A**) with (top right) or without (top left) the additional 5x alanine linker sequence. Next, these products were cloned into the PbAlp1_pET28a vector backbone using NcoI and XhoI restriction sites. Upon integration, the insert replaced the original N-terminally tagged *pbalp1* and incorporated the 6x histidine tag at the 3'-end (C-terminus). **(B)** The agarose gel of the test digestion with NcoI and XhoI (below) verifies the correct integration of the constructs. The clone number 3 of the C-His_pET28a and the number 4 of the C-His+5xAla_pET28a were confirmed by Sanger sequencing and subsequently used for the expression and solubilisation tests. **(C)** The western blot of the expression and solubilisation tests revealed strong degradation of PbAlp1, irrespective of the presence of a 5x alanine linker sequence or co-expression of the KJE8 chaperone set. M = marker. The red arrow indicates the target size (43 kDa) of PbAlp1.

3.1.1.5 Summary of the heterologous overexpression of PbAlp1 in *E. coli*

PbAlp1 was successfully expressed in the *E. coli* BL21 strain and solubilised through the co-expression of GroEL and GroES chaperones. In the optimum conditions, approximately 50% of the expressed PbAlp1 could be solubilised. However, this was found to be insufficient because the IMAC purification process resulted in the loss of the majority of the product. In order to address the issue, combinations of several different conditions were evaluated (**Table 2**). The results obtained indicate that the apparent problem in the purification process is the outcome of a combination of the chaperone contamination and the inefficient binding of the polyhistidine-tagged PbAlp1 to the purification column. It may be possible to overcome the contamination issue once a sufficient quantity of soluble PbAlp1 is obtained.

Table 2: Overview of the tested conditions for the production of recombinant PbAlp1. Chaperone set KJE8 (DnaK, DnaJ, GrpE, GroES, GroEL); Tf2 (GroES, GroEL, Tig); pGro7 (GroES, GroEL); Tf16 (Tig); LDAO (Lauryldimethylamine oxide); FC12 (Fos-choline-12); DM (Decylmaltoside); OG (Octyl-beta-Glucoside); CHAPs (3. -{Dimethyl [3-(3α,7α,12α-trihydroxy-5β-cholan-24-amido)propyl]azaniumyl} propane-1-sulfonate); Ni-NTA (Nickel-nitrilotriacetic acid); Co-CMA (Cobalt-carboxylmethylaspartate); Ni-TED (Nickel-tris-carboxymethyl ethylene diamine); ATP (Adenosine triphosphate).

Protein	*E. coli* strain	Vector	Solubilisation method	IMAC resin	Expression	Solubilisation	Purification
Alp1	BL21	pET28a	Buffer only	Ni-NTA			
			Chaperone (KJE8)	Ni-NTA			
				Ni-NTA + ATP-wash			
				Co-CMA			
				Co-CMA + ATP-wash			
				Ni-TED			
			Chaperone (Tf2)	Ni-NTA			
			Chaperone (pGro7)				
			Chaperone (Tf16)				
			LDAO + Chaperone (pGro7)				
			FC12				
			FC12 + Chaperone (pGro7)				
			DM + Chaperone (pGro7)				
			OG				
			CHAPs + Chaperone (pGro7)				
		pET28a C-term. His-tag	Buffer only				
	C41	pET28a	Buffer only				
			LDAO				
	C43		Buffer only				
			LDAO				
	LOBSTR		Buffer only				
			LDAO				

High
Low
Negligible

3.1.2 Overexpression and solubilisation of PbAlp2b

Plasmodium berghei alp2b (*pbalp2b*) integrated pET28a overexpression plasmid (**Figure 18A**) was previously generated by V. Sangel. A 6x histidine tag was incorporated at the N-terminus of PbAlp2b to allow for subsequent IMAC purification. The primary objective was to identify the optimal expression condition, achieved through testing different host *E. coli* strains, media, culture duration, and temperature. The best expression condition was determined to be with BL21 (DE3) strain, cultured in TB medium for four hours at 16°C following the induction with 0.5 mM IPTG (**Figure 18B**). In comparison to PbAlp1 (**3.1.1**), the expression level of PbAlp2b was observed to be generally lower and displayed slight degradation when the cells were cultured overnight or at a temperature exceeding 16°C. The determined culture condition was consistently applied for all subsequent PbAlp2b expressions described in this section.

A

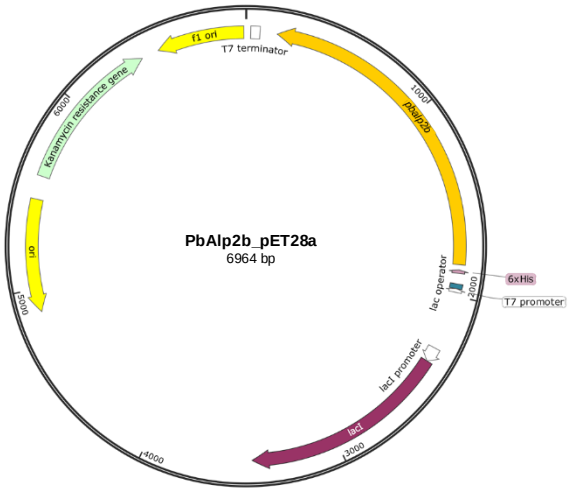

B

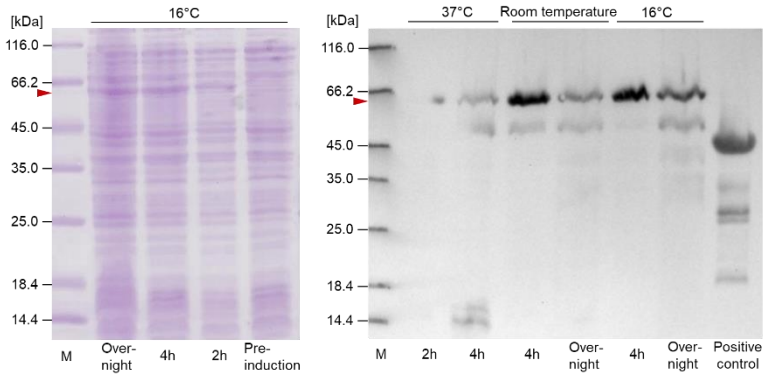

Figure 18: Plasmid map of PbAlp2b_pET28a expression vector and expression test of PbAlp2b. (A) *pbalp2b* sequence attached with a 6x histidine tag at the 5'-end is located downstream of the T7 promoter. The plasmid carries a kanamycin resistance gene for drug selection and a *lacI* gene encoding the lac repressor protein to regulate target gene expression. **(B)** The representative SDS-PAGE gel (left) showing overexpressed PbAlp2b (62 kDa) at 16°C with terrific broth (TB) medium (no chaperon co-expression). The α-his tag western blot (right) confirms the expression of polyhistidine-PbAlp2b, which is mostly intact only in the four hours culture at 16°C. M = marker, h= hours after IPTG induction. Red arrow indicates the target size (62 kDa) of PbAlp2b.

In contrast to *pbalp1*, the genomic sequence of *pbalp2b* was not codon-optimised for expression in the *E. coli* system. The differences in codon bias between *Plasmodium* and *E. coli* may have exerted additional pressure during heterologous expression, which might explain the reduced expression level of PbAlp2b in *E. coli*. To test this hypothesis, the pRAREII plasmid (Novagen) was co-expressed to provide a selection of tRNAs for *E. coli* rare codons, which could partially substitute for codon optimisation. However, the expression did not result in the desired enhancement (**Figure 19**). The solubilisation of PbAlp2b was initially attempted through the co-expression of the extensive chaperone set (KJE8) and cell lysis in a range of solubilisation buffers described previously (**Table 1**). Despite the expression with multiple chaperones, the solubilisation of PbAlp2b was not achieved.

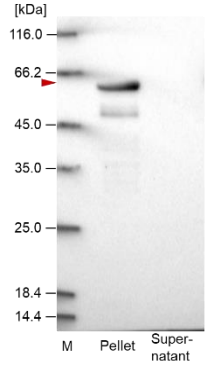

Figure 19: Expression and solubilisation test of PbAlp2b co-expressed with pRAREII. Non-codon-optimised *pbalp2b* was co-expressed with the pRAREII plasmid, which provides rare codon tRNAs for *E. coli* to ease the codon bias pressure. Western blot analysis revealed no enhancement in expression level. Solubilisation was conducted using the standard 50 mM HEPES solubilisation buffer (pH 8.0, 200 mM NaCl), yet no soluble PbAlp2b was obtained. M = marker. Red arrow indicates the target size (62 kDa) of PbAlp2b.

3.1.2.1 Minimal solubilisation of PbAlp2b achieved by the use of zwitterionic detergents

Insolubility of recombinant proteins can be a consequence of the hydrophobicity inherent to the natural characteristics of the target protein or the misfolding and aggregation, which expose hydrophobic regions (Royster et al., 2021). The use of amphiphilic agents, such as detergents, can facilitate alterations in the interaction affinity between the protein and the solvent. This is achieved through the formation of a protein-detergent complex, which increases the exposure of hydrophilic regions (Ratkeviciute et al., 2021). Some mild detergents, such as Triton and Tween, which were also occasionally included in the experimental solubilisation buffers, primarily interact with membrane lipid-associated proteins (Riske et al., 2017). In contrast, more powerful detergents can additionally disrupt protein-protein interactions, thereby liberating the target protein from aggregation (Soulié

et al., 2023). In order to examine the impact of detergents on persistently insoluble PbAlp2b, a range of detergents with varying potencies were selected and their capacity to solubilise the protein was evaluated. Consequently, 30 mM fos-choline-12 (FC12) was the sole detergent capable of producing a detectable quantity of soluble PbAlp2b on a western blot (**Figure 20A**). FC12 is a zwitterionic detergent, which is regarded to be particularly powerful due to their capacity to disrupt protein-protein interactions. Purification of the FC12-solubilised PbAlp2b was attempted via IMAC, resulting in the absence of enriched bands at the target PbAlp2b size (62 kDa) (**Figure 20B**). It is noteworthy that the utilisation of FC12 appeared to diminish the presence of chaperone contaminants. This may be due to the denaturing effect of FC12. However, the quantity of purified PbAlp2b remained insufficient.

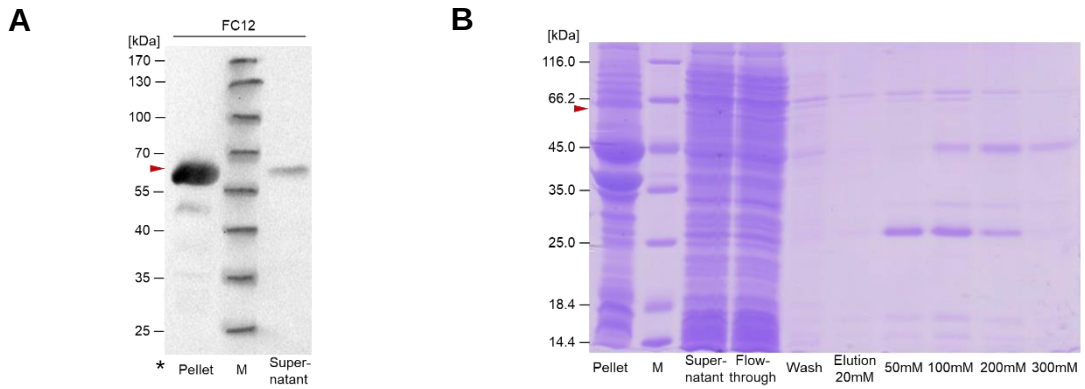

Figure 20: Solubilisation and IMAC purification of PbAlp2b treated with fos-choline-12 (FC12) detergent. **(A)** 30 mM of FC12 was added to the solubilisation buffer in order to reinforce the solubilisation of PbAlp2b. The western blot analysis revealed the presence of only a minimal amount of solubilised PbAlp2b. *The pellet sample load was erroneously doubled, thus the band does not accurately reflect the actual expression amount. **(B)** Ni-NTA IMAC purification of FC12-treated PbAlp2b. Given the limited initial quantity of solubilised PbAlp2b, it was not possible to observe target bands at 62 kDa in the eluted fractions. M = marker. Red arrow indicates the target size (62 kDa) of PbAlp2b.

3.1.2.2 SUMO tag improved PbAlp2b expression, but not solubilisation

The small ubiquitin-related modifier (SUMO) tag is a small protein fusion tag (Malakhov et al., 2004). Owing to its stable structure and chaperone effect, the tag has been reported to enhance the expression level and solubility of the target recombinant proteins when attached at the N-terminus. The *pbalp2b* gene was integrated into the multiple-cloning site of the pSUMO vector, positioned downstream of the 6x histidine tag and the *sumo* gene (**Figure 21A,B**). The PbAlp2b_pSUMO vector was transformed into BL21 cells and expressed under the standard condition previously described, without the use of chaperones. The level of expression appeared to be slightly elevated in the presence of the SUMO tag. However, no soluble PbAlp2b was detected in the supernatant (**Figure 21C**).

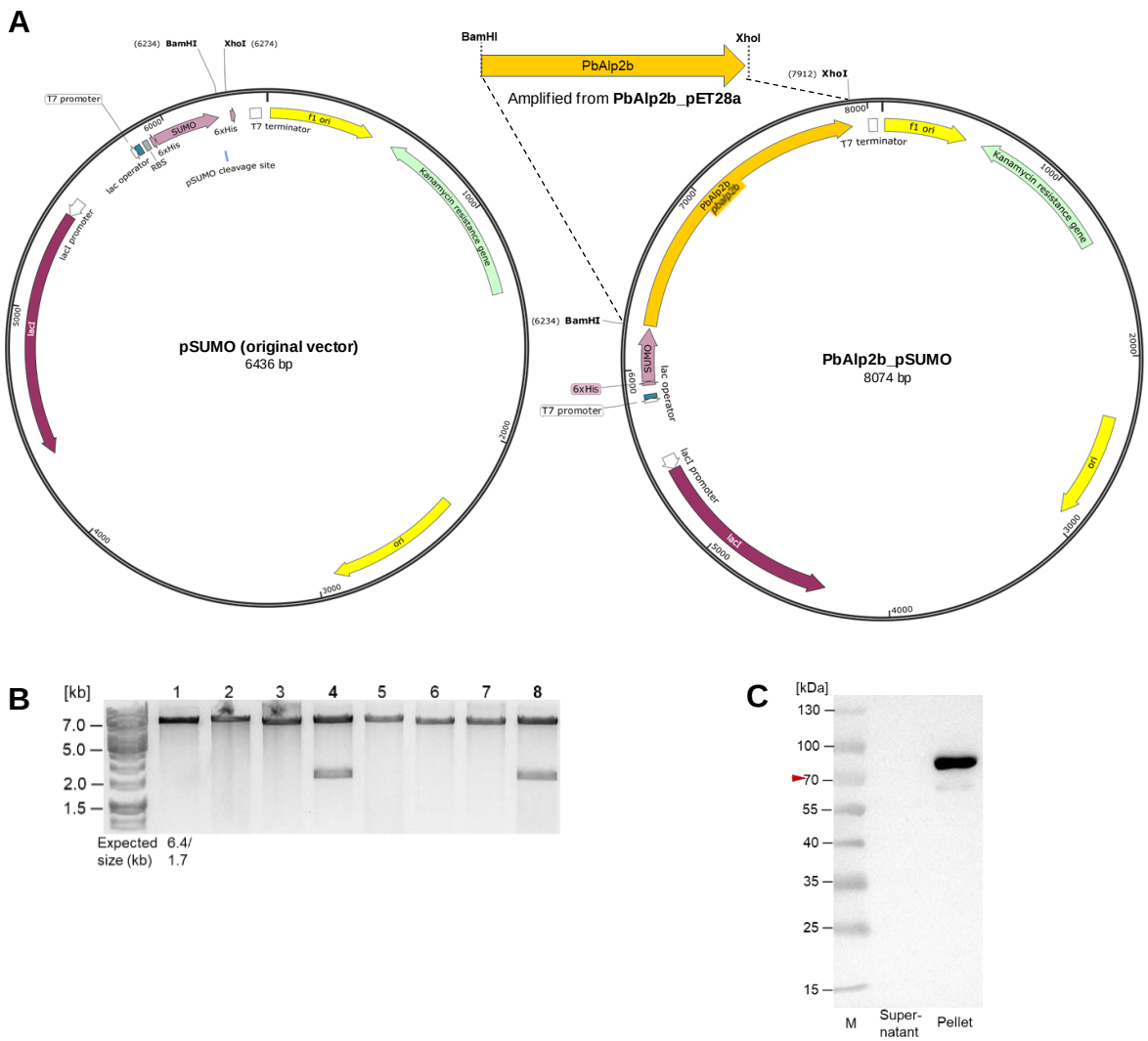

Figure 21: Plasmid maps and cloning test digestion of PbAlp2b_pSUMO and solubilisation test results. (A) *pbalp2b* was amplified via PCR from the PbAlp2b_pET28a (**Figure 18A**) vector and cloned into the pSUMO vector backbone (top left) using BamHI and XhoI restriction sites. Upon integration, *pbalp2b* was positioned downstream of 6x histidine tag and SUMO protein, enabling a production of tag-free PbAlp2b in the downstream processing (top right). The pSUMO plasmid drives the expression of the target via T7 promoter and carries a kanamycin resistance gene for drug selection, as well as a *LacI* gene encoding the lac repressor protein to regulate target gene expression. **(B)** The agarose gel of the test digestion with BamHI and XhoI (below) verifies the correct integration of *pbalp2b*. The clone number 4 was confirmed by Sanger sequencing and subsequently used for the expression and solubilisation tests. **(C)** The α-his tag western blot of the expression and solubilisation tests showed that the expression of PbAlp2b was moderately increased in the presence of SUMO tag, although the solubilisation of PbAlp2b was unsuccessful. M = marker. The red arrow indicates the target size (70 kDa) of SUMO-PbAlp2b.

3.1.2.3 Summary of the heterologous overexpression of PbAlp2b in *E. coli*

PbAlp2b was stably expressed in *E. coli* BL21 using pET28a vector. However, to prevent degradation, the protein had to be extracted within four hours following the induction. The reduced expression level and the sensitivity of PbAlp2b may be attributed to the non-codon-optimised DNA sequence. The anticipated enhancement was, however, not achieved through the co-expression of rare-codon tRNAs. The greatest challenge presently faced in

the production of recombinant PbAlp2b is to achieve a soluble state without compromising the structural integrity of the protein. Although the use of a potent detergent such as FC12 has been demonstrated to be an effective method for solubilisation, the excessive application may result in irreversible degradation. The data collected (**Table 3**) suggests that the primary area for optimisation may be the expression level, with the aim of obtaining a sufficient quantity of PbAlp2b to overcome the issue of low solubility or loss during detergent solubilisation. This could be accomplished through codon optimisation or by exploring alternative expression systems, such as insect cells.

Table 3: Overview of the tested conditions for the production of recombinant PbAlp2b. pRAREII (rare tRNA expressing plasmid); Chaperone set KJE8 (DnaK, DnaJ, GrpE, GroES, GroEL); LDAO (Lauryldimethylamine oxide); FC12 (Fos-choline-12); DM (Decylmaltoside); OG (Octyl-beta-Glucoside); CHAPs (3.-{Dimethyl [3-(3α,7α,12α-trihydroxy-5β-cholan-24-amido)propyl]azaniumyl} propane-1-sulfonate); Ni-NTA (Nickel-nitrilotriacetic acid)

Protein	*E. coli* strain	Vector	Solubilisation method	IMAC column/treatment	Expression	Solubilisation	Purification
Alp2b	BL21	pET28	Buffer only	Ni-NTA			
			pRARE II				
			Chaperone (KJE8)				
			LDAO + Chaperone (KJE8)				
			FC12				
			FC12 + Chaperone (KJE8)				
			DM + Chaperone (KJE8)				
			OG				
			CHAPs + Chaperone (KJE8)				
		pSUMO	Buffer only				
			FC12				
			LDAO				
	C41	pET28	Buffer only				
	C43						
	KRX						
	LOBSTR						
			LDAO				

High
Low
Negligible

3.2 Characterisation of Alp1 in *Plasmodium berghei*

Motility is a fundamental requirement for the survival of numerous parasites, including *Plasmodium*. The actin-like protein 1 (Alp1) plays a vital role in facilitating ookinete motility and reducing the mosquito midgut infection in *Plasmodium berghei* (Binder, 2020). This section presents detailed investigations into the functional relevance of Alp1 to the biology of *Plasmodium* and their molecular motor mechanism, which serve to illustrate the importance of this unique protein.

3.2.1 Phenotypic impact of PbAlp1 knock-out and cross-species complementation

In this study, Alp1 of *Plasmodium berghei* (PbAlp1) was either fully removed or replaced with *P. falciparum* Alp1 (PfAlp1) to observe its phenotypic effect on the parasite.

3.2.1.1 Generation of PbAlp1 full knock-out and complementation parasite lines

PbAlp1 full knock-out

In the initial study conducted by Binder (2020), *Plasmodium berghei alp1* (*pbalp1*) gene was knocked out (KO) using a PlasmoGEM vector (Gomes et al., 2015) (**Supplement 3**). This resulted in the removal of approximately 64% of the cDNA, leaving the C-terminus part of the protein. The impact of the KO was evident; however, the possibility of the residual part of the gene still being functionally active could not be dismissed. Thus, in order to fully characterise the phenotypic effects of PbAlp1 KO, a full KO construct was generated (**Figure 22A,B**).

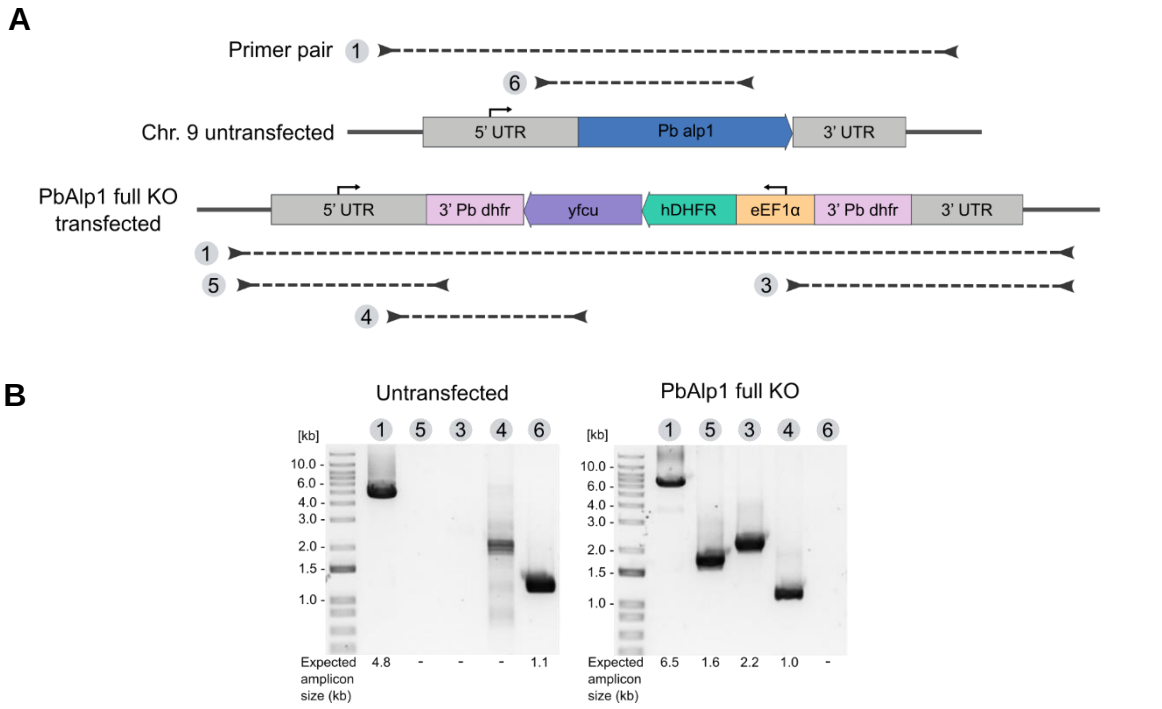

Figure 22:Transfection scheme of PbAlp1 full knock-out and the final genotyping result. (A) The entire *alp1* gene of wild-type *P. berghei* was replaced by the drug selection cassette via homologous recombination of the 5' and 3' UTRs of *pbalp1*. The selection cassette, which carries *hDHFR* and *yfcu* under the eEF1α promoter, allows for positive and negative selections, respectively. The presence of identical sequences of 3' Pb *dhfr* functions as a terminator as well as a recombination site for the negative selection. The small arrow indicates a promoter function. **(B)** The genotyping agarose gels of the isogenic KO parasites and the untransfected control confirm the successful generation of the target clone. The circled number and a dotted line indicate the primer pair used and its coverage for the genotyping. The reverse primer in the primer pair '5' partially binds to the construct backbone, therefore specific. UTR (untranslated region); 3' Pb *dhfr* (3' untranslated region of *P. berghei* dihydrofolate reductase); *hDHFR* (human dihydrofolate reductase); *yfcu* (yeast cytosine deaminase-uracil phosphoribosyl transferase); eEF1α (eukaryotic translation elongation factor 1 alpha).

PbAlp1 complementation – genotyping

To verify the phenotypic effects of PbAlp1 KO, complementation of *pbalp1* into the KO locus was performed. The complementation construct was previously generated and transfected by Binder (2020) (**Figure 23A**). For phenotypic characterisation, an isogenic line was obtained via limiting dilution and confirmed by a genotyping PCR (**Figure 23B**).

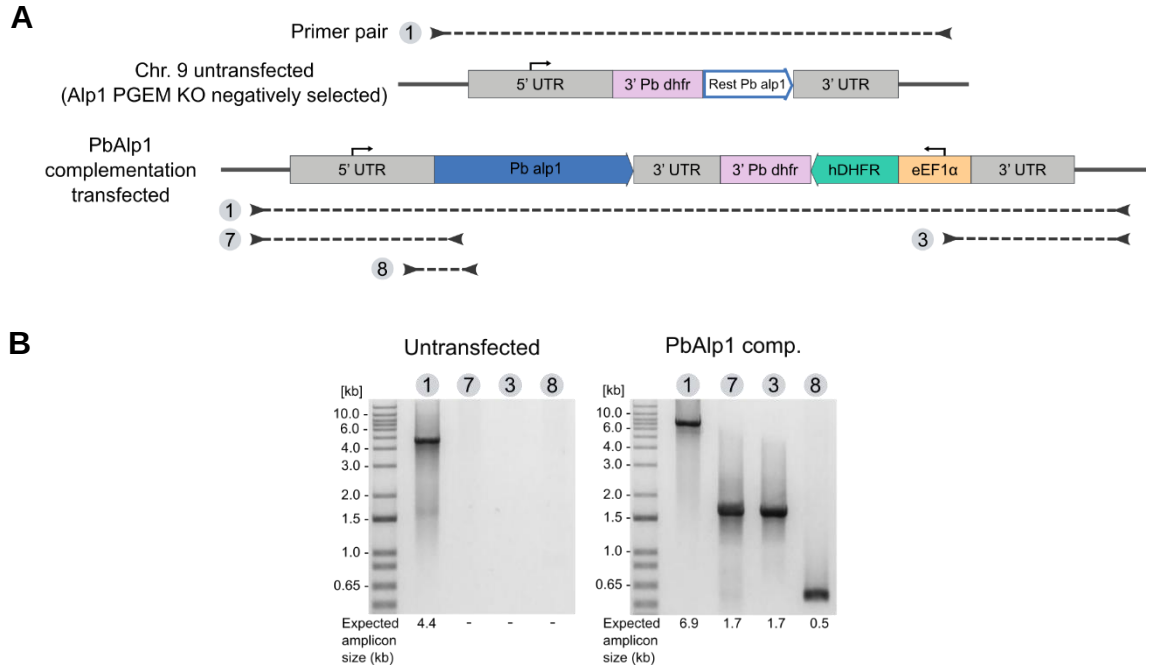

Figure 23: Transfection scheme of PbAlp1 complementation and the final genotyping result. (A) *pbalp1* was complemented into the negatively selected PlasmoGEM KO locus along with the positive selection cassette (*hDHFR*). The PlasmoGEM PbAlp1 KO, negative selection and the PbAlp1 complementation lines were generated by Binder (2020) (**Supplement 3**). The small arrow indicates a promoter function. **(B)** The genotyping agarose gels of the isogenic PbAlp1-complemented parasites and the untransfected control confirm the successful generation of the target clone. The circled number and a dotted line indicate the primer pair used and its coverage for the genotyping. UTR (untranslated region); 3' Pb *dhfr* (3' untranslated region of *P. berghei* dihydrofolate reductase); *hDHFR* (human dihydrofolate reductase); eEF1α (eukaryotic translation elongation factor 1 alpha).

PfAlp1 complementation

In addition to the full KO and complementation studies, the cross-species conservation of Alp1 was investigated by complementing *Plasmodium falciparum* Alp1 in *P. berghei*. The importance of studying the functional conservation of Alp1 between these species not only seeks the translational potential of our current research model for the human pathogenic species, but also allows genus-level investigation of the protein function. The general genomic structures of *P. berghei Alp1* and *P. falciparum Alp1* are similar. At the protein level, both molecules are composed of 378 amino acids, sharing 76% sequence identity and are predicted to have highly similar structures (**Figure 24A**). To increase the chance of intact expression of PfAlp1 in *P. berghei*, the cDNA sequence of *pfalp1* was used for this complementation to bypass the splicing process. The background parasite line (PbAlp1 full KO) was negatively selected by a 5FC treatment to remove the remaining selection cassette from the previous modification step (**Figure 24B**). The construct carrying *pfalp1* cDNA was then transfected into the same locus through homologous recombination (**Figure 24C**). Genotyping PCR was performed at each transfection step to confirm target gene integration and isogeneity of the parasite line (**Figure 24D,E**).

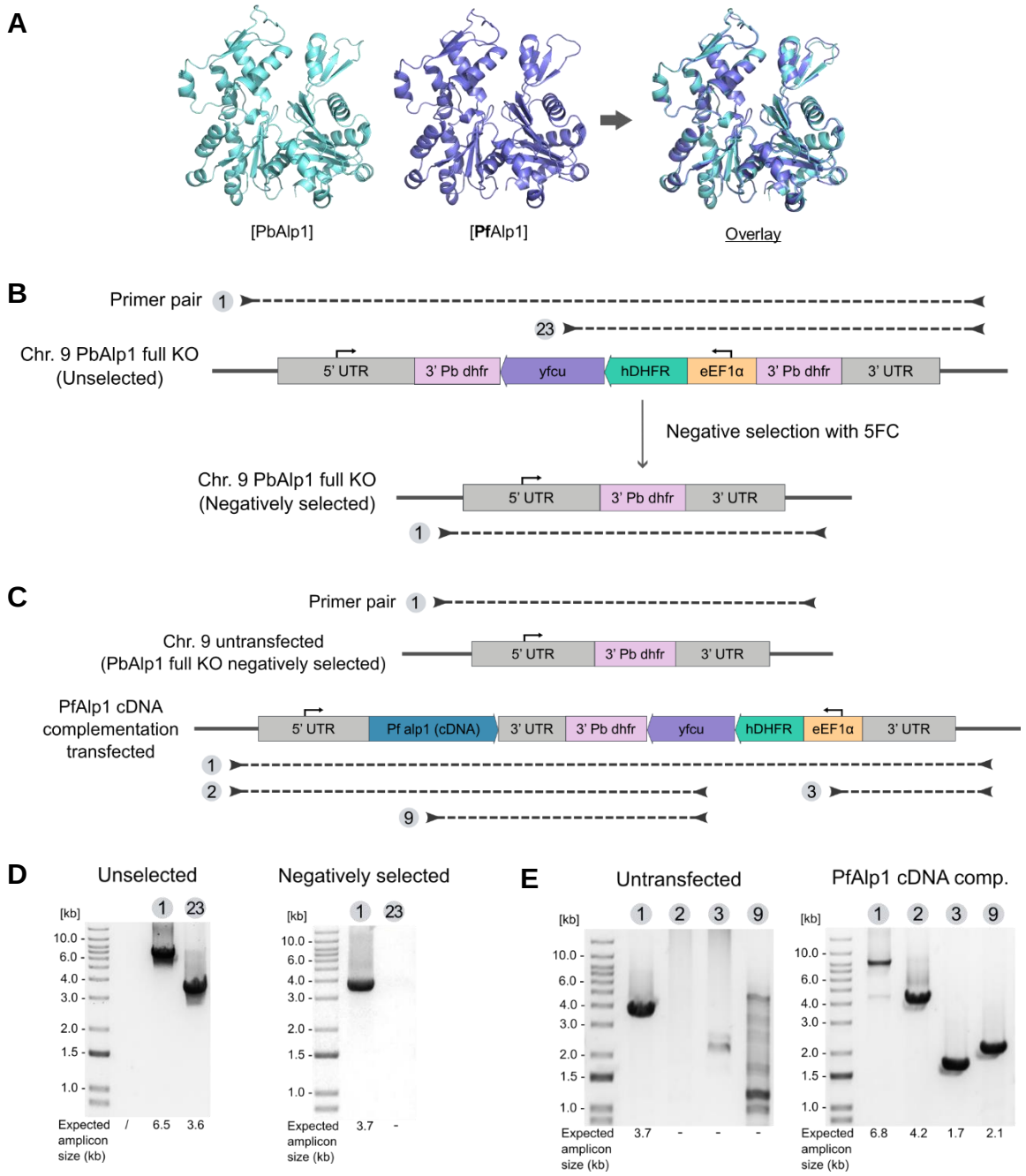

Figure 24: Transfection scheme of PfAlp1 complementation and the final genotyping result. (A) The AlphaFold-predicted structures of *P. berghei* Alp1 and *P. falciparum* Alp1, with the overlay structure, demonstrate the high degree of similarity between their protein structures. **(B)** Negative selection was performed on the PbAlp1 full KO line to remove the selection cassette from the target locus for subsequent PfAlp1 complementation study. **(C)** pfalp1 cDNA was transfected into the *P. berghei alp1* KO locus through homologous recombination. The expression of *pfalp1* was initiated by the native *pbalp1* promoter. The small arrow indicates a promoter function. **(D)** The genotyping agarose gels of the pre- and post-negative selection parasites and **(E)** the *pfalp1* cDNA complemented parasites with untransfected control confirm the successful generation of the target clones. The circled number and a dotted line indicate the primer pair used and its coverage for the genotyping. UTR (untranslated region); 3' Pb *dhfr* (3' untranslated region of *P. berghei* dihydrofolate reductase); *hDHFR* (human dihydrofolate reductase); *yfcu* (yeast cytosine deaminase-uracil phosphoribosyl transferase); eEF1α (eukaryotic translation elongation factor 1 alpha); 5FC (5-fluorocytosine).

3.2.1.2 Complete absence of Alp1 caused a modest delay in blood stage growth

The *in vivo* multiplication rates of the Alp1 KO and complemented *P. berghei* were determined following the injection of a single parasite into a naïve mouse. The parasite lacking Alp1 displayed a slight delay in asexual growth, with an approximate 8-fold increase per 24 hours, when compared to the PbAlp1 complementation control line generated in this study (**Figure 25A**). A spectrum of growth rates was observed in the PfAlp1 complemented parasites, which showed a pattern resembled either wild-type or Alp1 KO. The progression of parasitaemia of a wild-type-like parasite typically exhibited a sharp increase after reaching approximately 1%, as observed in the control (PbAlp1 comp.) parasites (**Figure 25B**). In contrast, the PbAlp1 KO parasites displayed a delayed onset of infection and appeared to slow down or struggle to grow around the 1% parasitaemia threshold. A comparable growth phenotype was also observed in the PbAlp1 partial KO line (Binder, 2020), suggesting that the residual C-terminus DNA sequence does not influence the blood stage growth. In the PfAlp1-complemented parasites, two of the clones showed continued rapid growth after reaching 1%, while the rest had difficulty progressing, as observed in the KO parasites. The results indicate that Alp1 plays a minor role in maintaining parasite blood stage growth, although it is not a critical factor.

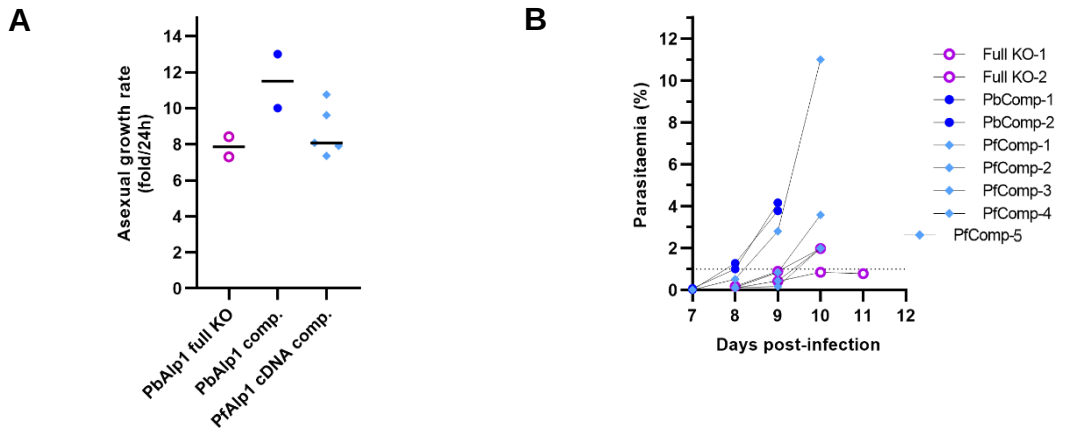

Figure 25: Blood stage growth comparison between the PbAlp1 knock-out (KO) and complemented (comp.) lines. (A) The *in vivo* multiplication rates of the asexual parasites in mice reveal a moderate growth delay of PbAlp1 KO parasites in comparison to the control PbAlp1 complemented line. The PfAlp1 complemented parasites partially displayed growth rates comparable to those of the PbAlp1 complemented line, while the remainder exhibited a growth delay. **(B)** Parasites that exhibited a delayed asexual growth rate appeared to encounter difficulties in maintaining progression after reaching approximately 1% parasitaemia (indicated by a dotted line). The mixed growth rates of PfAlp1-complemented parasites were also evident in their progression behaviour. KO (knock-out); comp. (complementation).

3.2.1.3 Alp1 is not required for ookinete development, but essential for motility

Despite the moderate delay in asexual growth, the Alp1 KO parasites were viable during the blood-stage of their life cycle and capable of forming gametocytes and exflagellating. To gain further insight into the potential impact of this growth phenotype on ookinete development, *ex vivo* ookinete cultures were set up. Following a 21-hour incubation period,

the parasites were purified and quantified according to their developmental stages (**Figure 26A,B**). In the quantification, both fertilised and unfertilised macrogametes were grouped under the same category as 'macrogamete/zygote', and the intermediate stages (early-, mid-, late-retort) before mature ookinete were categorised as 'retort' in general, in order to make a clearer visualisation of the number of ookinetes in development. Additionally, the PbAlp1 partial KO line generated by Binder (2020) was included in the assay for comparative purposes. In the wild-type (WT) population, the maturity rate of ookinetes among the sexual stage parasites was approximately 85%, with around 5% of retorts. The percentage of mature ookinetes was reduced to approximately 70% in both partial and full KO of PbAlp1. Although statistically significant, these differences are considered to be within the biological range. Importantly, the same level of ookinete maturation between the full and partial KO demonstrated that the residual Alp1 C-terminus does not play a role. Moreover, as expected from the KO results, no significant difference was observed between the WT and the PfAlp1 complemented ookinetes, indicating that Alp1 plays a minor role in asexual growth but is not essential for ookinete development.

The absence of Alp1 did not affect the maturation of ookinetes; however, it was found to have a critical impact on their motility (**Figure 26C**). The number of motile ookinetes, defined as individuals that are able to perform forward gliding motions for a minimum of one parasite length over a period of 15 minutes, was quantified using a 2D motility assay in each Alp1 KO and complementation population. In optimal conditions, motile ookinetes were capable of gliding at a speed of 3 to 8 µm per minute, potentially reaching even higher speed in our experimental setup (**Figure 26D**). Notably, over 99% of the partial KO and 100% of the full Alp1 KO ookinetes were classified as immotile, with many of them exhibiting a twitching type of motion or remaining completely still. The same phenotypic effects were observed in the PfAlp1 complemented population, which still retained a small population of weakly motile ookinetes with less than 2 µm per minute migration speed, representing less than 5% of the total. The strongly reduced motility and the compromised gliding speed demonstrated that the complementation of *P. falciparum alp1* cDNA in *P. berghei* was unable to replace PbAlp1. Given that healthy motile ookinetes typically exhibit vigorous gliding motility (**Figure 26E**), the impaired movement of KO parasites points to a critical function of Alp1 in facilitating *Plasmodium* gliding motility.

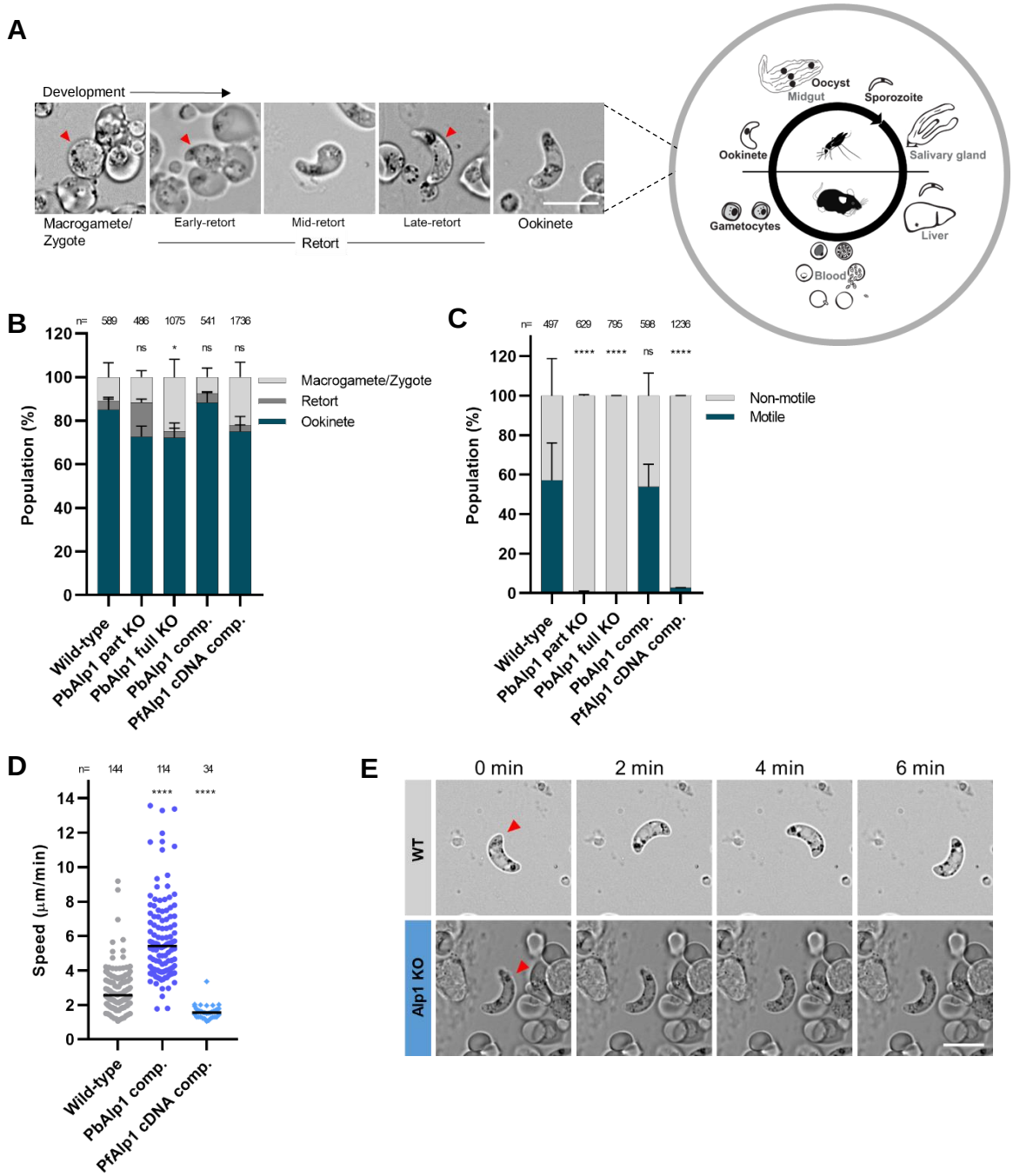

Figure 26: Effects of Alp1 KO and PfAlp1 complementation on ookinetes. (A) The life cycle of *P. berghei* and its developmental stages of ookinete. Life cycle figure was adapted from Douglas et al., (2018). **(B)** The quantification of mature ookinetes in the Alp1 KO and complemented populations revealed no biologically significant difference, thereby demonstrating that Alp1 does not play a role in ookinete development. The statistical analysis represents a level of significance against the wild-type mature ookinetes (Fisher's exact test, two-sided, ns = non-significant, * = P ≤ 0.05). **(C)** Quantification of motile ookinetes in the Alp1 KO and complemented populations demonstrated that Alp1 is essential for facilitating ookinete motility. Complementation with PfAlp1 did not rescue *P. berghei* ookinete motility. The statistical analysis represents a level of significance against the wild-type motile ookinetes (Fisher's exact test, two-sided, ns = non-significant, **** = P ≤ 0.0001). **(D)** An analysis of the gliding speeds of motile ookinetes indicates that the motility of the PfAlp1-complemented ookinetes is significantly compromised in comparison to the wild-type. From a biological perspective, however, this represents a relatively minor reduction. The higher speed of PbAlp1 complemented ookinetes may be due to an improvement in the researcher's sample handling, and thus unlikely to be a phenotype. The statistical analysis represents a level of significance against the wild-type (Mann-Whitney test, two-sided, **** = P ≤ 0.0001). **(E)** Typical motion types of wild-type (WT) and Alp1 KO ookinetes. WT ookinetes typically perform either circular or linear gliding motility. In contrast, Alp1 KO ookinetes showed a twitching back-and-forth motion or remained entirely still. The red arrow indicates the parasite in question. Scale bar = 10 µm. KO (knock-out); comp. (complementation).

3.2.2 Cellular localisation of Alp1 in *P. berghei*

The critical motility phenotype of Alp1 KO ookinetes provides compelling evidence for the involvement of Alp1 in the operation of locomotive machineries in the parasite. Elucidating the cellular localisation of Alp1 provides a deeper understanding of the protein's function and establishes further evidence for its potential mechanism of action and interaction partners. This study analyses the localisation of Alp1 in *P. berghei* through fluorescence microscopy by tagging the protein with enhanced green fluorescent protein (EGFP) and a 3x hemagglutinin (HA) tag.

3.2.2.1 Generation of EGFP-PbAlp1 and PbAlp1-3xHA parasite lines

EGFP-PbAlp1 endogenous tagging

EGFP is a 27 kDa fluorescent protein that is commonly utilised for the visualisation of proteins in *in vivo* localisation studies. It has successfully visualised actin in *P. berghei* (Angrisano et al., 2012) and Alp1 in *T. gondii* (Gordon et al., 2009, 2008). The use of EGFP in this assay offers the advantage of enabling live localisation studies of Alp1 in motile cells. The endogenous PbAlp1 was N-terminally tagged with an EGFP with an AAAAEFAAAA linker. The EGFP-Alp1 construct with a full selection cassette was transfected into the negatively-selected locus of the PbAlp1 partial KO parasites (**Figure 27A, Supplement 3**). Following the transfection, isogenic cells were selected and the integration of the target gene was confirmed by a genotyping PCR (**Figure 27B**). Furthermore, the expression of EGFP-tagged PbAlp1 was verified through α-GFP western blot analysis with protein of approximately $6x10^6$ blood stage parasites (**Figure 27C**). No conclusive band was detected at the anticipated molecular weight of EGFP-PbAlp1 (69 kDa). Instead, a faint band was observed at approximately 25 kDa, which could be indicative of the cleavage of the EGFP tag. Seeing also that the ookinetes in the subsequent test culture exhibited defective motility (**Figure 27D**), this tagging strategy was not pursued further.

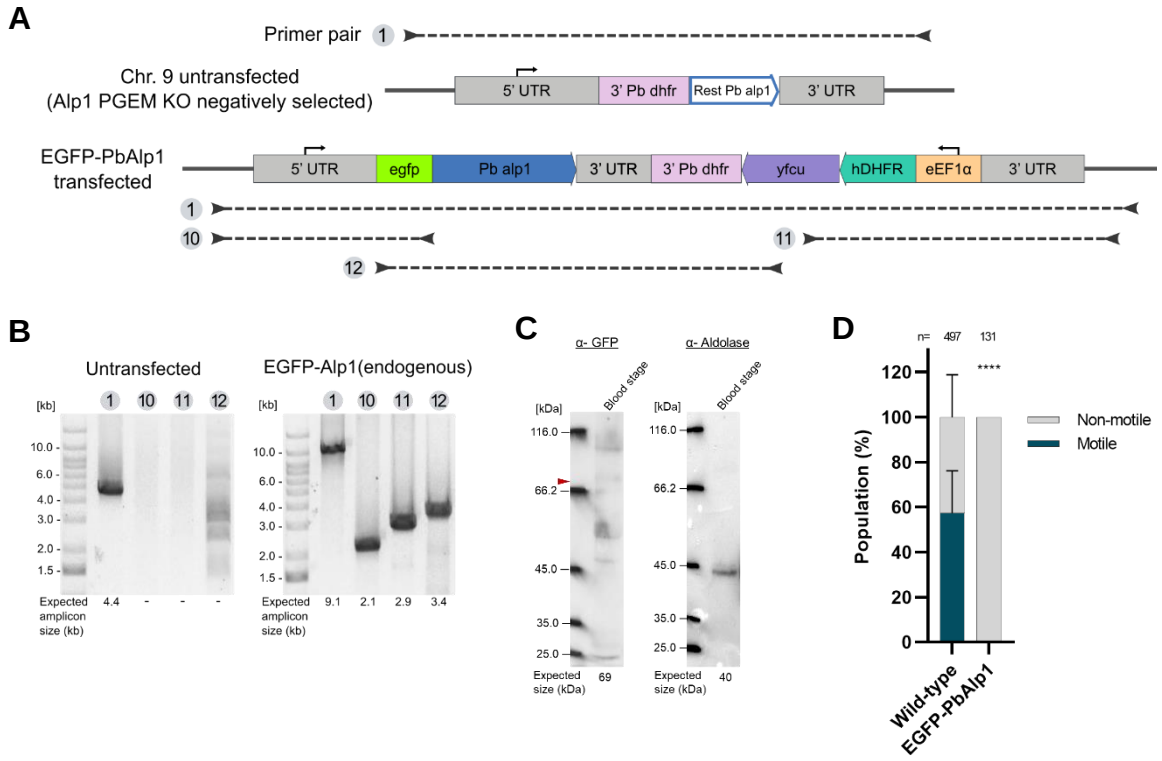

Figure 27: Transfection scheme of EGFP-PbAlp1 (endogenous) and the final expression and ookinete phenotype. (A) The negatively-selected locus of PbAlp1 partial KO was transfected with the EGFP-PbAlp1 construct via homologous recombination of the 5' and 3' UTRs of pbalp1. The selection cassette, which carries *hDHFR* and *yfcu* under the eEF1α promoter, allows for positive and negative selections, respectively. For the potential negative selection, the two identical segments of *pbalp1* 3' UTR act as the recombination site. The small arrow indicates a promoter function. **(B)** The genotyping agarose gels of the isogenic EGFP-PbAlp1 (endogenous) parasites and the untransfected control confirm the successful generation of the target clone. The circled number and a dotted line indicate the primer pair used and its coverage for the genotyping. **(C)** The α-GFP western blot (left) with protein of 6x10⁶ blood stage parasites revealed no expression of EGFP-PbAlp1 (69 kDa). Conversely, a faint band at approximately 25 kDa may indicate a cleavage of the EGFP tag. The α-aldolase blotting of the same membrane serves to validate the quality of the sample. The red arrow indicates the target size (69 kDa) of EGFP-PbAlp1. **(D)** The ookinetes with EGFP-tagged Alp1 showed non-motile phenotype. The statistical analysis represents a level of significance against the wild-type motile ookinetes (same data set as **Figure 26C**) (Fisher's exact test, two-sided, **** = P ≤ 0.0001). UTR (untranslated region); 3' Pb *dhfr* (3' untranslated region of *P. berghei* dihydrofolate reductase); *hDHFR* (human dihydrofolate reductase); *yfcu* (yeast cytosine deaminase-uracil phosphoribosyl transferase); eEF1α (eukaryotic translation elongation factor 1 alpha).

EGFP-PbAlp1 additional copy

The lack of expression and the defective motility of the endogenously-tagged EGFP-PbAlp1 parasites may indicate the sensitivity of this protein to manipulation. In order to maintain the function of the endogenous Alp1, a copy of *egfp-pbalp1* was additionally introduced into wild-type *P. berghei*. The same strategy was previously used to successfully visualise *Plasmodium* actin (Angrisano et al., 2012). The identical construct utilized for the endogenous tagging was used to introduce *egfp-pbalp1* to chromosome 12, which differs from the endogenous PbAlp1. This was achieved through homologous recombination of the 5' and 3' UTR sequences of the target integration site (**Figure 28A**). The genotyping agarose gel after transfection and limiting dilution (**Figure 28B**) revealed the presence of two amplicons at 9.7 kb and 1.6 kb in the whole locus (⑬) PCR product of the transfected line. The larger band represents the target locus with the correctly integrated construct, while the smaller band indicates the empty, untransfected target locus. The presence of additional integration-specific bands (⑭, ⑮ and ⑫) confirmed that the population consisted of both correctly transfected parasites (EGFP-PbAlp1 additional copy) and parasites with either no transfection (wild-type) or an incorrectly integrated construct to the endogenous Alp1 locus. Despite repeated transfections and limiting dilutions, the target clone could not be isolated. Nevertheless, to examine the intact expression of EGFP-PbAlp1, an α-GFP western blot analysis was conducted using approximately $2.6x10^4$ purified ookinetes and $7x10^6$ blood stage parasites (**Figure 28C**). As with the previous experiment, no expression of EGFP-PbAlp1 was detected, despite the α-aldolase control indicating sufficient amount of blood stage parasites. Assuming that intact EGFP-PbAlp1 were still correctly expressed, it is possible that the mixed population of blood stage parasites contained an insufficient amount of the protein. However, given the relatively higher expression of Alp1 during the blood stage (Howick et al., 2019), the complete absence of EGFP-PbAlp1 may rather indicate a critical inhibitory effect of this tag on the initiation of the expression process.

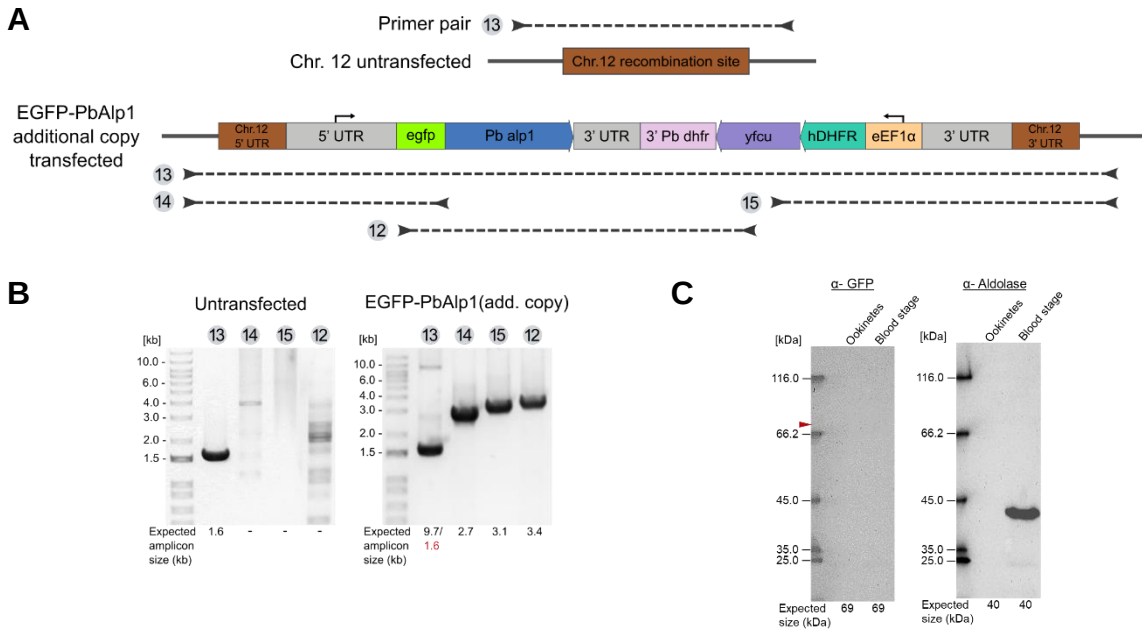

Figure 28: Transfection scheme of EGFP-PbAlp1 (additional copy) and the final genotyping and expression results. (A) The EGFP-PbAlp1 construct was transfected into the chromosome 12 of the wild-type parasite via homologous recombination of the 5' and 3' UTR sequences of the target integration site. The selection cassette, which carries *hDHFR* and *yfcu* under the eEF1α promoter, allows for positive and negative selections, respectively. For the potential negative selection, the two identical segments of *pbalp1* 3' UTR act as the recombination site. The small arrow indicates a promoter function. **(B)** The genotyping agarose gel of the limiting dilution-selected EGFP-PbAlp1 (additional copy) parasites showed that the final population consisted of a mixture of correctly transfected and untransfected wild-type parasites, as well as endogenously transfected parasites (due to incorrect recombination). Despite repeated attempts at multiple transfections and limiting dilutions, the isogenic EGFP-PbAlp1 additional copy line could not be obtained. The amplicon size highlighted in red indicates the size of the untransfected chromosome 12. The circled number and a dotted line indicate the primer pair used and its coverage for the genotyping. **(C)** The α-GFP western blot (left) using $2.6x10^4$ ookinetes and $7x10^6$ blood stage parasites showed no signals for EGFP-PbAlp1 (69 kDa). It can be inferred from the α-aldolase control that the amount of ookinete sample was insufficient. In addition, it is presumed that the mixed population of blood stage parasites contained an insufficient amount of EGFP-PbAlp1, or the expression was inhibited. The red arrow indicates the target size (69 kDa) of EGFP-PbAlp1. UTR (untranslated region); 3' Pb *dhfr* (3' untranslated region of *P. berghei* dihydrofolate reductase); *hDHFR* (human dihydrofolate reductase); *yfcu* (yeast cytosine deaminase-uracil phosphoribosyl transferase); eEF1α (eukaryotic translation elongation factor 1 alpha).

PbAlp1-3xHA additional copy

A further approach was made to tag PbAlp1 as an additional copy. In the previous attempt, the expression of EGFP-PbAlp1 was not successfully detected. This may be attributed to the EGFP tag sequence impeding protein expression, or alternatively, the instability of the N-terminus EGFP resulting in accelerated degradation of expressed Alp1. The EGFP tag is a prevalent strategy for live cell localisation studies. However, its relatively large size could also affect the dynamics of the tagged protein (Montecinos-Franjola et al., 2020). In order to mitigate the observed effects of tagging, a 3xHA tag was selected to tag the C-terminus of PbAlp1. The 3xHA tag is a 3 kDa epitope tag that is frequently employed for the visualisation of proteins through immunofluorescence staining. PbAlp2b, a member of the same protein family as PbAlp1, was previously tagged with a 3xHA tag at the C-terminus and could be expressed in its intact form, as demonstrated by Mikus (2020). Additionally,

the linker sequence AKIGSGG, adapted from Stortz et al., (2019), was implemented to enhance flexibility. Moreover, an extension of approximately 500 bp was incorporated at each end of the chromosome 12 homology arms (**Figure 29A**), with the objective of enhancing the efficiency of target site recombination. The construct was integrated into the chromosome 12 of wild-type *P. berghei* and successfully selected for the isogenic line (**Figure 29B**). The expression of intact PbAlp1-3xHA was confirmed by α-HA western blot analysis with protein of 1x10⁷ blood stage parasites, 17x10⁴ (I) and 24x10⁴ (II) ookinetes (**Figure 29C**). Furthermore, the western blood analysis highlighted that a minimum of 24×10⁴ ookinetes are necessary for adequate detection on a blot. Importantly, this tagging strategy did not result in any discernible phenotypic impacts on either the asexual growth rate or the motile ookinete population (**Supplement 4**), demonstrating that endogenous Alp1 is fully functional and was not affected by the additional expression of PbAlp1-3xHA.

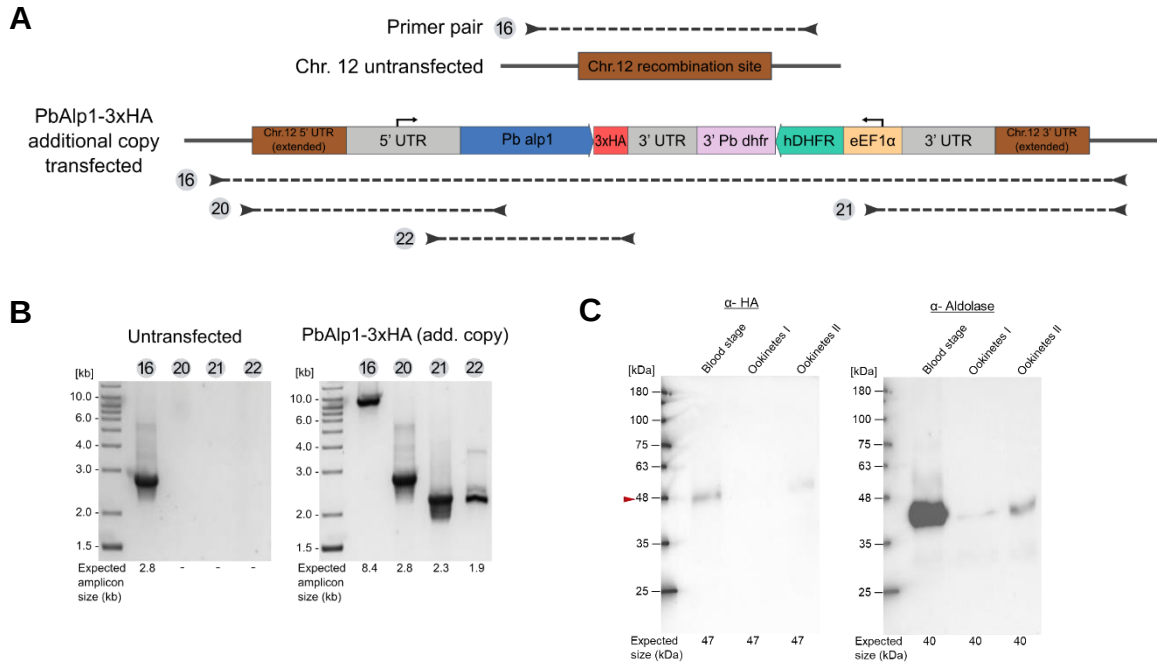

Figure 29: Transfection scheme of PbAlp1-3xHA (additional copy) and the final genotyping and expression result. (A) The PbAlp1-3xHA construct was transfected into the chromosome 12 of wild-type parasites via homologous recombination of the 5' and 3' UTR sequences of the target integration site. To enhance the efficiency of recombination, the homology arms were extended to approximately 1000 bp. The selection cassette, which carries *hDHFR* under the eEF1α promoter, enables positive selection. The outer 3' UTR of *pbalp1* serves as a 3' homology arm when this construct is introduced into the endogenous *pbalp1* locus. The small arrow indicates a promoter function. **(B)** The genotyping agarose gels of the isogenic PbAlp1-3xHA (additional copy) parasites and the untransfected control confirm the successful generation of the target clone. The circled number and a dotted line indicate the primer pair used and its coverage for the genotyping. **(C)** The α-HA western blot (left) with protein of 1x10⁷ blood stage parasites, 17x10⁴ (I) and 24x10⁴ (II) ookinetes confirmed the intact expression of PbAlp1-3xHA with the target band at 47 kDa. The α-aldolase blotting of the same membrane serves to validate the quality of the sample, indicating that a minimum of 24x10⁴ ookinetes are required for a western blot analysis. The red arrow indicates the target size (47 kDa) of PbAlp1-3xHA. UTR (untranslated region); 3' Pb *dhfr* (3' untranslated region of *P. berghei* dihydrofolate reductase); *hDHFR* (human dihydrofolate reductase); eEF1α (eukaryotic translation elongation factor 1 alpha).

3.2.2.2 PbAlp1-3xHA localisation was observed throughout the cytoplasm

Immunofluorescence (IF) staining of the 3xHA tag was performed to observe the localisation of Alp1 in *P. berghei* at different developmental stages, utilising the above described PbAlp1-3xHA additional copy line. The comparison across the different developmental stages demonstrates the parasite-specific fluorescent signals, while the unstained control confirms minimal background autofluorescence (**Figure 30A)**. A detailed analysis of the localisation signal was conducted on the ookinete stage, where Alp1 exhibited a critical for the parasite's motility. In general, two distinct signal types were observed in ookinetes (**Figure 30B**). The predominant type of signal appeared slightly aggregated and speckled, while a smaller number of cells exhibited a smooth and more diffuse signal (**Figure 30C**). Both were observed to be present throughout the cell, with no discernible sublocalisation identified. This may suggest that Alp1 primarily operates in the cytoplasm. However, given the sensitivity of Alp1 as shown through the EGFP tagging, this additional copy approach still cannot exclude the possibility of mislocalisation due to 3xHA-tagging. Therefore, this result alone is not yet sufficient to draw a definitive conclusion regarding any specific contribution of Alp1 to the parasite's motility.

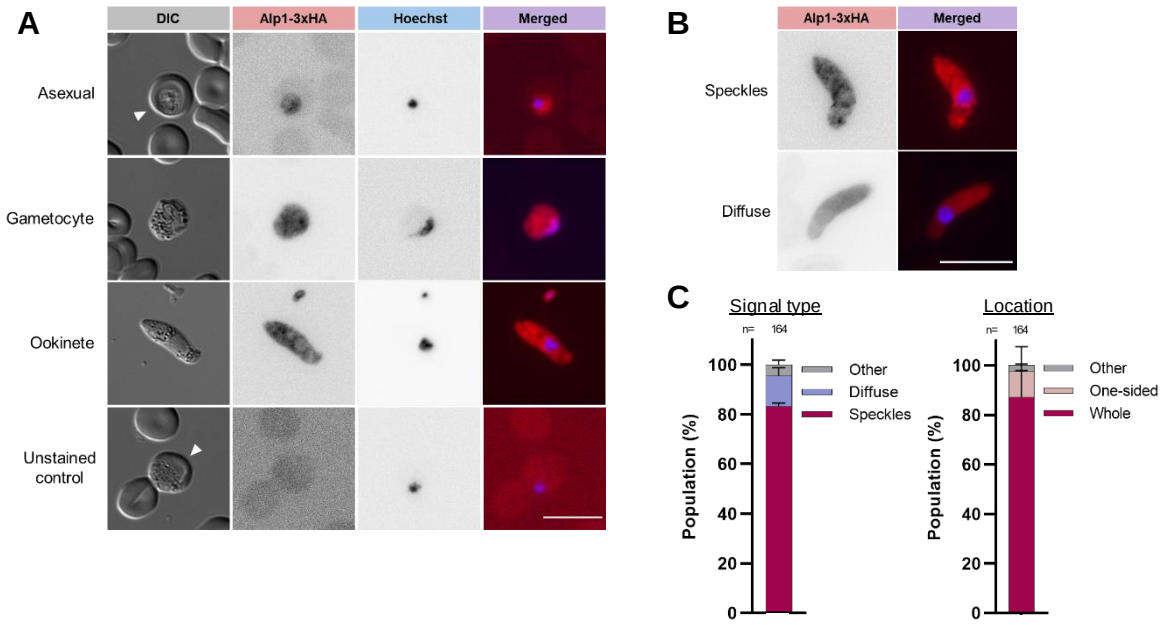

Figure 30: Immunofluorescence staining of PbAlp1-3xHA and its localisation in ookinetes. (A) The IF-stained PbAlp1-3xHA was visualised in the parasites at different developmental stages. The red fluorescent dye (Alexa Fluor 594) represents Alp1-3xHA, while the blue dye (Hoechst) represents the nucleus. The unstained control demonstrates minimal background autofluorescence and the specificity of the IF stain. The white arrow indicates the parasite in question. Merged = overlay of PbAlp1-3xHA and Hoechst channels. **(B)** Two distinct PbAlp1-3xHA signal types were observed in ookinetes, and **(C)** the localisation patterns were quantified. In the majority of ookinetes, PbAlp1-3xHA was observed to be distributed throughout the cell, exhibiting a predominantly speckled signal pattern. DIC (differential interference contrast); HA (hemagglutinin). Scale bar = 10 µm.

A tag-free localisation of PbAlp1 was additionally attempted with two α-PbAlp1 antibodies (synthesised by Eurogentec) (**Supplement 5**). One of the custom antibodies (α-PbAlp1 epitope 2) demonstrated a binding affinity towards recombinant PbAlp1, yet did not exhibit the same affinity towards the actual parasite Alp1 in a western blot analysis. This could be attributed to the expression level of PbAlp1 or other *in vivo* factors that interfere with antibody binding.

Overall, this study has demonstrated the cytoplasmic localisation of PbAlp1 through the tagging of an additional gene copy. Nevertheless, further validation of the result is required.

3.2.3 *In vivo* visualisation of actin in Alp1 knock-out *P. berghei*

The deletion of Alp1 in *P. berghei* resulted in the complete inhibition of ookinete gliding motility, which is facilitated by glideosome, an actin-based motor machinery. Given that Alp1 is a member of the actin-related proteins (Arps) family, it is plausible that Alp1 is similarly involved in the regulation or functional association with actin. To assess whether the absence of Alp1 would impact the actin dynamics, an actin chromobody (ChromoTek) was used to visualise total actin in *P. berghei* ookinetes. The actin chromobody is a fluorescent protein-fused nanobody directed against actin. It has been successfully employed to visualise actin in apicomplexan parasites (Periz et al., 2017; Yee et al., 2022). This study reveals the distinct localisation of actin in wild-type ookinetes and demonstrates how this can be altered under the influence of actin modulating compounds and in the absence of PbAlp1, illustrating the potential interaction between Alp1 and actin.

3.2.3.1 Generation of PbAlp1 KO – actin chromobody parasite line

The actin chromobody construct generated by Yee et al., (2022) was introduced into chromosome 12 of the negatively selected PbAlp1 KO parasite line (**Figure 31A**). The actin-directing chromobody, coupled with an Emerald fluorescent protein, was expressed under the regulation of the *P. berghei* actin1 promoter, along with the dihydrofolate synthase (*pbdhfs*) terminator sequence. The correct integration of the target construct was confirmed by genotyping (**Figure 31B**). The Alp1 KO locus was also included in the genotyping PCR to verify the absence of the gene.

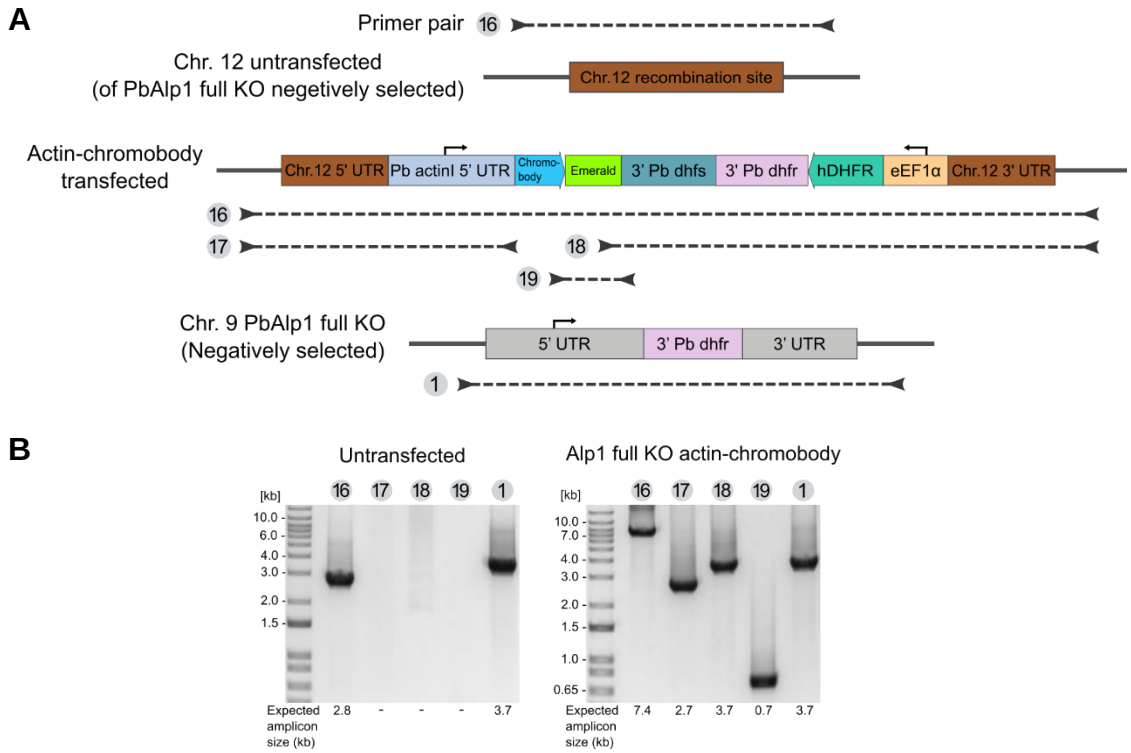

Figure 31: Transfection scheme of PbAlp1 KO - actin chromobody and the final genotyping result. (A) The actin chromobody-Emerald was integrated into the chromosome 12 of the PbAlp1 KO parasite line previously subjected to negative selection, together with the positive selection cassette (*hDHFR*). The PbActin1 promoter is responsible for the expression of the nanobody, while the 3' *pbdhfs* functions as a terminator. The small arrow indicates a promoter function. **(B)** The genotyping agarose gels of the isogenic PbAlp1 KO-actin chromobody parasites and the untransfected control confirm the successful generation of the target clone. The PbAlp1 KO locus was additionally genotyped to confirm the absence of the gene. The circled number and a dotted line indicate the primer pair used and its coverage for the genotyping. UTR (untranslated region); 3' Pb *dhfs* (3' untranslated region of *P. berghei* dihydrofolate synthase);3' Pb *dhfr* (3' untranslated region of *P. berghei* dihydrofolate reductase); *hDHFR* (human dihydrofolate reductase); eEF1α (eukaryotic translation elongation factor 1 alpha).

3.2.3.2. Expression of the actin chromobody does not compromise ookinete motility

The actin chromobody binds to actin filaments in a specific manner that preserves the fundamental dynamics of actin (Melak et al., 2017). The study of *P. berghei* sporozoites also demonstrated no significant impact on their motility patterns, with only minor effects on salivary gland invasion and motility speed (Yee et al., 2022). In this study, the impact of actin chromobody on ookinete motility was evaluated using a 2D assay previously outlined in **3.2.1.3**. A comparison of the motile population revealed that the actin chromobody-expressing ookinetes exhibited a higher percentage of motility than the wild-type (**Figure 32A**) and also showed a slightly faster migration speed (**Figure 32B**). Nevertheless, it seems unlikely that these statistically significant values truly reflect a genuine biological difference between the two ookinete populations. The results of this study demonstrate that actin chromobody does not negatively impact ookinete motility, indicating that actin dynamics are not measurably affected.

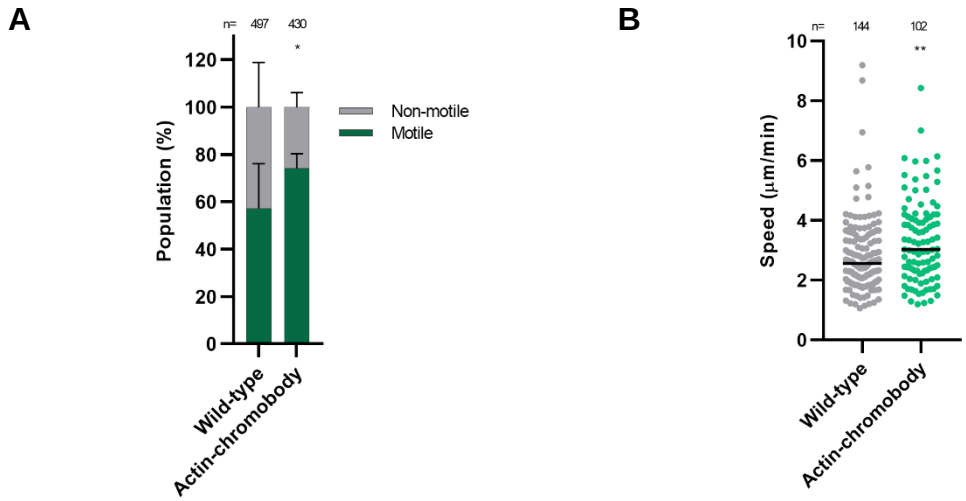

Figure 32: Effect of actin chromobody on ookinete motility. (A) Quantification of motile ookinetes in the actin chromobody and wild-type (same data set as **Figure 26C**) populations demonstrate that actin chromobody-expressing ookinetes are slightly more motile. The statistical analysis represents a level of significance against the wild-type motile ookinetes (Fisher's exact test, two-sided, * = P ≤ 0.05). **(B)** An analysis of the gliding speeds of motile ookinetes indicates that the motility of the actin chromobody-expressing ookinetes are significantly enhanced in comparison to the wild-type (same data set as **Figure 26D**). From a biological perspective, however, this represents a minimal effect. The statistical analysis represents a level of significance against the wild-type (Mann-Whitney test, two-sided, ** = P ≤ 0.01).

3.2.3.3 Alp1 is potentially involved in actin regulation

The actin chromobody-expressing *P. berghei* ookinetes with either a wild-type or an Alp1 KO background were chemically fixed and observed under a fluorescence microscope.

In both wild-type and Alp1 KO ookinetes, the chromobody-actin signal was predominantly observed as a whole cell structure comprising a combination of thick and finer tubules, or an almost mesh-like structure (**Figure 33**). The thick tubule was frequently observed to be positioned more posteriorly to the nucleus. It is noteworthy that these tubules occasionally exhibited a ring-like structure (**Supplement 6**), similar to that observed by Yee (2019). The function of the actin ring in ookinetes remains unknown. However, it may suggest a nucleus-associated role during development, as both wild-type and PbAlp1 KO ookinetes exhibited comparable numbers of the ring-like structure. Approximately 20% of the wild-type ookinetes exhibited chromobody-actin localisation at the nucleus, with half of these additionally displaying a tubular signal at either the anterior or posterior end. The observed variability in the location of the actin signal may suggest that it is susceptible to biological factors, such as parasite fitness, degree of maturation, or state of movement at the time of fixation.

In order to investigate the impact of altered actin filament dynamics on the observed actin localisation, the ookinetes were treated with 5 nM jasplakinolide (Jas) and 100 nM cytochalasin D (Cyto D). The actin filament stabiliser, Jas-treated ookinetes exhibited a

distinctive two-part localisation at the opposing tips of the cell, defined as 'front + back'. In many cases, a whisk-like structure was observed at the posterior end, accompanied by a condensed signal at the opposite end. In contrast, treatment with Cyto D, an actin filament destabiliser, resulted in a diffuse actin signal distributed throughout the cell with enhanced nuclear localisation, which is defined as 'nucleus'. The obvious alterations in the chromobody-actin signal validate the specificity and reliability of the chromobody as a research tool in this study. Moreover, the mislocalisation of actin through chemical inhibition of polymerisation dynamics demonstrates that F-actin localisation in ookinetes is determined by its dynamic filament turnover.

A comparison of actin signals between the wild-type and the Alp1 KO ookinetes revealed no apparent difference in actin localisation. The thick tubules and the mesh-like structures were also observed in the KO ookinetes, being predominantly located in the whole cell. This indicates that the non-motile phenotype of Alp1 KO ookinetes is not attributable to a mislocalisation of actin. Moreover, the structural resemblance of the actin signals between the wild-type and the Alp1 KO ookinetes could suggest that Alp1 plays a relatively minor role in maintaining actin filament integrity. A noteworthy observation was made in the presence of Jas, where a significantly higher proportion of Alp1 KO ookinetes exhibited the 'front + back' localisation, indicative of enhanced responsiveness to the actin filament stabiliser. In contrast, the effect of actin filament destabilisation by Cyto D was not discernible between the wild-type and the Alp1 KO ookinetes.

A

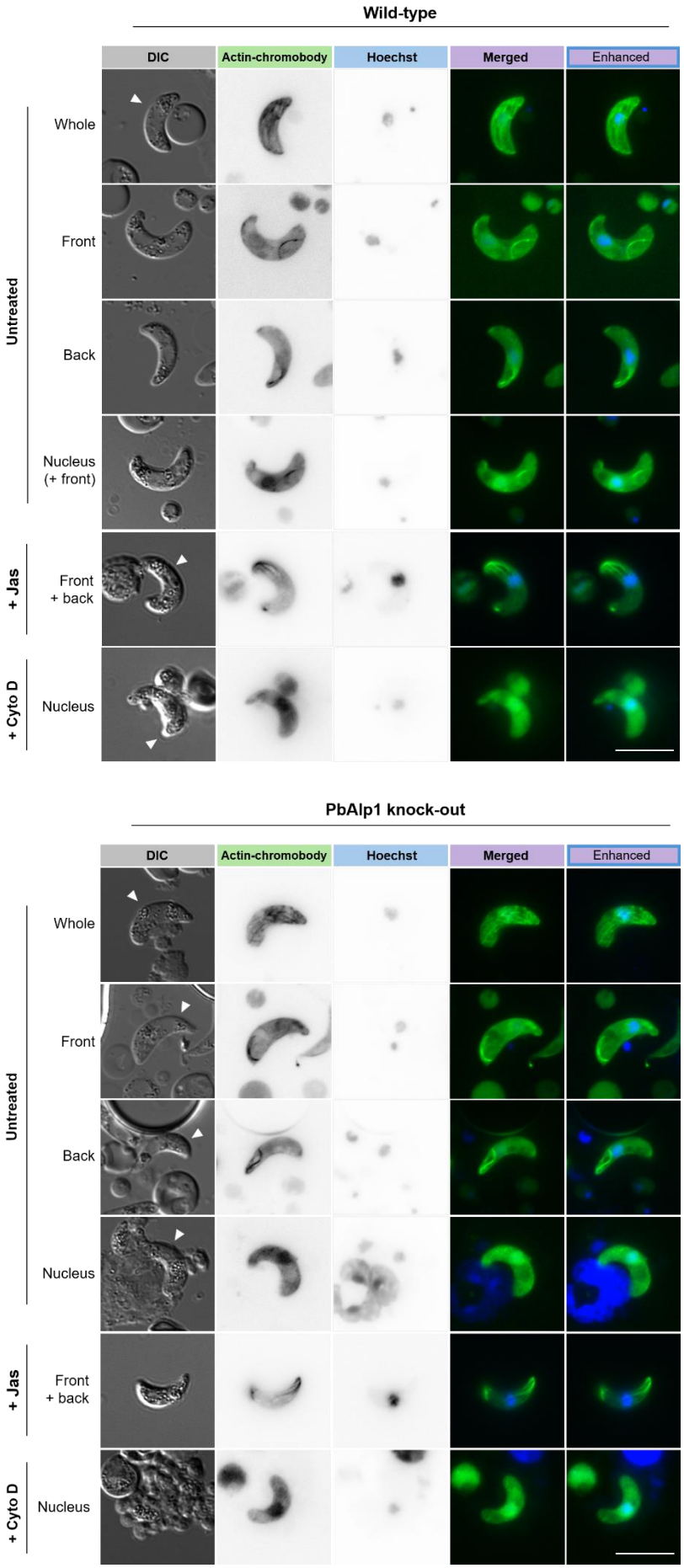
Wild-type
DIC
Actin-chromobody
Hoechst
Merged
Enhanced
Untreated
Whole
Front
Back
Nucleus (+ front)
+ Jas
Front + back
+ Cyto D
Nucleus
PbAlp1 knock-out
DIC
Actin-chromobody
Hoechst
Merged
Enhanced
Untreated
Whole
Front
Back
Nucleus
+ Jas
Front + back
+ Cyto D
Nucleus

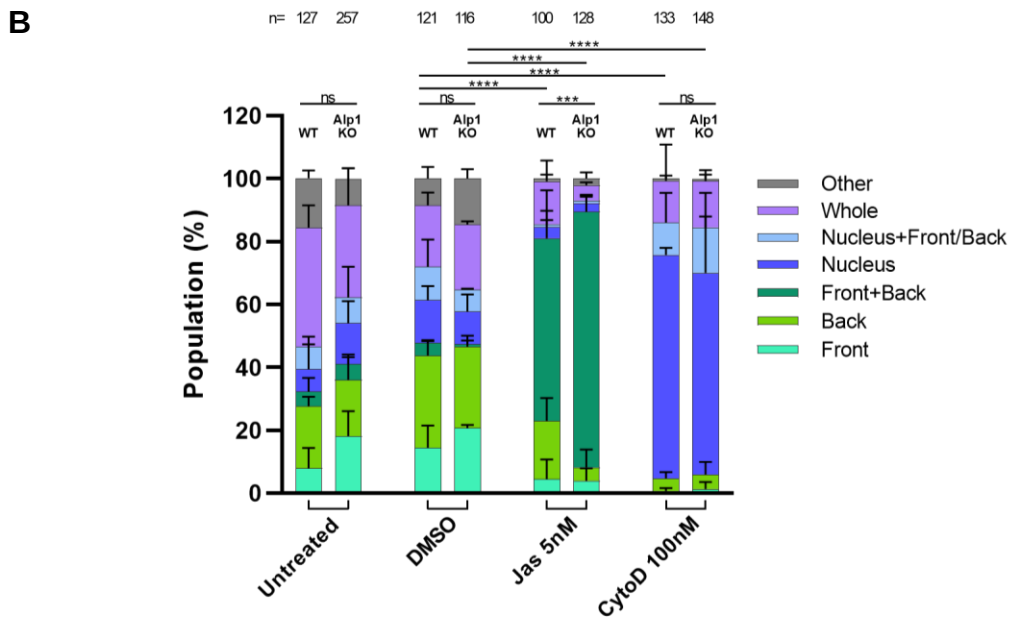

Figure 33: Localisation of actin in the wild-type and Alp1 KO ookinetes using actin chromobody. (A) Fluorescent microscopy images of actin chromobody-expressing wild-type and Alp1 KO ookinetes. Actin (green) displays a vine-like thick tubular and a fine mesh-like structure in both wild-type and Alp1 ookinetes, with occasional localisation in the nucleus. The actin signal was observed to be split into two distinct regions within the cell, the anterior and the posterior. These regions displayed a condensed signal structure and a whisk-like signal structure, respectively. In contrast, Cyto D-treated ookinetes exhibited a predominantly diffuse actin pattern, with a notable accumulation of signal in the nucleus. The blue Hoechst stain was used to label the nucleus, and the merged images show the overlay of the actin and the nucleus. The enhanced images present the Hoechst signal with an increased intensity. The white arrow indicates ookinete. Scale bar = 10 µm. **(B)** In both wild-type and Alp1 KO ookinetes, the actin signal is mostly observed in the entire cell, followed by the posterior and anterior regions. No significant difference in actin localisation was observed between the untreated wild-type and the Alp1 KO ookinetes. The statistical analysis represents a level of significance between the 'whole' population. The actin signal under Jas treatment showed predominantly 'Front + Back' localisation, whereas Cyto D treatment showed enhanced 'Nucleus' localisation in both wild-type and Alp1 KO ookinetes. While no Alp1 KO-relevant effect was observed in Cyto D-treated ookinetes, Jas-treated Alp1 KO ookinetes showed a significantly higher 'Front + Back' population, suggesting increased sensitivity to Jas treatment. The statistical analyses of the Jas treated ookinetes represent a level of significance between the 'Front + Back' population, while the analyses of the Cyto D-treated ookinetes shows a significance between the 'Nucleus' population. There is no major statistical difference between the untreated and DMSO control groups in terms of actin localisation (**Supplement 7**) (Fisher's exact test, two-sided, ns = non-significant, *** = P ≤ 0.001, **** = P ≤ 0.0001). DIC (differential interference contrast); DMSO (dimethyl sulfoxide); Jas (jasplakinolide); Cyto D (cytochalasin D).

In the preceding comparison, a significantly more pronounced response to Jas treatment was observed in ookinetes lacking Alp1, indicating that actin filaments in the absence of Alp1 are more susceptible to chemical stabilisation. Given that Alp1 exerts no direct influence on the cellular distribution of actin, it is possible that Alp1 plays a more prominent role in the regulation of actin filaments. To gain further insight into the specific effects of Alp1 on actin filament dynamics, the sensitivity of these filaments to varying concentrations of Jas and Cyto D was evaluated. The actin signal was subsequently classified according to its shape in response to specific treatments (**Figure 34A**). In the case of Jas-treated ookinetes, a "whisk-like" split structure was prominently observed, whereas more "diffuse nuclear" accumulation of the signal was identified under Cyto D treatments. In untreated

and less treatment-affected ookinetes, the actin filaments exhibited a tubular structure (**Figure 34B**). The quantification of Jas and Cyto D-treated ookinetes demonstrates that the effect of actin filament modulation becomes increasingly prevalent in a concentration-dependent manner. No statistically significant difference in sensitivity was observed between the wild-type and Alp1 KO upon 5 nM Jas treatment. However, the 0.5 nM treatment revealed that the Alp1 KO ookinetes were more sensitive to the Jas treatment. This result confirms that actin filaments are more susceptible to the stabilising modification in the absence of Alp1, implying that Alp1 may play a role in actin filament destabilisation. It appears that lacking Alp1 does not result in enhanced sensitivity of actin to Cyto D treatments. This provides further evidence that Alp1 is unlikely to counteract the destabilising effect of Cyto D. Given the potential role of Alp1 in actin filament destabilisation, an attempt was made to compensate for the impaired motility of the PbAlp1 KO ookinetes by treating them with different concentrations of Cyto D (**Supplement 8**). This experiment, however, did not succeed in restoring the motility of the Alp1 KO ookinetes, suggesting that Alp1 destabilises actin filaments through a different mode of action from that of Cyto D.

Overall, the utilisation of actin chromobody successfully demonstrated the *in vivo* localisation of actin in *P. berghei* ookinetes. The chemical modulation of actin filaments further revealed that Alp1 moderately influences the stability of actin filaments, which may consequently impact the parasite's motility.

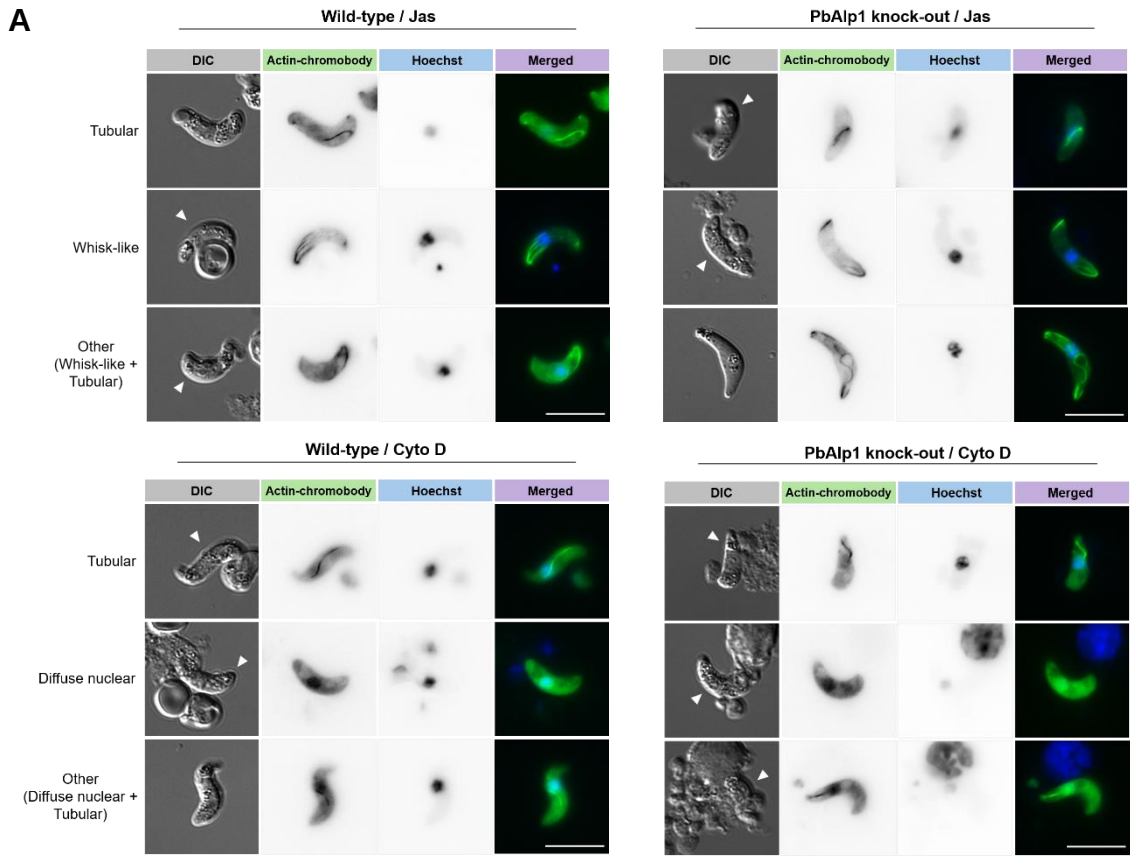

B

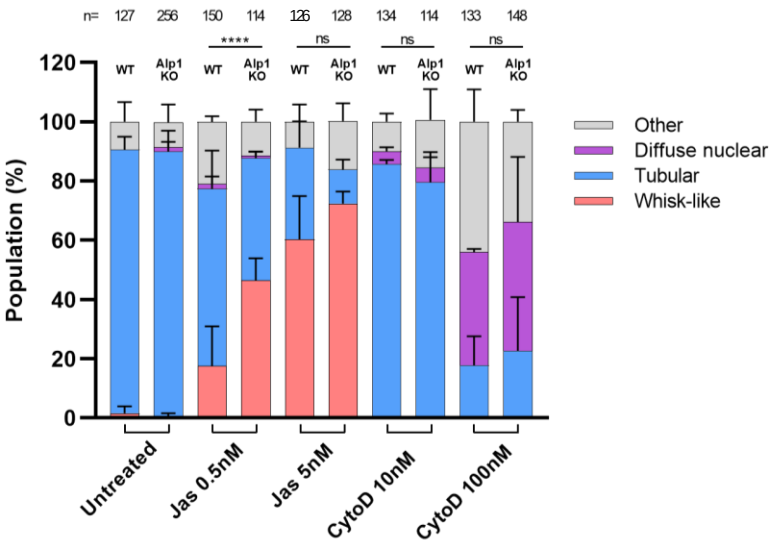

Figure 34: Sensitivity of actin in the wild-type and Alp1 KO ookinetes to jasplakinolide and cytochalasin D. (A) Categorisation of actin signals in response to Jas and Cyto D treatments. The 'tubular' actin signal was predominantly observed in untreated ookinetes, whereas the 'whisk-like' and 'diffuse nuclear' actin signals were typically displayed in Jas and Cyto D-susceptible ookinetes, respectively. The blue Hoechst stain was used to label the nucleus, and the merged images show the overlay of actin and the nucleus. The white arrow indicates ookinete. Scale bar = 10 µm. **(B)** Both the wild-type and Alp1 KO ookinetes responded to Jas treatment in a concentration-dependent manner. A treatment with 0.5 nM Jas revealed an enhanced sensitivity of Alp1 KO ookinetes, indicative of stabilisation-prone actin filaments. Thus, Alp1 demonstrates its potential role in destabilising actin filaments. The Cyto D treatment effectively altered actin dynamics in both the wild-type and Alp1 KO ookinetes, particularly at the 0.1 µM concentration. The absence of Alp1 did not result in any discernible difference in sensitivity. The same data sets (ookinetes) from **Figure 33B** were re-analysed to obtain the 'untreated', 'Jas 5nM' and 'Cyto D 100 nM' results. The statistical analyses of the Jas-treated WT and Alp1 KO ookinetes represent a level of significance between the 'whisk-like' population, while Cyto D-treated ookinetes were compared based on the 'diffuse nuclear' population. (Fisher's exact test, two-sided, ns = non-significant, **** = P ≤ 0.0001). DIC (differential interference contrast); Jas (jasplakinolide); Cyto D (cytochalasin D).

In conclusion, the characterisation of Alp1 in *P. berghei* demonstrated its essential role in facilitating ookinete gliding motility. The complete deletion of Alp1 resulted in the formation of non-motile ookinetes, while their blood stage growth and ookinete development were not significantly affected. Despite the relatively high protein sequence identity, the cDNA of *P. falciparum alp1* was unable to rescue the motility of *P. berghei* ookinetes, indicating the potential involvement of the *alp1* introns in maintaining protein expression. Alp1 appears to be distributed throughout the cytoplasm in ookinetes, however, no specific subcellular localisation could be identified. The visualisation of actin using an actin chromobody revealed the presence of distinct structures and the dynamic localisation of actin filaments in ookinetes. The absence of Alp1 resulted in a slight enhancement of the sensitivity of actin filaments to Jas treatment, which suggests that Alp1 may be involved in the destabilisation of actin filaments and, consequently, in the regulation of gliding motility.

3.3 Characterisation of Alp2b in *Plasmodium berghei*

The transmission of *Plasmodium* to mosquitoes involves a fertilisation process that allows the parasites to transform into an invasive form, thus ensuring their midgut colonisation. This crucial phase necessitates the involvement of actively motile male gametes, which are produced during the gametogenesis (Douglas et al., 2015). This is followed by a simultaneous egression, referred to as exflagellation. The actin-like protein 2b (Alp2b) has been observed to play a critical role in facilitating exflagellation (Binder, 2020; Mikus, 2020). This section investigates the function and critical regions of PbAlp2b through a series of targeted mutations, complementation, temporal and spatial analysis of the exflagellation process.

3.3.1 Phenotypic impact of PbAlp2b knock-out and cross-species complementation

In this study, *P. berghei* Alp2b was replaced with the *P. falciparum* Alp2b (cross-species complementation) and the impact on blood stage growth was evaluated. Moreover, an assay was devised for the quantitative comparison of exflagellation activity across the wild-type, PbAlp2b knock-out (KO) and PfAlp2b complemented parasite lines.

3.3.1.1 Generation of PfAlp2b complementation parasite line

Cross-species complementation constitutes an important aspect of protein characterisation, allowing the study of functional conservation and the deepening of current understanding of protein properties. Alp2b in *P. berghei* and *P. falciparum* share approximately 64% protein sequence identity, and their structural compositions are both characterised by enlarged outer structures, such as the D-loop and H-plug (**Figure 35A**). As their genomic sequences do not contain introns, *pfalp2b* was directly complemented into the corresponding locus of *pbalp2b*. The complementation construct was generated using *E. coli* and linearised prior to transfection into the previously generated PbAlp2b KO negatively selected parasite line (Binder, 2020) (**Supplement 9**). The construct carrying *pfalp2b* and a positive selection cassette was integrated into the target locus through means of homologous recombination of the 5' and 3' untranslated regions (UTRs) of *pbalp2b* (**Figure 35B**). Subsequently, the transfected parasites were subjected to positive selection through pyrimethamine treatment, and isogenic clones were isolated by limiting dilution. The target clone carrying *pfalp2b* was confirmed by genotyping PCR (**Figure 35C**).

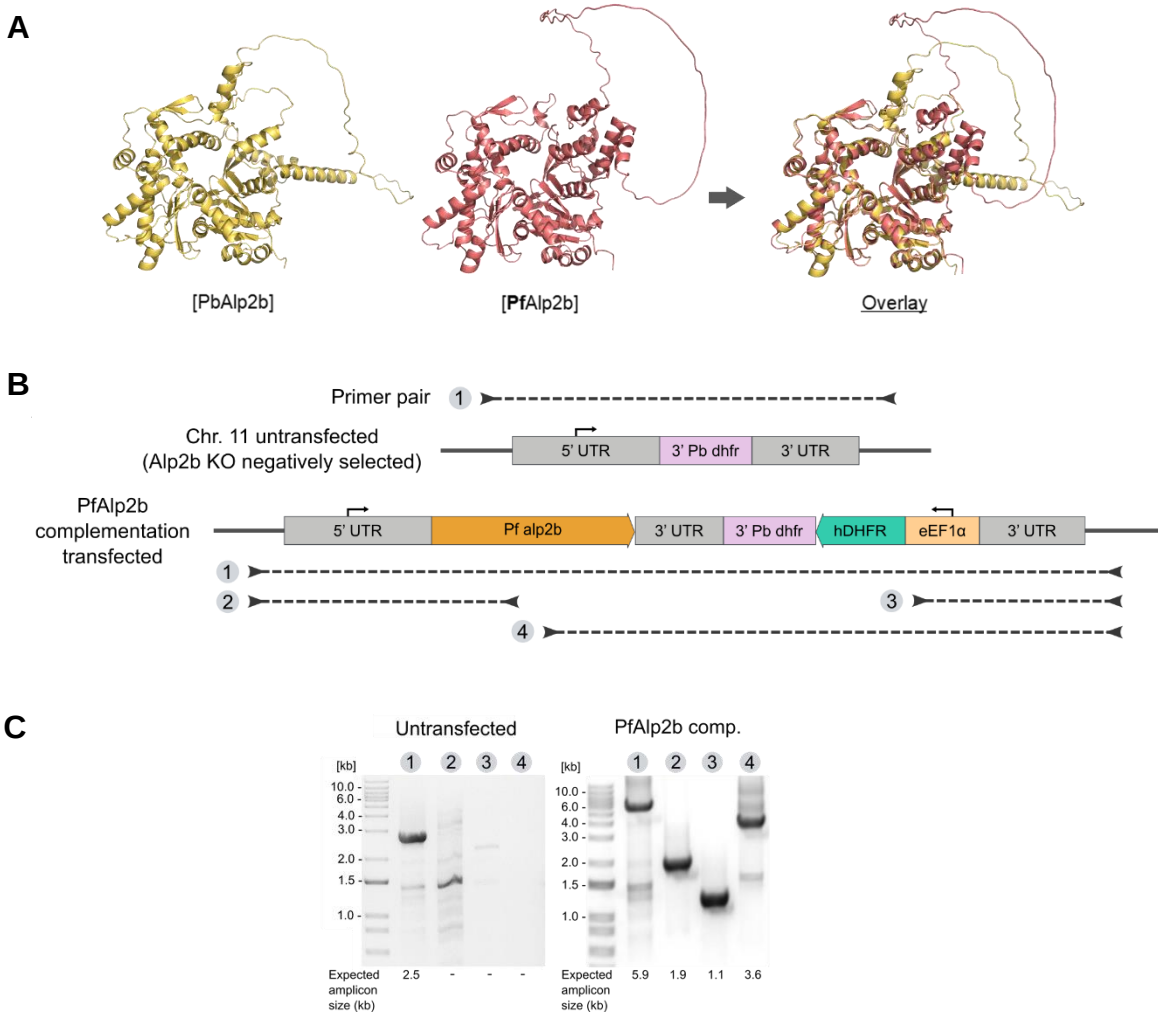

Figure 35: Transfection scheme of PfAlp2b complementation and the final genotyping result. (A) The AlphaFold-predicted structures of *P. berghei* Alp2b and *P. falciparum* Alp2b, with the overlay structure, demonstrate the overall structural similarity between these two proteins. **(B)** *pfalp2b* was transfected into the negatively selected *P. berghei alp2b* KO locus through homologous recombination along with the positive selection cassette (*hDHFR*). The expression of *pfalp2b* was initiated by the native *pbalp2b* promoter. The small arrow indicates a promoter function. **(C)** The genotyping agarose gels of the PfAlp2b complemented parasites with untransfected control confirm the successful generation of the target clone. The circled number and a dotted line indicate the primer pair used and its coverage for the genotyping. UTR (untranslated region); 3' Pb *dhfr* (3' untranslated region of *P. berghei* dihydrofolate reductase); *hDHFR* (human dihydrofolate reductase); eEF1α (eukaryotic translation elongation factor 1 alpha); comp. (complementation).

Prior to the phenotypic study on the sexual stage, the growth rate of the blood stage PfAlp2b complemented (comp.) parasites was evaluated by calculating the *in vivo* multiplication rate. A slight delay in growth was observed with the PfAlp2b comp. parasites when compared to the PbAlp2b complemented parasite line (= 10.2) reported by Binder (2020) (**Figure 36A**). Nevertheless, no issues in the parasitaemia progression were identified (**Figure 36B**). Given that PbAlp2b KO did not affect parasitaemia progression (Binder, 2020), Alp2b is likely to be a non-essential factor in blood stage growth.

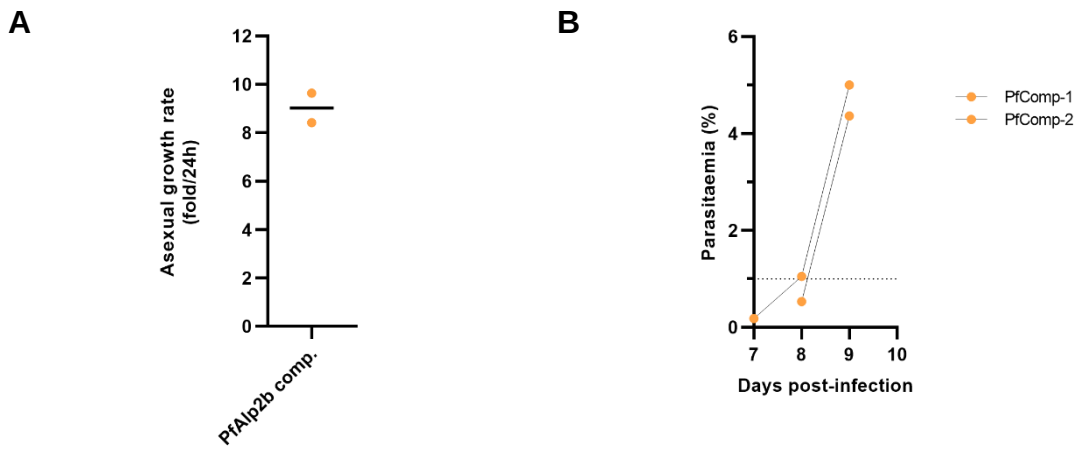

Figure 36: Blood stage growth of the PfAlp2b complementation parasites. (A) The *in vivo* multiplication rates of the asexual parasites in mice reveal a slight growth delay of PfAlp2b comp. parasites in comparison to the PbAlp2b complemented parasites (= 10.2) (Binder, 2020). **(B)** Despite a slightly slower onset of infection, the parasites demonstrated no difficulties in the subsequent progression of parasitaemia. The dotted line indicates the 1% parasitaemia threshold, which becomes relevant when the parasites exhibit a growth phenotype. Comp. (complementation).

3.3.1.2 Absence of Alp2b inhibited exflagellation in *P. berghei*, while complementation with PfAlp2b partially rescued

It has been reported that *P. berghei* lacking Alp2b is incompetent for transmission to mosquitoes due to impaired exflagellation (Binder, 2020; Mikus, 2020). Despite the clear description of the effect of this phenotype, a quantitative analysis of exflagellation had yet to be conducted. As this study is primarily interested in elucidating the critical regions of Alp2b, it was also essential to establish a standardised assay that can discern the subtle phenotypic differences. The assay was designed to present the number of exflagellation events per 100 gametocytes, calculated based on gametocytaemia and *in vivo* quantified exflagellation centres (male gametocyte with egressing gametes) (**Figure 37A**). In this assay, the PbAlp2b KO and complementation lines, previously generated by Binder (2020) (**Supplement 9**), were also analysed. The quantification revealed that the abolished exflagellation by PbAlp2b KO was fully rescued by the complementation of PbAlp2b, while the cross-species complementation with PfAlp2b demonstrated a partial rescue effect (**Figure 37B**). Up to 26 exflagellation events per 100 gametocytes were observed in the PfAlp2b complemented line, and these parasites were able to develop into motile ookinetes (**Supplement 10**), suggesting that a degree of functional conservation is present between *P. berghei* and *P. falciparum* Alp2b.

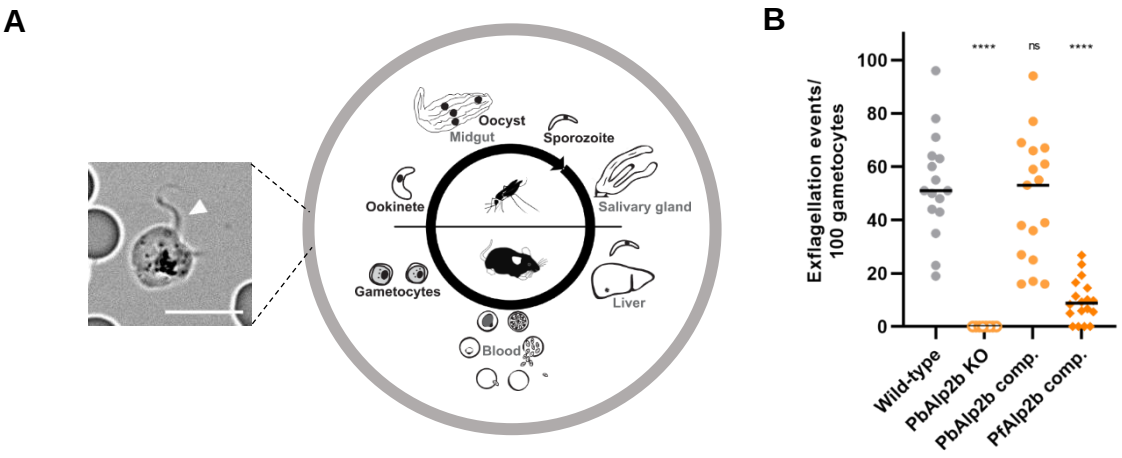

Figure 37: Quantified exflagellation events of PbAlp2b knock-out and complemented lines. (A) The simplified life cycle of *P. berghei* (right) depicting the time point of exflagellation. Exflagellation centre (left) showing a male gametocyte with egressing gametes. The white arrow indicates an egressing gamete. Scale bar = 10 µm. Life cycle figure was adapted from Douglas et al., (2018) **(B)** The quantification of exflagellation events demonstrates a complete inhibition of this process in the absence of Alp2b, which can be effectively rescued by PbAlp2b complementation. Furthermore, PfAlp2b was observed to partially rescue exflagellation, illustrating a degree of cross-species conservation of Alp2b function. Each data point represents a technical repeat. The statistical analysis represents a level of significance against the wild-type (Mann-Whitney test, two-sided, ns = non-significant, **** = P ≤ 0.0001).

3.3.2 Targeted mutations of PbAlp2b unique regions and their phenotypic impacts

The protein sequence of Alp2b contains a number of distinctive insertions when compared to actin1 (**Figure 38**). These insertions, interestingly, result in a notable expansion of some key protein structures. The DNase I-binding loop (D-loop) and the hydrophobic plug (H-plug) of actin, for instance, play a pivotal role in the formation of a polymer by initiating major inter-subunit interactions with the adjacent monomers (Chou and Pollard, 2019; Dominguez, 2019). It is as yet unclear whether Alp2b is capable of forming a filament. However, the enlargement of these specific regions may indicate a particular function of Alp2b beyond polymerisation. Given that Alp2b is essential for exflagellation, it is arguable that they are also involved in facilitating the process. In order to first investigate the structural significance of the expanded D-loop and the H-plug of Alp2b, the respective sizes of these features were reduced by replacing them with the corresponding protein sequences of *P. berghei* actin1 (Mikus, 2020). For this study, the sequences were specifically adapted from actin in order to minimise the influence of non-native amino acid residues. The impact of these modifications was then evaluated in relation to the number of exflagellation events. Subsequently, the same regions of the D-loop and H-plug were subjected to more subtle mutations to further identify functionally critical residues.

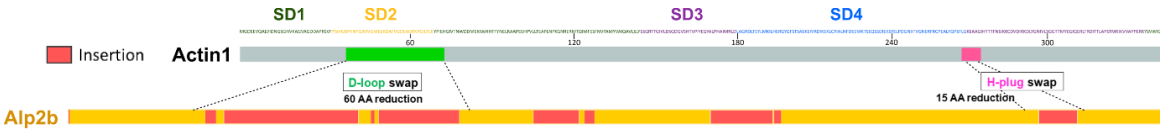

Figure 38: Unique insertions of Alp2b relative to the actin1 protein sequence. Alp2b has a number of distinctive insertions in comparison to *P. berghei* actin1. Notable insertions have been identified within the known essential regions of actin, including the D-loop and H-plug. In order to investigate the significance of such structural expansions, the corresponding protein sequences of actin were complemented into Alp2b, resulting in D-loop and H-plug regions that are 60 and 15 amino acids smaller, respectively. SD = subdomain, AA = amino acid.

3.3.2.1 Generation of PbAlp2b mutant parasite lines

PbAlp2b actin D-loop mutant

The size of the D-loop structure in PbAlp2b was reduced by swapping the target protein region with the corresponding region of Pbactin1 (**Supplement 2**), resulting in a reduction of 60 amino acid residues (**Figure 39A**). In the predicted structure, the smaller D-loop does not appear to induce any significant conformational changes to the core structure of PbAlp2b. The generation of the construct and the selection of isogenic mutant lines were conducted by Mikus (2020) (**Figure 39B**).

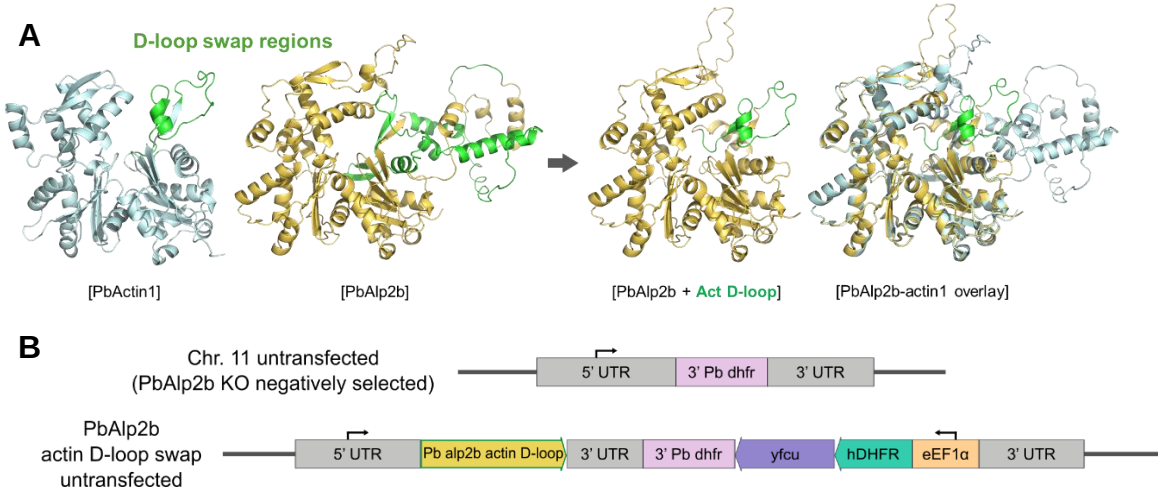

Figure 39: Predicted structure of PbAlp2b-actin D-loop and the construct generated by Mikus (2020). **(A)** The AlphaFold-predicted structures of *P. berghei* actin1, Alp2b and the PbAlp2b-actin D-loop show no major conformational changes associated with the reduced D-loop structure. The green highlighted regions indicate the D-loop structures that were swapped. **(B)** The PbAlp2b-actin D-loop transfection scheme, as generated and transfected by Mikus (2020). The construct features a selection cassette comprising positive (*dDHFR*) and negative (*yfcu*) selection genes, which are driven under the eEF1α promoter. UTR (untranslated region); 3' Pb *dhfr* (3' untranslated region of *P. berghei* dihydrofolate reductase); *hDHFR* (human dihydrofolate reductase); *yfcu* (yeast cytosine deaminase-uracil phosphoribosyl transferase); eEF1α (eukaryotic translation elongation factor 1 alpha).

PbAlp2b D-loop$^{Y52\text{-}K59}$ alanine substitution mutant

While the structural significance of the enlarged D-loop was investigated by reducing the total size, a targeted mutation in one of the unique insertion regions was attempted in order to elucidate the possible contribution of these residues to the function of the protein. Given the high degree of sequence divergence between PbAlp2b and actin1 (**Supplement 2**), the

mutation design was based on the conservation of the amino acids across the major human pathogenic *Plasmodium* species and *P. berghei*. In the preceding cross-species complementation study, *P. falciparum* Alp2b was observed to only partially complement *P. berghei* Alp2b function. Considering the general structural similarities between these proteins, it is possible that the main obstructing factor may be the interspecific variance of their amino acid sequences, which are probably required for specialised interactions to permit full functionality. It is noteworthy that some distinctive insertion regions, such as the D-loop and H-plug, exhibit pronounced divergence across the species, which may be indicative of underlying biological differences. Conversely, the conserved residues within such regions may imply a universally crucial role in *Plasmodium*.

The hypothesis was tested by replacing the eight amino acid residues (Y52 - K59) that are perfectly conserved in the upstream region of the PbAlp2b D-loop with alanine (A) residues, thereby neutralising their activities (**Figure 40A**). In the AlphaFold-predicted structure, the selected mutation region is shown as an outward-facing small hook-like structure located at the interface between the conserved actin core and the unique insertion of the D-loop. The alanine substitution appears to alter the overall conformation of the D-loop into a more stretched state, although the core actin-fold and the target region structures remain comparable (**Figure 40B**). It is noteworthy that the D-loop is a dynamic structure and generally presented with low prediction confidence. Therefore, the shown conformational change may not accurately reflect the true effect of the mutation. In addition to cross-species conservation, the target region was also selected on the basis of higher structure prediction confidence (>70%), with the objective of optimising the mutation design. The mutant Alp2b (D-loop$^{Y52\text{-}K59}$ ala. sub.) was generated via overlapping PCR and transfected into the negatively selected PbAlp2b KO locus, together with the standard selection cassette (**Figure 40C**). The successfully transfected and selected isogenic clone was confirmed by genotyping PCR for subsequent characterisation (**Figure 40D**).

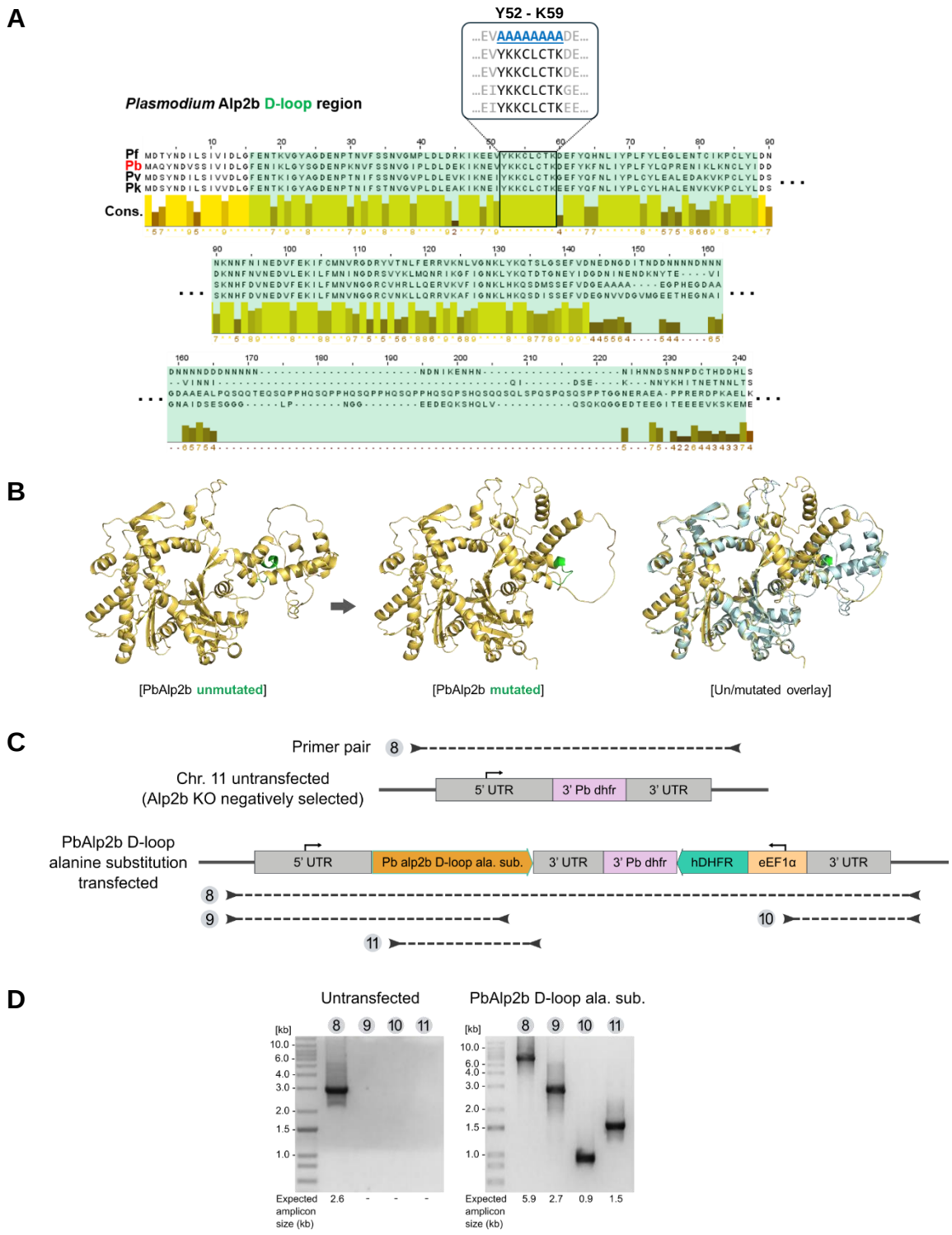

Figure 40: Generation and transfection result of PbAlp2b D-loop$^{Y52\text{-}K59}$ alanine substitution mutant. (A) The multiple sequence alignment of the *Plasmodium* Alp2b D-loop region (highlighted in green), depicting the conserved residues Y52–K59, which have been replaced with eight alanine residues (blue). Pf (*P. falciparum*); Pb (*P. berghei*); Pv (*P. vivax*); Pk (*P. knowlesi*); Cons. (conservation). **(B)** The AlphaFold-predicted structures of PbAlp2b, indicating the mutated region (green), exhibit no significant conformational alterations associated with the alanine substitution. **(C)** *pbalp2b* D-loop$^{Y52\text{-}K59}$ ala. sub. mutant was transfected into the negatively selected *pbalp2b* KO locus through homologous recombination along with the positive selection cassette (*hDHFR*). The small arrow indicates a promoter function. **(D)** The genotyping agarose gels confirm the successful generation of the target PbAlp2b mutant clone. The circled number and a dotted line indicate the primer pair used and its coverage for the genotyping. UTR (untranslated region); 3' Pb *dhfr* (3' untranslated region of *P. berghei* dihydrofolate reductase); *hDHFR* (human dihydrofolate reductase); eEF1α (eukaryotic translation elongation factor 1 alpha); ala. (alanine); sub. (substitution).

PbAlp2b actin H-plug mutant

In order to reduce the physical size of the enlarged PbAlp2b H-plug, 20 amino acids from the unique insertion region were removed and complemented with the corresponding actin1 H-plug sequence (**Supplement 2**). The AlphaFold-predicted structure of the PbAlp2b Act H-plug mutant exhibits a subtle alteration in the D-loop structure relative to the pre-mutation model (**Figure 41A**). In light of the dynamic nature of the actin D-loop and the extremely low confidence in the predictions for this region in general, this alternation is not considered to be a consequence of the mutation. The construct generated by Mikus (2020) was transfected into the PbAlp2b KO parasites that underwent negative selection (**Figure 41B**), and the target isogenic clone was selected via limiting dilution. The resulting clone was subsequently confirmed by genotyping (**Figure 41C**).

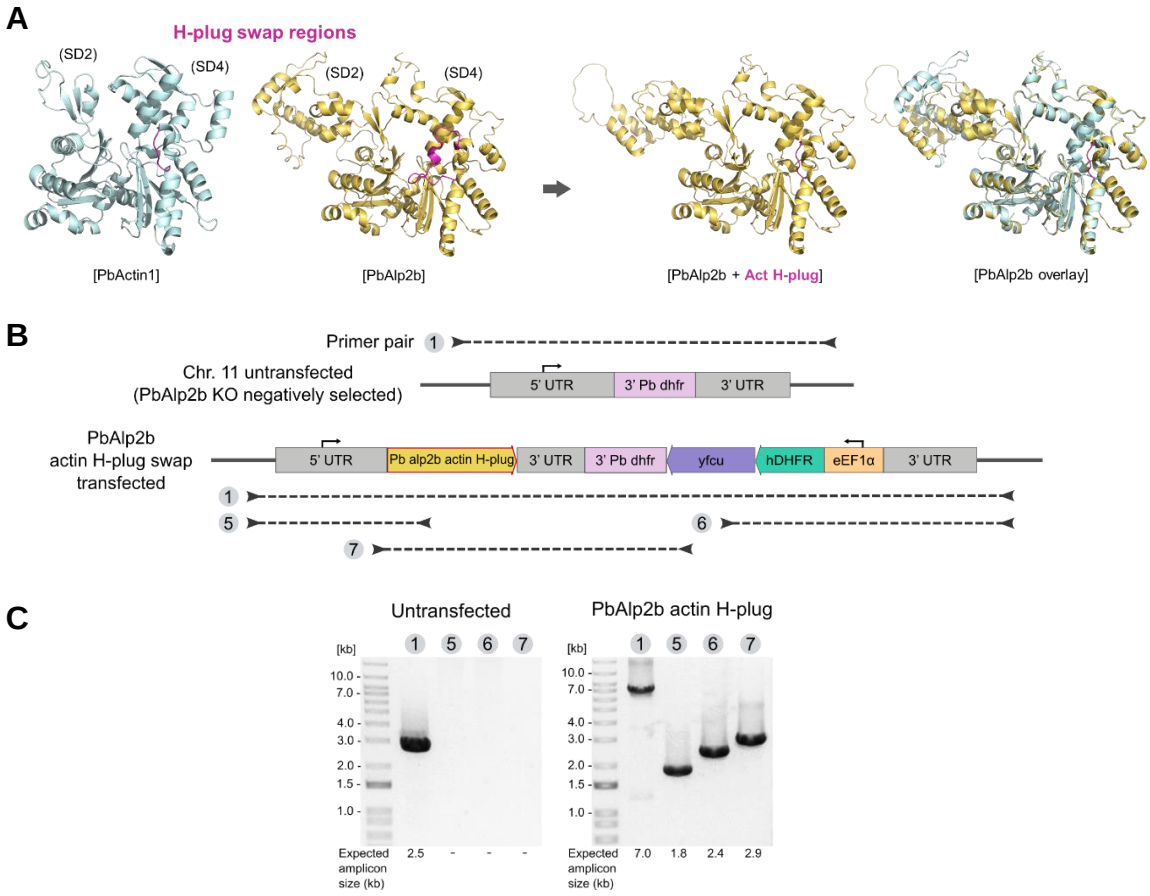

Figure 41: Predicted structure of PbAlp2b-actin H-plug and the construct generated by Mikus (2020). **(A)** The AlphaFold-predicted structures of *P. berghei* actin1, Alp2b and the PbAlp2b-actin H-plug show no major conformational changes associated with the reduced H-plug structure. The pink highlighted regions indicate the H-plug structures that were swapped. SD = subdomain. **(B)** The PbAlp2b-actin H-plug construct generated by Mikus (2020) was transfected into the negatively selected PbAlp2b KO parasites. The construct features a selection cassette comprising positive (*dDHFR*) and negative (*yfcu*) selection genes, which are driven under the eEF1α promoter. **(C)** The genotyping agarose gels confirm the successful generation of the target PbAlp2b mutant clone. The circled number and a dotted line indicate the primer pair used and its coverage for the genotyping. UTR (untranslated region); 3' Pb *dhfr* (3' untranslated region of *P. berghei* dihydrofolate reductase); *hDHFR* (human dihydrofolate reductase); *yfcu* (yeast cytosine deaminase-uracil phosphoribosyl transferase); eEF1α (eukaryotic translation elongation factor 1 alpha).

PbAlp2b H-plug$^{N438\text{-}K442}$ actin sequence substitution mutant

Precisely at the apex of the expanded H-plug of Alp2b, five conserved amino acid residues (N438 - K442) were identified. Three of them (PbN438, L439 and K442) are perfectly conserved across all aligned *Plasmodium* species, while the other two (Y440 and T441) are partially conserved (**Figure 42A,B**). Interestingly in actin, three crucial amino acids (G269, K270 and E271) are present in the corresponding region, facilitating the formation of lateral contacts with neighbouring subunits and thereby contributing to the polymerisation process (Douglas et al., 2018; Pospich et al., 2017). To investigate whether the conserved tip of the PbAlp2b H-plug can be substituted with the actin counterpart, the region of interest was replaced with the actin amino acid residues GKEAA, and the resulting impact on exflagellation was evaluated. The generation of the mutant PbAlp2b was achieved through overlapping PCR, followed by transfection into the *pbalp2b* KO locus of the negatively selected *P. berghei* with a selection cassette (**Figure 42C**). The subsequent parasites were selected via pyrimethamine drug selection and limiting dilution, and finally confirmed by genotyping for the correct isogenic clone (**Figure 42D**). It is important to note that the parasite line generated in this experiment exhibited a markedly slower blood stage growth compared to other mutant lines (**Figure 42E**). However, as neither undesirable mutations nor frameshift in the transfected *alp2b* locus, nor impaired gametocyte development were observed (**Figure 42F**), the line was still included in this phenotypic study. Furthermore, the observation that more drastic mutation in the same region (PbAlp2b actin H-plug) did not result in any growth delay suggests that this was a biological variation of the clone.

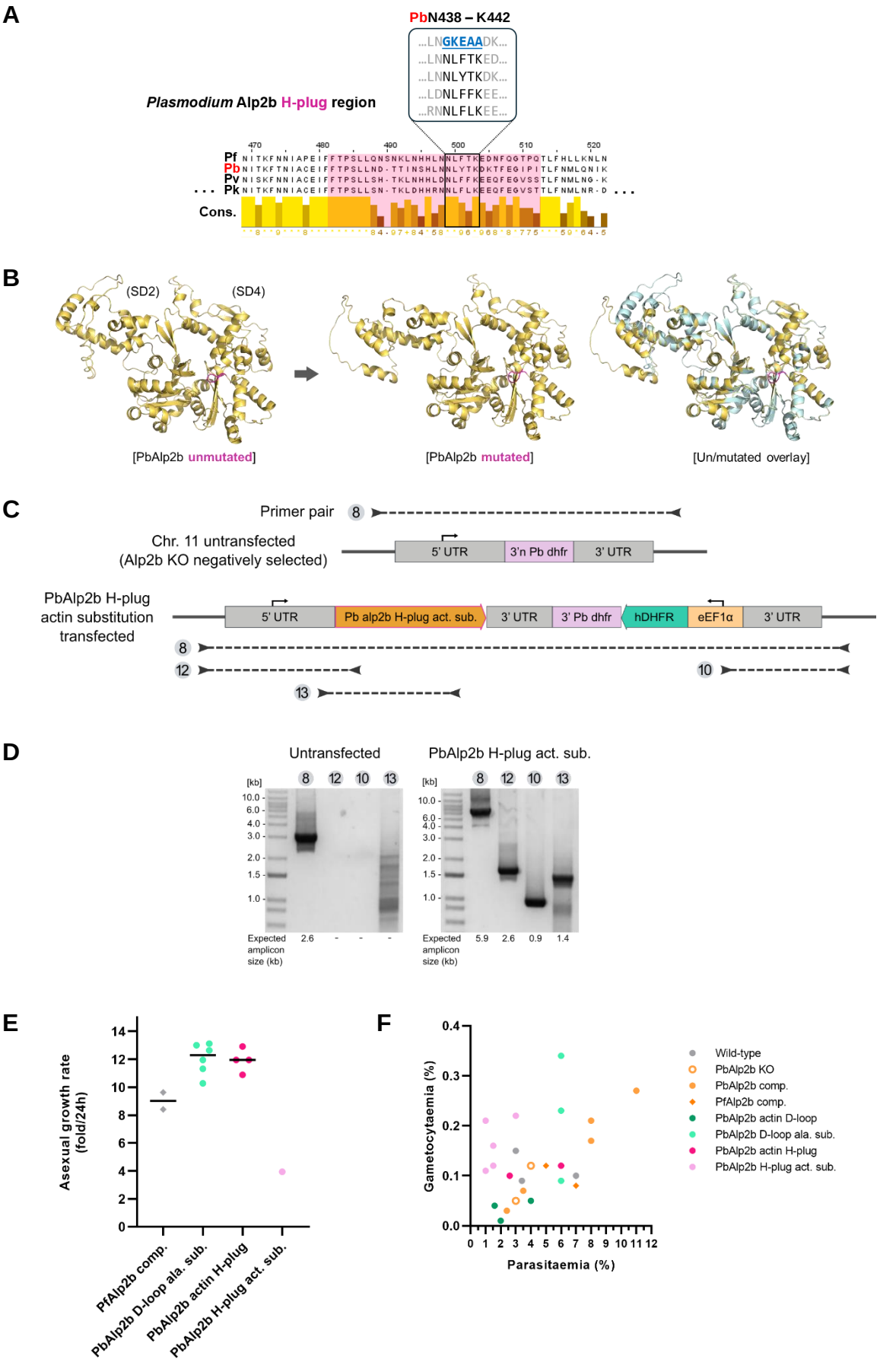
A
PbN438 – K442
...LNGKEAADK...
...LNNLFTKED...
...LNNLYTKDK...
...LDNLFFKEE...
...RNNLFLKEE...
Plasmodium Alp2b H-plug region
Pf
Pb
Pv
Pk
Cons.
B
(SD2)
(SD4)
[PbAlp2b unmutated]
[PbAlp2b mutated]
[Un/mutated overlay]
C
Primer pair 8
Chr. 11 untransfected
(Alp2b KO negatively selected)
5' UTR
3'n Pb dhfr
3' UTR
PbAlp2b H-plug
actin substitution
transfected
5' UTR
Pb alp2b H-plug act. sub.
3' UTR
3' Pb dhfr
hDHFR
eEF1α
3' UTR
8
12
10
13
D
Untransfected
PbAlp2b H-plug act. sub.
[kb]
Expected amplicon size (kb)
2.6
5.9
0.9
1.4
E
Asexual growth rate (fold/24h)
PfAlp2b comp.
PbAlp2b D-loop ala. sub.
PbAlp2b actin H-plug
PbAlp2b H-plug act. sub.
F
Gametocytaemia (%)
Parasitaemia (%)
Wild-type
PbAlp2b KO
PbAlp2b comp.
PfAlp2b comp.
PbAlp2b actin D-loop
PbAlp2b D-loop ala. sub.
PbAlp2b actin H-plug
PbAlp2b H-plug act. sub.

Figure 42: Generation and transfection result of PbAlp2b H-plug$^{N438\text{-}K442}$ actin sequence substitution mutant. (A) The multiple sequence alignment of the *Plasmodium* Alp2b H-plug region, depicting the conserved residues PbY438–K442, which have been replaced with the corresponding actin1 H-plug residues (blue). Pf (*P. falciparum*); Pb (*P. berghei*); Pv (*P. vivax*); Pk (*P. knowlesi*). Conc. (conservation). **(B)** The AlphaFold-predicted structures of PbAlp2b, indicating the mutated region (pink), exhibit no significant conformational alterations associated with the actin sequence substitution. The mutated region remains at the apex of the H-plug, retaining an almost identical loop structure to the original PbAlp2b H-plug. **(C)** *pbalp2b* H-plug$^{Y438\text{-}K442}$ act. sub. mutant was transfected into the negatively selected *pbalp2b* KO locus through homologous recombination along with the positive selection cassette (*hDHFR*). The small arrow indicates a promoter function. **(D)** The genotyping agarose gels confirm the successful generation of the target PbAlp2b mutant clone. The circled number and a dotted line indicate the primer pair used and its coverage for the genotyping. **(E)** The *in vivo* blood stage growth was documented during the limiting dilution process. No growth delays were caused by the alanine substitution of the conserved region of D-loop (D-loop ala. sub.) or the size reduction of the H-plug structure (actin H-plug). In contrast, the mutant with the actin sequence substituting the conserved H-plug region showed a notably slower growth. The mutated locus was confirmed by Sanger sequencing to exclude possibilities of undesirable mutations of frameshift. The PfAlp2b comp. data was adapted from **Figure 36A**. **(F)** A comparison of the gametocytaemia of wild-type and the PbAlp2b mutant parasites relative to their parasitaemia. In the majority of cases, gametocytaemia was observed to fall within the range of 0.3 to 1.5%, although there were some exceptions. The H-plug act. sub. mutant, which exhibited a growth delay (E), exhibited comparable gametocytaemia to other parasite lines including wild-type. In contrast, the smaller D-loop mutant (actin D-loop) exhibited generally lower gametocytaemia, although no growth issues were reported (Mikus, 2020). UTR (untranslated region); 3' Pb *dhfr* (3' untranslated region of *P. berghei* dihydrofolate reductase); *hDHFR* (human dihydrofolate reductase); eEF1α (eukaryotic translation elongation factor 1 alpha); act. (actin); sub. (substitution); ala. (alanine).

3.3.2.2 PbAlp2b D-loop residues are critical, while mutated H-plug is functional

The *P. berghei* Alp2b D-loop and H-plug mutants described in the prior sections were injected into naïve mice, and their *in vivo* exflagellation rates were quantified in accordance with the KO and complementation studies (**3.3.1**). Firstly, the reduction in size of the D-loop (PbAlp2b actin D-loop) and H-plug (PbAlp2b actin H-plug) both resulted in the complete cessation of exflagellation (**Figure 43**). The results indicate that Alp2b requires either the physical presence of the expanded D-loop or H-plug structures, or the specific residues present within the unique insertions to facilitate exflagellation. This is further substantiated by the alanine substitution assay of the eight conserved amino acid residues in the D-loop unique insertion region (PbAlp2b D-loop ala. sub.), which resulted in the complete inhibition of exflagellation, suggesting that these residues may convey a specific function. Notably, the actin sequence (GKEAA) substitution of the H-plug unique region retained the parasite's ability to exflagellate. Given the fact that the presence of the exact same actin sequence did not yield any rescue effect in the preceding size reduction mutation (where the Alp2b H-plug sequence was replaced with the respective actin sequence), it is possible that the replaced conserved residues were simply not essential, or that the physical presence of the larger H-plug does play a role in facilitating exflagellation.

In conclusion, the results of this study demonstrate that the enlarged D-loop and the H-plug structures are both essential for the function of Alp2b and cannot be replaced by the actin equivalents. Moreover, the highly conserved eight amino acid residues at the base region of the D-loop appear to provide a molecular contribution to the function of Alp2b, while the

conserved region at the apex of the H-plug may be less relevant to the process of exflagellation.

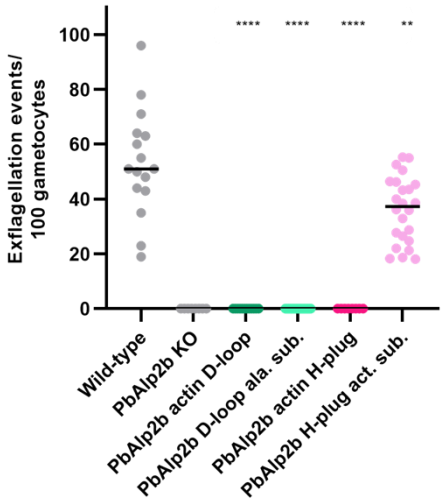

Figure 43: PbAlp2b D-loop and H-plug are essential for exflagellation. The quantification of exflagellation events reveals that the smaller D-loop and H-plug mutants (actin D-loop and actin H-plug, respectively) exhibit clear inhibition, emphasising the importance of their enlarged structures for the function of Alp2b. Furthermore, the alanine substitution of the conserved amino acids in the D-loop (D-loop ala. sub.) also fully inhibited exflagellation, thus successfully locating the region that is critical for function. In contrast, the conserved residues at the apex of the H-plug exhibited significantly milder effects on exflagellation when substituted with the corresponding actin sequence. The wild-type and PbAlp2b KO reference values were adapted from **Figure 37B**. Each data point represents a technical repeat. The statistical analysis represents a level of significance against the wild-type (Mann-Whitney test, two-sided, ** = P ≤ 0.01, **** = P ≤ 0.0001). ala. (alanine); act. (actin); sub. (substitution).

3.3.3 Cellular localisation of Alp2b in *P. berghei*

As previously outlined in section **3.2.2**, elucidating the cellular localisation constitutes an important aspect of protein characterisation. However, as yet, no studies have successfully determined the localisation of Alp2b. This section will discuss the localisation strategies using a fluorescent protein and the α-PbAlp2b antibody.

3.3.3.1 Generation of EGFP-PbAlp2b additional copy parasite line

Despite a number of attempts employing different strategies, the tagging of endogenous Alp2b has not yet been achieved. The tagging of the N-terminus and C-terminus with EGFP and 3xHA, respectively, both resulted in the inhibition of exflagellation (Mikus, 2020). In order to preserve the function of the endogenous Alp2b, the N-terminally tagged Alp2b was introduced to *P. berghei* as an additional copy. The EGFP tag was selected based on the successful localisation of *Plasmodium* actin (Angrisano et al., 2012), as well as the possibility of observing live localisation under a fluorescent microscope.The construct containing *egfp-pbalp2b* that is linked with the AAAAEFAAAA sequence was integrated into the chromosome 12 recombination site of *P. berghei* via homologous recombination (**Figure 44A**). As this parasite line was intended for further mutation or colocalisation

studies, the full-size selection cassette, including the negative selection gene (*yfcu*), was employed. The chromosome 12 5' and 3' homology arms were purposely kept shorter to reduce the total size of the construct. Subsequently, the isogenic parasite clones were selected through limiting dilution and confirmed to carry the target genes by genotyping (**Figure 44B**). The western blot analysis prior to fluorescent microscopy revealed the presence of a very faint signal, approximately corresponding to the size of EGFP-PbAlp2b (90 kDa) (**Figure 44C**). However, the detection of a distinct band at 25 kDa provides compelling evidence for the proteolytic cleavage of the EGFP protein, a phenomenon that was also observed with the endogenously tagged PbAlp1 (**3.2.2**). It is currently unclear whether this cleavage is caused by the linker sequence used or the nature of the proteins. However, as this consistently occurs across different proteins and biological repeats, it can be concluded that this strategy is not feasible for this research purpose.

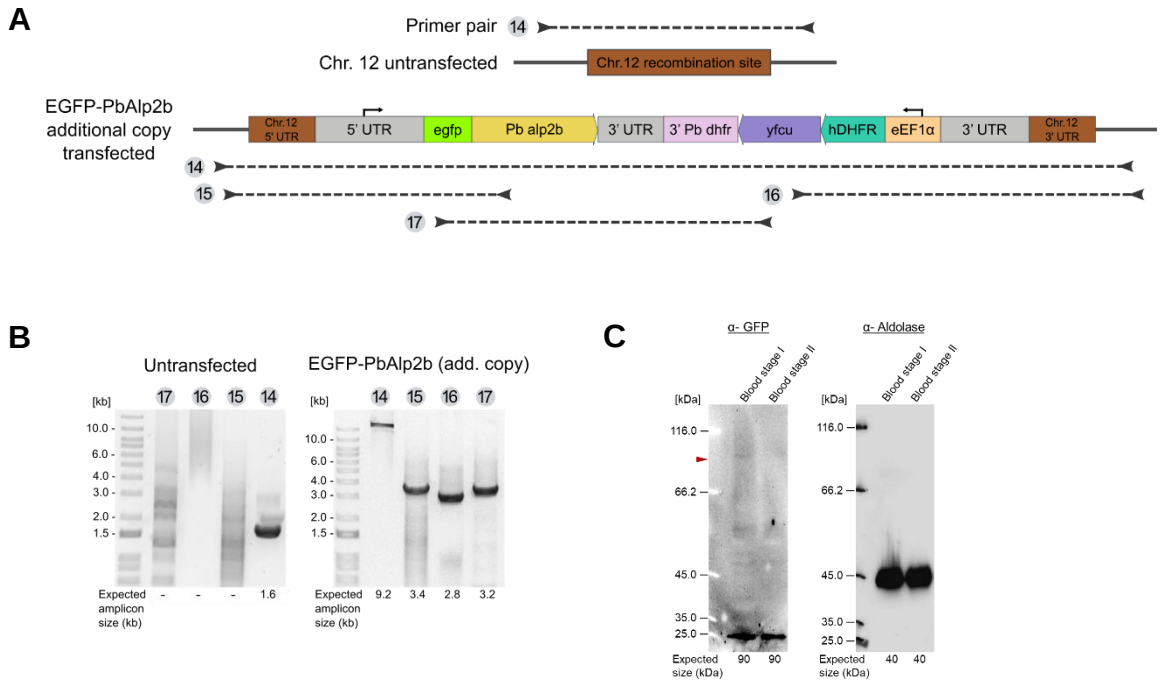

Figure 44: Transfection scheme of EGFP-PbAlp2b (additional copy) and the final genotyping and expression results. (A) The EGFP-PbAlp2b construct was transfected into the chromosome 12 of wild-type *P. berghei* via homologous recombination of the 5' and 3' UTR sequences of the target integration site. The selection cassette, which carries *hDHFR* and *yfcu* under the eEF1α promoter, allows for positive and negative selections, respectively. For the potential negative selection, the two identical segments of *pbalp2b* 3' UTR act as the recombination site. The small arrow indicates a promoter function. **(B)** The genotyping agarose gel of the limiting dilution-selected EGFP-PbAlp2b (additional copy) parasites confirms the correct integration of the target genes. The circled number and a dotted line indicate the primer pair used and its coverage for the genotyping. **(C)** The α-GFP western blot (left) using 2x10⁷ blood stage parasites from two mice (I & II) revealed a faint signal for potential EGFP-PbAlp2b (90 kDa). The clear bands at 25 kDa in both samples indicate the potential cleavage of the EGFP tag. The α-aldolase western blot serves to ensure the quality of the parasite samples used. Due to a technical issue during the imaging process, the marker on the α-GFP is displayed in white. The red arrow indicates the target size (90 kDa) of EGFP-PbAlp2b. UTR (untranslated region); 3' Pb *dhfr* (3' untranslated region of *P. berghei* dihydrofolate reductase); *hDHFR* (human dihydrofolate reductase); *yfcu* (yeast cytosine deaminase-uracil phosphoribosyl transferase); eEF1α (eukaryotic translation elongation factor 1 alpha).

Similarly to Alp1, two custom antibodies directed against PbAlp2b were synthesised (Eurogentec) for the purpose of tag-free localisation studies (**Supplement 11**). Both antibodies demonstrated successful binding to the recombinantly expressed Alp2b in *E. coli*. However, the anticipated binding capacity was not observed in the actual parasite lysate. Further validation is required before proceeding with the localisation study.

3.3.4 Visualisation of microgametogenesis in *P. berghei* Alp2b mutant gametocytes

Exflagellation is a male-specific developmental step that releases eight motile microgametes, which are required for fertilisation. The process of exflagellation, so-called microgametogenesis, follows an activation of male gametocytes, three sets of genome replication, simultaneous assembly and organisation of axonemes and ultimately active egress of mature microgametes along with the individually allocated nucleus (Dash et al., 2022). Thus far, Alp2b has been demonstrated to play a pivotal role in facilitating exflagellation in *Plasmodium*. To attain insight into the molecular-level involvement of Alp2b, immunostaining of α-tubulin in gametocytes was performed to monitor their mitotic activity and axonemal development during the microgametogenesis.

3.3.4.1 PbAlp2b knock-out gametocytes can form axonemes, but not egress

The fluorescence microscopy images of wild-type gametocytes present a progressive transformation of the axonemal structures occurring during gametogenesis (**Figure 45**). At eight minutes post-activation (mpa), the formation of multiple basal bodies is identified in the form of discrete dots, along with the short, newly formed axonemes that are attached. These structures frequently appear less oriented in comparison to the more mature axonemes observed in the 10 and 12 mpa gametocytes. In the period preceding exflagellation, the axonemes are typically wrapped around the aggregated nuclei present in the centre of the cell. During this process, the attached basal body pulls a nucleus along, enabling it to be taken with the egressing microgamete. The semi-multi-nucleated state observed at 14 mpa serves as an illustrative example. The 16 mpa gametocyte provides a classical image of exflagellation, exhibiting the egress of multiple microgametes from a gametocyte. Additionally, the Hoechst staining indicates nuclear migration into individual microgametes. The post-exflagellation gametocyte, as represented in the 20 mpa image, occasionally showed a residual DNA content and microgametes, which presumably failed to egress from the cell.

In gametocytes lacking Alp2b, the formation of basal bodies and the nucleation of short axonemes were also observed. These axonemes were capable of elongating and attaining the morphology comparable to that of the wild-type. The positioning of the basal bodies and

the tubular structures that coil around the nuclei further indicate that the axonemes are organised in a similar manner to wild-type gametocytes preparing for exflagellation. In contrast to the overall developmental similarity observed, however, none of the axonemes in the Alp2b KO gametocytes were able to fully develop into microgametes that could egress. This suggests that the inhibition of exflagellation observed in the Alp2b KO is likely due to a failure in the maturation of the microgametes.

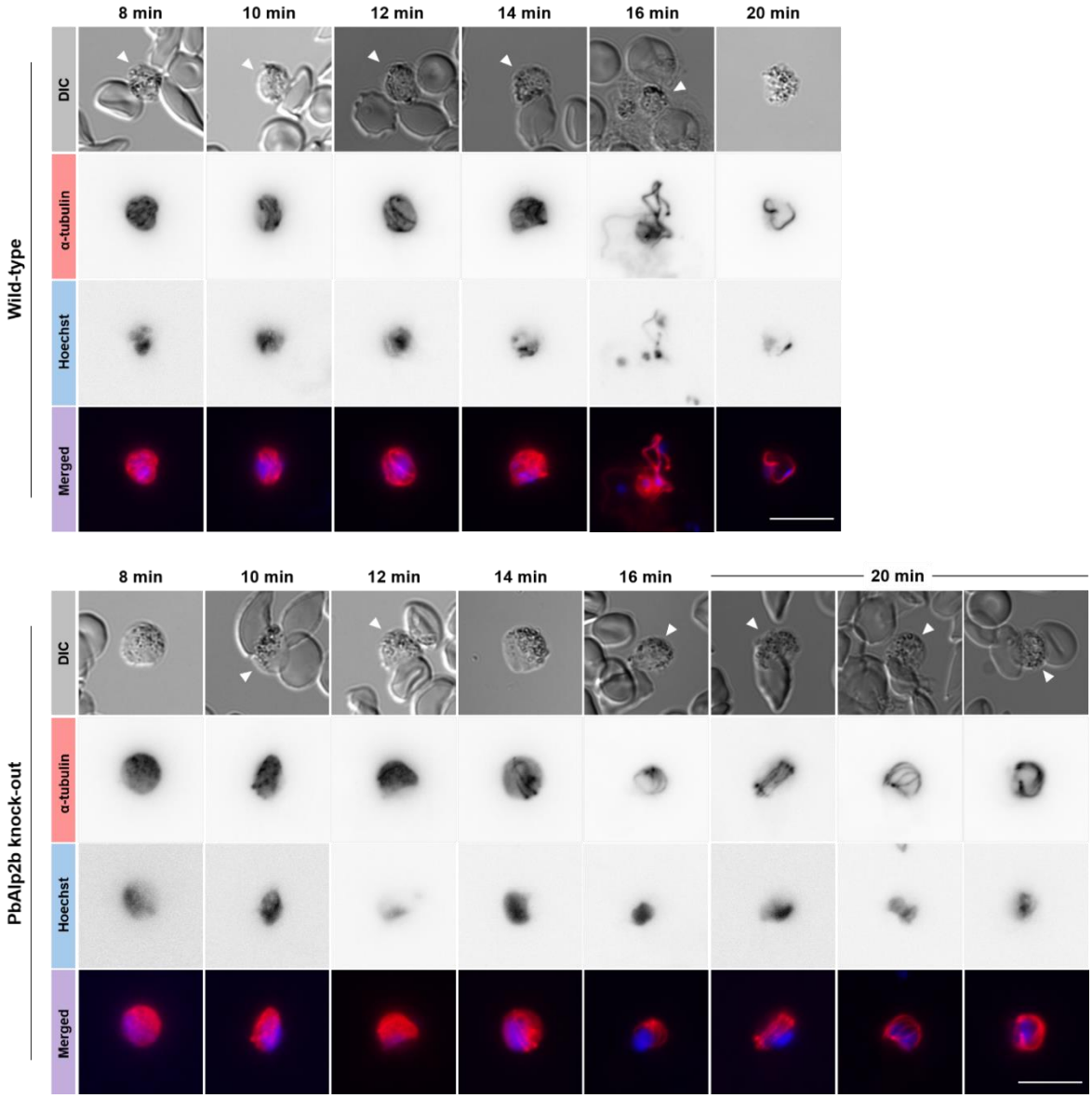

Figure 45: Microgametogenesis and exfllagellation of wild-type and PbAlp2b KO gametocytes visualised by α-tubulin immunostaining. The labelling of α-tubulin (red) reveals the presence of basal bodies and nucleated axonemes in both wild-type and PbAlp2b KO gametocytes between eight and ten minutes post-activation (mpa). In both cases, the axonemes underwent further elongation to form premature microgametes, which were positioned around the aggregated nuclei (blue) in the centre of the cell. In the wild-type gametocyte at 14 mpa, the aggregated nuclei were observed to be pulled apart and to shift their positions towards the individual microgametes, which subsequently egressed from the cell (exflagellation), as shown at 16 mpa. By 20 mpa, some gametocytes were observed to have reached the post-exflagellation state, with a residual trace of DNA content and, occasionally, the presence of left-behind microgametes. In contrast, the axonemal structure in the PbAlp2b KO gametocytes did not exhibit any indication of further progression beyond the initial localisation around the nucleus. This indicates that the absence of Alp2b hinders the final maturation stages of microgametes, thereby impairing the process of exflagellation. The white arrow indicates a gametocyte and the time indicates the minutes post-activation (mpa). Merged = overlay of α-tubulin and Hoechst images. Scale bar = 10 µm. DIC (differential interference contrast).

3.3.4.2 Alp2b is essential for reaching the multi-nucleated stage before exflagellation

The visualisation of microgametogenesis in PbAlp2b KO gametocytes provided a clear indication that Alp2b plays a critical role during the pre-exflagellation step. It is evident that the non-exflagellating phenotype is caused by immature microgametes, which are unable to proceed to egress after positioning themselves against the cell membrane. In order to gain deeper insight into this abnormal morphology and possible developmental issues, the microgametogenesis and exflagellation processes were categorised into seven distinct steps based on α-tubulin and nucleus localisation patterns and ordered according to the time point observed (**Figure 46A**). The term 'non-specific' localisation is used to describe a diffuse α-tubulin signal that does not exhibit any structures associated with the axoneme or basal body. This may also include some non-activated gametocytes. In gametocytes designated as 'spindle/basal bodies', the presence of rod-like structures (spindles) and discrete dots (basal bodies) is observed. These structures are not attached to one another. Both the "early axonemes" and the "late axonemes" are defined by the presence of multiple basal bodies and prominent tubular structures, which are projected from the basal bodies. The 'early axonemes' are typically shorter in length, whist the 'late axonemes' are longer than the diameter of the cell. Additionally, the latter are often aligned in a single direction while coiling around the nuclei. The 'multi-nucleated' state of gametocytes is characterised by the visible segregation of multiple nuclei distributed to individual microgametocytes, which are often aggregated against the cellular membrane. This is the final phase of microgametogenesis prior to the onset of 'exflagellation', whereby multiple microgametes emerge from a gametocyte and detach (egress). The characteristic of 'post-exflagellation' gametocytes is weak residual DNA signal, with the occasional presence of a ‘left-behind’ microgamete/axonemal structure inside the cell.

In the wild-type population, the majority of male gametocytes (>60%) exhibited axoneme formation at 8 minutes post-activation (mpa), with more than one-third of them already at the late axoneme step (**Figure 46B**). The population of mature axonemes continued to expand at a rapid rate until 12 mpa, at which point the first exflagellation event was identified. The transition from the late axonemes to exflagellation is characterised by the multi-nucleated step. This essential process appears to be transient, and therefore the population was observed to remain at a low level. The number of exflagellating individuals reached its peak at 16 mpa, together with the post-exflagellation population demonstrating that over 50% of male gametocytes had exflagellated. By the termination of this assay at 20 mpa, all the gametocytes had formed mature axonemes. In stark contrast, PbAlp2b KO male gametocytes appeared to encounter two major impediments during their development. The initial threshold is the transition between the formation of the basal body and the nucleation

of the axoneme. While the majority of wild-type gametocytes were observed to reach the point of axoneme formation by 8 mpa, the PbAlp2b KO gametocytes were found to remain at the basal body formation phase, with this population representing the majority until 12 mpa. It is of interest to note that the maturation of the axonemes did not appear to be much influenced once the initial formation had been overcome. The population exhibiting a mature axonemal structure continued to grow until 20 mpa. The second and most significant impediment is, indeed, exflagellation, which is completely blocked by the absence of Alp2b. The observation revealed that no multi-nucleated gametocytes were present in this population, implying potential issues in nuclei organisation or axoneme function that hinder the uptake of the nucleus by microgametes. Furthermore, the *P. falciparum* Alp2b-complemented gametocytes (**Supplement 12**) were analysed to determine whether they manifest similar developmental issues to the PbAlp2b KO parasites. As shown previously (**3.3.1.2**), these gametocytes exhibited an intermediate exflagellation phenotype, with a reduction of approximately 80% compared to wild type. The developmental behaviour presented in the time course analysis showed a comparable progression of microgametogenesis to the wild type, accompanied by a reduced number of exflagellations, consistent with the results of the previous quantification assay. Given that microgametogenesis was unaffected, the reduction in exflagellation is also considered to be a consequence of an inefficient transition to the exflagellation phase.

The results of these analyses provide valuable insights into the role of Alp2b in the different phases of microgametogenesis. In the early phase, the absence of Alp2b causes gametocytes to struggle with the initial formation of axoneme. As this delay is exclusive to the initiation phase and not observed in the PfAlp2b-complemented parasites, the role of Alp2b in this phase is likely to be less critical than in the later phase, where Alp2b may be involved in the distribution of nuclei to mature microgametes. This is evidenced by the absence of multi-nucleated gametocytes in the PbAlp2b KO population that ultimately could not exflagellate.

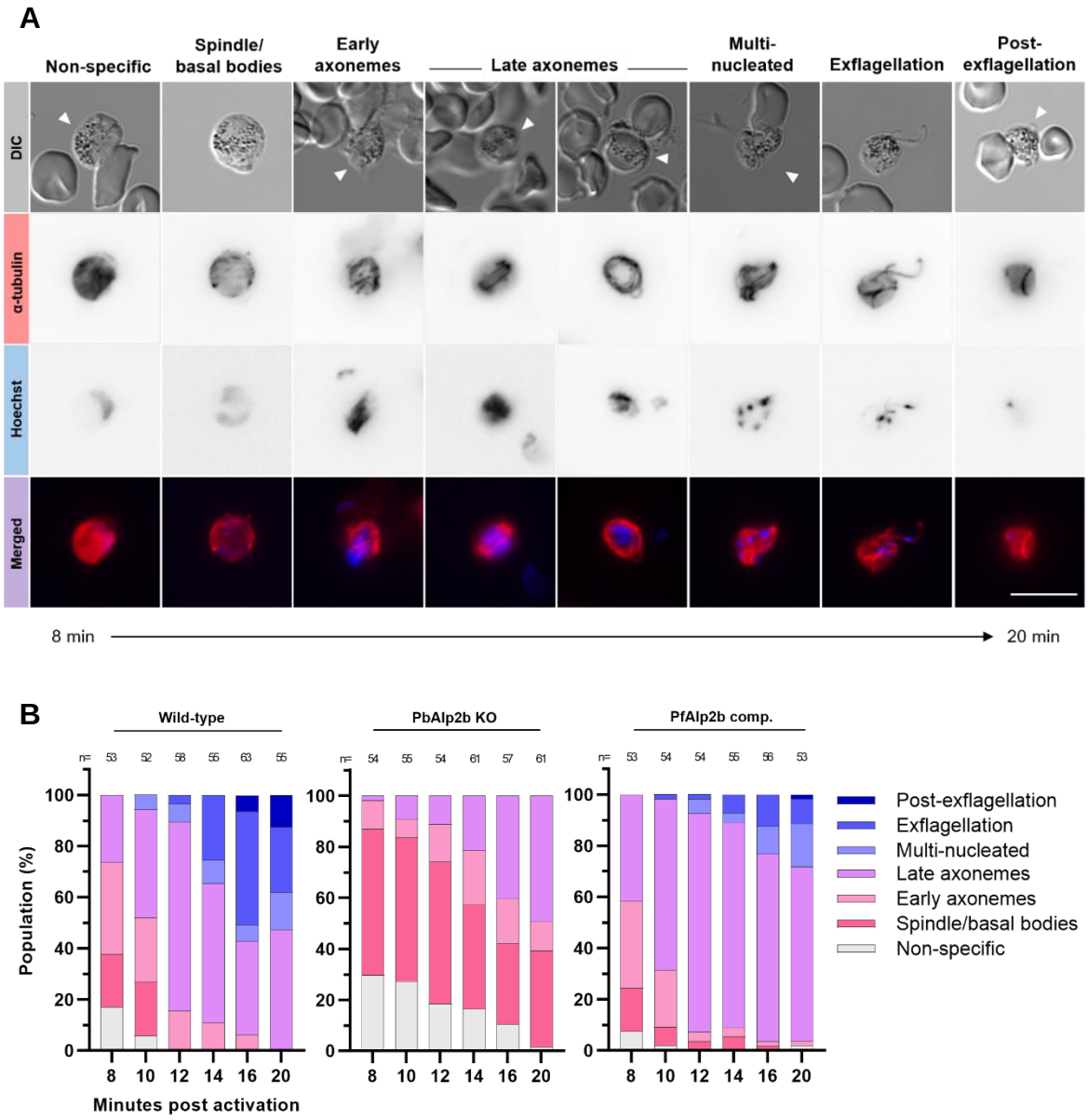

Figure 46: Quantitative analysis of the microgametogenesis and exflagellation process of wild-type and Alp2b mutant male gametocytes. (A) A detailed categorisation of the microgametogenesis and exflagellation process is presented, based on the localisation pattern of α-tubulin (red) and the nucleus (blue). Non-specific: diffuse signal with no association with axonemal structures. Spindle/basal bodies: rod-like (spindle) and dotted (basal bodies) signals, which are not conjoined. Early axonemes: Short tubular structures (axoneme) with attached basal bodies. No specific orientation. Late axonemes: Longer and aligned axonemal structures with basal bodies. Mostly coiled around the nuclei. Multi-nucleated: Similar axonemal structures to late axonemes, but with distinct nuclear signals that are segregated and pulled towards individual microgametes. Exflagellation: microgametes with a nucleus emerging from a gametocyte body. Post-exflagellation: residual DNA content in an almost empty gametocyte. Occasionally some microgametes are trapped inside but not egressing. The white arrow indicates a gametocyte. Merged = overlay of α-tubulin and Hoechst images. Scale bar = 10 µm. **(B)** Microgametogenesis and exflagellation process visualised based on the categorisation in (A). In comparison to the wild-type, the PbAlp2b KO gametocytes exhibited a markedly prolonged period before initiating axoneme formation, ultimately failing to progress to the multi-nucleated state necessary for exflagellation. These results suggest that Alp2b plays a non-essential role in the initial stages of microgametogenesis but is crucial for enabling exflagellation, potentially by contributing to nucleus distribution. The PfAlp2b-complemented gametocytes were observed to reach the exflagellation stage within a timeframe comparable to the wild-type, although the overall population was compromised. It may be inferred that PfAlp2b-complemented gametocytes also encounter difficulties in transitioning from the late axonemal stage to exflagellation, potentially for the same reason as the wild-type. DIC (differential interference contrast).

In conclusion, this study successfully established and utilised a quantitative exflagellation assay to identify the precise phenotypic effects of Alp2b KO, complementation and mutations in *P. berghei*. The mutations in the D-loop and H-plug demonstrated their indispensable role in the function of Alp2b. The highly conserved amino acid residues within the Alp2b unique insertion region were identified to be critical for exflagellation, while the conserved apex residues of the H-plug could be substituted with the corresponding sequence of actin. The visualisation of the microgametogenesis process has revealed that Alp2b may play a role in the initiation of axoneme formation and the final phase of exflagellation, potentially related to nuclear organisation.

4 Discussion

4.1 Production of recombinant *Plasmodium berghei* Alp1 and Alp2b

The production of recombinant proteins allows for an array of *in vitro* assays, including studies on the biochemical properties and molecular interactions, as well as the determination of crystal structures (Rosano and Ceccarelli, 2014). The obtained proteins can be further utilised for the generation of custom antibodies and *in vitro* binding studies. This information provides a reliable foundation for *in silico* docking studies, facilitating the identification of inhibitory ligands as part of drug development. The heterologous expression system using *Escherichia coli* is a robust and accessible system that has been employed to express various *Plasmodium* proteins belonging to the actin superfamily (Chen et al., 2018; Day et al., 2019; Dillenberger et al., 2023; Shonhai et al., 2008) and actin-binding proteins (Kursula et al., 2008; Schüler et al., 2005b). Moreover, the system was also used to express some yeast and plant actin-related proteins (Harata et al., 1999; March-Díaz et al., 2007).

4.1.1 Purification issues of PbAlp1

In this study, *P. berghei* Alp1 (PbAlp1) was successfully expressed using pET28a vector in the *E. coli* BL21 strain, and was rendered soluble through the co-expression of the *E. coli* chaperone set containing GroEL and GroES (**Figure 11**, **Figure 12**) The subsequent IMAC purification with Ni-NTA resin, however, revealed that the purified fractions contained several protein contaminants and the total yield of the recombinant Alp1 was insufficient for additional purification processes (**Figure 13**). Based on their molecular weights, some of the persistent contaminants appeared to be a mixture of histidine-rich proteins derived from *E. coli*, such as ArnA (74 kDa) and SlyD (28 kDa) (Andersen et al., 2013), and the chaperones, such as GroEL (60 kDa), that were co-expressed. The latter is particularly problematic as these chaperones are essential for the solubilisation of PbAlp1. One potential cause of contamination during IMAC is the binding specificity of the purification resin. During the protein binding step, Ni-NTA resin offers two Ni^{2+} ions for a polyhistidine tag to interact with, which results in a higher yield of his-tagged target protein (Block et al., 2009). However, this also compromises the specificity and may necessitate additional purification steps, such as size exclusion chromatography, to achieve the desired product purity. This would not be an issue if the solubilised pre-purification protein amount were sufficient to permit some yield loss during the process. However, given the limited quantity of solubilised PbAlp1, Ni-NTA may not have been the optimal choice. Ni-TED is yet another nickel-based purification resin, offering only one Ni^{2+} ion for interaction with the side chain

of a polyhistidine tag (Block et al., 2009). Alternatively, Co-CMA is a cobalt-based purification resin with two Co^{2+} ion binding sites that exhibit a weaker binding affinity for histidine (Bornhorst and Falke, 2000; Rubiyana et al., 2015). It minimises non-specific binding while favouring interaction with the polyhistidine tag. As anticipated, IMAC purifications with Ni-TED and Co-CMA resins resulted in a reduction of certain background impurities (**Figure 14**). However, these methods proved ineffective in removing the major contaminants, and the amount of purified PbAlp1 remained low, indicating that unspecific histidine binding is not the cause of poor yield of recombinant PbAlp1 and that the persistent contaminants are likely to have originated from the chaperones.

The contamination of recombinant proteins through chaperones can occur when they remain attached to the target protein during the purification process (Morales et al., 2019). ATP-dependent chaperones, such as GroEL/GroES and DnaK, can be promoted to release their interacting proteins through the addition of Mg-ATP to the purification column prior to the elution step (Imamoglu et al., 2020; Lin and Rye, 2006), thereby leaving the contaminant-free product. The Mg-ATP treatment successfully reduced one of the major contaminants of 60 kDa, which is likely to be residual GroEL (**Figure 16A**). Nevertheless, the overall product purity remained inadequate. These results strongly point to the necessity of increasing the amount of solubilised pre-purification PbAlp1 in order to enable additional purification steps to obtain the desired level of purity.

Despite the fact that a reasonable quantity of the expressed PbAlp1 could be solubilised under the optimal conditions, a considerable proportion was lost during purification due to its suboptimal binding to the IMAC resin. It is possible that the polyhistidine tag was misfolded into the protein or became cleaved, or that there were insufficient free histidine binding sites available due to the contaminants. It is unlikely that the cleavage had occurred, as the flow-through fraction following the IMAC resin binding step still contained intact histidine-tagged PbAlp1. The possibility of histidine binding site competition with nonspecific proteins was previously disproven, as the reduction of those contaminants did not result in an increase of bound PbAlp1. As a result, an attempt was made to optimise the exposure of the polyhistidine tag by relocating it from the N-terminus to the C-terminus of PbAlp1. Consequently, however, there was critical degradation of the expressed protein (**Figure 17**). This result demonstrated the limitations of the current polyhistidine tagging approach and the necessity for alternative affinity tags together with fundamental improvements to recombinant PbAlp1 solubility to overcome the poor IMAC resin binding affinity.

4.1.2 Persistent insolubility of PbAlp2b

The heterologous expression of *P. berghei* Alp2b (PbAlp2b) was successfully achieved in *E. coli*, although in a lesser abundance than PbAlp1 (**Figure 18**). This may be due to the fact that the genomic sequence of *pbalp2b* was not codon optimised for the *E. coli* expression system. The *Plasmodium* genome is considerably AT-rich (Honma et al., 2016; Weber, 1987), and its codon usage differs significantly from that of *E. coli* (Baca and Hol, 2000). The supplementation of *E. coli* tRNAs for rare codons (e.g., AUA, AGA, and GGA) through the co-expression of the pRAREII plasmid did not lead to an enhanced expression level of PbAlp2b (**Figure 19**). This suggests either that the tRNAs were insufficient to compensate for the codon bias, or that Alp2b is a challenging protein to express. Additionally, the potential toxicity of the recombinant PbAlp2b could be excluded, as the best expression level was observed in the standard BL21 strain, rather than in the so-called "toxic protein-resistant" C41 and C43 strains (Dumon-Seignovert et al., 2004). Interestingly, there was a slight elevation in the expression level when a SUMO tag was fused at the N-terminus of *pbalp2b* **(Figure 21)**. This may be the consequence of the structural stabilisation of the N-terminus and the reported chaperone effect of the SUMO protein (Malakhov et al., 2004).

Unlike PbAlp1, PbAlp2b was unable to be solubilised by the co-expression of *E. coli* chaperones (**Figure 19**). This may indicate the persistent misfolding or aggregation of the expressed PbAlp2b, which is attributed to the biochemical properties of the target protein, the biological limitation of the expression host, and the activity of the chaperones. For example, the formation of disulfide bonds between the cysteine residues in side chains is essential for the proper folding of the protein. However, the reducing environment of the *E. coli* cytoplasm makes this challenging (Makrides, 1996). The structural analysis of PbAlp2b based on the AlphaFold structure, using VADAR (Willard et al., 2003) revealed no potential disulfide bond formations. Moreover, the expression of PbAlp2b in a more oxidative periplasmic environment has also failed to yield soluble PbAlp2b (Diers, 2022). The available evidence suggests that a lack of disulfide bonds is an unlikely cause of the misfolding of PbAlp2b.

Post-translational modifications (PTMs) represent another challenge to the expression of eukaryotic proteins in *E. coli*. Some PTMs, such as phosphorylation, acetylation and ubiquitination, are inadequately provided in the *E. coli* system (Levin-Kravets et al., 2018; Sahdev et al., 2008) and the absence of these modifications can affect the stability and solubility of recombinant proteins (Tokmakov et al., 2012). As predicted by PTMGPT2 (Shrestha et al., 2024), PbAlp2b contains seven and three potentially ubiquitinated and acetylated residues throughout the protein, respectively, which may be indicative of the

insolubility observed in the *E. coli* system. The transient expression of PbAlp2b in insect cells, which provide a wider range of PTMs including ubiquitination and acetylation, however, also did not result in the production of soluble PbAlp2b (Diers, 2022). This outcome does not necessarily diminish the significance of PTMs. Rather, it may indicate underlying issues in the present solubilisation protocol, which is ineffective in both *E. coli* and insect systems.

Given that the solubilisation of PbAlp1 was dependent on the chaperone activity, it is also possible that the chaperone functions were somewhat compromised during the PbAlp2b expression. PbAlp2b is approximately 20 kDa larger than PbAlp1, and in general, the folding process of larger proteins is slower and involves several unstable intermediate forms, which are more prone to aggregation (Lin and Rye, 2006). Furthermore, some of the chaperones employed, such as GroEL/GroES, require regulated coordination for optimal protein folding (Dahiya and Chaudhuri, 2014). Considering the reduced expression level of PbAlp2b, it is possible that the overexpression of this larger protein was exerting undue pressure on the *E. coli* expression system, subsequently impairing chaperone activity and leading to the observed insolubility. An alternative possibility is that *E. coli* chaperones are incompatible with *Plasmodium* Alp2b. While it has been demonstrated that the co-expression of *P. falciparum* Hsp70-1 (a homologue of *E. coli* DnaK) also did not solubilise PbAlp2b (Moll, 2024), it is possible that Alp2b requires the assistance of multiple chaperones for its correct folding.

It is worth noting that the partial solubilisation of PbAlp2b was achieved through the application of the zwitterionic detergent FC12, which disrupts protein-protein interactions and releases the target protein from aggregation (Soulié et al., 2023). However, this method ultimately resulted in the degradation of PbAlp2b (**Figure 20**).

4.1.3 Prospective optimisation of recombinant PbAlp1 and PbAlp2b production

In summary, both PbAlp1 and PbAlp2b were successfully expressed in *E. coli*. Further optimisation is required to enhance the purification yield of PbAlp1. The current polyhistidine tag should be replaced with an alternative affinity tag that offers higher purification efficacy and reduced aggregation/misfolding. It may be beneficial to test whether larger protein-based tags, such as the haloalkane dehalogenase (Halo) tag and the maltose-binding protein (MBP) tag, can still be tolerated by the overexpression and the chaperones. The MBP tag has also been reported to enhance recombinant protein expression and solubility (Kimple et al., 2013). Some *P. falciparum* proteins were successfully solubilised using the tag (Goh et al., 2003; Shakya et al., 2017). PbAlp2b

proved to be the most challenging to solubilise, and the accumulated evidence indicates that *E. coli* may not be the optimal heterologous expression host for this protein. Consequently, alternative expression systems, such as insect cells (Bookwalter et al., 2017; Lee et al., 2019) and yeast (LaCount et al., 2009; Molbaek et al., 2020), should be explored to achieve a more feasible expression level and solubilisation. Although insect cells had previously been explored for the expression of PbAlps (Diers, 2022), there was considerable potential for optimisation. In addition, it would be advisable to consider the appropriate codon optimisation.

4.2 Critical role of Alp1 in facilitating ookinete gliding motility

The ookinete is the first infective form of *Plasmodium* to emerge during an infection of the mosquito host. They can move actively and are capable of penetrating the peritrophic matrix and epithelial tissues of the mosquito midgut (Douglas et al., 2015). Gliding motility is an essential mechanism for establishing the infection.

In this study, the complete removal of the *alp1* gene in *P. berghei* resulted in the abolishment of gliding motility in ookinetes (**Figure 26C**). This result aligns with the previous observation by Binder (2020), in which *pbalp1* was partially depleted using PlasmoGEM knock-out (KO) construct. In addition to the defect in motility, parasites with either a partial or complete Alp1 knockout exhibited a slightly delayed onset of infection during blood stage (**Figure 25A**). Some of the parasite clones appeared to struggle maintaining their growth after reaching 1% parasitaemia (**Figure 25B**). Nevertheless, this did not affect the ultimate development of ookinetes, and the effect of Alp1 KO on parasite growth was minor (**Figure 26B**). In the PlasmoGEM knock-out, approximately 36% of the cDNA sequence was still present in the C-terminus side of *pbalp1*. The complete removal of the gene in this study demonstrated that the residual C-terminal sequence has no impact on parasite growth or development. This finding indicates that Alp1 plays a crucial role in ookinete gliding motility and that partial gene removal is sufficient to significantly impair its function.

The function of *P. berghei* Alp1 could not be restored by the complementation with the cDNA of *P. falciparum* (Pf) *alp1* (**Figure 26C**). Given the moderately high amino acid sequence identity (76%) and the considerable structural similarity in the prediction, it was initially hypothesised that the cDNA of *pfalp1* would be sufficient to rescue the ookinete motility to a certain level. In contrast, the *pfalp1* cDNA-complemented ookinetes were entirely immotile, underscoring the potential involvement of introns as gene regulatory elements. Both *P. berghei* and *P. falciparum alp1* contain three introns, which share 53-59% sequence identities. Remarkably, in the subsequent complementation study with the

hybrid *alp1* comprising Pf-exons and Pb-introns, the ookinete motility was nearly fully restored (Busse, 2023), demonstrating the functional significance of *alp1* introns as well as the high degree of cross-species conservation. In eukaryotes, introns play a role in various aspects of gene expression, including alternative splicing, upregulation of expression and mRNA transport (Jo and Choi, 2015). In *Plasmodium*, the expression of certain proteins has been observed to be influenced by the presence of introns. For instance, *α2-tubulin* introns demonstrably enhance the expression of complemented *α1-tubulin* exons (Aguirre Botero, 2019), whereas the expression level of complemented *α2-tubulin* exons is observed to decline with the *α1-tubulin* introns (Spreng et al., 2019). Moreover, the presence of introns in profilin (*pfn*) affects gene expression in a life stage-specific manner (Moreau et al., 2017). The observations indicate that introns play a role in regulating gene expression in *Plasmodium*, with effects that vary depending on the functional locus and life stage. In the two isoforms of *Plasmodium* actin, only *actin2* contains an intron (Wesseling et al., 1989). The involvement of RNA helicase 'development of zygote inhibited' (DOZI) and the sm-like factor 'homolog of worm CAR-I and fly Trailer Hitch' (CITH) in the female-specific translational repression (Andreadaki et al., 2014; Mair et al., 2010) may indicate the potential role of the *actin2* intron in expression regulation. Furthermore, the introns of *var* genes of *P. falciparum* have been reported to mediate the relocation of transcriptionally active genes to the perinuclear compartment by recruiting actin filaments (Zhang et al., 2011). It is yet unclear whether *alp1* requires the same active gene regulation mechanisms. However, it is conceivable that the three introns of *alp1* may harbour comparable functions. According to the RNA-Seq result (Farr et al., 2021; Howick et al., 2019) (**Figure 47**), the expression of *pbalp1* is markedly upregulated during the developmentally active liver, trophozoite and male gametocyte stages, which are followed by a pronounced decline. This further suggests the necessity of a gene expression regulatory mechanism, which might be undertaken by the introns. To conclusively answer this question, the actual mRNA levels of *pfalp1* cDNA and the Pb-intron/Pf-exon hybrid *alp1* in *P. berghei* should be quantified through RT-PCR-based methods.

Despite the critical function of Alp1 in facilitating ookinete motility, the gene expression during the gliding motility-dependent stages (ookinete, sporozoite and merozoite) is relatively low. The shown upregulation in the liver and trophozoite stages may indicate a greater involvement of Alp1 in parasite development or the maturation of specific organelles that are subsequently required for motility. In *Toxoplasma gondii*, Alp1 has been shown to play a role in the formation of daughter cells during endodyogeny (Gordon et al., 2008). It could be hypothesised that *Plasmodium* Alp1 has a comparable role in schizogony, assisting in the correct organisation of cellular components but to less of a critical extent.

This could be linked to the slight growth delay observed in the Alp1 KO parasites during the blood stage, where the merozoites possibly emerged from incomplete schizogony or maturation with compromised gliding motility, resulting in lower infectivity and thus slower parasitaemia progression. The male-biased upregulation of *alp1* expression must be considered carefully, as the post-fertilisation development-related proteins are generally more actively synthesised in female gametocytes (Dash et al., 2022; Khan et al., 2005). Nevertheless, it might be possible that Alp1 performs a number of functions of varying levels of importance that extend beyond facilitating ookinete gliding motility, encompassing also cellular development. In this study, the maturity of ookinetes was morphologically determined. In order to investigate the potential involvement of Alp1 in parasite development and subsequent impact on motility, it would be useful to examine the developmental status of the glideosome by observing the cellular localisation of individual components, such as myosin A, GAPs and MTIP (Green et al., 2017; Ridzuan et al., 2012; Siden-Kiamos et al., 2020). In addition, the surface adhesin circumsporozoite- and TRAP-related protein (CTRP) would also serve to indicate the functionality of the apical complex and glideosome in ookinete gliding motility (Ramakrishnan et al., 2011).

To summarise, this study demonstrates the essential role of Alp1 in ookinete gliding motility. The partial (64%) removal of the upstream region of *alp1* drastically reduced the motility of ookinetes, while the full KO of the gene resulted in the complete abolition of the motility. The results suggest that the C-terminus may exert a lesser influence on Alp1 function than the N-terminus. Furthermore, the cDNA complementation of *pfalp1* reveals the functional importance of the introns, which may play a role in regulating gene expression. The objective of the prospective study is to elucidate the precise molecular mechanism by which Alp1 facilitates gliding motility. Furthermore, the scope of observation should be extended to other motile stages, such as sporozoites, which, interestingly, show no expression of Alp1, as well as non-motile liver stage parasites that display markedly elevated levels of Alp1 expression. Further investigation of the function of Alp1 can be conducted in conjunction with its localisation, as demonstrated through fluorescent tagging.

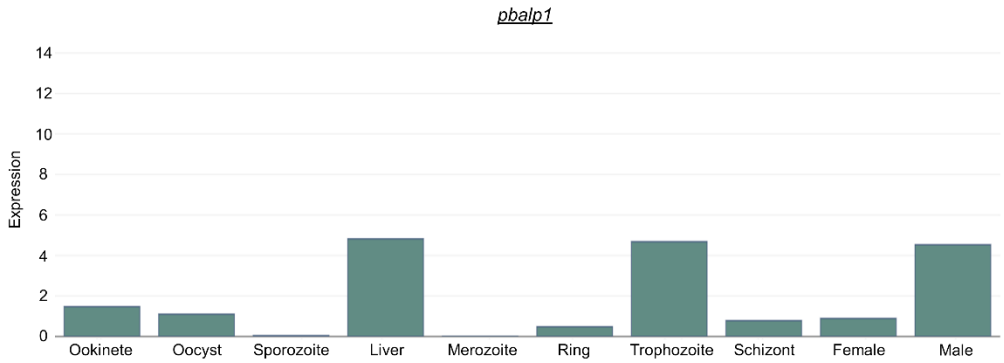

Figure 47: Gene expression profile of *P. berghei alp1* throughout the life cycle. Despite the critical role of Alp1 during the ookinete stage, other stages (liver, trophozoite and male gametocyte) involving or in close association with asexual replication exhibit comparably elevated *alp1* expression. Expression unit in relative expression level. The graph retrieved from SPOT profiling (Farr et al., 2021), generated based on the Malaria Cell Atlas (Howick et al., 2019).

4.3 Localisation of Alp1 in *P. berghei* ookinete

The fusion of *egfp* to the endogenous *pbalp1* resulted in the inhibition of gliding motility in ookinetes (**Figure 27D**). Consequently, the *egfp-pbalp1* construct was expressed as an additional copy, which successfully maintained the function of the endogenous *alp1*. However, the desired isogenic line could not be obtained, and no intact EGFP-PbAlp1 expression was detected in the subsequent western blot analysis (**Figure 28**). Ultimately, the 3xHA tag was used to visualise the additional copy of Alp1 in ookinetes. Fluorescent protein tags, such as EGFP, are an excellent tool for capturing the live localisation of target proteins. The EGFP tag has been used to visualise actin in a number of organisms, including *Drosophila melanogaster* (Verkhusha et al., 1999), *Saccharomyces cerevisiae* (Doyle and Botstein, 1996), *Dictyostelium discoideum* (amoeba) (Westphal et al., 1997) as well as actins in *Plasmodium* (Andreadaki et al., 2014; Angrisano et al., 2012; Deligianni et al., 2011) and Alp1 in *Toxoplasma gondii* (Gordon et al., 2009, 2008). However, its relatively large size (27 kDa) could potentially impact the function and stability of the tagged protein (Montecinos-Franjola et al., 2020). It is conceivable that the presence of EGFP and the ten-amino-acid linker upstream of the *alp1* open reading frame may have interfered with the transcription process by the native *pbalp1* promoter and potentially relevant introns. The absence of intact protein expression precludes the possibility of protein aggregation. However, it is also conceivable that Alp1 naturally has a high turnover rate, which renders it undetectable by western blot. In contrast, the 3xHA tag is considerably smaller (3 kDa) and has been commonly used to visualise several *Plasmodium* proteins of cytoskeletal, cytosolic and nuclear origins (Cepeda Diaz et al., 2023; Collier et al., 2023; Liu et al., 2020). However, as it is an epitope tag, it automatically excludes the live microscopy option.

In motile *P. berghei* ookinetes, Alp1-3xHA was observed to be localised throughout the cytoplasmic compartment of the cell (**Figure 30**). The signal patterns exhibited multiple speckles and small aggregates, yet no discernible subcellular localisations were identified, including the inner membrane complex, where the glideosome is located. In comparison to the myosin A localisation (Green et al., 2017), it is evident that Alp1 is absent from the apical tip and the periphery of mature ookinetes. The presence of similar cytoplasmic speckles and a slight accumulation around the nucleus were also observed with Arp1 (Siden-Kiamos et al., 2010) and *Toxoplasma* Alp1 (Gordon et al., 2008). However, the general density of the observed Alp1 speckles appear markedly higher, and no obvious sign of co-localisation between the Arp1 and Alp1 could be recognised. In relation to actin1 (Angrisano et al., 2012), no discernible pellicular localisation of Alp1 was observed, while both proteins were found to be present in the cytoplasm. Instead, the localisation pattern observed with actin2 (Andreadaki et al., 2014) is more comparable to Alp1. Actin2 is known to be essential for both exflagellation and sexual stage development, and its expression is also significantly upregulated in male gametocytes (Andreadaki et al., 2014; Deligianni et al., 2011; Lopez et al., 2023). Functionally, however, actin2 does not influence ookinete motility (Andreadaki et al., 2014). In this thesis, an actin chromobody was employed for the visualisation of total actin in ookinetes (**4.4**). Similarly, no common localisation patterns were observed between Alp1 and chromobody-actin. The collective observation suggests that Alp1 is unlikely to co-localise with actin, despite its critical contribution to gliding motility.

Overall, the generation and expression of PbAlp1-3xHA was successfully achieved, and Alp1 was predominantly found in the cytoplasm of ookinetes. The interpretation of the localisation result nevertheless requires careful evaluation, as there are potential issues with tag cleavage and mislocalisation of non-functional Alp1. While the small size of the 3xHA is advantageous in minimising the tagging effect on the target protein, it is also challenging to detect the cleavage. It is probable that the western blot analysis conducted in this study was unable to detect the 3 kDa cleaved 3xHA tag. Secondly, the functional impairment of the endogenous Alp1 observed in the EGFP tagging could also be applicable to the additional Alp1-3xHA. In this case, as the endogenous Alp1 remains functional, it is not feasible to phenotypically assess the functionality of the tagged Alp1. Although the non-functional GFP-actin has been observed to correctly localise in yeast (Doyle and Botstein, 1996), the possibility of mislocalisation due to functional impairment of Alp1-3xHA still cannot be excluded. In this context, further tagging attempts of endogenous Alp1 should be included in future experiments. The 3xHA tag on the endogenous Alp1 has yet to be tested. Alternatively, another epitope tag, FLAG, has been successfully utilised in *Plasmodium* (Lopez et al., 2023; Takano et al., 2019). Assuming that Alp1 is a cytosolic protein, the split

GFP system with the small FP11 tag (< 2 kDa) (Kamiyama et al., 2016) may represent a viable alternative for achieving live localisation while minimising the tagging impact on gene expression. Nevertheless, it is essential to conduct a detailed examination of the functional tolerance of Alp1 in the presence of an EGFP tag.

4.4 Visualisation of F-actin in *P. berghei* ookinete and the role of Alp1 in actin dynamics

While Alp1 is a critical factor for gliding motility, its cellular localisation does not appear to correspond with that of the glideosome at the pellicle. This raises the question of whether Alp1 exerts an indirect influence on the glideosome, thus affecting gliding motility. To ascertain whether Alp1 interacts with actin, a central component of the glideosome, fluorescent visualisation of total actin in *P. berghei* was conducted. The dynamic properties of apicomplexan actin pose a significant challenge when it comes to direct visualisation. Many conventional methods, including the widely used LifeAct (Riedl et al., 2008), have shown their limitations in effectively visualising the actin polymer structures in apicomplexan cells (Das et al., 2021; Melak et al., 2017). The actin chromobody is a nanobody directed against actin, which is conjugated with a fluorescent protein (Melak et al., 2017). It is highly specific and has been successfully employed to visualise apicomplexan actin without interfering with the polymerisation dynamics and the cellular viability (Del Rosario et al., 2019; Hvorecny et al., 2024; Periz et al., 2017; Stortz et al., 2019). In *Plasmodium*, the chromobody has visualised actin in sexual stage parasites, gametocytes (Collier et al., 2023; Stortz et al., 2019) and sporozoites (Yee et al., 2022). This study therefore focuses on ookinetes and successfully reveals unique actin localisations, which are strongly linked to the polymerisation dynamics. Moreover, the role of Alp1 in actin dynamics was elucidated through the visualisation of chemically modulated actin filaments. Of note, the actin chromobody did not measurably affect the motility of the parasites in this assay (**Figure 32**), thus proving itself to be a robust tool for the study of *Plasmodium* actin.

4.4.1 Heterogeneous localisation of actin in wild-type and Alp1 knock-out ookinetes

In mature wild-type ookinetes, actin filaments (F-actin) were frequently observed assembling into tubular structures of varying thickness, often extended from the either end of the parasite's longitudinal axis. In some cases, a mesh-like actin network was observed to connect the apical and basal poles by stretching across the cell (**Figure 33A**). These localisations, particularly the mesh-like network, bear resemblance to the previously observed F-actin flow in *Toxoplasma gondii* tachyzoites, where the accumulated F-actin at

the apical tip was distributed towards the Golgi apparatus and the basal body via dynamic network formation (Del Rosario et al., 2019). The fluorescent signals of chromobody-actin in ookinetes were detected in the apical and basal tips, the nuclear region, and in combinations of these locations (**Figure 33B**). The observed heterogeneity of cellular location patterns may indicate the transient localisation of F-actin, as previously observed in *Toxoplasma* (Del Rosario et al., 2019), and the dynamic retrograde flow of F-actin across the cell. Almost identical F-actin localisations were observed in the ookinetes lacking Alp1 (**Figure 33B)**. Despite the critical impairment of gliding motility, no specific polarisation of actin signals was identified. Similarly, the thick F-actin tubular structure was also present in a comparable manner to that observed in wild-type ookinetes (**Supplement 6**). These results indicate that the defective motility of Alp1 KO ookinetes is not caused by the mislocalisation of actin and that Alp1 plays a minimal role in maintaining F-actin integrity. Given that the dynamic F-actin flow is postulated to underlie the operational mechanism of gliding motility (Martinez et al., 2023; Tosetti et al., 2019), the comparable variance in cellular F-actin locations between Alp1 KO and wild-type ookinetes may imply the possibility that Alp1 is involved in local regulation of gliding machineries rather than in the universal organisation of actin.

4.4.2 Functional implications of F-actin cellular locations

Both wild-type and Alp1 KO ookinetes exhibited comparable variance in the distribution of F-actin signals (**Figure 33B**). The F-actin signals were most frequently observed in the entire cell as a combination of cytosolic tubules and a network, as well as an accumulation at either or both ends of the parasite. It has been demonstrated that the apically nucleated F-actin is associated with gliding motility and is channelled into the pellicular space by conoidal flux, where it is subsequently translocated along the inner membrane complex (IMC) surface towards the basal end in *Toxoplasma* and *Cryptosporidium*. (Dos Santos Pacheco et al., 2022; Martinez et al., 2023; Tosetti et al., 2019). *Plasmodium*, which lacks the classical conoidal structure, also demonstrates comparable pellicular F-actin translocation (Pražák et al., 2024). Given that some conoid-associated members are also present in *Plasmodium* (Bertiaux et al., 2021; Wall et al., 2016), a similar mechanism may be responsible for sustaining the dynamic distribution of glideosome-associated actin.

The cytosolic actin network has been described in the context of cytokinesis during the intra-erythrocytic schizogony (Stortz et al., 2019). The assembly of the network is governed by formin2, one of the principal F-actin nucleators in *Plasmodium* (Baum et al., 2008b; Stortz et al., 2019). Although ookinetes do not undergo cytokinesis, the linkage between

the major F-actin nucleation sites at the apical and basal poles may indicate the potential function of the F-actin network in coordinating these two sites or facilitating intracellular material exchange (Del Rosario et al., 2019; Periz et al., 2017).

Of particular interest is the thick tubule observed to run along the longitudinal axis from either the apical or basal poles of ookinetes. The length of the thick tubule ranged from a few microns to almost the entire length of the parasite, exhibiting both linear and mild coiling patterns. Interestingly, a comparable tubular structure has been observed in replicating *Toxoplasma gondii*, which facilitates the synchronous maturation of daughter cells (Periz et al., 2017). This function is not directly relevant for ookinetes. However, as with the cytosolic actin network, it can be postulated to function as a means of intracellular transport or communication. An alternative interpretation is that the thick tubular formation of F-actin may be associated with the cell rigidity or maintenance of physical balance during the gliding motility. In *Cryptosporidium* sporozoites, F-actin was observed to be positioned parallel to the spirally elongated filaments on the external surface of the IMC, suggesting its involvement in the helical gliding motility (Martinez et al., 2023). Although the actin-tubules observed in ookinetes did not take an obvious spiral form, the tendency towards slightly coiled longitudinal elongation might also imply an association with the helical motion. While several potential functions of thick actin tubules have been considered, it is important to note that in the majority of cases, only a single thick actin tubule structure was observed per ookinete. This may favour the speculative functions in cellular transport or organisation, given that gliding motility generally requires coordination of multiple smaller structural components rather than a single, solid apparatus.

The visualisation of F-actin in ookinetes demonstrated that the overall localisation and structures remain unaltered by the absence of Alp1. Therefore, further investigation was conducted into the role of Alp1 in actin polymerisation dynamics through the use of chemical modulators.

4.4.3 Chemical modulation of actin and the role of Alp1 in polymerisation

While Alp1 does not influence the cellular distribution of F-actin in ookinetes, it is not yet clear whether Alp1 plays a role in regulating F-actin formation. The apicomplexan gliding motility is facilitated by a molecular motor called the glideosome (Opitz and Soldati, 2002). Actin is a central component of this machinery, and its dynamic polymerisation and depolymerisation properties exert a significant influence on the parasite's gliding motility. (Münter et al., 2009). To investigate whether the impaired motility of Alp1 KO ookinetes is attributed to misregulation of F-actin dynamics in the glideosome, the *in vivo* vulnerability

of F-actin towards chemical stabilisation and destabilisation was evaluated in the absence of Alp1. The actin filament modulators jasplakinolide (Jas) and cytochalasin D (Cyto D) are commonly used compounds for the study of actin polymerisation dynamics. Jas is a cyclic peptide that promotes the nucleation and stabilisation of actin filaments (Bubb et al., 2000). In contrast, Cyto D inhibits the polymerisation and depolymerisation of the filament by capping the growing barbed end binding to monomers, which leads to the destabilisation of the actin filament (Shoji et al., 2012).

The impact of Alp1 KO on actin polymerisation was assessed by examining the sensitivities to Jas and Cyto D treatments. In both wild-type and Alp1 KO ookinetes, the treatments with these compounds resulted in significant alterations to the localisation patterns of actin. The actin filament destabiliser, Cyto D, induced the degradation of both tubular and network structures in a concentration-dependent manner, resulting in the diffuse actin signals within the cytoplasm (**Figure 34B,C**). Interestingly, in response to cytoplasmic F-actin depolymerisation, a notable accumulation of F-actin signals was observed at the nucleus. It could be proposed that the excessive amount of monomeric actin in the cytoplasm promoted the polymerisation of nuclear actin (Scheffler et al., 2022). However, the actin chromobody utilised in this study lacks nuclear localisation signals, and it is unclear whether it can still access nuclear F-actin to the same extent. Given the specificity of the chromobody to F-actin (Periz et al., 2017), it seems unlikely that the chromobody was imported to the nucleus along with monomeric actin. Therefore, it can be postulated that the accumulated F-actin is situated at the periphery of the nucleus. It is possible that specific elements from the nucleus, such as transcriptionally active mRNA (Zhang et al., 2011), may be exerting an opposing effect on the depolymerisation impact of Cyto D in this particular region. Nevertheless, no difference in sensitivity to Cyto D was identified between the wild-type and Alp1 KO ookinetes, indicating that the function of Alp1 is less likely related to the stabilisation of F-actin (**Figure 34C**).

The stabilisation of F-actin by Jas treatment resulted in a strongly polarised localisation to the apical and basal tips of the parasite (**Figure 34A**). This response is comparable to that observed in Jas-treated sporozoites (Yee et al., 2022), and the distinct signal pattern with whisk-like split tubules resembles the alignment of subpellicular microtubules (SPMT) and IMC surface filaments (Bertiaux et al., 2021; Dos Santos Pacheco et al., 2022; Qian et al., 2022). The accumulation of F-actin at the apical and basal ends of the parasite may be indicative of the actin polymerisation and depolymerisation centres, respectively. One of the isoforms of an actin nucleator, formin1, is also localised at the apical tip of the parasite and provides the necessary F-actin to facilitate gliding motility (Baum et al., 2008b; Douglas et al., 2018; Tosetti et al., 2019). On the other hand, the basal end appears to be the point

of collection for F-actin, which is mobilised from the apical tip through the dynamic retrograde flow (Del Rosario et al., 2019; Dos Santos Pacheco et al., 2022; Pražák et al., 2024). The prevalence of pore structures connecting the IMC and the cytoplasm may suggest that the basal end serves as a recycling centre for actin (Martinez et al., 2023; Pražák et al., 2024). This process may involve coronin disassembling actin filaments through the recruitment of actin depolymerising factor (ADF) (Bane et al., 2016; Douglas et al., 2018). In *Toxoplasma* tachyzoites lacking ADF, F-actin exhibited a similar localisation pattern to that observed in the Jas treatment, with an enhanced signal at the basal end (Periz et al., 2017). This may represent a congestion of the F-actin turnover gateway due to the over-stabilised filaments, which could be comparable to the Jas treatment in this assay. Altogether, the accumulation of F-actin at specific cellular locations is indicative of disrupted F-actin dynamics due to inadequate depolymerisation. This ultimately impedes the relocation of adhesion sites (Münter et al., 2009) and inhibits gliding motility.

The sensitivity of F-actin to Jas treatment was increased in Alp1 KO ookinetes compared to wild type (**Figure 34C**), indicating that F-actin becomes more susceptible to the stabilising effect in the absence of Alp1. Conversely, Alp1 may be responsible for maintaining F-actin dynamics by facilitating filament destabilisation. As Alp1 does not regulate the overall integrity of the F-actin network, its function is likely to have a mild effect on individual actin filaments. The potential actin depolymerisation mechanism of Alp1 can be speculated as both direct and indirect interaction with the filaments. Since the destabilising effect of Alp1 could not be compensated by Cyto D (**Supplement 8**), it is possible that Alp1 destabilises the filaments in a way other than barbed end capping, for example by promoting disassembly or sequestering of monomers. The structural similarity between Alp1 and actin may permit copolymerisation, as observed with Arp1 in the dynactin complex (Fokin et al., 2021). This could result in the formation of an unstable actin-Alp1 hybrid filament due to differing inter-subunit interactions. The expansion of the Alp1 D-loop structure (the key polymerisation contributor) through the insertion of the actin sequence did not affect ookinete motility (Busse, 2023), suggesting that actin and Alp1 could be interchangeable in possible copolymerisation. An *in vitro* polymerisation assay with recombinant Alp1 might reveal unconventional actin filament formation in *Plasmodium*. If Alp1 would not engage in copolymerisation, it could instead be a constituent of a complex that influences the stability of F-actin, or that coordinates with F-actin destabilising ABPs. Given the multiple unique insertions and deletions (InDels) that are predominantly located on the outer surface of the protein (**Figure 7**), it appears more probable that Alp1 may constitute a subunit of a larger complex. It can be hypothesised that the structural alterations resulting from the InDels may be necessary for mediating specific substrate

interactions. The replacement of the individual InDel regions has been shown not to affect the function of Alp1 (Busse, 2023). However, this does not preclude the possibility of Alp1 interacting with its partners via multiple contact points. In order to test the potential existence of Alp1 in a complex, a pull-down assay can be conducted following the establishment of an appropriate endogenous tagging method for Alp1. Furthermore, the simultaneous mutation of multiple InDel regions may assist in elucidating the conformational arrangement of potential interaction partners.

This study presents one of the first detailed analyses of chromobody-actin localisation in *Plasmodium* ookinetes. While certain observations align with the previous localisation studies utilising other actin visualisation systems, some atypical actin structures were also observed. The actin chromobody successfully elucidated the destabilising role of Alp1 on F-actin, which appears to exert a moderate effect on actin dynamics. Given the central role of actin in gliding motility, it is entirely conceivable that a minor misregulation could result in a critical failure of the entire motor machinery. The potential interaction of Alp1 with other proteins associated with gliding motility should be further investigated as part of a future study. Nevertheless, the Alp1 KO-actin chromobody parasite line established in this study will also permit observation of the impact of Alp1 deletion in other stages, such as trophozoites and male gametocytes, where gene expression is markedly upregulated. This will provide valuable insight for the comprehensive characterisation of this protein.

4.5 Critical role of Alp2b in male gametocytes

The sexual reproduction of *Plasmodium* occurs exclusively in mosquitoes following the ingestion of gametocytes (Kuehn and Pradel, 2010). Upon reaching the mosquito midgut, environmental stimuli, such as temperature, pH and mosquito-derived xanthurenic acid, activate sex-specific developments (Billker et al., 1997). Male gametocytes are subject to microgametogenesis, a process obligatory for the fertilisation of female gametocytes. Subsequently, the motile microgametes emerge from the parent gametocyte through a process called exflagellation and proceed to fertilise the female (Billker et al., 2004).

This study demonstrated that the deletion of Alp2b resulted in the complete inhibition of exflagellation of *P. berghei* gametocytes (**Figure 37B**). This observation aligns with the previously reported phenotype, wherein these gametocytes also failed to produce any oocysts (Binder, 2020). A further study by Mikus (2020) utilising a sex reporter line corroborated that the absence of Alp2b does not result in sex ratio distortion. This implies that male gametocytes were still produced, yet remained incapable of exflagellating. The establishment of a systematic quantification method for exflagellation has greatly

contributed to elucidating the subtle phenotypic differences between the Alp2b complemented and mutated parasite lines. The quantification analysis revealed that the KO parasites complemented with PbAlp2b exhibited a comparable exflagellation rate to wild-type controls, thereby verifying the crucial role of Alp2b in facilitating exflagellation.

In order to investigate whether the function of Alp2b is conserved between other *Plasmodium* species, the *alp2b* gene of *P. falciparum* was introduced into *P. berghei* (**Figure 35**). The quantitative analysis of exflagellation revealed that PfAlp2b was capable of restoring *P. berghei* exflagellation by approximately 20% (**Figure 37B**), indicating that the function of Alp2b in microgametogenesis is conserved to a certain degree in these two species, and potentially in other *Plasmodium* species. Conversely, the relatively low phenotypic rescue may also suggest the functional contribution of species-specific protein sequence, which could be required for interaction with specific proteins within the respective species. This, in turn, emphasises the capacity of conserved amino acid sequences to maintain Alp2b functionality.

While it is evident that Alp2b is essential for exflagellation, its function in female parasites is yet to be elucidated. The single-cell transcriptomics indicate that Alp2b is generally expressed at low levels, yet with no notable difference between male and female gametocytes (Farr et al., 2021; Howick et al., 2019) (**Figure 48**). Moreover, despite its critical function during microgametogenesis, Alp2b is more abundantly expressed during the ookinete and oocyst stages. It would be beneficial to generate a conditional Alp2b KO line utilising the dimerisable Cre (DiCre) recombinase system (Das et al., 2017; Fernandes et al., 2020) in order to investigate the role of Alp2b in the post-fertilisation stages. To examine the potential female-specific function of Alp2b, the protein could be expressed under a sex-specific promoter, such as the *ccp2* promoter, which is employed in the *P. berghei* 820cl1m1cl1 fluorescent reporter line (Ponzi et al., 2009) previously used for sex ratio determination (Mikus, 2020). An alternative approach would be to cross the current Alp2b KO line with a sterile female gametocyte line, thus enabling observation of whether Alp2b affects female fertility. For example, parasites lacking the macrogamete-contributed factor essential for transmission (*MaCFET*) gene can develop normally during the blood stage but produce only fertile male gametocytes (Kumar et al., 2022). Such a parasite line would be an optimal candidate for the crossing experiment. Overall, this study has identified a critical function of Alp2b in male gametocytes, which completely blocks the transmission of *Plasmodium* to mosquitoes.

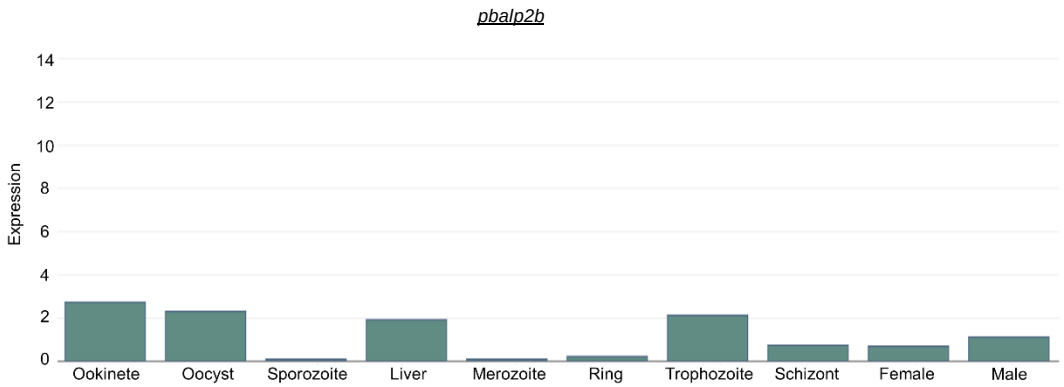

Figure 48: Gene expression profile of *P. berghei alp2b* throughout the life cycle. Despite the critical function of Alp2b in male gametocytes, higher expression levels are observed in the ookinete and oocyst stages. Furthermore, the expression of *alp2b* in female gametocytes implies the potential role of Alp2b during this stage. Expression unit in relative expression level. The graph retrieved from SPOT profiling (Farr et al., 2021), generated based on the Malaria Cell Atlas (Howick et al., 2019).

4.6 Unique insertions of D-loop and H-plug in Alp2b

Alp2b is notably larger than actin1 due to a number of extensive insertions into the actin fold core structure (**Figure 7A**). The majority of these insertions are conserved across the *Plasmodium* species, with a tendency to accumulate in specific locations within the subdomains (SDs) 2 and 4 (**Figure 49**). The largest patch of insertions is located in SD2 resulting in a substantial enlargement of the D-loop structure (**Figure 7B**). The downstream insertion within the D-loop demonstrates significantly reduced interspecies conservation, exhibiting only 24% amino acid sequence identity, as opposed to the upstream insertion which displays 66% identity. This could signify that the downstream insertion determines the dimensions and the species-specific characteristics of the Alp2b D-loop, while the conserved upstream insertion may play a role in the core function of the protein. Between SD3 and SD4, the smaller insertion results in an extension of the H-plug structure. The H-plug, along with the D-loop, is a crucial element in the polymerisation of actin (Chou and Pollard, 2019; Dominguez, 2019). The substantial alteration of these structures in Alp2b may be indicative of its non-polymerising characteristics, as observed in many Arps (Muller et al., 2005). For example, Arp4, the closest phylogenetic relative of Alp2b (Gordon and Sibley, 2005), is canonically known to form chromatin-remodelling complexes with actin and other Arps, rather than polymerising itself (Oma and Harata, 2011). *Plasmodium* Arp4 also does not seem to form a filament (Liu et al., 2020). While no homologue has been annotated in *Plasmodium*, Arp8 exhibits an intriguing structural similarity to Alp2b, characterised by enlarged D-loop and H-plug (Muller et al., 2005). Arp8 is a subunit of the human and yeast INO80 chromatin remodelling complexes, and binds both actin and Arp4 (Kunert et al., 2022). The extended D-loop of Arp8 blocks its own pointed end through internal interactions,

while the altered H-plug orients itself towards the neighbouring actin, presumably obstructing conventional polymerisation (Gerhold et al., 2012). It is conceivable that the unique insertions of the D-loop and H-plug in Alp2b may similarly interfere with the polymerisation process, or mediate certain protein-protein interactions either directly or through conformational change to fulfil Alp2b-specific functions.

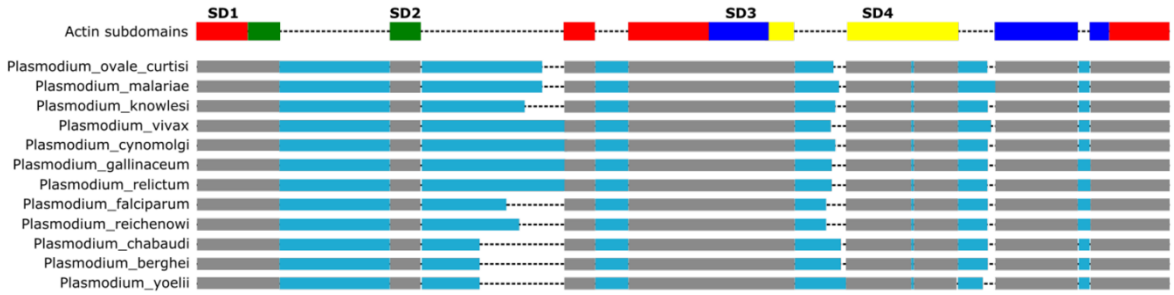

Figure 49: Alp2b protein sequence from different *Plasmodium* species aligned in relation to actin. The multiple sequence alignment reveals the presence of insertion hotspots in subdomains 2 and 4. The substantial insertions observed in subdomain 2 and the smaller insertion between subdomains 3 and 4 result in the enlargement of the D-loop and H-plug structures, respectively. The grey bars represent regions that could be aligned with actin1, while the blue bars indicate the relative size and location of insertions. SD = subdomain. Figure was adapted from Mikus (2020).

4.6.1 Functional contribution of Alp2b D-loop to exflagellation

The replacement of the Alp2b D-loop with the actin1 D-loop resulted in the chimera Alp2b harbouring a 60 amino acids shorter D-loop (**Figure 38, Figure 39A**) (Mikus, 2020). As anticipated, the substantial downsizing of the key structure led to the complete abolishment of exflagellation in the mutant parasites. (**Figure 43**). This indicates that the physical presence of the expanded D-loop may play a role in maintaining Alp2b function. Furthermore, the loss of Alp2b-specific amino acid residues may also have had a significant impact. A further mutation, focusing on the unique insertions of D-loop, demonstrated that the highly conserved eight amino acid residues at Y52-K59 are essential for exflagellation. (**Figure 40A, Figure 43**). The mutation was conducted through alanine substitution of the target residues, thereby preserving the original size of the D-loop. This indicates that these amino acid residues are not merely placeholders for the larger D-loop, but rather serve a specific function in facilitating exflagellation. The two positively charged lysine residues (K58-K59) in this region, and their location in the base of the D-loop, may imply a role in facilitating specific conformational changes through internal interactions, as observed in Arp8 (Gerhold et al., 2012). In the AlphaFold prediction model, the alanine substitution of the conserved Y52-K59 residues exhibited a marked orientation shift of the major alpha helix and the formation of a small secondary loop in SD2 (**Figure 40B**). Despite the fact that this dynamic region generally exhibits reduced prediction confidence, this structural alteration could still be caused by the neutralisation of the mutated region's net charge,

which further suggests that these conserved residues may play a role in maintaining the conformational change of Alp2b.

4.6.2 Functional contribution of Alp2b H-plug to exflagellation

The H-plug of Alp2b was replaced with the actin1 H-plug, which reduced the size of the original structure by 15 amino acids (**Figure 38, Figure 41A**). The introduction of a smaller H-plug also resulted in the inhibition of exflagellation (**Figure 43**), thus identifying the H-plug as a critical contributor to the function of Alp2b. The multiple sequence alignment and mapping on the AlphaFold predicted structure identified five conserved amino acid residues (N438-K442) located at the tip of the H-plug (**Figure 42A,B**). It may be posited that these residues indicate conserved protein or chemical interactions across the species. The substitution of the conserved H-plug tip with the corresponding region of the actin1 H-plug (G269-A273) resulted in a minor reduction in the exflagellation rate (**Figure 43**), indicating that the function of the conserved H-plug tip may be compensated for by the actin1 residues. In actin1, the tip of the H-plug contains three crucial amino acid residues, G269, K270 and E271, which engage in intersubunit contacts during polymerisation (Douglas et al., 2018; Pospich et al., 2017). The moderate phenotypic effect observed in the presence of crucial actin residues may suggest that the H-plug in Alp2b and actin facilitate protein function in a similar manner. It is noteworthy that the first complementation with the complete actin1 H-plug sequence also contained these three critical amino acids, yet no exflagellation was observed. This implies that, in addition to the functional residues, the enlarged structure of the H-plug itself is also necessary to facilitate exflagellation. It should be noted, however, that the question of whether the exflagellation was mediated by the compatible actin residues or through the presence of other functionally critical residues within Alp2b remains unanswered. In order to answer this question, it would be necessary to either neutralise the H-plug tip through alanine substitution or to perform a mutation of other conserved residues.

The enlarged D-loop and H-plug of Alp2b both contain several unique insertions that are highly conserved across the *Plasmodium* species. The findings of this study indicate that the conserved tip region of the H-plug can be replaced by the corresponding actin1 sequence, provided that the original length is maintained. Additionally, the residues at the base of the D-loop are crucial for exflagellation, potentially due to their role in the conformational shift of the protein, given their hydrophilic nature. Considering the structural resemblance to Arp8 (Muller et al., 2005), it would be interesting to observe whether Alp2b interacts with actin and Arp4, as found in the INO80 complex (Oma and Harata, 2011). The presence of RUVBL homologues in *Plasmodium* (Ahmad and Tuteja, 2012; Sen et al., 2018), which are essential subunits of the INO80 complex (Jónsson et al., 2004), lends

further support to the idea that Alp2b might represent a highly divergent variant of Arp8 that participates in an INO80-like complex. Here, protein pulldown or colocalisation assays with RUVBL (Sen et al., 2018) through Alp2b tagging would be useful to answer this question.

4.7 Inhibition of microgametogenesis in the absence of Alp2b

Prior to exflagellation, a male gametocyte produces up to eight motile haploid gametes through a rapid and complex process known as microgametogenesis (Dash et al., 2022). This process entails the cytoplasmic assembly of axonemes and three rounds of genome replication (mitosis I, II and III), which are facilitated by two distinct microtubule organising centres (MTOCs) (Zeeshan et al., 2022). The two MTOCs span the nuclear envelope via a transmembrane linkage (Rashpa and Brochet, 2022). Following the activation of microgametogenesis, the intranuclear MTOC orchestrates the formation of a total of eight MTOC-hemispindle cores, facilitating endomitotic replications (Rashpa and Brochet, 2022). In *Plasmodium* gametocytes, all the requisite genome replications are completed within the nucleus prior to the condensation of the DNA and subsequent nuclear segregation (Wall et al., 2018). Consequently, the eight haploid nuclei are only visible in the final phase of microgametogenesis, during which each nucleus is allocated to an individual gamete that subsequently exflagellates (Yang et al., 2023). The assembly of the flagellar axonemes is concomitantly facilitated by the MTOCs that are located on the cytoplasmic side of the nuclear envelope. Axoneme is a microtubule-based cytoskeleton that plays an essential role in the ciliary motility of male gametes (Sinden et al., 2010). In contrast to the intranuclear MTOCs, which are duplicated at each mitotic stage, the complete set of eight cytoplasmic MTOCs are formed simultaneously at the outset of microgametogenesis, thereby commencing the nucleation of axonemes (Rashpa and Brochet, 2022). During mitosis I, four cytoplasmic MTOCs are associated with each of the two intranuclear MTOCs, while only two become linked to each of the four intranuclear MTOCs during mitosis II. Ultimately, each cytoplasmic MTOC (also referred to as a basal body) becomes coupled to a single intranuclear MTOC with a fully grown axoneme, namely the gamete (Rashpa and Brochet, 2022).

The deletion of Alp2b inhibits exflagellation (**Figure 37B**). The fluorescent staining of α-tubulin and DNA in this study revealed the abnormal progression of microgametogenesis and the critical impediment of nuclear segregation (**Figure 46B**). While elongated axonemal structures are typically observed at 8 minutes post-activation (mpa) in wild-type gametocytes, those lacking Alp2b exhibited evidently fewer, or only shorter axonemes. The protracted onset of axoneme elongation has visibly impacted the overall progression of

gametogenesis. At 20 mpa, nearly 40% of the gametocytes remained without axonemes, but only with basal bodies. Notably, the subsequent axoneme elongation did not appear to be affected once they overcame the nucleation stage. This observation suggests that Alp2b does not affect MTOC organisations, but is moderately involved in the initiation of early stage axoneme formation. Some gametocytes, despite the sustained axoneme formation, still developed elongated axonemes with a basal body appropriately anchored to the nuclear membrane. However, none of them exhibited indication of DNA condensation, an essential step preceding nuclear segregation (**Figure 45, Figure 46B**). Consequently, the gametocytes were unable to complete the endomitosis, and the exflagellation process was fully arrested, indicating the crucial role of Alp2b in facilitating nuclear segregation.

As previously discussed, Alp2b exhibits structural similarity to Arp8, a subunit of the chromatin remodelling complex INO80. Notably, Arp8 has been demonstrated to bind to both single- and double-stranded DNA (Gerhold et al., 2012; Osakabe et al., 2014). This may indicate the potential ability of Alp2b to interact with DNA strands during mitosis. If Alp2b were to constitute a component of a chromatin remodelling complex, as Arp8 does, it could also regulate gene expression (Xue et al., 2015; Zahedi et al., 2023). One potential target could be tubulin, which would ultimately impact both axoneme formation and nuclear segregation. Interestingly, the INO80 complex has been shown to directly interact with mitotic spindles, thereby facilitating their assembly (Hur et al., 2010; Park et al., 2011). A comparative analysis of tubulin expression levels in wild-type and Alp2b KO gametocytes might reveal potential role of Alp2b in gene expression regulation including tubulin.

A comparable endomitosis defect has been described in the absence of the end-binding 1 (EB1) protein, which facilitates chromosome segregation by mediating the attachment of mitotic spindles to the kinetochore (Yang et al., 2023). Similarly, the deficiency of ARPC1, the *Plasmodium* homologue of the actin-related protein 2/3 complex subunit (Gordon and Sibley, 2005), has also resulted in incomplete nuclear divisions (Hentzschel et al., 2023). ARPC1 has been suggested to form a non-canonical Arp2/3-like complex together with Alp5a and Alp5b, thereby securing the linkage between the spindles and kinetochores through the interaction with Akit7 (Brusini et al., 2021; Hentzschel et al., 2023). It may be the case that Alp2b performs a related function in cytokinesis. However, as neither the depletion of EB1 nor ARPC1 resulted in any observable impact on axoneme assembly or exflagellation, it is likely that Alp2b has a broader function, which may encompass the regulation of more ubiquitous cellular components or the initiation of microgametogenesis itself. Given that Alp2b is a member of the Arp family, it is possible that it is also capable of interacting with actin. Specifically, actin2 is essential for exflagellation and its depletion abolishes gamete motility, while axoneme formation remained unaffected (Deligianni et al.,

2011). This phenotype aligns with the observed characteristics of Alp2b KO gametes, which could suggest a critical role of Alp2b in regulating actin2.

The process of microgametogenesis is dependent on the precise cell cycle regulation of a number of protein kinases and phosphatases, including the calcium-dependent protein kinase 4 (CDPK4), the serine/arginine-rich protein kinase 1 (SRPK1) and the protein phosphatase 1 (PP1), respectively. The essential roles of CDPK4 and SRPK1 have been documented in the phosphoregulation of mitosis, DNA replication and flagellar motility-related proteins (Fang et al., 2017; Invergo et al., 2017; Tewari et al., 2010). Meanwhile, axoneme development is dependent on PP1 (Zeeshan et al., 2021). The diverse effect of the Alp2b deletion on both axoneme formation and nuclear segregation may be explained by postulating that Alp2b interacts with a variety of protein-regulating enzymes. Another possibility is that Alp2b is involved in the transition between mitotic stages. For example, the anaphase-promoting complex 3 (APC3) plays a critical role in proceeding to anaphase, thereby permitting DNA condensation and exflagellation (Wall et al., 2018). It is possible that Alp2b serves as a key activator of specific cellular processes.

So far, the present study has demonstrated the critical role of Alp2b in facilitating the multi-nucleated stage prior to exflagellation. However, the precise molecular mechanism of this process remains to be elucidated. To gain deeper insight into how nuclear segregation is ultimately affected, it is crucial to examine the accuracy of genome replication by measuring the DNA contents throughout microgametogenesis. Should replication proceed independently of Alp2b, an octoploid nucleus should be identified by the point of inhibition. Furthermore, an ultrastructural analysis of the axonemes using transmission electron microscopy (TEM) combined with RT-PCR-based tubulin expression level determination may reveal any potential abnormalities in axoneme assembly that could not be identified by the tubulin immunostaining alone in this study. The detection of irregular tubulin expression levels in the absence of Alp2b may also provide insights into the potential gene regulatory function of this protein. For the visualisation of MTOCs and intracellular flagellar organisations, expansion microscopy represents an excellent option (Rashpa and Brochet, 2022). This could be combined with the fluorescently-tagged Alp2b and actin chromobody, which may serve as a powerful indicator of possible molecular interactions. The tagging of Alp2b has yet to be accomplished due to the substantial cleavage of the EGFP tag (**Figure 44C**), which may be attributed to its dynamic structural characteristics. Further optimisation of the tagging strategy is essential for this study, as it enables not only localisation studies but also pull-down assays of potential interaction partners. Altogether, the future study will seek to uncover the molecular basis of the Alp2b function during microgametogenesis.

4.8 Concluding remarks

On the whole, this study has demonstrated the critical roles of Alp1 and Alp2b at different stages of *Plasmodium* transmission to mosquitoes. Alp1 is localised throughout the cytoplasm and plays a crucial role in facilitating ookinete gliding motility. It does not appear to be a component of the glideosome apparatus. However, it may play a role in destabilising F-actin, which is essential for the dynamic operation of glideosome. It is plausible that Alp1 performs multifaceted functions, including regulatory and cellular maintenance roles, which may collectively impact the gliding motility of ookinetes. Alp2b is a critical factor for male gametocytes to complete their microgametogenesis. It promotes the initial phase of axoneme assembly and facilitates nuclear segregation at the final phase of endomitosis. The microgametes lacking Alp2b were unable to exflagellate and exhibited a complete loss of ciliary motility. However, this phenotype was partially rescued by the cross-species complementation of Alp2b. Given the observation that neutralising the highly *Plasmodium*-specific residues in the D-loop region also resulted in the complete inhibition of exflagellation, it can be inferred that the function of Alp2b is dependent on some of the conserved amino acid residues. In contrast, the conserved residues in the H-plug could be substituted with the corresponding residues of actin, provided that the original size of the H-plug was preserved. This also suggests that dimensional integrity may also be a determining factor in Alp2b function.

Finally, in light of the findings, this study emphasises the prospective value of Alp1 and Alp2b as potential targets for transmission-blocking anti-malarial drugs. The objective of the future study is to provide further insight into the molecular function of these Alps and to investigate their biochemical properties by obtaining recombinant Alp1 and Alp2b. The extensive understanding of the Alps will certainly provide a foundation for greater comprehension of the intricate *Plasmodium* biology as well as the uncharted branches of the actin superfamily.

References

Adl, S.M., Leander, B.S., Simpson, A.G.B., Archibald, J.M., Anderson, O.Roger., Bass, D., Bowser, S.S., Brugerolle, G., Farmer, M.A., Karpov, S., Kolisko, M., Lane, C.E., Lodge, D.J., Mann, D.G., Meisterfeld, R., Mendoza, L., Moestrup, Ø., Mozley-Standridge, S.E., Smirnov, A.V., Spiegel, F., 2007. Diversity, nomenclature, and taxonomy of Protists. Syst. Biol. 56, 684–689. https://doi.org/10.1080/10635150701494127

Aguirre Botero, M., 2019. Analysis of α-tubulin isotypic differences and the role of a nexin candidate in *Plasmodium berghei* microgametes (Master's thesis). Faculty of Biosciences of the Ruprecht-Karls-University Heidelberg.

Ahmad, M., Tuteja, R., 2012. *Plasmodium falciparum* RuvB proteins. Commun. Integr. Biol. 5, 350–361. https://doi.org/10.4161/cib.20005

Amimo, F., Lambert, B., Magit, A., Sacarlal, J., Hashizume, M., Shibuya, K., 2020. *Plasmodium falciparum* resistance to sulfadoxine-pyrimethamine in Africa: A systematic analysis of national trends. BMJ Glob. Health 5, e003217. https://doi.org/10.1136/bmjgh-2020-003217

Amino, R., Thiberge, S., Martin, B., Celli, S., Shorte, S., Frischknecht, F., Ménard, R., 2006. Quantitative imaging of *Plasmodium* transmission from mosquito to mammal. Nat. Med. 12, 220–224. https://doi.org/10.1038/nm1350

Andersen, K.R., Leksa, N.C., Schwartz, T.U., 2013. Optimized *Escherichia coli* expression strain LOBSTR eliminates common contaminants from His-tag purification. Proteins 81, 1857–1861. https://doi.org/10.1002/prot.24364

Andreadaki, M., Morgan, R.N., Deligianni, E., Kooij, T.W.A., Santos, J.M., Spanos, L., Matuschewski, K., Louis, C., Mair, G.R., Siden-Kiamos, I., 2014. Genetic crosses and complementation reveal essential functions for the *Plasmodium* stage-specific actin2 in sporogonic development. Cell. Microbiol. 16, 751–767. https://doi.org/10.1111/cmi.12274

Angrisano, F., Delves, M.J., Sturm, A., Mollard, V., McFadden, G.I., Sinden, R.E., Baum, J., 2012. A GFP-Actin reporter line to explore microfilament dynamics across the malaria parasite lifecycle. Molecular and Biochemical Parasitology 182, 93–96. https://doi.org/10.1016/j.molbiopara.2011.11.008

Arredondo, S.A., Schepis, A., Reynolds, L., Kappe, S.H.I., 2021. Secretory organelle function in the *Plasmodium* sporozoite. Trends Parasitol. 37, 651–663. https://doi.org/10.1016/j.pt.2021.01.008

Arrow, K.J., Panosian, C., Gelband, H., 2004. Antimalarial drugs and drug resistance, in: saving lives, buying time: Economics of malaria drugs in an age of resistance. NAP (US). https://doi.org/10.17226/11017

Ashley, E.A., Pyae Phyo, A., Woodrow, C.J., 2018. Malaria. Lancet 391, 1608–1621. https://doi.org/10.1016/S0140-6736(18)30324-6

Baca, A.M., Hol, W.G.J., 2000. Overcoming codon bias: A method for high-level overexpression of *Plasmodium* and other AT-rich parasite genes in *Escherichia coli*. Int. J. Parasitol. 30, 113–118. https://doi.org/10.1016/S0020-7519(00)00019-9

Bahl, A., Brunk, B., Crabtree, J., Fraunholz, M.J., Gajria, B., Grant, G.R., Ginsburg, H., Gupta, D., Kissinger, J.C., Labo, P., Li, L., Mailman, M.D., Milgram, A.J., Pearson, D.S., Roos, D.S., Schug, J., Stoeckert, C.J., Whetzel, P., 2003. PlasmoDB: the *Plasmodium* genome resource. A database integrating experimental and computational data. Nucleic Acids Res. 31, 212–215.

Baker, R.P., Wijetilaka, R., Urban, S., 2006. Two *Plasmodium* rhomboid proteases preferentially cleave different adhesins implicated in all invasive stages of Malaria. PLOS Pathog. 2, e113. https://doi.org/10.1371/journal.ppat.0020113

Bane, K.S., Lepper, S., Kehrer, J., Sattler, J.M., Singer, M., Reinig, M., Klug, D., Heiss, K., Baum, J., Mueller, A.-K., Frischknecht, F., 2016. The actin filament-binding protein coronin regulates motility in *Plasmodium* sporozoites. PLOS Pathog. 12, e1005710. https://doi.org/10.1371/journal.ppat.1005710

Baum, J., Gilberger, T.-W., Frischknecht, F., Meissner, M., 2008a. Host-cell invasion by malaria parasites: Insights from *Plasmodium* and *Toxoplasma*. Trends Parasitol. 24, 557–563. https://doi.org/10.1016/j.pt.2008.08.006

Baum, J., Tonkin, C.J., Paul, A.S., Rug, M., Smith, B.J., Gould, S.B., Richard, D., Pollard, T.D., Cowman, A.F., 2008b. A malaria parasite formin regulates actin polymerization and localizes to the parasite-erythrocyte moving junction during invasion. Cell Host Microbe 3, 188–198. https://doi.org/10.1016/j.chom.2008.02.006

Bennink, S., Kiesow, M.J., Pradel, G., 2016. The development of malaria parasites in the mosquito midgut. Cell. Microbiol. 18, 905–918. https://doi.org/10.1111/cmi.12604

Bergmann, A., Floyd, K., Key, M., Dameron, C., Rees, K.C., Thornton, L.B., Whitehead, D.C., Hamza, I., Dou, Z., 2020. *Toxoplasma gondii* requires its plant-like heme biosynthesis pathway for infection. PLOS Pathog. 16, e1008499. https://doi.org/10.1371/journal.ppat.1008499

Bertiaux, E., Balestra, A.C., Bournonville, L., Louvel, V., Maco, B., Soldati-Favre, D., Brochet, M., Guichard, P., Hamel, V., 2021. Expansion microscopy provides new insights into the cytoskeleton of malaria parasites including the conservation of a conoid. PLOS Biol. 19, e3001020. https://doi.org/10.1371/journal.pbio.3001020

Bertola, L.D., Ott, E.B., Griepsma, S., Vonk, F.J., Bagowski, C.P., 2008. Developmental expression of the alpha-skeletal actin gene. BMC Evol. Biol. 8, 166. https://doi.org/10.1186/1471-2148-8-166

Bhatt, S., Weiss, D.J., Cameron, E., Bisanzio, D., Mappin, B., Dalrymple, U., Battle, K., Moyes, C.L., Henry, A., Eckhoff, P.A., Wenger, E.A., Briët, O., Penny, M.A., Smith, T.A., Bennett, A., Yukich, J., Eisele, T.P., Griffin, J.T., Fergus, C.A., Lynch, M., Lindgren, F., Cohen, J.M., Murray, C.L.J., Smith, D.L., Hay, S.I., Cibulskis, R.E., Gething, P.W., 2015. The effect of malaria control on *Plasmodium falciparum* in Africa between 2000 and 2015. Nature 526, 207–211. https://doi.org/10.1038/nature15535

Billker, O., Dechamps, S., Tewari, R., Wenig, G., Franke-Fayard, B., Brinkmann, V., 2004. Calcium and a calcium-dependent protein kinase regulate gamete formation and mosquito transmission in a malaria parasite. Cell 117, 503–514. https://doi.org/10.1016/S0092-8674(04)00449-0

Billker, O., Shaw, M.K., Margos, G., Sinden, R.E., 1997. The roles of temperature, pH and mosquito factors as triggers of male and female gametogenesis of *Plasmodium* berghei *in vitro*. Parasitology 115, 1–7. https://doi.org/10.1017/S0031182097008895

Binder, A., 2020. The role of actin-like proteins in *Plasmodium berghei* transmission (Master's thesis). Faculty of Biosciences of the Ruprecht-Karls-University Heidelberg.

Blanchoin, L., Pollard, T.D., 1999. Mechanism of interaction of *Acanthamoeba* actophorin (ADF/cofilin) with actin filaments. JBC 274, 15538–15546. https://doi.org/10.1074/jbc.274.22.15538

Blanchoin, L., Pollard, T.D., 1998. Interaction of actin monomers with *Acanthamoeba* actophorin (ADF/cofilin) and profilin. JBC 273, 25106–25111. https://doi.org/10.1074/jbc.273.39.25106

Block, H., Maertens, B., Spriestersbach, A., Brinker, N., Kubicek, J., Fabis, R., Labahn, J., Schäfer, F., 2009. Chapter 27 Immobilized-Metal Affinity Chromatography (IMAC): A review, in: Burgess, R.R., Deutscher, M.P. (Eds.), Methods Enzymol., Guide to Protein Purification, 2nd Edition. Academic Press, 439–473. https://doi.org/10.1016/S0076-6879(09)63027-5

Bookwalter, C.S., Tay, C.L., McCrorie, R., Previs, M.J., Lu, H., Krementsova, E.B., Fagnant, P.M., Baum, J., Trybus, K.M., 2017. Reconstitution of the core of the malaria parasite glideosome with recombinant *Plasmodium* class XIV myosin A and *Plasmodium* actin. JBC 292, 19290. https://doi.org/10.1074/jbc.M117.813972

Bornhorst, J.A., Falke, J.J., 2000. Purification of proteins using polyhistidine affinity tags. Methods Enzymol. 326, 245–254. https://doi.org/10.1016/S0076-6879(00)26058-8

Boucher, L.E., Hopp, C.S., Muthinja, J.M., Frischknecht, F., Bosch, J., 2018. Discovery of *Plasmodium* (M)TRAP-aldolase interaction stabilizers interfering with sporozoite motility and invasion. ACS Infect. Dis. 4, 620–634. https://doi.org/10.1021/acsinfecdis.7b00225

Braks, J.A.M., Franke-Fayard, B., Kroeze, H., Janse, C.J., Waters, A.P., 2006. Development and application of a positive–negative selectable marker system for use in reverse genetics in *Plasmodium*. Nucleic Acid Res. 34, e39. https://doi.org/10.1093/nar/gnj033

Braumann, F., Klug, D., Kehrer, J., Song, G., Feng, J., Springer, T.A., Frischknecht, F., 2023. Conformational change of *Plasmodium* TRAP is essential for sporozoite migration and transmission. EMBO Rep. 24, e57064. https://doi.org/10.15252/embr.202357064

Brusini, L., Pacheco, N.D.S., Soldati-Favre, D., Brochet, M., 2022. Composition and organization of kinetochores show plasticity in apicomplexan chromosome segregation. J. Cell Biol. 5;221(9). https://doi.org/10.1101/2021.11.03.466924

Bubb, M.R., Spector, I., Beyer, B.B., Fosen, K.M., 2000. Effects of jasplakinolide on the kinetics of actin polymerization: An explanation for certain *in vivo* observations. JBC 275, 5163–5170. https://doi.org/10.1074/jbc.275.7.5163

Bugyi, B., Carlier, M.-F., 2010. Control of actin filament treadmilling in cell motility. Annu. Rev. Biophys. 39, 449–470. https://doi.org/10.1146/annurev-biophys-051309-103849

Bullen, H.E., Tonkin, C.J., O'Donnell, R.A., Tham, W.-H., Papenfuss, A.T., Gould, S., Cowman, A.F., Crabb, B.S., Gilson, P.R., 2009. A novel family of apicomplexan glideosome-associated proteins with an inner membrane-anchoring role. JBC 284, 25353–25363. https://doi.org/10.1074/jbc.M109.036772

Burda, P.-C., Caldelari, R., Heussler, V.T., 2017. Manipulation of the host cell membrane during *Plasmodium* liver stage egress. mBio. 8, e00139-17. https://doi.org/10.1128/mBio.00139-17

Burtnick, L.D., Koepf, E.K., Grimes, J., Jones, E.Y., Stuart, D.I., McLaughlin, P.J., Robinson, R.C., 1997. The crystal structure of plasma gelsolin: Implications for actin severing, capping, and nucleation. Cell 90, 661–670. https://doi.org/10.1016/S0092-8674(00)80527-9

Busse, C., 2023. Generation and phenotypic characterisation of *Plasmodium berghei* Alp1 mutants (Master's thesis). Institute of Nutritional Science, Depertment of Biochemistry and Molecular Biology, Justus-Liebig University Giessen.

Carruthers, V.B., Sibley, L.D., 1997. Sequential protein secretion from three distinct organelles of *Toxoplasma gondii* accompanies invasion of human fibroblasts. Eur. J. Cell Biol. 73, 114–123.

Cepeda Diaz, A.K., Rudlaff, R.M., Farringer, M., Dvorin, J.D., 2023. Essential function of alveolin PfIMC1g in the *Plasmodium falciparum* asexual blood stage. mBio. 14, e01507-23. https://doi.org/10.1128/mbio.01507-23

Chen, K., Wang, L., Yu, Z., Yu, J., Ren, Y., Wang, Q., Xu, Y., 2024. Structure of the human TIP60 complex. Nat. Commun. 15, 7092. https://doi.org/10.1038/s41467-024-51259-z

Chen, Y., Murillo-Solano, C., Kirkpatrick, M.G., Antoshchenko, T., Park, H.-W., Pizarro, J.C., 2018. Repurposing drugs to target the malaria parasite unfolding protein response. Sci. Rep. 8, 10333. https://doi.org/10.1038/s41598-018-28608-2

Chhabra, E.S., Higgs, H.N., 2007. The many faces of actin: matching assembly factors with cellular structures. Nat. Cell Biol. 9, 1110–1121. https://doi.org/10.1038/ncb1007-1110

Chou, S.Z., Pollard, T.D., 2019. Mechanism of actin polymerization revealed by cryo-EM structures of actin filaments with three different bound nucleotides. PNAS 116, 4265–4274. https://doi.org/10.1073/pnas.1807028115

Collier, S., Pietsch, E., Dans, M., Ling, D., Tavella, T.A., Lopaticki, S., Marapana, D.S., Shibu, M.A., Andrew, D., Tiash, S., McMillan, P.J., Gilson, P., Tilley, L., Dixon, M.W.A., 2023. *Plasmodium falciparum* formins are essential for invasion and sexual stage development. Commun. Biol. 6, 1–15. https://doi.org/10.1038/s42003-023-05233-y

Collins, K.A., Snaith, R., Cottingham, M.G., Gilbert, S.C., Hill, A.V.S., 2017. Enhancing protective immunity to malaria with a highly immunogenic virus-like particle vaccine. Sci. Rep. 7, 46621. https://doi.org/10.1038/srep46621

Coravos, J.S., Mason, F.M., Martin, A.C., 2017. Actomyosin pulsing in tissue integrity maintenance during morphogenesis. Trends Cell Biol. 27, 276–283. https://doi.org/10.1016/j.tcb.2016.11.008

Cox, F.E., 2010. History of the discovery of the malaria parasites and their vectors. Parasit. Vectors 3, 5. https://doi.org/10.1186/1756-3305-3-5

Dahiya, V., Chaudhuri, T.K., 2014. Chaperones GroEL/GroES accelerate the refolding of a multidomain protein through modulating on-pathway intermediates. JBC 289, 286–298. https://doi.org/10.1074/jbc.M113.518373

Das, S., Ge, P., Oztug Durer, Z.A., Grintsevich, E.E., Zhou, Z.H., Reisler, E., 2020. D-loop dynamics and near-atomic-resolution cryo-EM structure of phalloidin-bound F-actin. Structure 28, 586-593.e3. https://doi.org/10.1016/j.str.2020.04.004

Das, S., Lemgruber, L., Tay, C.L., Baum, J., Meissner, M., 2017. Multiple essential functions of *Plasmodium falciparum* actin-1 during malaria blood-stage development. BMC Biol. 15, 70. https://doi.org/10.1186/s12915-017-0406-2

Das, S., Stortz, J.F., Meissner, M., Periz, J., 2021. The multiple functions of actin in apicomplexan parasites. Cell. Microbiol. 23. https://doi.org/10.1111/cmi.13345

Dash, M., Sachdeva, S., Bansal, A., Sinha, A., 2022. Gametogenesis in *Plasmodium*: Delving deeper to connect the dots. Front. Cell. Infect. Microbiol. 12. https://doi.org/10.3389/fcimb.2022.877907

Datoo, M.S., Dicko, A., Tinto, H., Ouédraogo, J.-B., Hamaluba, M., Olotu, A., Beaumont, E., Lopez, F.R., Natama, H.M., Weston, S., Chemba, M., Compaore, Y.D., Issiaka, D., Salou, D., Some, A.M., Omenda, S., Lawrie, A., Bejon, P., Rao, H., Chandramohan, D., Roberts, R., Bharati, S., Stockdale, L., Gairola, S., Greenwood, B.M., Ewer, K.J., Bradley, J., Kulkarni, P.S., Shaligram, U., Hill, A.V.S., Mahamar, A., Sanogo, K., Sidibe, Y., Diarra, K., Samassekou, M., Attaher, O., Tapily, A., Diallo, M., Dicko, O.M., Kaya, M., Maguiraga, S.O., Sankare, Y.,

Yalcouye, H., Diarra, S., Niambele, S.M., Thera, I., Sagara, I., Sylla, M., Dolo, A., Misidai, N., Simando, S., Msami, H., Juma, O., Gutapaka, N., Paul, R., Mswata, S., Sasamalo, I., Johaness, K., Sultan, M., Alexander, A., Kimaro, I., Lwanga, K., Mtungwe, M., Khamis, K., Rugarabam, L., Kalinga, W., Mohammed, M., Kamange, J., Msangi, J., Mwaijande, B., Mtaka, I., Mhapa, M., Mlaganile, T., Mbaga, T., Yerbanga, R.S., Samtouma, W., Sienou, A.A., Kabre, Z., Ouedraogo, W.J.M., Yarbanga, G.A.B., Zongo, I., Savadogo, H., Sanon, J., Compaore, J., Kere, I., Yoni, F.L., Sanre, T.M., Ouattara, S.B., Provstgaard-Morys, S., Woods, D., Snow, R.W., Amek, N., Ngetsa, C.J., Ochola-Oyier, L.I., Musyoki, J., Munene, M., Mumba, N., Adetifa, U.J., Muiruri, C.M., Mwawaka, J.S., Mwaganyuma, M.H., Ndichu, M.N., Weya, J.O., Njogu, K., Grant, J., Webster, J., Lakhkar, A., Ido, N.F.A., Traore, O., Tahita, M.C., Bonko, M. dit A., Rouamba, T., Ouedraogo, D.F., Soma, R., Millogo, A., Ouedraogo, E., Sorgho, F., Konate, F., Valea, I., 2024. Safety and efficacy of malaria vaccine candidate R21/Matrix-M in African children: A multicentre, double-blind, randomised, phase 3 trial. Lancet 403, 533–544. https://doi.org/10.1016/S0140-6736(23)02511-4

Day, J., Passecker, A., Beck, H.-P., Vakonakis, I., 2019. The *Plasmodium falciparum* Hsp70-x chaperone assists the heat stress response of the malaria parasite. FASEB J. 33, 14611–14624. https://doi.org/10.1096/fj.201901741R

de Koning-Ward, T.F., Fidock, D.A., Thathy, V., Menard, R., van Spaendonk, R.M.L., Waters, A.P., Janse, C.J., 2000. The selectable marker human dihydrofolate reductase enables sequential genetic manipulation of the *Plasmodium berghei* genome. Mol. Biochem. Parasitol. 106, 199–212. https://doi.org/10.1016/S0166-6851(99)00189-9

Del Rosario, M., Periz, J., Pavlou, G., Lyth, O., Latorre-Barragan, F., Das, S., Pall, G.S., Stortz, J.F., Lemgruber, L., Whitelaw, J.A., Baum, J., Tardieux, I., Meissner, M., 2019. Apicomplexan F-actin is required for efficient nuclear entry during host cell invasion. EMBO Rep. 20, e48896. https://doi.org/10.15252/embr.201948896

Deligianni, E., Morgan, R.N., Bertuccini, L., Kooij, T.W.A., Laforge, A., Nahar, C., Poulakakis, N., Schüler, H., Louis, C., Matuschewski, K., Siden-Kiamos, I., 2011. Critical role for a stage-specific actin in male exflagellation of the malaria parasite. Cell. Microbioi. 13, 1714–1730. https://doi.org/10.1111/j.1462-5822.2011.01652.x

Diers, A., 2022. Heterologous Expression of *Plasmodium berghei* Alp1 and Alp2b and characterization of Alp5a in parasite transmission (Master's thesis). Institute of Nutritional Science, Depertment of Biochemistry and Molecular Biology, Justus-Liebig University Giessen.

Dillenberger, M., Werner, A.-D., Velten, A.-S., Rahlfs, S., Becker, K., Fritz-Wolf, K., 2023. Structural analysis of *Plasmodium falciparum* hexokinase provides novel information about catalysis due to a *Plasmodium*-specific insertion. Int. J. Mol. Sci. 24, 12739. https://doi.org/10.3390/ijms241612739

Dominguez, R., 2019. Nucleotide-dependent conformational changes in the actin filament: subtler than expected. Proc. Natl. Acad. Sci. U.S.A. 116, 3959–3961. https://doi.org/10.1073/pnas.1900799116

Dominguez, R., 2007. A common binding site for actin-binding proteins on the actin surface, in: actin-monomer-binding proteins, Molecular Biology Intelligence Unit. Springer New York, 107–115. https://doi.org/10.1007/978-0-387-46407-7_10

Dominguez, R., Holmes, K.C., 2011. Actin structure and function. Annu. Rev. Biophys. 40, 169–186. https://doi.org/10.1146/annurev-biophys-042910-155359

Dondorp, A., Nosten, F., Stepniewska, K., Day, N., White, N., South East Asian Quinine Artesunate Malaria Trial (SEAQUAMAT) group, 2005. Artesunate versus quinine for treatment

of severe *falciparum* malaria: A randomised trial. Lancet 366, 717–725. https://doi.org/10.1016/S0140-6736(05)67176-0

Dos Remedios, C.G., Chhabra, D., Kekic, M., Dedova, I.V., Tsubakihara, M., Berry, D.A., Nosworthy, N.J., 2003. Actin binding proteins: Regulation of cytoskeletal microfilaments. Physiol. Rev. 83, 433–473. https://doi.org/10.1152/physrev.00026.2002

Dos Santos Pacheco, N., Brusini, L., Haase, R., Tosetti, N., Maco, B., Brochet, M., Vadas, O., Soldati-Favre, D., 2022. Conoid extrusion regulates glideosome assembly to control motility and invasion in Apicomplexa. Nat. Microbiol. 7, 1777–1790. https://doi.org/10.1038/s41564-022-01212-x

Douamba, Z., Dao, N.G.L., Zohoncon, T.M., Bisseye, C., Compaoré, T.R., Kafando, J.G., Sombie, B.C., Ouermi, D., Djigma, F.W., Ouedraogo, P., Ghilat, N., Pietra, V., Colizzi, V., Simpore, J., 2014. Mother-to-children *Plasmodium falciparum* asymptomatic malaria transmission at Saint Camille Medical Centre in Ouagadougou, Burkina Faso. Malar. Res. Treat. 2014, 390513. https://doi.org/10.1155/2014/390513

Douglas, R.G., Amino, R., Sinnis, P., Frischknecht, F., 2015. Active migration and passive transport of malaria parasites. Trends Parasitol. 31, 357–362. https://doi.org/10.1016/j.pt.2015.04.010

Douglas, R.G., Nandekar, P., Aktories, J.-E., Kumar, H., Weber, R., Sattler, J.M., Singer, M., Lepper, S., Sadiq, S.K., Wade, R.C., Frischknecht, F., 2018. Inter-subunit interactions drive divergent dynamics in mammalian and *Plasmodium* actin filaments. PLOS Biol. 16, e2005345. https://doi.org/10.1371/journal.pbio.2005345

Douse, C.H., Green, J.L., Salgado, P.S., Simpson, P.J., Thomas, J.C., Langsley, G., Holder, A.A., Tate, E.W., Cota, E., 2012. Regulation of the *Plasmodium* motor complex: Phosphorylation of myosin A tail-interacting protein (MTIP) loosens its grip on MyoA. JBC 287, 36968–36977. https://doi.org/10.1074/jbc.M112.379842

Doyle, T., Botstein, D., 1996. Movement of yeast cortical actin cytoskeleton visualized *in vivo*. PNAS 93, 3886–3891. https://doi.org/10.1073/pnas.93.9.3886

Duffy, P.E., Gorres, J.P., Healy, S.A., Fried, M., 2024. Malaria vaccines: a new era of prevention and control. Nat. Rev. Microbiol. 1–17. https://doi.org/10.1038/s41579-024-01065-7

Dumon-Seignovert, L., Cariot, G., Vuillard, L., 2004. The toxicity of recombinant proteins in *Escherichia coli*: a comparison of overexpression in BL21(DE3), C41(DE3), and C43(DE3). Protein Expr. and Purif. 37, 203–206. https://doi.org/10.1016/j.pep.2004.04.025

Durer, Z.A.O., Kudryashov, D.S., Sawaya, M.R., Altenbach, C., Hubbell, W., Reisler, E., 2012. Structural states and dynamics of the D-loop in actin. Biophys. J. 103, 930–939. https://doi.org/10.1016/j.bpj.2012.07.030

Eckley, D.M., Gill, S.R., Melkonian, K.A., Bingham, J.B., Goodson, H.V., Heuser, J.E., Schroer, T.A., 1999. Analysis of dynactin subcomplexes reveals a novel actin-related protein associated with the Arp1 minifilament pointed end. J. Cell Biol. 147, 307–320. https://doi.org/10.1083/jcb.147.2.307

Edwards, M., Zwolak, A., Schafer, D.A., Sept, D., Dominguez, R., Cooper, J.A., 2014. Capping protein regulators fine-tune actin assembly dynamics. Nat. Rev. Mol. Cell Biol. 15, 677–689. https://doi.org/10.1038/nrm3869

Eustermann, S., Schall, K., Kostrewa, D., Lakomek, K., Strauss, M., Moldt, M., Hopfner, K.-P., 2018. Structural basis for ATP-dependent chromatin remodelling by the INO80 complex. Nature 556, 386–390. https://doi.org/10.1038/s41586-018-0029-y

Fang, H., Klages, N., Baechler, B., Hillner, E., Yu, L., Pardo, M., Choudhary, J., Brochet, M., 2017. Multiple short windows of calcium-dependent protein kinase 4 activity coordinate distinct cell cycle events during *Plasmodium* gametogenesis. eLife 6, e26524. https://doi.org/10.7554/eLife.26524

Farr, E.B., Sattler, J.M., Frischknecht, F., 2021. SPOT: A web-tool enabling swift profiling of transcriptomes. Bioinformatics 38, 284–285. https://doi.org/10.1093/bioinformatics/btab541

Fenn, S., Breitsprecher, D., Gerhold, C.B., Witte, G., Faix, J., Hopfner, K.-P., 2011. Structural biochemistry of nuclear actin-related proteins 4 and 8 reveals their interaction with actin: Structural biochemistry of nuclear Arp4 and Arp8. EMBO J. 30, 2153–2166. https://doi.org/10.1038/emboj.2011.118

Fernandes, P., Briquet, S., Patarot, D., Loubens, M., Hoareau-Coudert, B., Silvie, O., 2020. The dimerisable Cre recombinase allows conditional genome editing in the mosquito stages of *Plasmodium berghei*. PLOS One 15, e0236616. https://doi.org/10.1371/journal.pone.0236616

Ferron, F., Rebowski, G., Lee, S.H., Dominguez, R., 2007. Structural basis for the recruitment of profilin-actin complexes during filament elongation by Ena/VASP. EMBO J. 26, 4597–4606. https://doi.org/10.1038/sj.emboj.7601874

Flaherty, K.M., McKay, D.B., Kabsch, W., Holmes, K.C., 1991. Similarity of the three-dimensional structures of actin and the ATPase fragment of a 70-kDa heat shock cognate protein. PNAS 88, 5041–5045.

Fokin, A.I., David, V., Oguievetskaia, K., Derivery, E., Stone, C.E., Cao, L., Rocques, N., Molinie, N., Henriot, V., Aumont-Nicaise, M., Hinckelmann, M.-V., Saudou, F., Le Clainche, C., Carter, A.P., Romet-Lemonne, G., Gautreau, A.M., 2021. The Arp1/11 minifilament of dynactin primes the endosomal Arp2/3 complex. Sci. Adv. 7, eabd5956. https://doi.org/10.1126/sciadv.abd5956

Francia, M.E., Dubremetz, J.-F., Morrissette, N.S., 2016. Basal body structure and composition in the apicomplexans *Toxoplasma* and *Plasmodium*. Cilia 5, 3. https://doi.org/10.1186/s13630-016-0025-5

Frénal, K., Dubremetz, J.-F., Lebrun, M., Soldati-Favre, D., 2017. Gliding motility powers invasion and egress in Apicomplexa. Nat Rev Microbiol 15, 645–660. https://doi.org/10.1038/nrmicro.2017.86

Frénal, K., Krishnan, A., Soldati-Favre, D., 2020. The actomyosin systems in Apicomplexa. In: Coluccio, L. (eds) Myosins. Advances in experimental medicine and biology, vol 1239. Springer, Cham. https://doi.org/10.1007/978-3-030-38062-5_14

Frischknecht, F., Matuschewski, K., 2017. *Plasmodium* Sporozoite Biology. Cold Spring Harb. Perspect. Med. 7, a025478. https://doi.org/10.1101/cshperspect.a025478

Fujiwara, I., Vavylonis, D., Pollard, T.D., 2007. Polymerization kinetics of ADP- and ADP-P_i -actin determined by fluorescence microscopy. PNAS 104, 8827–8832. https://doi.org/10.1073/pnas.0702510104

Gandhi, M., Goode, B.L., 2008. Coronin: The Double-Edged Sword of Actin Dynamics, in: Clemen, C.S., Eichinger, L., Rybakin, V. (Eds.), The coronin family of proteins: Subcellular biochemistry, subcellular biochemistry. Springer, New York, 72–87. https://doi.org/10.1007/978-0-387-09595-0_7

Gerhold, C.B., Winkler, D.D., Lakomek, K., Seifert, F.U., Fenn, S., Kessler, B., Witte, G., Luger, K., Hopfner, K.-P., 2012. Structure of actin-related protein 8 and its contribution to nucleosome binding. Nucleic Acids Res. 40, 11036–11046. https://doi.org/10.1093/nar/gks842

Ghosh, A.K., Jacobs-Lorena, M., 2009. *Plasmodium* sporozoite invasion of the mosquito salivary gland. Curr. Opin. Microbiol. 12, 394–400. https://doi.org/10.1016/j.mib.2009.06.010

Goh, L.L., Loke, P., Singh, M., Sim, T.S., 2003. Soluble expression of a functionally active *Plasmodium falciparum* falcipain-2 fused to maltose-binding protein in *Escherichia coli*. Prot. Expr. Purif. 32, 194–201. https://doi.org/10.1016/S1046-5928(03)00225-0

Goley, E.D., Welch, M.D., 2006. The ARP2/3 complex: An actin nucleator comes of age. Nat. Rev. Mol. Cell Biol. 7, 713–726. https://doi.org/10.1038/nrm2026

Gomes, A.R., Bushell, E., Schwach, F., Girling, G., Anar, B., Quail, M.A., Herd, C., Pfander, C., Modrzynska, K., Rayner, J.C., Billker, O., 2015. A genome-scale vector resource enables high-throughput reverse genetic screening in a malaria parasite. Cell Host Microbe 17, 404–413. https://doi.org/10.1016/j.chom.2015.01.014

Goode, B.L., Eck, M.J., 2007. Mechanism and function of formins in the control of actin assembly. Annu. Rev. Biochem. 76, 593–627. https://doi.org/10.1146/annurev.biochem.75.103004.142647

Goodson, H.V., Hawse, W.F., 2002. Molecular evolution of the actin family. J. Cell Sci. 115, 2619–2622. https://doi.org/10.1242/jcs.115.13.2619

Goodson, H.V., Jonasson, E.M., 2018. Microtubules and microtubule-associated proteins. Cold Spring Harb. Perspect. Biol. 10, a022608. https://doi.org/10.1101/cshperspect.a022608

Gordon, J.L., Beatty, W.L., Sibley, L.D., 2008. A novel actin-related protein is associated with daughter cell formation in *Toxoplasma gondii*. Eukaryot. Cell 7, 1500–1512. https://doi.org/10.1128/EC.00064-08

Gordon, J.L., Buguliskis, J.S., Buske, P.J., Sibley, L.D., 2009. Actin-like protein 1 (ALP1) is a component of dynamic, high molecular weight complexes in *Toxoplasma gondii*. Cell Motil. Cytoskeleton. https://doi.org/10.1002/cm.20414

Gordon, J.L., Sibley, L.D., 2005. Comparative genome analysis reveals a conserved family of actin-like proteins in apicomplexan parasites. BMC 6, 179. https://doi.org/10.1186/1471-2164-6-179

Goswami, D., Kumar, S., Betz, W., Armstrong, J.M., Haile, M.T., Camargo, N., Parthiban, C., Seilie, A.M., Murphy, S.C., Vaughan, A.M., Kappe, S.H.I., 2022. A *Plasmodium falciparum* ATP-binding cassette transporter is essential for liver stage entry into schizogony. iScience 25, 104224. https://doi.org/10.1016/j.isci.2022.104224

Green, J.L., Wall, R.J., Vahokoski, J., Yusuf, N.A., Ridzuan, M.A.M., Stanway, R.R., Stock, J., Knuepfer, E., Brady, D., Martin, S.R., Howell, S.A., Pires, I.P., Moon, R.W., Molloy, J.E., Kursula, I., Tewari, R., Holder, A.A., 2017. Compositional and expression analyses of the glideosome during the *Plasmodium* life cycle reveal an additional myosin light chain required for maximum motility. JBC 292, 17857–17875. https://doi.org/10.1074/jbc.M117.802769

Grossman-Haham, I., 2023. Towards an atomic model of a beating ciliary axoneme. Curr. Opin. Struct. Biol. 78, 102516. https://doi.org/10.1016/j.sbi.2022.102516

Guggisberg, A.M., Amthor, R.E., Odom, A.R., 2014. Isoprenoid biosynthesis in *Plasmodium falciparum*. Eukaryot. Cell 13, 1348–1359. https://doi.org/10.1128/EC.00160-14

Gunning, P.W., Ghoshdastider, U., Whitaker, S., Popp, D., Robinson, R.C., 2015. The evolution of compositionally and functionally distinct actin filaments. J. Cell Sci. 128, 2009–2019. https://doi.org/10.1242/jcs.165563

Haase, R., Dos Santos Pacheco, N., Soldati-Favre, D., 2022. Nanoscale imaging of the conoid and functional dissection of its dynamics in Apicomplexa. Curr. Opin. Microbiol. 70, 102226. https://doi.org/10.1016/j.mib.2022.102226

Hakala, M., 2020. Revising the actin disassembly machinery: The role of GMF and twinfilin in turnover of dendritic actin arrays (Doctoral thesis). Faculty of Biological and Environmental Sciences University of Helsinki.

Hammesfahr, B., Kollmar, M., 2012. Evolution of the eukaryotic dynactin complex, the activator of cytoplasmic dynein. BMC Evol. Biol. 12, 95. https://doi.org/10.1186/1471-2148-12-95

Harata, M., Oma, Y., Mizuno, S., Jiang, Y.W., Stillman, D.J., Wintersberger, U., 1999. The nuclear actin-related protein of *Saccharomyces cerevisiae*, Act3p/Arp4, interacts with core histones. Mol. Biol. Cell 10, 2595–2605.

Harris, H.E., Weeds, Alan.G., 1984. Plasma gelsolin caps and severs actin filaments. FEBS Lett. Elsevier Science Publishers B. V. 177. https://doi.org/10.1016/0014-5793(84)81280-6

Heinzelman, M.B., 2015. Gliding motility in apicomplexan parasites | Elsevier Enhanced Reader. Semin. Cell Dev. Biol. 46, 135–142. https://doi.org/10.1016/j.semcdb.2015.09.020

Hentzschel, F., Jewanski, D., Sokolowski, Y., Agarwal, P., Kraeft, A., Hildenbrand, K., Dorner, L., Singer, M., Frischknecht, F., Marti, M., 2023. A non-canonical Arp2/3 complex is essential for *Plasmodium* DNA segregation and transmission of malaria. Biorxiv. https://doi.org/10.1101/2023.10.25.563799

Hilton, D.M., Aguilar, R.M., Johnston, A.B., Goode, B.L., 2018. Species-specific functions of twinfilin in actin filament depolymerization. J Mol Biol 430, 3323–3336. https://doi.org/10.1016/j.jmb.2018.06.025

Hirai, M., Arai, M., Kawai, S., Matsuoka, H., 2006. PbGCβ is essential for *Plasmodium* ookinete motility to invade midgut cells and for successful completion of parasite life cycle in mosquitoes. J. Biochem. 140, 747–757. https://doi.org/10.1093/jb/mvj205

Hoang, A.N., Jones, C.N., Dimisko, L., Hamza, B., Martel, J., Kojic, N., Irimia, D., 2013. Measuring neutrophil speed and directionality during chemotaxis, directly from a droplet of whole blood. Technology (Singap. World. Sci.) 1, 49. https://doi.org/10.1142/S2339547813500040

Holmes, K.C., Popp, D., Gebhard, W., Kabsch, W., 1990. Atomic model of the actin filament. Nature 347, 44–49. https://doi.org/10.1038/347044a0

Honma, H., Niikura, M., Kobayashi, F., Horii, T., Mita, T., Endo, H., Hirai, M., 2016. Mutation tendency of mutator *Plasmodium berghei* with proofreading-deficient DNA polymerase δ. Sci. Rep. 6, 36971. https://doi.org/10.1038/srep36971

Howick, V.M., Russell, A.J.C., Andrews, T., Heaton, H., Reid, A.J., Natarajan, K., Butungi, H., Metcalf, T., Verzier, L.H., Rayner, J.C., Berriman, M., Herren, J.K., Billker, O., Hemberg, M., Talman, A.M., Lawniczak, M.K.N., 2019. The Malaria Cell Atlas: Single parasite transcriptomes across the complete *Plasmodium* life cycle. Science 365, eaaw2619. https://doi.org/10.1126/science.aaw2619

Hu, K., Roos, D.S., Murray, J.M., 2002. A novel polymer of tubulin forms the conoid of *Toxoplasma gondii*. J. Cell Biol. 156, 1039–1050. https://doi.org/10.1083/jcb.200112086

Hur, S.-K., Park, E.-J., Han, J.-E., Kim, Y.-A., Kim, J.-D., Kang, D., Kwon, J., 2010. Roles of human INO80 chromatin remodeling enzyme in DNA replication and chromosome segregation suppress genome instability. Cell. Mol. Life Sci. 67, 2283–2296. https://doi.org/10.1007/s00018-010-0337-3

Hurley, J.H., 1996. The sugar kinase/heat shock protein 70/actin superfamily: implications of conserved structure for mechanism. Annu. Rev. Biophys. Biomol. Struct. 25, 137–162. https://doi.org/10.1146/annurev.bb.25.060196.001033

Hvorecny, K.L., Sladewski, T.E., De La Cruz, E.M., Kollman, J.M., Heaslip, A.T., 2024. *Toxoplasma gondii* actin filaments are tuned for rapid disassembly and turnover. Nat. Commun. 15, 1840. https://doi.org/10.1038/s41467-024-46111-3

Ibrahim, A.O., Bello, I.S., Ajetunmobi, A.O., Ayodapo, A., Afolabi, B.A., Adeniyi, M.A., 2023. Prevalence of asymptomatic malaria infection by microscopy and its determinants among residents of Ido-Ekiti, Southwestern Nigeria. PLOS One 18, e0280981. https://doi.org/10.1371/journal.pone.0280981

Idro, R., Marsh, K., John, C.C., Newton, C.R.J., 2010. Cerebral malaria: mechanisms of brain injury and strategies for improved neurocognitive outcome. Pediatr. Res. 68, 267–274. https://doi.org/10.1203/PDR.0b013e3181eee738

Imamoglu, R., Balchin, D., Hayer-Hartl, M., Hartl, F.U., 2020. Bacterial Hsp70 resolves misfolded states and accelerates productive folding of a multi-domain protein. Nat. Commun. 11, 365. https://doi.org/10.1038/s41467-019-14245-4

Imlay, L., Odom, A.R., 2014. Isoprenoid metabolism in apicomplexan parasites. Curr. Clin. Microbiol. Rep. 1, 37–50. https://doi.org/10.1007/s40588-014-0006-7

Invergo, B.M., Brochet, M., Yu, L., Choudhary, J., Beltrao, P., Billker, O., 2017. Sub-minute Phosphoregulation of cell cycle systems during *Plasmodium* gamete formation. Cell Rep. 21, 2017–2029. https://doi.org/10.1016/j.celrep.2017.10.071

Ishikawa, T., 2017. Axoneme structure from motile cilia. Cold Spring Harb. Perspect. Biol. 9, a028076. https://doi.org/10.1101/cshperspect.a028076

Iwasa, J.H., Mullins, R.D., 2007. Spatial and temporal relationships between actin-filament nucleation, capping, and disassembly. Curr. Biol. 17, 395–406. https://doi.org/10.1016/j.cub.2007.02.012

Jaiswal, R., Breitsprecher, D., Collins, A., Corrêa, I.R., Xu, M.-Q., Goode, B.L., 2013. The formin Daam1 and fascin directly collaborate to promote filopodia formation. Curr. Biol. 23, 1373–1379. https://doi.org/10.1016/j.cub.2013.06.013

Janse, C.J., Ramesar, J., Waters, A.P., 2006. High-efficiency transfection and drug selection of genetically transformed blood stages of the rodent malaria parasite *Plasmodium berghei*. Nat. Protoc. 1, 346–356. https://doi.org/10.1038/nprot.2006.53

Jo, B.-S., Choi, S.S., 2015. Introns: The functional benefits of introns in genomes. Genomics Inform. 13, 112–118. https://doi.org/10.5808/GI.2015.13.4.112

Jónsson, Z.O., Jha, S., Wohlschlegel, J.A., Dutta, A., 2004. Rvb1p/Rvb2p recruit Arp5p and assemble a functional Ino80 chromatin remodeling complex. Mol. Cell 16, 465–477. https://doi.org/10.1016/j.molcel.2004.09.033

Jumper, J., Evans, R., Pritzel, A., Green, T., Figurnov, M., Ronneberger, O., Tunyasuvunakool, K., Bates, R., Žídek, A., Potapenko, A., Bridgland, A., Meyer, C., Kohl, S.A.A., Ballard, A.J., Cowie, A., Romera-Paredes, B., Nikolov, S., Jain, R., Adler, J., Back, T., Petersen, S., Reiman, D., Clancy, E., Zielinski, M., Steinegger, M., Pacholska, M., Berghammer, T., Bodenstein, S., Silver, D., Vinyals, O., Senior, A.W., Kavukcuoglu, K., Kohli, P., Hassabis, D., 2021. Highly accurate protein structure prediction with AlphaFold. Nature 596, 583–589. https://doi.org/10.1038/s41586-021-03819-2

Kabsch, W., Holmes, K.C., 1995. The actin fold. FASEB J. 9, 167–174. https://doi.org/10.1096/fasebj.9.2.7781919

Kabsch, W., Mannherz, H., Georg, Suck, D., Pai, Emil.F., Holmes, K.C., 1990. Atomic structure of the actin: DNase I complex. Nature 347. https://doi.org/10.1038/347037a0

Kamiyama, D., Sekine, S., Barsi-Rhyne, B., Hu, J., Chen, B., Gilbert, L.A., Ishikawa, H., Leonetti, M.D., Marshall, W.F., Weissman, J.S., Huang, B., 2016. Versatile protein tagging in cells with split fluorescent protein. Nat. Commun. 7, 11046. https://doi.org/10.1038/ncomms11046

Kan, A., Tan, Y., Angrisano, F., Hanssen, E., Rogers, K.L., Whitehead, L., Mollard, V.P., Cozijnsen, A., Delves, M.J., Crawford, S., Sinden, R.E., McFadden, G.I., Leckie, C., Bailey, J., Baum, J., 2014. Quantitative analysis of *Plasmodium* ookinete motion in three dimensions suggests a critical role for cell shape in the biomechanics of malaria parasite gliding motility. Cell Microbiol. 16, 734–750. https://doi.org/10.1111/cmi.12283

Kapoor, P., Chen, M., Winkler, D.D., Luger, K., Shen, X., 2013. Evidence for monomeric actin function in INO80 chromatin remodeling. Nat. Struct. Mol. Biol. 20, 426–432. https://doi.org/10.1038/nsmb.2529

Kappe, S.H.I., Buscaglia, C.A., Bergman, L.W., Coppens, I., Nussenzweig, V., 2004. Apicomplexan gliding motility and host cell invasion: overhauling the motor model. Trends Parasitol. 20, 13–16. https://doi.org/10.1016/j.pt.2003.10.011

Ke, H., Sigala, P.A., Miura, K., Morrisey, J.M., Mather, M.W., Crowley, J.R., Henderson, J.P., Goldberg, D.E., Long, C.A., Vaidya, A.B., 2014. The heme biosynthesis pathway is essential for *Plasmodium falciparum* development in mosquito stage but not in blood stages. J. Biol. Chem. 289, 34827–34837. https://doi.org/10.1074/jbc.M114.615831

Kelvin, J.M., Darlington, T.P., Rodriguez, J.A., Zarinshenas, R., Zou, Y., Bruinsma, R., Bradley, P.J., Miao, J., 2012. Three-dimensional real-time imaging of gliding motility in apicomplexan parasites using 4D dark field microscopy. Biophys. J. 102, 192a. https://doi.org/10.1016/j.bpj.2011.11.1050

Khan, S.M., Franke-Fayard, B., Mair, G.R., Lasonder, E., Janse, C.J., Mann, M., Waters, A.P., 2005. Proteome analysis of separated male and female gametocytes reveals novel sex-specific *Plasmodium* biology. Cell 121, 675–687. https://doi.org/10.1016/j.cell.2005.03.027

Kimple, M.E., Brill, A.L., Pasker, R.L., 2013. Overview of affinity tags for protein purification. Curr Protoc Protein Sci 73, Unit-9.9. https://doi.org/10.1002/0471140864.ps0909s73

Kissinger, J.C., Gajria, B., Li, L., Paulsen, I.T., Roos, D.S., 2003. ToxoDB: accessing the *Toxoplasma gondii* genome. Nucleic Acids Res. 31, 234–236. https://doi.org/10.1093/nar/gkg072

Kita, A.M., Swider, Z.T., Erofeev, I., Halloran, M.C., Goryachev, A.B., Bement, W.M., 2019. Spindle–F-actin interactions in mitotic spindles in an intact vertebrate epithelium. MBoC 30, 1645–1654. https://doi.org/10.1091/mbc.E19-02-0126

Klein, E.Y., 2013. Antimalarial drug resistance: a review of the biology and strategies to delay emergence and spread. Int. J. Antimicrob. Agents 41, 311–317. https://doi.org/10.1016/j.ijantimicag.2012.12.007

Klenchin, V.A., Allingham, J.S., King, R., Tanaka, J., Marriott, G., Rayment, I., 2003. Trisoxazole macrolide toxins mimic the binding of actin-capping proteins to actin. Nat. Struct. Biol. 10, 1058–1063. https://doi.org/10.1038/nsb1006

Klug, D., Frischknecht, F., 2017. Motility precedes egress of malaria parasites from oocysts. eLife 6, e19157. https://doi.org/10.7554/eLife.19157

Knoll, K.R., Eustermann, S., Niebauer, V., Oberbeckmann, E., Stoehr, G., Schall, K., Tosi, A., Schwarz, M., Buchfellner, A., Korber, P., Hopfner, K.-P., 2018. The nuclear actin-containing Arp8 module is a linker DNA sensor driving INO80 chromatin remodeling. Nat. Struct. Mol. Biol. 25, 823–832. https://doi.org/10.1038/s41594-018-0115-8

Koreny, L., Zeeshan, M., Barylyuk, K., Tromer, E.C., van Hooff, J.J.E., Brady, D., Ke, H., Chelaghma, S., Ferguson, D.J.P., Eme, L., Tewari, R., Waller, R.F., 2021. Molecular characterization of the conoid complex in *Toxoplasma* reveals its conservation in all apicomplexans, including *Plasmodium* species. PLOS Biol. 19(3). https://doi.org/10.1371/journal.pbio.3001081

Kuehn, A., Pradel, G., 2010. The coming-out of malaria gametocytes. J. Biomed. Biotechnol. 2010, 976827. https://doi.org/10.1155/2010/976827

Kumar, S., Abatiyow, B.A., Haile, M.T., Oualim, K.M.Z., Leeb, A.S., Vaughan, A.M., Kappe, S.H.I., 2022. A putative *Plasmodium* RNA-binding protein plays a critical role in female gamete fertility and parasite transmission to the mosquito vector. Front. Cell Dev. Biol. 10, 825247. https://doi.org/10.3389/fcell.2022.825247

Kunert, F., Metzner, F.J., Jung, J., Höpfler, M., Woike, S., Schall, K., Kostrewa, D., Moldt, M., Chen, J.-X., Bantele, S., Pfander, B., Eustermann, S., Hopfner, K.-P., 2022. Structural mechanism of extranucleosomal DNA readout by the INO80 complex. Sci. Adv. 8, eadd3189. https://doi.org/10.1126/sciadv.add3189

Kursula, I., Kursula, P., Ganter, M., Panjikar, S., Matuschewski, K., Schüler, H., 2008. Structural basis for parasite-specific functions of the divergent profilin of *Plasmodium falciparum*. Structure 16, 1638–1648. https://doi.org/10.1016/j.str.2008.09.008

LaCount, D.J., Schoenfeld, L.W., Fields, S., 2009. Selection of yeast strains with enhanced expression of *Plasmodium falciparum* proteins. Mol. Biochem. Parasitol. 163, 119–122. https://doi.org/10.1016/j.molbiopara.2008.10.003

Laurens, M.B., 2019. RTS,S/AS01 vaccine (Mosquirix™): an overview. Hum. Vaccin. Immunother. 16, 480–489. https://doi.org/10.1080/21645515.2019.1669415

Lee, D.-H., Chu, K.-B., Kang, H.-J., Lee, S.-H., Chopra, M., Choi, H.-J., Moon, E.-K., Inn, K.-S., Quan, F.-S., 2019. Protection induced by malaria virus-like particles containing codon-optimized AMA-1 of *Plasmodium* berghei. Malar. J. 18, 394. https://doi.org/10.1186/s12936-019-3017-2

Lee, S.H., Hayes, D.B., Rebowski, G., Tardieux, I., Dominguez, R., 2007. Toxofilin from *Toxoplasma gondii* forms a ternary complex with an antiparallel actin dimer. PNAS 104, 16122–16127. https://doi.org/10.1073/pnas.0705794104

Legesse, G., Tafesse, W., Kenea, D., Subussa, B.W., Alemayehu, G.S., Kebede, T., Golassa, L., Ali, M.M., Hailu, A., 2024. Asymptomatic malaria and predictors among migrant farmworkers East Shewa zone Oromia Ethiopia. Sci. Rep. 14, 16187. https://doi.org/10.1038/s41598-024-65470-x

Lettermann, L., Ziebert, F., Schwarz, U.S., 2024. A geometrical theory of gliding motility based on cell shape and surface flow. PNAS 121, e2410708121. https://doi.org/10.1073/pnas.2410708121

Levin-Kravets, O., Keren-Kaplan, T., Attali, I., Sharon, I., Tanner, N., Shapira, D., Rathi, R., Persaud, A., Shohat, N., Shusterman, A., Prag, G., 2018. *Escherichia coli*-based selection and expression systems for discovery, characterization, and purification of ubiquitylated proteins. Methods Mol. Biol. 1844, 155–166. https://doi.org/10.1007/978-1-4939-8706-1_11

Lin, S., Wu, S., He, J., Wang, X., Grossman, A.R., 2024. Shining light on dinoflagellate photosystem I. Nat. Commun. 15, 3337. https://doi.org/10.1038/s41467-024-47797-1

Lin, Z., Rye, H.S., 2006. GroEL-mediated protein folding: making the impossible, possible. Crit Rev Biochem Mol Biol 41, 211–239. https://doi.org/10.1080/10409230600760382

Liu, H., Cui, X.-Y., Xu, D.-D., Wang, F., Meng, L.-W., Zhao, Y.-M., Liu, M., Shen, S.-J., He, X.-H., Fang, Q., Tao, Z.-Y., Jiang, C.-Z., Zhang, Q.-F., Gu, L., Xia, H., 2020. Actin-related protein Arp4 regulates euchromatic gene expression and development through H2A.Z deposition in blood-stage *Plasmodium falciparum*. Parasit. Vectors. 13, 314. https://doi.org/10.1186/s13071-020-04139-6

Lopez, A.J., Andreadaki, M., Vahokoski, J., Deligianni, E., Calder, L.J., Camerini, S., Freitag, A., Bergmann, U., Rosenthal, P.B., Sidén-Kiamos, I., Kursula, I., 2023. Structure and function of *Plasmodium* actin II in the parasite mosquito stages. PLOS Pathog. 19, e1011174. https://doi.org/10.1371/journal.ppat.1011174

Lu, H., Fagnant, P.M., Trybus, K.M., 2019. Unusual dynamics of the divergent malaria parasite PfAct1 actin filament. PNAS 116, 20418–20427. https://doi.org/10.1073/pnas.1906600116

Mair, G.R., Lasonder, E., Garver, L.S., Franke-Fayard, B.M.D., Carret, C.K., Wiegant, J.C.A.G., Dirks, R.W., Dimopoulos, G., Janse, C.J., Waters, A.P., 2010. Universal features of post-transcriptional gene regulation are critical for *Plasmodium* zygote development. PLOS Pathog. 6, e1000767. https://doi.org/10.1371/journal.ppat.1000767

Makrides, S.C., 1996. Strategies for achieving high-level expression of genes in *Escherichia coli*. Microbiol. Rev. 60, 512–538. https://doi.org/10.1128/mr.60.3.512-538.1996

Malakhov, M.P., Mattern, M.R., Malakhova, O.A., Drinker, M., Weeks, S.D., Butt, T.R., 2004. SUMO fusions and SUMO-specific protease for efficient expression and purification of proteins. J. Struct. Func. Genom. 5, 75–86. https://doi.org/10.1023/B:JSFG.0000029237.70316.52

Marbach, A., Bettenbrock, K., 2012. lac operon induction in *Escherichia coli*: Systematic comparison of IPTG and TMG induction and influence of the transacetylase LacA. J. Biotech. 157, 82–88. https://doi.org/10.1016/j.jbiotec.2011.10.009

March-Díaz, R., García-Domínguez, M., Florencio, F.J., Reyes, J.C., 2007. SEF, a new protein required for flowering repression in *Arabidopsis*, interacts with PIE1 and ARP6. Plant. Physiol. 143, 893–901. https://doi.org/10.1104/pp.106.092270

Marti, M., Good, R.T., Rug, M., Knuepfer, E., Cowman, A.F., 2004. Targeting malaria virulence and remodeling proteins to the host erythrocyte. Science 306, 1930–1933. https://doi.org/10.1126/science.1102452

Martinez, M., Mageswaran, S.K., Guérin, A., Chen, W.D., Thompson, C.P., Chavin, S., Soldati-Favre, D., Striepen, B., Chang, Y.-W., 2023. Origin and arrangement of actin filaments for gliding motility in apicomplexan parasites revealed by cryo-electron tomography. Nat. Commun. 14, 4800. https://doi.org/10.1038/s41467-023-40520-6

Matuschewski, K., Nunes, A.C., Nussenzweig, V., Ménard, R., 2002. *Plasmodium* sporozoite invasion into insect and mammalian cells is directed by the same dual binding system. EMBO J. 21, 1597–1606. https://doi.org/10.1093/emboj/21.7.1597

McFadden, G.I., Yeh, E., 2017. The apicoplast: now you see it, now you don't. Int. J. Parasitol. 47, 137–144. https://doi.org/10.1016/j.ijpara.2016.08.005

Mehta, S., Sibley, L.D., 2011. Actin depolymerizing factor controls actin turnover and gliding motility in *Toxoplasma gondii*. MBoC 22, 1290–1299. https://doi.org/10.1091/mbc.e10-12-0939

Meissner, M., Schlüter, D., Soldati, D., 2002. Role of *Toxoplasma gondii* myosin A in powering parasite gliding and host cell invasion. Science 298, 837–840. https://doi.org/10.1126/science.1074553

Melak, M., Plessner, M., Grosse, R., 2017. Actin visualization at a glance. J. Cell Sci. 130, 525–530. https://doi.org/10.1242/jcs.189068

Mikati, M.A., Breitsprecher, D., Jansen, S., Reisler, E., Goode, B.L., 2015. Coronin enhances actin filament severing by recruiting cofilin to filament sides and altering F-actin conformation. J. Mol. Bio. 427, 3137–3147. https://doi.org/10.1016/j.jmb.2015.08.011

Mikus, F., 2020. Tagging and mutant generation of the Actin-like protein Alp2b of *Plasmodium berghei* and analysis of its role in gametogenesis (Master's thesis). Faculty of Biosciences of the Ruprecht-Karls-University Heidelberg.

Miller, R.L., Ikram, S., Armelagos, G.J., Walker, R., Harer, W.B., Shiff, C.J., Baggett, D., Carrigan, M., Maret, S.M., 1994. Diagnosis of *Plasmodium falciparum* infections in mummies using the rapid manual ParaSight™-F test. Trans. R. Soc. Trop. Med. Hyg. 88, 31–32. https://doi.org/10.1016/0035-9203(94)90484-7

Mockrin, S.C., Korn, E.D., 1980. *Acanthamoeba* profilin interacts with G-actin to increase the rate of exchange of actin-bound adenosine 5'-triphosphate. Biochemistry 19, 5359–5362. https://doi.org/10.1021/bi00564a033

Molbaek, K., Tejada, M., Ricke, C.H., Scharff-Poulsen, P., Ellekvist, P., Helix-Nielsen, C., Kumar, N., Klaerke, D.A., Pedersen, P.A., 2020. Purification and initial characterization of *Plasmodium falciparum* K+ channels, PfKch1 and PfKch2 produced in Saccharomyces cerevisiae. MCFs 19, 183. https://doi.org/10.1186/s12934-020-01437-7

Moll, A., 2024. Phenotypic characterization of a PbAlp1 mutant and influence of insect cells on ookinetes (Master's thesis). Institute of Nutritional Science, Depertment of Biochemistry and Molecular Biology, Justus-Liebig University Giessen.

Montecinos-Franjola, F., Bauer, B.L., Mears, J.A., Ramachandran, R., 2020. GFP fluorescence tagging alters dynamin-related protein 1 oligomerization dynamics and creates disassembly-refractory puncta to mediate mitochondrial fission. Sci. Rep. 10, 14777. https://doi.org/10.1038/s41598-020-71655-x

Morales, E.S., Parcerisa, I.L., Ceccarelli, E.A., 2019. A novel method for removing contaminant Hsp70 molecular chaperones from recombinant proteins. Protein Sci. 28, 800–807. https://doi.org/10.1002/pro.3574

Moreau, C.A., Bhargav, S.P., Kumar, H., Quadt, K.A., Piirainen, H., Strauss, L., Kehrer, J., Streichfuss, M., Spatz, J.P., Wade, R.C., Kursula, I., Frischknecht, F., 2017. A unique profilin-actin interface is important for malaria parasite motility. PLOS Pathog. 13, e1006412. https://doi.org/10.1371/journal.ppat.1006412

Moreau, C.A., Quadt, K.A., Piirainen, H., Kumar, H., Bhargav, S.P., Strauss, L., Tolia, N.H., Wade, R.C., Spatz, J.P., Kursula, I., Frischknecht, F., 2020. A function of profilin in force generation during malaria parasite motility independent of actin binding. JCS 233775. https://doi.org/10.1242/jcs.233775

Mota, M.M., Pradel, G., Vanderberg, J.P., Hafalla, J.C.R., Frevert, U., Nussenzweig, R.S., Nussenzweig, V., Rodríguez, A., 2001. Migration of *Plasmodium* sporozoites through cells before infection. Science 291, 141–144. https://doi.org/10.1126/science.291.5501.141

Mouilleron, S., Langer, C.A., Guettler, S., McDonald, N.Q., Treisman, R., 2011. Structure of a pentavalent G-Actin•MRTF-A complex reveals how G-actin controls nucleocytoplasmic shuttling

of a transcriptional coactivator. Science Signaling 4, ra40–ra40. https://doi.org/10.1126/scisignal.2001750

Moxon, C.A., Grau, G.E., Craig, A.G., 2011. Malaria: modification of the red blood cell and consequences in the human host. Br. J. Haematol. 154, 670–679. https://doi.org/10.1111/j.1365-2141.2011.08755.x

Muller, J., Oma, Y., Vallar, L., Friederich, E., Poch, O., Winsor, B., 2005. Sequence and comparative genomic analysis of actin-related proteins. Mol. Bio. Cell 16, 13.

Münter, S., Sabass, B., Selhuber-Unkel, C., Kudryashev, M., Hegge, S., Engel, U., Spatz, J.P., Matuschewski, K., Schwarz, U.S., Frischknecht, F., 2009. *Plasmodium* sporozoite motility is modulated by the turnover of discrete adhesion sites. Cell Host Microbe 6, 551–562. https://doi.org/10.1016/j.chom.2009.11.007

Mzilahowa, T., McCall, P.J., Hastings, I.M., 2007. "Sexual" population structure and genetics of the malaria agent *P. falciparum*. PLOS One 2, e613. https://doi.org/10.1371/journal.pone.0000613

Nag, S., Larsson, M., Robinson, R.C., Burtnick, L.D., 2013. Gelsolin: The tail of a molecular gymnast. Cytoskeleton 70, 360–384. https://doi.org/10.1002/cm.21117

Neuhaus, J.M., Wanger, M., Keiser, T., Wegner, A., 1983. Treadmilling of actin. J. Muscle. Res. Cell. Motil. 4, 507–527. https://doi.org/10.1007/BF00712112

Oda, T., Aihara, T., Wakabayashi, K., 2016. Early nucleation events in the polymerization of actin, probed by time-resolved small-angle x-ray scattering. Sci. Rep. 6, 34539. https://doi.org/10.1038/srep34539

Ojala, P., Paavilainen, V., Vartiainen, M., Tuma, R., Weeds, A., Lappalainen, P., 2002. The two ADF-H domains of twinfilin play functionally distinct roles in interactions with actin monomers. Mol. Bio. Cell 13, 3811–3821. https://doi.org/10.1091/mbc.E02-03-0157

Olshina, M.A., Angrisano, F., Marapana, D.S., Riglar, D.T., Bane, K., Wong, W., Catimel, B., Yin, M.-X., Holmes, A.B., Frischknecht, F., Kovar, D.R., Baum, J., 2015. *Plasmodium falciparum* coronin organizes arrays of parallel actin filaments potentially guiding directional motility in invasive malaria parasites. Malar. J. 14, 280. https://doi.org/10.1186/s12936-015-0801-5

Oma, Y., Harata, M., 2011. Actin-related proteins localized in the nucleus: from discovery to novel roles in nuclear organization. Nucleus 2, 38–46. https://doi.org/10.4161/nucl.2.1.14510

Oosawa, F., Asakura, S., Hotta, K., Imai, N., Ooi, T., 1959. G-F transformation of actin as a fibrous condensation. J. Polym. Sci. 37, 323–336. https://doi.org/10.1002/pol.1959.1203713202

Oosterheert, W., Blanc, F.E.C., Roy, A., Belyy, A., Sanders, M.B., Hofnagel, O., Hummer, G., Bieling, P., Raunser, S., 2023. Molecular mechanisms of inorganic-phosphate release from the core and barbed end of actin filaments. Nat. Struct. Mol. Biol. 30, 1774–1785. https://doi.org/10.1038/s41594-023-01101-9

Opitz, C., Soldati, D., 2002. 'The glideosome': a dynamic complex powering gliding motion and host cell invasion by *Toxoplasma gondii*. Mol. Microbiol. 45, 597–604. https://doi.org/10.1046/j.1365-2958.2002.03056.x

Osakabe, A., Takahashi, Y., Murakami, H., Otawa, K., Tachiwana, H., Oma, Y., Nishijima, H., Shibahara, K., Kurumizaka, H., Harata, M., 2014. DNA binding properties of the Actin-related protein Arp8 and its role in DNA repair. PLOS ONE 9, e108354. https://doi.org/10.1371/journal.pone.0108354

Park, E.-J., Hur, S.-K., Lee, H.-S., Lee, S.-A., Kwon, J., 2011. The human INO80 binds to microtubule via the E-hook of tubulin: implications for the role in spindle assembly. Biochem. Biophys. Res. Commun. 416, 416–420. https://doi.org/10.1016/j.bbrc.2011.11.069

Patra, K.P., Kaur, H., Kolli, S.K., Wozniak, J.M., Prieto, J.H., Yates, J.R., Gonzalez, D.J., Janse, C.J., Vinetz, J.M., 2021. A hetero-multimeric chitinase-containing *Plasmodium falciparum* and *Plasmodium gallinaceum* ookinete-secreted protein complex involved in mosquito midgut invasion. Front .Cell Infect. Microbiol. 10, 615343. https://doi.org/10.3389/fcimb.2020.615343

Pazicky, S., Dhamotharan, K., Kaszuba, K., Mertens, H.D.T., Gilberger, T., Svergun, D., Kosinski, J., Weininger, U., Löw, C., 2020. Structural role of essential light chains in the apicomplexan glideosome. Commun. Biol. 3, 1–14. https://doi.org/10.1038/s42003-020-01283-8

Periz, J., Whitelaw, J., Harding, C., Gras, S., Del Rosario Minina, M.I., Latorre-Barragan, F., Lemgruber, L., Reimer, M.A., Insall, R., Heaslip, A., Meissner, M., 2017. *Toxoplasma gondii* F-actin forms an extensive filamentous network required for material exchange and parasite maturation. eLife 6, e24119. https://doi.org/10.7554/eLife.24119

Pollard, T.D., 2016. Actin and actin-binding proteins. Cold Spring Harb. Perspect. Biol. 8, a018226. https://doi.org/10.1101/cshperspect.a018226

Pollard, T.D., 1984. Polymerization of ADP-actin. J. Cell. Biol. 99, 769–777. https://doi.org/10.1083/jcb.99.3.769

Ponzi, M., Sidén-Kiamos, I., Bertuccini, L., Currà, C., Kroeze, H., Camarda, G., Pace, T., Franke-Fayard, B., Laurentino, E.C., Louis, C., Waters, A.P., Janse, C.J., Alano, P., 2009. Egress of *Plasmodium berghei* gametes from their host erythrocyte is mediated by the MDV-1/PEG3 protein. Cell. Microbiol. 11, 1272–1288. https://doi.org/10.1111/j.1462-5822.2009.01331.x

Pospich, S., Kumpula, E.-P., von der Ecken, J., Vahokoski, J., Kursula, I., Raunser, S., 2017. Near-atomic structure of jasplakinolide-stabilized malaria parasite F-actin reveals the structural basis of filament instability. PNAS 114, 10636–10641. https://doi.org/10.1073/pnas.1707506114

Pražák, V., Vasishtan, D., Grünewald, K., Douglas, R.G., Ferreira, J.L., 2024. Molecular architecture of glideosome and nuclear F-actin in *Plasmodium falciparum*. BioRxiv. https://doi.org/10.1101/2024.04.22.590301

Przyborski, J., Lanzer, M., 2004. The malarial secretome. Science 306, 1897–1898. https://doi.org/10.1126/science.1107072

Pukrittayakamee, S., Jittamala, P., Watson, J.A., Hanboonkunupakarn, B., Leungsinsiri, P., Poovorawan, K., Chotivanich, K., Bancone, G., Chu, C.S., Imwong, M., Day, N.P., Taylor, W.R., White, N.J., 2024. Primaquine in glucose-6-phosphate dehydrogenase deficiency: an adaptive pharmacometric assessment of ascending dose regimens in healthy volunteers. eLife 12, RP87318. https://doi.org/10.7554/eLife.87318

Qian, P., Wang, X., Guan, C., Fang, X., Cai, M., Zhong, C., Cui, Y., Li, Y., Yao, L., Cui, H., Jiang, K., Yuan, J., 2022. Apical anchorage and stabilization of subpellicular microtubules by apical polar ring ensures *Plasmodium* ookinete infection in mosquito. Nat. Commun. 13, 7465. https://doi.org/10.1038/s41467-022-35270-w

Qu, K., Chen, K., Wang, H., Li, X., Chen, Z., 2022. Structure of the NuA4 acetyltransferase complex bound to the nucleosome. Nature 610, 569–574. https://doi.org/10.1038/s41586-022-05303-x

Ramakrishnan, C., Dessens, J.T., Armson, R., Pinto, S.B., Talman, A.M., Blagborough, A.M., Sinden, R.E., 2011. Vital functions of the malarial ookinete protein CTRP reside in the A domains. Int. J. Parasitol. 41, 1029–1039. https://doi.org/10.1016/j.ijpara.2011.05.007

Ramasamy, R., 2014. Zoonotic Malaria – Global Overview and Research and Policy Needs. Front. Public Health 2. https://doi.org/10.3389/fpubh.2014.00123

Rashpa, R., Brochet, M., 2022. Expansion microscopy of *Plasmodium* gametocytes reveals the molecular architecture of a bipartite microtubule organisation centre coordinating mitosis with axoneme assembly. PLOS Pathog. 18, e1010223. https://doi.org/10.1371/journal.ppat.1010223

Ratkeviciute, G., Cooper, B.F., Knowles, T.J., 2021. Methods for the solubilisation of membrane proteins: the micelle-aneous world of membrane protein solubilisation. Biochem. Soc. Trans. 49, 1763–1777. https://doi.org/10.1042/BST20210181

Ridzuan, M.A.M., Moon, R.W., Knuepfer, E., Black, S., Holder, A.A., Green, J.L., 2012. Subcellular location, phosphorylation and assembly into the motor complex of GAP45 during *Plasmodium falciparum* schizont development. PLOS One 7, e33845. https://doi.org/10.1371/journal.pone.0033845

Riedl, J., Crevenna, A.H., Kessenbrock, K., Yu, J.H., Neukirchen, D., Bista, M., Bradke, F., Jenne, D., Holak, T.A., Werb, Z., Sixt, M., Wedlich-Soldner, R., 2008. Lifeact: a versatile marker to visualize F-actin. Nat. Methods. 5, 605–607. https://doi.org/10.1038/nmeth.1220

Riske, K.A., Domingues, C.C., Casadei, B.R., Mattei, B., Caritá, A.C., Lira, R.B., Preté, P.S.C., de Paula, E., 2017. Biophysical approaches in the study of biomembrane solubilization: quantitative assessment and the role of lateral inhomogeneity. Biophys. Rev. 9, 649–667. https://doi.org/10.1007/s12551-017-0310-6

Rodal, A.A., Sokolova, O., Robins, D.B., Daugherty, K.M., Hippenmeyer, S., Riezman, H., Grigorieff, N., Goode, B.L., 2005. Conformational changes in the Arp2/3 complex leading to actin nucleation. Nat. Struct. Mol. Biol. 12, 26–31. https://doi.org/10.1038/nsmb870

Rosano, G.L., Ceccarelli, E.A., 2014. Recombinant protein expression in *Escherichia coli*: advances and challenges. Front. Microbiol. 5. https://doi.org/10.3389/fmicb.2014.00172

Rotty, J.D., Wu, C., Bear, J.E., 2013. New insights into the regulation and cellular functions of the ARP2/3 complex. Nat. Rev. Mol. Cell Biol. 14, 7–12. https://doi.org/10.1038/nrm3492

Royster, A., Mir, S., Mir, M.A., 2021. A novel approach for the purification of aggregation prone proteins. PLOS One 16, e0260143. https://doi.org/10.1371/journal.pone.0260143

Rubiyana, Y., Santoso, A., Batubara, I., 2015. Comparison of immobilized metal affinity chromatography Ni-NTA and Co-TALON for the purification of recombinant human erythropoietin. Makara Journal of Science 19. https://doi.org/10.7454/mss.v19i4.5167

Saeed, S., Tremp, A.Z., Dessens, J.T., 2023. *Plasmodium* sporozoite excystation involves local breakdown of the oocyst capsule. Sci. Rep. 13, 22222. https://doi.org/10.1038/s41598-023-49442-1

Sahdev, S., Khattar, S.K., Saini, K.S., 2008. Production of active eukaryotic proteins through bacterial expression systems: a review of the existing biotechnology strategies. Mol. Cell Biochem. 307, 249–264. https://doi.org/10.1007/s11010-007-9603-6

Schafer, D.A., Gill, S.R., Cooper, J.A., Heuser, J.E., Schroer, T.A., 1994. Ultrastructural analysis of the dynactin complex: an actin-related protein is a component of a filament that resembles F-actin. J. Cell Biol. 126, 403–412. https://doi.org/10.1083/jcb.126.2.403

Schafer, D.A., Schroer, T.A., 1999. Actin-Related Proteins 25. Annu. Rev. Cell Dev. Biol., 15:341-63. https://doi.org/10.1146/annurev.cellbio.15.1.341

Scheffler, K., Giannini, F., Lemonnier, T., Mogessie, B., 2022. The prophase oocyte nucleus is a homeostatic G-actin buffer. J. Cell Sci. 135, jcs259807. https://doi.org/10.1242/jcs.259807

Schindelin, J., Arganda-Carreras, I., Frise, E., Kaynig, V., Longair, M., Pietzsch, T., Preibisch, S., Rueden, C., Saalfeld, S., Schmid, B., Tinevez, J.-Y., White, D.J., Hartenstein, V., Eliceiri, K., Tomancak, P., Cardona, A., 2012. Fiji: an open-source platform for biological-image analysis. Nat. Methods 9, 676–682. https://doi.org/10.1038/nmeth.2019

Schroer, T.A., 2004. Dynactin. Annu. Rev. Cell Dev. Biol. 20, 759–779. https://doi.org/10.1146/annurev.cellbio.20.012103.094623

Schroer, T.A., Fyrberg, E., Cooper, J.A., Waterson, R.H., Helfman, D., Pollard, T.D., Meyer, D.I., 1994. Actin-related protein nomenclature and classification. J. Cell Biol. 127, 1777–1778.

Schüler, H., Matuschewski, K., 2006. *Plasmodium* motility: actin not actin' like actin. Trends Parasitol. 22, 146–147. https://doi.org/10.1016/j.pt.2006.02.005

Schüler, H., Mueller, A.-K., Matuschewski, K., 2005a. Unusual properties of *Plasmodium falciparum* actin: new insights into microfilament dynamics of apicomplexan parasites. FEBS Lett. 579, 655–660. https://doi.org/10.1016/j.febslet.2004.12.037

Schüler, H., Mueller, A.-K., Matuschewski, K., 2005b. A *Plasmodium* actin-depolymerizing factor that binds exclusively to actin monomers. Mol. Biol. Cell 16, 4013–4023. https://doi.org/10.1091/mbc.E05-02-0086

Sebastian, S., Brochet, M., Collins, M.O., Schwach, F., Jones, M.L., Goulding, D., Rayner, J.C., Choudhary, J.S., Billker, O., 2012. A *Plasmodium* calcium-dependent protein kinase controls zygote development and transmission by translationally activating repressed mRNAs. Cell Host Microbe 12, 9–19. https://doi.org/10.1016/j.chom.2012.05.014

Segireddy, R.R., Belda, H., Yang, A.S.P., Dundas, K., Knoeckel, J., Galaway, F., Wood, L., Quinkert, D., Knuepfer, E., Treeck, M., Wright, G.J., Douglas, A.D., 2024. A screen for *Plasmodium falciparum* sporozoite surface protein binding to human hepatocyte surface receptors identifies novel host–pathogen interactions. Malar. J. 23, 151. https://doi.org/10.1186/s12936-024-04913-2

Selden, L.A., Kinosian, H.J., Estes, J.E., Gershman, L.C., 1999. Impact of profilin on actin-bound nucleotide exchange and actin polymerization dynamics. Biochemistry 38, 2769–2778. https://doi.org/10.1021/bi981543c

Sen, U., Saxena, H., Khurana, J., Nayak, A., Gupta, A., 2018. *Plasmodium falciparum* RUVBL3 protein: a novel DNA modifying enzyme and an interacting partner of essential HAT protein MYST. Sci. Rep. 8, 10917. https://doi.org/10.1038/s41598-018-29137-8

Shakya, B., Penn, W.D., Nakayasu, E.S., LaCount, D.J., 2017. The *Plasmodium falciparum* exported protein PF3D7_0402000 binds to erythrocyte ankyrin and band 4.1. Mol. Biochem. Parasitol. 216, 5–13. https://doi.org/10.1016/j.molbiopara.2017.06.002

Shoji, K., Ohashi, K., Sampei, K., Oikawa, M., Mizuno, K., 2012. Cytochalasin D acts as an inhibitor of the actin–cofilin interaction. BBRC 424, 52–57. https://doi.org/10.1016/j.bbrc.2012.06.063

Shonhai, A., Botha, M., de Beer, T.A.P., Boshoff, A., Blatch, G.L., 2008. Structure-function study of a *Plasmodium falciparum* Hsp70 using three dimensional modelling and in vitro analyses. Protein Pept. Lett. 15, 1117–1125. https://doi.org/10.2174/092986608786071067

Shrestha, P., Kandel, J., Tayara, H., Chong, K.T., 2024. Post-translational modification prediction via prompt-based fine-tuning of a GPT-2 model. Nat. Commun. 15, 6699. https://doi.org/10.1038/s41467-024-51071-9

Siden-Kiamos, I., Goosmann, C., Buscaglia, C.A., Brinkmann, V., Matuschewski, K., Montagna, G.N., 2020. Polarization of MTIP is a signature of gliding locomotion in *Plasmodium* ookinetes and sporozoites. Mol. Biochem. Parasitol. 235, 111247. https://doi.org/10.1016/j.molbiopara.2019.111247

Siden-Kiamos, I., Pinder, J.C., Louis, C., 2006. Involvement of actin and myosins in *Plasmodium berghei* ookinete motility. Mol. Biochem. Parasitol. 150, 308–317. https://doi.org/10.1016/j.molbiopara.2006.09.003

Siden-Kiamos, I., Schüler, H., Liakopoulos, D., Louis, C., 2010. Arp1, an actin-related protein, in *Plasmodium berghei*. Mol. Biochem. Parasitol. 173, 88–96. https://doi.org/10.1016/j.molbiopara.2010.05.008

Silvie, O., Franetich, J.-F., Charrin, S., Mueller, M.S., Siau, A., Bodescot, M., Rubinstein, E., Hannoun, L., Charoenvit, Y., Kocken, C.H., Thomas, A.W., van Gemert, G.-J., Sauerwein, R.W., Blackman, M.J., Anders, R.F., Pluschke, G., Mazier, D., 2004. A role for apical membrane antigen 1 during invasion of hepatocytes by *Plasmodium falciparum* sporozoites. JBC 279, 9490–9496. https://doi.org/10.1074/jbc.M311331200

Sinden, R., Talman, A., Marques, S., Wass, M., Sternberg, M., 2010. The flagellum in malarial parasites. Curr. Opin. Microbiol., Host–Microbe Interactions: Fungi/Parasites/Viruses 13, 491–500. https://doi.org/10.1016/j.mib.2010.05.016

Sinden, R.E., Croll, N.A., 1975. Cytology and Kinetics of microgametogenesis and fertilization in *Plasmodium yoelii nigeriensis*. Parasitology 70, 53–65. https://doi.org/10.1017/S0031182000048861

Skillman, K.M., Diraviyam, K., Khan, A., Tang, K., Sept, D., Sibley, L.D., 2011. Evolutionarily divergent, unstable filamentous actin is essential for gliding motility in apicomplexan parasites. PLOS Pathog. 7, e1002280. https://doi.org/10.1371/journal.ppat.1002280

Skrzypek, R., Callaghan, R., 2017. The “pushmi-pullyu” of resistance to chloroquine in malaria. Essays. Biochem. 61, 167–175. https://doi.org/10.1042/EBC20160060

Smith, J.D., Rowe, J.A., Higgins, M.K., Lavstsen, T., 2013. Malaria’s deadly grip: cytoadhesion of *Plasmodium falciparum* infected erythrocytes. Cell Microbiol. 15, 10.1111/cmi.12183. https://doi.org/10.1111/cmi.12183

Smith, M.L., Styczynski, M.P., 2018. Systems biology-based investigation of host-*Plasmodium* interactions. Trends Parasitol 34, 617–632. https://doi.org/10.1016/j.pt.2018.04.003

Soulié, M., Deletraz, A., Wehbie, M., Mahler, F., Bouchemal, I., Le Roy, A., Petit-Härtlein, I., Keller, S., Meister, A., Pebay-Peyroula, E., Breyton, C., Ebel, C., Durand, G., 2023. Zwitterionic fluorinated detergents: From design to membrane protein applications. Biochimie, Membranes Proteins 205, 40–52. https://doi.org/10.1016/j.biochi.2022.11.003

Spreng, B., Fleckenstein, H., Kübler, P., Di Biagio, C., Benz, M., Patra, P., Schwarz, U.S., Cyrklaff, M., Frischknecht, F., 2019. Microtubule number and length determine cellular shape and function in *Plasmodium*. EMBO J. 38, e100984. https://doi.org/10.15252/embj.2018100984

Srinivasan, P., Beatty, W.L., Diouf, A., Herrera, R., Ambroggio, X., Moch, J.K., Tyler, J.S., Narum, D.L., Pierce, S.K., Boothroyd, J.C., Haynes, J.D., Miller, L.H., 2011. Binding of *Plasmodium* merozoite proteins RON2 and AMA1 triggers commitment to invasion. PNAS 108, 13275–13280. https://doi.org/10.1073/pnas.1110303108

Stewart, L.B., Freville, A., Voss, T.S., Baker, D.A., Awandare, G.A., Conway, D.J., 2022. *Plasmodium falciparum* sexual commitment rate variation among clinical isolates and diverse laboratory-adapted lines. Microbiol. Spectr. 10, e02234-22. https://doi.org/10.1128/spectrum.02234-22

Stortz, J.F., Del Rosario, M., Singer, M., Wilkes, J.M., Meissner, M., Das, S., 2019. Formin-2 drives polymerisation of actin filaments enabling segregation of apicoplasts and cytokinesis in *Plasmodium* falciparum. eLife 8, e49030. https://doi.org/10.7554/eLife.49030

Straub, K.W., Peng, E.D., Hajagos, B.E., Tyler, J.S., Bradley, P.J., 2011. The moving junction protein RON8 facilitates firm attachment and host cell invasion in *Toxoplasma gondii*. PLOS Pathog. 7, e1002007. https://doi.org/10.1371/journal.ppat.1002007

Sturm, A., Amino, R., van de Sand, C., Regen, T., Retzlaff, S., Rennenberg, A., Krueger, A., Pollok, J.-M., Menard, R., Heussler, V.T., 2006. Manipulation of host hepatocytes by the malaria parasite for delivery into liver sinusoids. Science 313, 1287–1290. https://doi.org/10.1126/science.1129720

Suh, P.F., Elanga-Ndille, E., Tchouakui, M., Sandeu, M.M., Tagne, D., Wondji, C., Ndo, C., 2023. Impact of insecticide resistance on malaria vector competence: a literature review. Malar. J. 22, 19. https://doi.org/10.1186/s12936-023-04444-2

Sulimenko, V., Dráberová, E., Dráber, P., 2022. γ-Tubulin in microtubule nucleation and beyond. Front. Cell Dev. Biol. 10. https://doi.org/10.3389/fcell.2022.880761

Sultan, A.A., Thathy, V., Frevert, U., Robson, K.J.H., Crisanti, A., Nussenzweig, V., Nussenzweig, R.S., Ménard, R., 1997. TRAP is necessary for gliding motility and infectivity of *Plasmodium* sporozoites. Cell 90, 511–522. https://doi.org/10.1016/S0092-8674(00)80511-5

Sun, S.Y., Segev-Zarko, L., Pintilie, G.D., Kim, C.Y., Staggers, S.R., Schmid, M.F., Egan, E.S., Chiu, W., Boothroyd, J.C., 2024. Cryogenic electron tomography reveals novel structures in the apical complex of *Plasmodium falciparum*. mBio 15, e02864-23. https://doi.org/10.1128/mbio.02864-23

Svitkina, T.M., 2018. The actin cytoskeleton and actin-based motility. Cold Spring Harb. Perspect. Biol. 10, a018267. https://doi.org/10.1101/cshperspect.a018267

Svitkina, T.M., Bulanova, E.A., Chaga, O.Y., Vignjevic, D.M., Kojima, S., Vasiliev, J.M., Borisy, G.G., 2003. Mechanism of filopodia initiation by reorganization of a dendritic network. J. Cell Biol. 160, 409–421. https://doi.org/10.1083/jcb.200210174

Sweeney, H.L., Holzbaur, E.L.F., 2018. Motor proteins. Cold Spring Harb. Perspect. Biol. 10, a021931. https://doi.org/10.1101/cshperspect.a021931

Tabor, S., 1990. Expression using the T7 RNA polymerase/promoter system. Curr. Protoc. Mol. Biol. 11, 16.2.1-16.2.11. https://doi.org/10.1002/0471142727.mb1602s11

Takano, R., Kozuka-Hata, H., Kondoh, D., Bochimoto, H., Oyama, M., Kato, K., 2019. A high-resolution map of SBP1 interactomes in *Plasmodium falciparum*-infected erythrocytes. iScience 19, 703–714. https://doi.org/10.1016/j.isci.2019.07.035

Tewari, R., Straschil, U., Bateman, A., Böhme, U., Cherevach, I., Gong, P., Pain, A., Billker, O., 2010. The systematic functional analysis of *Plasmodium* protein kinases identifies essential regulators of mosquito transmission. Cell Host Microbe 8, 377–387. https://doi.org/10.1016/j.chom.2010.09.006

Tham, W.-H., Lim, N.T.Y., Weiss, G.E., Lopaticki, S., Ansell, B.R.E., Bird, M., Lucet, I., Dorin-Semblat, D., Doerig, C., Gilson, P.R., Crabb, B.S., Cowman, A.F., 2015. *Plasmodium falciparum*

adhesins play an essential role in signalling and activation of invasion into human erythrocytes. PLOS Pathog. 11. https://doi.org/10.1371/journal.ppat.1005343

Titus, M.A., 2018. Myosin-Driven Intracellular Transport. Cold Spring Harb. Perspect. Biol. 10, a021972. https://doi.org/10.1101/cshperspect.a021972

Tokmakov, A.A., Kurotani, A., Takagi, T., Toyama, M., Shirouzu, M., Fukami, Y., Yokoyama, S., 2012. Multiple Post-translational Modifications Affect Heterologous Protein Synthesis. J. Biol. Chem. 287, 27106–27116. https://doi.org/10.1074/jbc.M112.366351

Tosetti, N., Dos Santos Pacheco, N., Soldati-Favre, D., Jacot, D., 2019. Three F-actin assembly centers regulate organelle inheritance, cell-cell communication and motility in *Toxoplasma gondii*. eLife 8, e42669. https://doi.org/10.7554/eLife.42669

Urnavicius, L., Zhang, K., Diamant, A.G., Motz, C., Schlager, M.A., Yu, M., Patel, N.A., Robinson, C.V., Carter, A.P., 2015. The structure of the dynactin complex and its interaction with dynein 7. Science 347. https://doi.org/10.1126/science.aaa4080

Vahokoski, J., Bhargav, S.P., Desfosses, A., Andreadaki, M., Kumpula, E.-P., Martinez, S.M., Ignatev, A., Lepper, S., Frischknecht, F., Sidén-Kiamos, I., Sachse, C., Kursula, I., 2014. Structural differences explain diverse functions of *Plasmodium* actins. PLOS Pathog. 10, e1004091. https://doi.org/10.1371/journal.ppat.1004091

Vega-Rodríguez, J., Ghosh, A.K., Kanzok, S.M., Dinglasan, R.R., Wang, S., Bongio, N.J., Kalume, D.E., Miura, K., Long, C.A., Pandey, A., Jacobs-Lorena, M., 2014. Multiple pathways for *Plasmodium* ookinete invasion of the mosquito midgut. PNAS 111, E492–E500. https://doi.org/10.1073/pnas.1315517111

Venugopal, K., Hentzschel, F., Valkiūnas, G., Marti, M., 2020. *Plasmodium* asexual growth and sexual development in the haematopoietic niche of the host. Nat. Rev. Microbiol. 18, 177–189. https://doi.org/10.1038/s41579-019-0306-2

Verkhusha, V.V., Tsukita, S., Oda, H., 1999. Actin dynamics in lamellipodia of migrating border cells in the *Drosophila* ovary revealed by a GFP-actin fusion protein. FEBS Lett. 445, 395–401. https://doi.org/10.1016/S0014-5793(99)00124-6

Vignjevic, D., Kojima, S., Aratyn, Y., Danciu, O., Svitkina, T., Borisy, G.G., 2006. Role of fascin in filopodial protrusion. J. Cell. Biol. 174, 863–875. https://doi.org/10.1083/jcb.200603013

Virtanen, J.A., Vartiainen, M.K., 2017. Diverse functions for different forms of nuclear actin. COCEBI, Cell Nucleus 46, 33–38. https://doi.org/10.1016/j.ceb.2016.12.004

von der Ecken, J., Müller, M., Lehman, W., Manstein, D.J., Penczek, P.A., Raunser, S., 2015. Structure of the F-actin–tropomyosin complex. Nature 519, 114–117. https://doi.org/10.1038/nature14033

Votýpka, J., Modrý, D., Oborník, M., Šlapeta, J., Lukeš, J., 2017. Apicomplexa, in: Archibald, J.M., Simpson, A.G.B., Slamovits, C.H., Margulis, L., Melkonian, M., Chapman, D.J., Corliss, J.O. (Eds.), Handbook of the Protists. Springer International Publishing, Cham, 1–58. https://doi.org/10.1007/978-3-319-32669-6_20-1

Wadman, M., 2023. First malaria vaccine slashes early childhood mortality [WWW Document]. URL https://www.science.org/content/article/first-malaria-vaccine-slashes-early-childhood-deaths (accessed 28/02/25).

Wall, R.J., Ferguson, D.J.P., Freville, A., Franke-Fayard, B., Brady, D., Zeeshan, M., Bottrill, A.R., Wheatley, S., Fry, A.M., Janse, C.J., Yamano, H., Holder, A.A., Guttery, D.S., Tewari, R., 2018. *Plasmodium* APC3 mediates chromosome condensation and cytokinesis during atypical

mitosis in male gametogenesis. Sci. Rep. 8, 5610. https://doi.org/10.1038/s41598-018-23871-9

Wall, R.J., Roques, M., Katris, N.J., Koreny, L., Stanway, R.R., Brady, D., Waller, R.F., Tewari, R., 2016. SAS6-like protein in *Plasmodium* indicates that conoid-associated apical complex proteins persist in invasive stages within the mosquito vector. Sci. Rep. 6, 28604. https://doi.org/10.1038/srep28604

Walton, T., Gui, M., Velkova, S., Fassad, M.R., Hirst, R.A., Haarman, E., O'Callaghan, C., Bottier, M., Burgoyne, T., Mitchison, H.M., Brown, A., 2023. Axonemal structures reveal mechanoregulatory and disease mechanisms. Nature 618, 625–633. https://doi.org/10.1038/s41586-023-06140-2

Wartel, M., Ducret, A., Thutupalli, S., Czerwinski, F., Gall, A.-V.L., Mauriello, E.M.F., Bergam, P., Brun, Y.V., Shaevitz, J., Mignot, T., 2013. A versatile class of cell surface directional motors gives rise to gliding motility and sporulation in *Myxococcus xanthus*. PLOS Biol. 11, e1001728. https://doi.org/10.1371/journal.pbio.1001728

Weber, J.L., 1987. Analysis of sequences from the extremely A + T-rich genome of *Plasmodium falciparum*. Gene 52, 103–109. https://doi.org/10.1016/0378-1119(87)90399-4

Wegner, A., 1976. Head to tail polymerization of actin. J. Mol. Biol. 108, 139–150. https://doi.org/10.1016/S0022-2836(76)80100-3

Weisse, T., 2017. Functional diversity of aquatic ciliates, Integrating the three dimensions of ciliate diversity: function, taxonomy, and genetics. Eur. J. Protistol. 61, 331–358. https://doi.org/10.1016/j.ejop.2017.04.001

Wesseling, J.G., Smits, M.A., Schoenmakers, J.G., 1988. Extremely diverged actin proteins in *Plasmodium falciparum*. Mol. Biochem. Parasitol. 30, 143–153. https://doi.org/10.1016/0166-6851(88)90107-7

Wesseling, J.G., Snijders, P.J.F., van Someren, P., Jansen, J., Smits, M.A., Schoenmakers, J.G.G., 1989. Stage-specific expression and genomic organization of the actin genes of the malaria parasite *Plasmodium falciparum*. Mol. Biochem. Parasitol. 35, 167–176. https://doi.org/10.1016/0166-6851(89)90119-9

Westphal, M., Jungbluth, A., Heidecker, M., Mühlbauer, B., Heizer, C., Schwartz, J.-M., Marriott, G., Gerisch, G., 1997. Microfilament dynamics during cell movement and chemotaxis monitored using a GFP–actin fusion protein. Curr. Biol. 7, 176–183. https://doi.org/10.1016/S0960-9822(97)70088-5

WHO, 2023. World malaria report 2023. World Health Organization. https://www.who.int/teams/global-malaria-programme/reports/world-malaria-report-2023

Wiese, C., Zheng, Y., 2000. A new function for the γ -tubulin ring complex as a microtubule minus-end cap. Nat. Cell Biol. 2, 358–364. https://doi.org/10.1038/35014051

Willard, L., Ranjan, A., Zhang, H., Monzavi, H., Boyko, R.F., Sykes, B.D., Wishart, D.S., 2003. VADAR: a web server for quantitative evaluation of protein structure quality. Nucleic Acids Res. 31, 3316–3319.

Wilson, L.G., Carter, L.M., Reece, S.E., 2013. High-speed holographic microscopy of malaria parasites reveals ambidextrous flagellar waveforms. PNAS 110, 18769–18774. https://doi.org/10.1073/pnas.1309934110

Wong, W., Skau, C.T., Marapana, D.S., Hanssen, E., Taylor, N.L., Riglar, D.T., Zuccala, E.S., Angrisano, F., Lewis, H., Catimel, B., Clarke, O.B., Kershaw, N.J., Perugini, M.A., Kovar, D.R., Gulbis, J.M., Baum, J., 2011. Minimal requirements for actin filament disassembly revealed by

structural analysis of malaria parasite actin-depolymerizing factor 1. PNAS 108, 9869–9874. https://doi.org/10.1073/pnas.1018927108

Woodrow, C.J., White, N.J., 2017. The clinical impact of artemisinin resistance in Southeast Asia and the potential for future spread. FEMS Microbiol. Rev. 41, 34–48. https://doi.org/10.1093/femsre/fuw037

Xue, B., Leyrat, C., Grimes, J.M., Robinson, R.C., 2014. Structural basis of thymosin-β4/profilin exchange leading to actin filament polymerization. PNAS 111, E4596–E4605. https://doi.org/10.1073/pnas.1412271111

Xue, Y., Van, C., Pradhan, S.K., Su, T., Gehrke, J., Kuryan, B.G., Kitada, T., Vashisht, A., Tran, N., Wohlschlegel, J., Peterson, C.L., Kurdistani, S.K., Carey, M.F., 2015. The INO80 complex prevents invasion of euchromatin into silent chromatin. Genes Dev. 29, 350–355. https://doi.org/10.1101/gad.256255.114

Yahata, K., Hart, M.N., Davies, H., Asada, M., Wassmer, S.C., Templeton, T.J., Treeck, M., Moon, R.W., Kaneko, O., 2021. Gliding motility of *Plasmodium* merozoites. PNAS 118, e2114442118. https://doi.org/10.1073/pnas.2114442118

Yahiya, S., Jordan, S., Smith, H.X., Gaboriau, D.C.A., Famodimu, M.T., Dahalan, F.A., Churchyard, A., Ashdown, G.W., Baum, J., 2022. Live-cell fluorescence imaging of microgametogenesis in the human malaria parasite *Plasmodium falciparum*. PLOS Pathog. 18, e1010276. https://doi.org/10.1371/journal.ppat.1010276

Yang, A.S.P., Dutta, D., Kretzschmar, K., Hendriks, D., Puschhof, J., Hu, H., Boonekamp, K.E., van Waardenburg, Y., Chuva de Sousa Lopes, S.M., van Gemert, G.-J., de Wilt, J.H.W., Bousema, T., Clevers, H., Sauerwein, R.W., 2023. Development of *Plasmodium falciparum* liver-stages in hepatocytes derived from human fetal liver organoid cultures. Nat. Commun. 14, 4631. https://doi.org/10.1038/s41467-023-40298-7

Yang, C., Czech, L., Gerboth, S., Kojima, S., Scita, G., Svitkina, T., 2007. Novel Roles of formin mDia2 in Lamellipodia and Filopodia formation in motile cells. PLOS Biol. 5, e317. https://doi.org/10.1371/journal.pbio.0050317

Yang, S., Cai, M., Huang, J., Zhang, S., Mo, X., Jiang, K., Cui, H., Yuan, J., 2023. EB1 decoration of microtubule lattice facilitates spindle-kinetochore lateral attachment in *Plasmodium* male gametogenesis. Nat. Commun. 14, 2864. https://doi.org/10.1038/s41467-023-38516-3

Yao, W., Beckwith, S.L., Zheng, T., Young, T., Dinh, V.T., Ranjan, A., Morrison, A.J., 2015. Assembly of the Arp5 (Actin-related Protein) Subunit involved in distinct INO80 chromatin remodeling activities. J. Biol. Chem. 290, 25700–25709. https://doi.org/10.1074/jbc.M115.674887

Yee, M., 2019. Characterization of actin subdomain 3 mutants and visualization of actin dynamics in *Plasmodium berghei* (Mastr's thesis). Faculty of Biosciences of the Ruprecht-Karls-University Heidelberg.

Yee, M., Walther, T., Frischknecht, F., Douglas, R.G., 2022. Divergent *Plasmodium* actin residues are essential for filament localization, mosquito salivary gland invasion and malaria transmission. PLOS Pathog. 18, e1010779. https://doi.org/10.1371/journal.ppat.1010779

Yoo, Y., Wu, X., Guan, J.L., 2007. A novel role of the actin-nucleating Arp2/3 complex in the regulation of RNA polymerase II-dependent transcription. J. Biol. Chem. 282(10):7616-23. https://doi.org/10.1074/jbc.M607596200

Zahedi, Y., Zeng, S., Ekwall, K., 2023. An essential role for the Ino80 chromatin remodeling complex in regulation of gene expression during cellular quiescence. Chromosome Res. 31, 14. https://doi.org/10.1007/s10577-023-09723-x

Zeeshan, M., Brady, D., Markus, R., Vaughan, S., Ferguson, D., Holder, A.A., Tewari, R., 2022. *Plasmodium* SAS4: basal body component of male cell which is dispensable for parasite transmission. Life Sci. Alliance 5, e202101329. https://doi.org/10.26508/lsa.202101329

Zeeshan, M., Pandey, R., Subudhi, A.K., Ferguson, D.J.P., Kaur, G., Rashpa, R., Nugmanova, R., Brady, D., Bottrill, A.R., Vaughan, S., Brochet, M., Bollen, M., Pain, A., Holder, A.A., Guttery, D.S., Tewari, R., 2021. Protein phosphatase 1 regulates atypical mitotic and meiotic division in *Plasmodium* sexual stages. Commun. Biol. 4, 1–14. https://doi.org/10.1038/s42003-021-02273-0

Zhang, Q., Huang, Y., Zhang, Y., Fang, X., Claes, A., Duchateau, M., Namane, A., Lopez-Rubio, J.-J., Pan, W., Scherf, A., 2011. A critical role of perinuclear filamentous actin in spatial repositioning and mutually exclusive expression of virulence genes in malaria parasites. Cell Host Microbe 10, 451–63. https://doi.org/10.1016/j.chom.2011.09.013

Zhang, R., Alushin, G.M., Brown, A., Nogales, E., 2015. Mechanistic origin of microtubule dynamic instability and its modulation by EB proteins. Cell 162, 849–859. https://doi.org/10.1016/j.cell.2015.07.012

Zhou, Y., Hatzakis, K., MacMillen, Z., Laohajaratsang, M., Grieser, A.M., Itsara, L.S., Do, J., Davie, J.W., Ghosh, A.K., Avril, M., 2024. Full maturation of in vitro *Plasmodium falciparum* oocysts using the AlgiMatrix 3D culture system. Malar. J. 23, 251. https://doi.org/10.1186/s12936-024-05079-7

Zsolnay, V., Katkar, H.H., Chou, S.Z., Pollard, T.D., Voth, G.A., 2020. Structural basis for polarized elongation of actin filaments. PNAS 117, 30458–30464. https://doi.org/10.1073/pnas.2011128117

Supplementary data

CLUSTAL O (1.2.4) multiple sequence alignment **PbActin1** vs **PbAlp1**

```
PbActin1      MGDEEVQALVIDNGSGNVKAGVAGDDAPRSVFPSIVGRPKNPGIMVGMEEKDAFVGDEAQ      60
PbAlp1        ---MDNNTIVIDNGSGYMKVGLNTHNLPAIVFPTVVGNSRNKDV------NQTYVGDEAF      51
                  : :::******* :*.*:  .: *  ***::**. :* .:      ::::*****

PbActin1      TKRGILTLKYPIEHGIVTNWDDMEKIWHHTFYNELRAAPEEHPVLLTEAPLNPKGNRERM      120
PbAlp1        FHESELSIYRPFDHGHISDWDLANNIWDYAISC-VDPNKSVKSALLTEPPLCSISHRKNM      110
               :.. *::  *::** :::**  ::**.:::   :    . : .**** **   .:*:.*

PbActin1      TQIMFESFNVPAMYVAIQAVLSLYSSGRTTGIVLDSGDGVSHTVPIYEGYALPHAIMRLD      180
PbAlp1        GEIFFENFGFESINISVSGLMSIYAAGLTTGLVLDIGEGVTQCIPIFDGYIEKNSVIRSD      170
               :*:**.*.. :: :::..::*:*::* ***:*** *:**:: :**::**   ::::* *

PbActin1      LAGRDLTEYLMKILHERGYGFSTSAEKEIVRDIKEKLCYIALNFDEEMKTSEQSSDIEKS      240
PbAlp1        FGGEELTMFMQKLICDIGYNMTTRKSYEYVKIMKETLCFCSLNPPKD----QLRDDLTVT      226
              :.*.:** :: *:: : **.::*  . * *: :**.**: :**  ::    :  .*:  :

PbActin1      YELPDGNIIT-------VGNERFRCPEALFQPSFLGKEAAGIHTTTFNSIKKCDVDIRKD      293
PbAlp1        YTLPDGDVLRDGYSTIEISHERFYVPEALFNPLLCHRDNLSISDIVCKSILSCPIENRKI      286
              * ****:::        :.:***  *****:* :  ::  .*   . :** .* :: **

PbActin1      LYGNIVLSGGTTMYEGIGERLTRDITTLAPSTMK--IKVVAPPERKYSVWIGGSILSSLS      351
PbAlp1        LSSYIILSGGCSLFPNLVERLEREIKNNSPENARSAVKVHAHENRGIMAWCGAQIFSQPE      346
              * . *:**** ::: .: *** *:*.. :*.. :  :** *  :*   .* *..*:*. .

PbActin1      ---TFQQMWITKEEYDESGPSIVHRKCF----  376   D-loop
PbAlp1        LRDAQRGVWVSKDEYEEIGDNIFLIKATLKLT  378   H-plug
                 : : :*::*:**:* * .*.  *.
```

Supplement 1: Protein sequence alignment of *P. berghei* actin1 and Alp1. Generated by Clustal Omega (EMBL). The green-underlined region and the pink-underlined region in actin1 represent the DNase I-binding loop (D-loop) and the hydrophobic plug (H-plug) respectively. * = identical amino acids, **:** = conserved amino acids, **.** = semi-conserved amino acids.

CLUSTAL O (1.2.4) multiple sequence alignment **PbActin1** vs **PbAlp2b**

```
PbActin1        -MGDEEVQALVIDNGSGNVKAGVAGDDAPRSVFPSIVGRPKNPGIMVGMEE-------KD      52
PbAlp2b         MAQYNDVSSIVIDLGFENIKLGYSGDENPKNVFSSNVGIPLDLDEKIKNEVYKKCLCTKD      60
                    ::*.::*** *  *:* * :**: *:.** * ** * : .  :  *        **

PbActin1        A-----------------------------------------------------------      53
PbAlp2b         EFYKFNLIYPLFYLQPRENIKLKNCLYIDDKNNFNVNEDVLEKILFMNINGDRSVYKLMQ      120


PbActin1        -----FVGDEAQT--KR---------------------------------GILTLKYPIE      73
PbAlp2b         NRIKGFIGNKLYKQTDTGNEYIDGDNINENDKNYTEVINNIQIDSEKNNYKHITNETNNL      180
                     *:*::  .  .                                      :* :

PbActin1        HGIVTNWDDMEKIWHHTF-----------------YNEL----RAAPEEHPVLLTEAPLN      112
PbAlp2b         TSTLKEWNEENCYFDLDIIENSHIDICGIKNMLNKYNNVSCGLNENMGNFPYVFSLPNKR      240
                 . :.:*:: :  :.  :                 **::    .    :.* :::    .

PbActin1        PKGNRERMTQIMFESFNVPAMYVAIQAVLSLYSSGRTTGIVLDSGDGVSHTVPIYEGYAL      172
PbAlp2b         NKKIKTKIAELLFEKYEIPAIYFNSKSILTGFAYNKKVCSVVDVGSCYSDFSICNDGIID      300
                 *  : ::::::**.:::**:*.  :::*: :: .:..  *:* *.  *.     :*

PbActin1        PHAIMRLDLAGRDLTEYLMKILHER----------------------G-------YGFS      202
PbAlp2b         DKNYNIYNIGGTSVDMFLEELLQKYNNSSLVPYYESSKEKNMHTNKKASYNSDNVHIDYY      360
                 :     ::.* .:  :* ::*::                        .        .:

PbActin1        TSAEKEIVRDIKEKLCYIALNFDEEMKTS-EQSSDIEKSYELPDGNIITVGNERFRCPEA      261
PbAlp2b         TKAKYIPLRDLKCYLCEVANSENEINKAKNITFNEHVDIYILPDGQNINITKFTNIACEI      420
                *.*:   :**:*  ** :* . :*  *:.    .:  . * ****: *.: :    . *

PbActin1        LFQPSFLGKEAA---------------GIHTTTFNSIKK-CDVDIRKDLYGNIVLSGGTT      305
PbAlp2b         FFTPSLLNDTTINSHLNNLYTKDKTFEGIPITLFNMLQNIKSIDHRQELLNNIILTGSST      480
                :* **:*.. :               **  * ** :::  .:* *::* .**:*:*.:*

PbActin1        MYEGIGERLTRDITTLAPS------TMKIKVVAPPERKYSVWIGGSILSSLSTFQQMWIT      359
PbAlp2b         LFQNFNERFINEFANLDMLNNTNFQNYQVLNNGKEFKKYSSWKGGSILSSFKSFNSFFVT      540
                :::.:.**: .::::.*         . ::   .   :*** * *******:.:*:.:::*

PbActin1        KEEYDESGPSIVHRKCF 376
PbAlp2b         RKEYEEFGFEIVNRKC- 556
                ::**:* * .**:***
```

D-loop
H-plug
Swapped region

Supplement 2: Protein sequence alignment of *P. berghei* actin1 and Alp2b. Generated by Clustal Omega (EMBL). The green-underlined region and the pink-underlined region in actin1 represent the DNase I-binding loop (D-loop) and the hydrophobic plug (H-plug) respectively. The blue-underlined regions indicate the swapped regions in the PbAlp2b-actin D-loop or H-plug mutants. * = identical amino acids, **:** = conserved amino acids, **.** = semi-conserved amino acids.

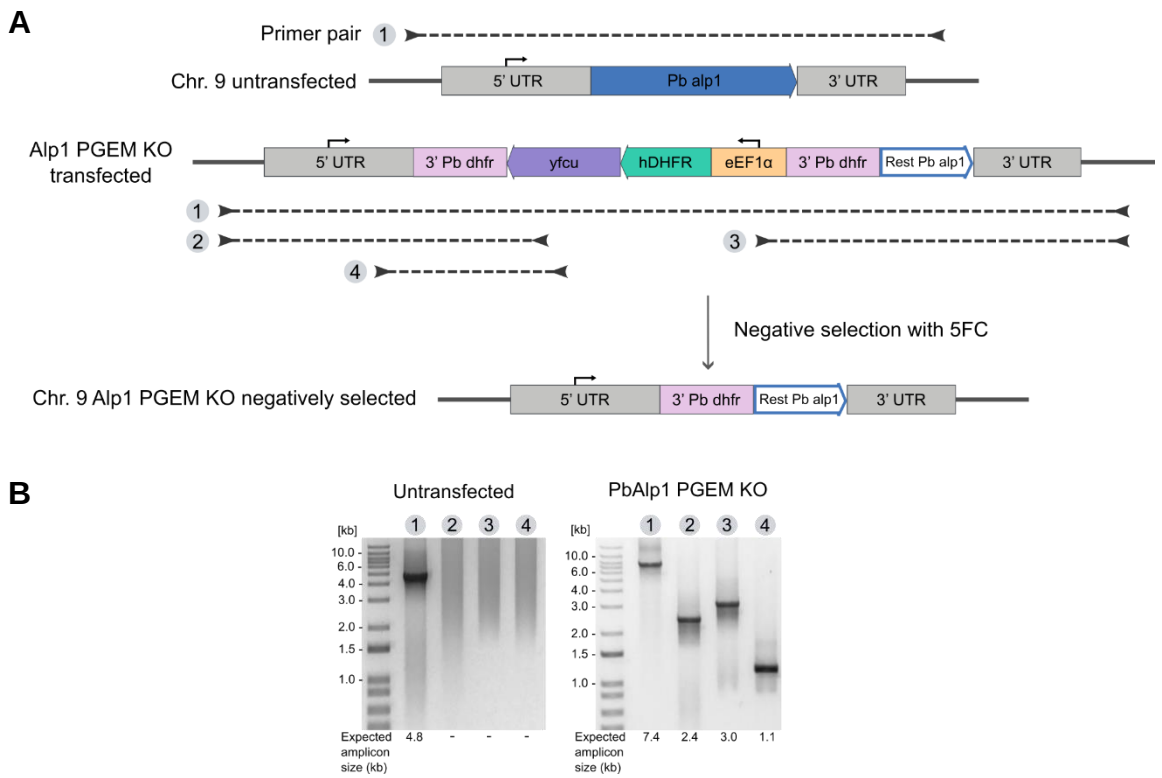

Supplement 3: PbAlp1 knock-out and negative selection using PlasmoGEM vector, conducted by Binder (2020) and genotyping. (A) *pbalp1* was replaced by the PlasmoGEM (PGEM) knock-out (KO) construct by homologous recombination of the 5' and 3' untranslated regions (UTR) of *pbalp1*. In addition to the drug selection cassette carrying *hDHFR* (positive selection) and *yfcu* (negative selection) under the eEF1α promoter, the construct also retains residual sequence from *pbalp1*, resulting in a partial KO of the target gene. The selection cassette was then excised under negative selection with 5FC, leaving a 3' Pb *dhfr* segment as a result of negative selection-induced recombination. The small arrow indicates a promoter function. **(B)** Quality control genotyping was conducted on the PbAlp1 PGEM KO line. The agarose gels confirm the correct integration of the target construct. The circled number and a dotted line indicate the primer pair used and its coverage for the genotyping. UTR (untranslated region); 3' Pb *dhfr* (3' untranslated region of *P. berghei* dihydrofolate reductase); *hDHFR* (human dihydrofolate reductase); *yfcu* (yeast cytosine deaminase-uracil phosphoribosyl transferase); eEF1α (eukaryotic translation elongation factor 1 alpha); 5FC (5-fluorocytosine).

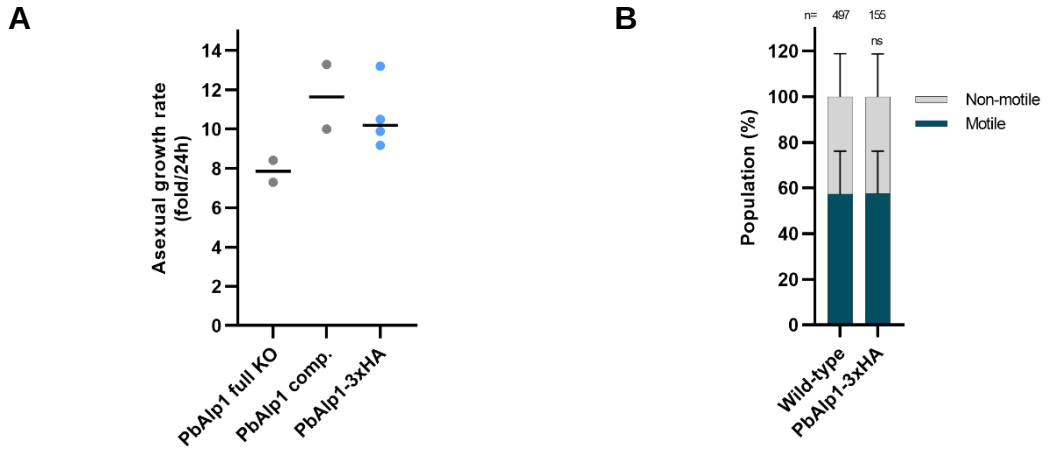

Supplement 4: Blood stage growth and motile ookinetes percentage of PbAlp1-3xHA. (A) The comparable blood stage growth of PbAlp1-3xHA parasites to the PbAlp1 complemented parasites indicates this parasite line does not have a growth phenotype. The PbAlp1 KO line, with the slower growth phenotype, is shown as a reference. The values of PbAlp1 full KO and comp. were adapted from **Figure 25A. (B)** Quantification of motile PbAlp1-3xHA ookinetes reveals comparable motility to wild-type (value was adapted from **Figure 26C)**. The statistical analyses represent a level of significance against the wild-type motile ookinetes (Fisher's exact test, two-sided, ns = non-significant.

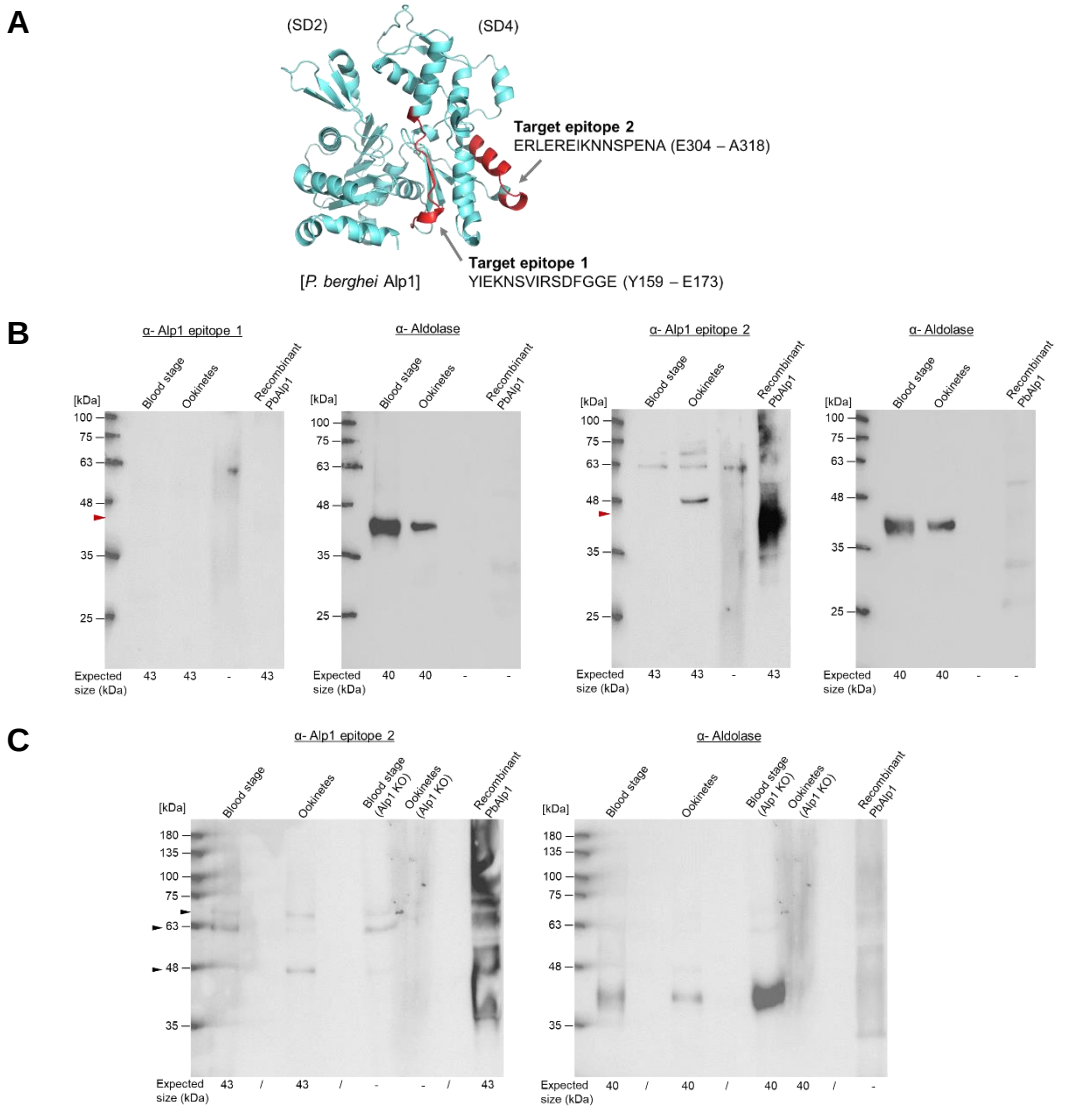

Supplement 5: Evaluation of binding capability and specificity of α-PbAlp1 antibody. (A) Two target epitopes in PbAlp1 were selected to generate α-PbAlp1 antibodies. The epitopes are located outside the PbAlp1 unique insertion and deletion regions and are not homologous to other *P. berghei* proteins. Additionally, a BLAST search against *Mus musculus* (mouse) provided a negative outcome. **(B)** A comparison of two antibodies directed against epitopes 1 and 2 on western blots demonstrated that the α-epitope 2 antibody is capable of binding to recombinant PbAlp1. Furthermore, some signals were observed in the vicinity of the target protein size (43 kDa, indicated with the red arrow). 1:5000 antibody concentration, 1 x 10^7 blood-stage parasites and 65 x 10^4 ookinetes were blotted. **(C)** The additional western blot with the protein of PbAlp1 KO parasites reveals non-specific binding of the α-epitope 2 antibody. The identical signals observed between the wild-type and the PbAlp1 KO negative control parasites indicate that the antibody binds to non-specific *P. berghei* proteins, but not to PbAlp1. To enhance detection, 1.8 x 10^7 blood stage parasites and 75 x 10^4 ookinetes were used with 1:2000 antibody concentration. Some of the parasite samples were found to be degraded as a result of inadequate storage conditions. While this does not impact the final interpretation of the outcome, it is essential to apply greater care in future experiments. Black arrows point to the signals indicating unspecific binding of α-epitope 2 antibody. SD2/SD4 = subdomain 2/ subdomain 4.

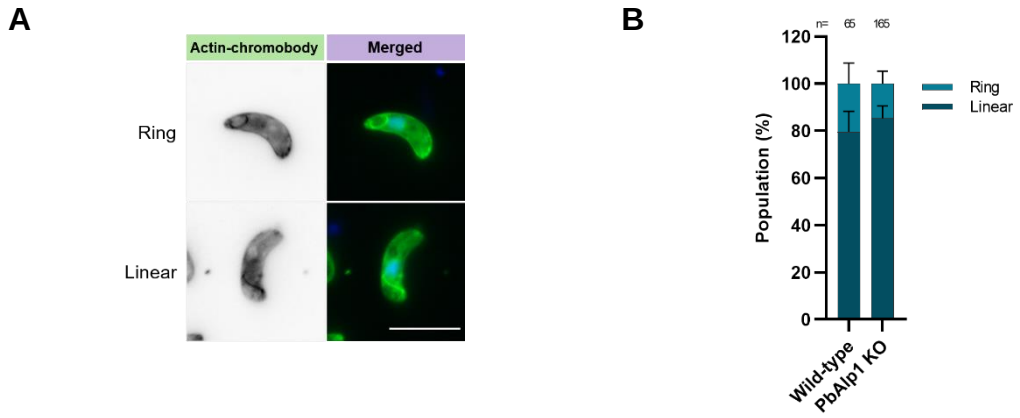

Supplement 6: Liner and ring-like forms of thick actin tubules. (A) Examples of linear and ring-like structures. The merged images show an overlay of actin (green) and the nucleus (blue). Scale bar = 10 µm. **(B)** Proportions of liner and ring-like structures in the wild-type and Alp1 KO ookinetes showing that the ring-like structure is a minority but present in both ookinete populations.

Untreated vs DMSO control

Element	P-value	Interpretation
WT Whole	0.0078	**
WT Front	0.2582	ns
WT Back	0.1881	ns
Alp1 KO Whole	0.1941	ns
Alp1 KO Front	0.1266	ns
Alp1 KO Back	0.2319	ns

Supplement 7: Statistical comparison of chromobody actin localisations between untreated and DMSO control. No significant difference in actin localisation patterns was observed at the statistical level, with the exception of the 'whole' populations in the wild-type ookinetes, which demonstrated a minor reduction under DMSO treatment. In conclusion, the data indicate that DMSO does not have an adverse effect overall (Fisher's exact test, two-sided, ns = non-significant, ** = P ≤ 0.01).

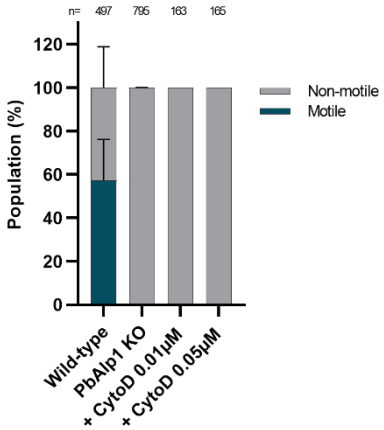

Supplement 8: Effect of cytochalasin D on PbAlp1 KO ookinete motility. In order to assess the potential actin filament-destabilising effect of Alp1, Alp1 KO ookinetes were treated with 0.01 and 0.05 µM of Cyto D and their motility rates were evaluated. However, no motility rescue effect was observed, indicating that the destabilising effect of Cyto D may differ from that of Alp1. The values of wild-type and PbAlp1 KO were adapted from **Figure 26C**. Cyto D (cytochalasin D).

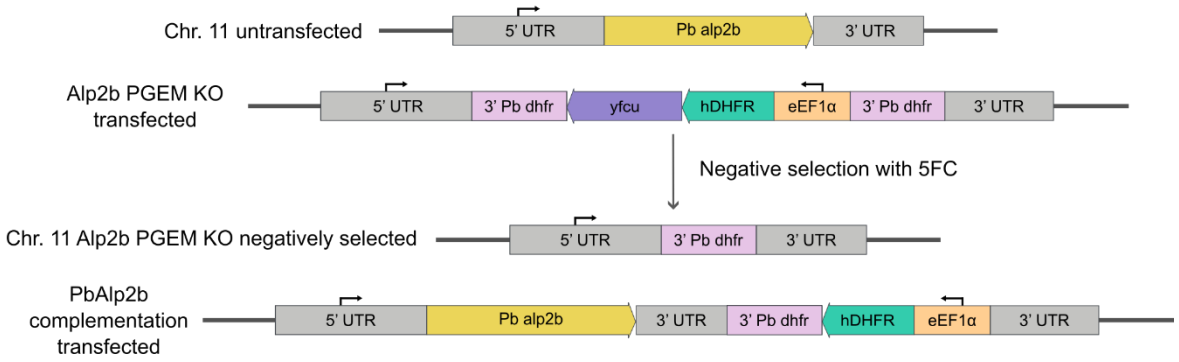

Supplement 9: PbAlp2b knock-out and negative selection using PlasmoGEM vector, and PbAlp2b complementation conducted by Binder (2000). *pbalp2b* was replaced by the PlasmoGEM (PGEM) knock-out (KO) construct by homologous recombination of the 5' and 3' untranslated regions (UTR) of *pbalp2b*. The construct comes with the drug selection cassette carrying *hDHFR* (positive selection) and *yfcu* (negative selection) under the eEF1α promoter. The selection cassette was then excised under negative selection with 5FC, leaving a 3' Pb *dhfr* segment as a result of negative selection-induced recombination. The negatively selected knockout locus was subsequently complemented with the *pbalp2b* gene in order to verify the observed knockout phenotypic effect. The complementation construct contains solely the positive selection cassette (*hDHFR*). The small arrow indicates a promoter function. UTR (untranslated region); 3' Pb *dhfr* (3' untranslated region of *P. berghei* dihydrofolate reductase); *hDHFR* (human dihydrofolate reductase); *yfcu* (yeast cytosine deaminase-uracil phosphoribosyl transferase); eEF1α (eukaryotic translation elongation factor 1 alpha); 5FC (5-fluorocytosine).

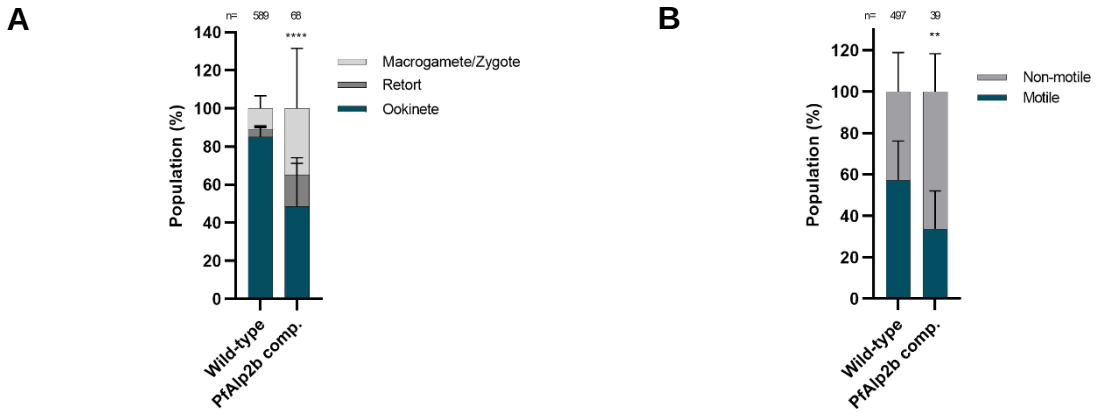

Supplement 10: Development and motility of PfAlp2b-complemented ookinetes. (A) Approximately 50% of the sexual stage parasites developed into mature ookinetes. The elevated number of macrogamete/zygote may include non-exflagellating microgametes, which could not be differentiated from this category. The statistical analysis represents a level of significance between the wild-type and PfAlp2b comp. mature ookinetes. (Fisher's exact test, two-sided, **** = P ≤ 0.0001). **(B)** Some ookinetes were identified as motile. Given the relatively low number of mature ookinetes evaluated (n=39), it is possible that the motility presented may not accurately reflect the true phenotype. Nevertheless, the data set indicates that the exflagellated PfAlp2b-complemented parasites were able to develop into motile ookinetes. This suggests that Alp2b function is likely to be more relevant at the exflagellation stage than at the ookinete stage. The statistical analysis represents a level of significance between the wild-type (value was adapted from **Figure 26C**) and PfAlp2b comp. motile ookinetes. (Fisher's exact test, two-sided, ** = P ≤ 0.01). Comp. (complementation).

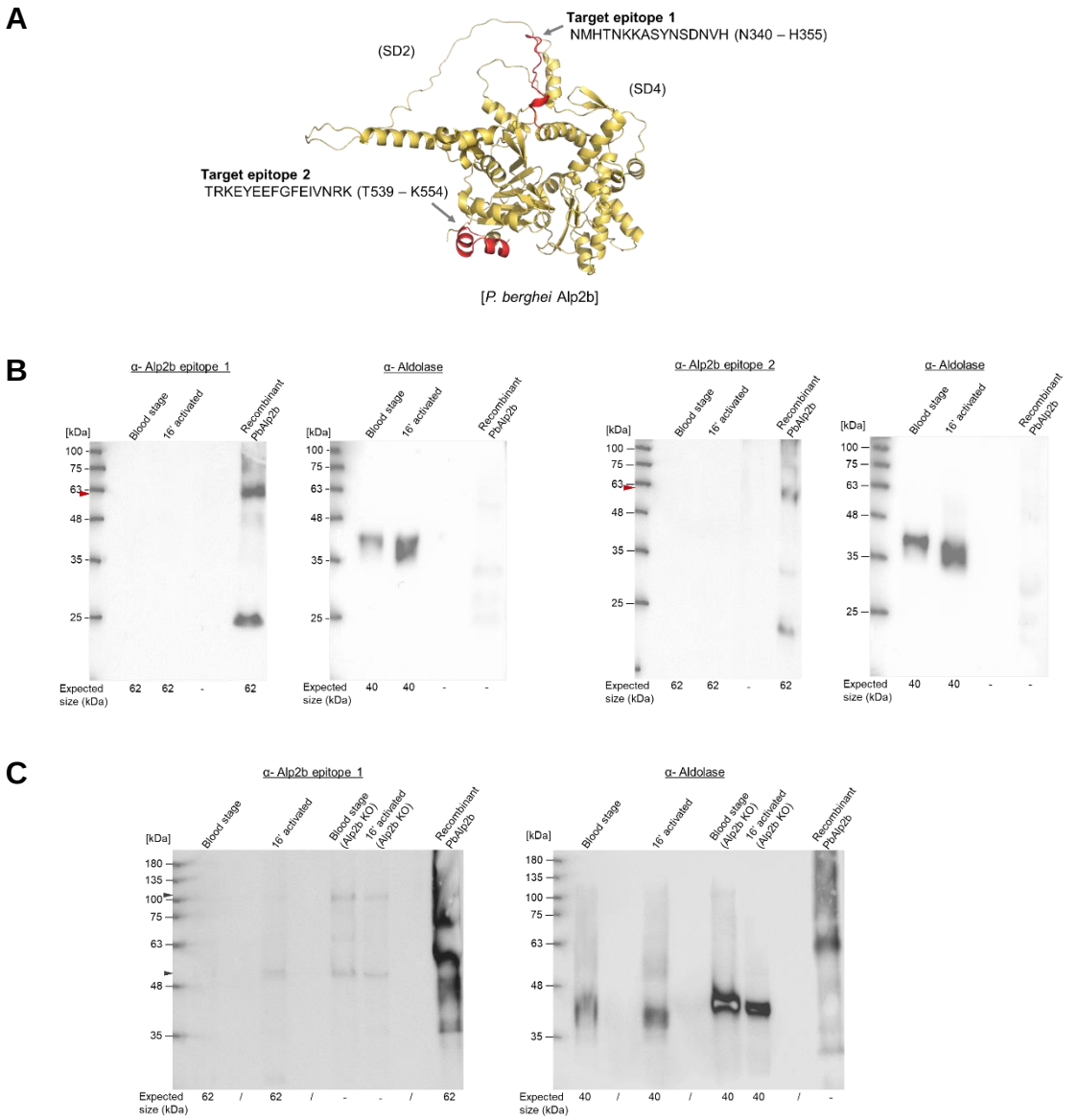

Supplement 11: Evaluation of binding capability and specificity of α-PbAlp2b antibody. (A) Two target epitopes in PbAlp2b were selected to generate α-PbAlp2b antibodies. The epitopes are located outside the PbAlp2b unique insertion regions and are not homologous to other *P. berghei* proteins. Additionally, a BLAST search against *Mus musculus* (mouse) provided a negative outcome. **(B)** A comparison of two antibodies directed against epitopes 1 and 2 on western blots demonstrated that the α-epitope 1 antibody showed a higher binding affinity to recombinant PbAlp2b. Nevertheless, no target bands corresponding to PbAlp2b (62 kDa, indicated with the red arrow) were observed in either the blood stage or sexually activated (16' activated) parasites. 1:5000 antibody concentration, 1 x 10^7 blood-stage and sexually activated parasites (16' activated) were blotted. **(C)** The additional western blot with the protein of PbAlp2b KO parasites reveals non-specific binding of the α-epitope 1 antibody. The identical signals observed between the wild-type and the PbAlp2b KO negative control parasites indicate that the antibody binds to non-specific *P. berghei* proteins, but not to PbAlp2b. To enhance the efficacy of the detection, the number of blood stage parasites was increased to 1.8 x 10^7 (with the sexually activated parasites remaining at 1 x 10^7 for practical reasons). An increased concentration of antibody (1:2000) was also used. Some of the parasite samples were found to be degraded as a result of inadequate storage conditions. While this does not impact the final interpretation of the outcome, it is essential to apply greater care in future experiments. Black arrows point to the signals indicating unspecific binding of α-epitope 1 antibody. SD2/SD4 = subdomain 2/ subdomain 4.

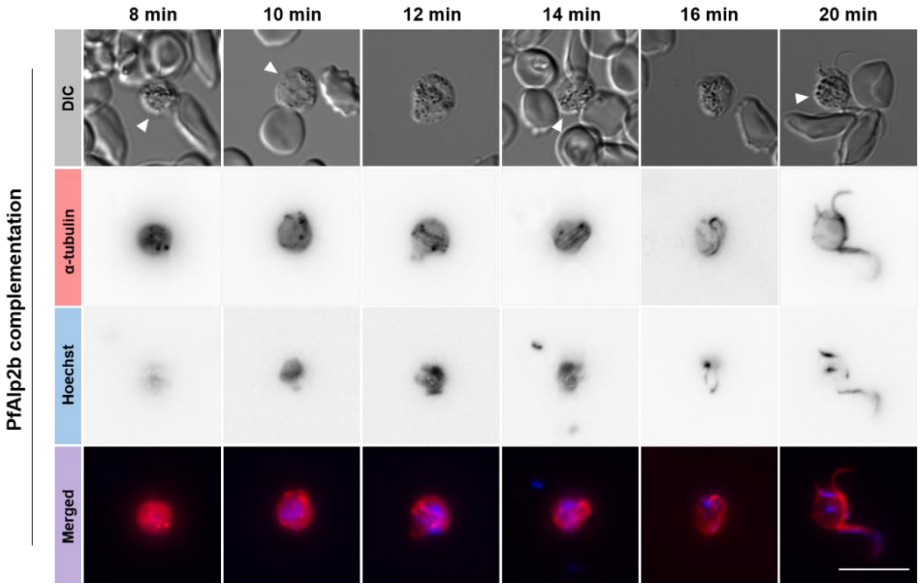

Supplement 12: Microgametogenesis and exfllagellation of PfAlp2b-complemented gametocytes visualised by α-tubulin immunostaining. The labelling of α-tubulin (red) reveals the comparable development to the wild-type gametocytes (**Figure 45**) with the presence of basal bodies and nucleated axonemes between eight and ten minutes post-activation (mpa). The axonemes underwent further elongation to form premature microgametes, which were positioned around the aggregated nuclei (blue) in the centre of the cell. At 16 mpa, a multi-nucleated signal indicates the imminent onset of exflagellation, as represented at 20 mpa. The white arrow indicates a gametocyte and the time indicates the minutes post-activation (mpa). Merged = overlay of α-tubulin and Hoechst images. Scale bar = 10 µm. DIC (differential interference contrast).